

**DESIGN & SYNTHESIS OF A FEW
PHARMACEUTICAL
COCRYSTALS/SALTS BY CRYSTAL
ENGINEERING APPROACH AND
STUDY OF THEIR
PHYSICOCHEMICAL PROPERTIES**

Thesis

Submitted in Partial Fulfillment of Requirements for the

Degree of

DOCTOR OF PHILOSOPHY

by

SUNIL KUMAR N



**DEPARTMENT OF CHEMISTRY
NATIONAL INSTITUTE OF TECHNOLOGY
KARNATAKA, SURATHKAL
MANGALORE-575025**

July, 2018

DECLARATION

I hereby declare that the Research Thesis entitled “**Design & Synthesis of A Few Pharmaceutical Cocrystals/Salts by Crystal Engineering Approach and Study of Their Physicochemical Properties**” which is being submitted to the **National Institute of Technology Karnataka, Surathkal** in partial fulfilment of the requirements for the award of the Degree of Doctor of Philosophy in Chemistry is a bonafide report of the research work carried out by me. The material contained in this Research Thesis has not been submitted to any University or Institution for the award of any degree.

Sunil Kumar N
Reg. No. 148002CY14F06
Department of Chemistry

Place: NITK - Surathkal
Date:

CERTIFICATE

This is to certify that the Research Thesis entitled “**Design & Synthesis of A Few Pharmaceutical Cocrystals/Salts by Crystal Engineering Approach and Study of Their Physicochemical Properties**” submitted by Mr. Sunil Kumar N (Register Number: 148002CY14F06) as the record of the research work carried out by him is accepted as the Research Thesis submission in partial fulfilment of the requirements for the award of degree of Doctor of Philosophy.

Dr. Darshak R. Trivedi
Research Guide
Date:

Chairman – DRPC
Date:

**DEDICATED TO
MY PARENTS AND FAMILY**

ACKNOWLEDGEMENT

My heartfelt acknowledgement to National Institute of Technology Karnataka (NITK), Surathkal for providing me a wonderful research environment and research facilities. I am obliged to NITK for providing research fellowship throughout my research work. I would like to extend my sincere thanks to Dr. Darshak R. Trivedi, Research guide for his support and encouragement during my research work. It wouldn't be possible without his support and timely guidance. I am sure that the experience I gained from NITK Surathkal will definitely boost my life and career in a positive direction. I take this opportunity to thank all my friends and colleagues who supported me directly or indirectly throughout my research work.

I am thankful to Prof. D. K. Bhat, Head, Department of Chemistry and Chairman-DRPC, RPAC members Prof. A. N. Shetty, Department of Chemistry and Prof. Jagannath Nayak, Department of Metallurgical and Materials Engineering for their support, guidance and valuable suggestions during my research progress. Their timely suggestions and inputs were highly noticeable during my research work. I thank all the faculty members of department of chemistry for their encouragement, timely help, and support. I thank Prof. Nagaraj, Prof. Kartick Tarafder, and Prof. Udayshankar from the department of physics, NITK Surathkal for extending their support. I extend my gratitude to Department of Science and Technology (DST), Govt. of India for providing SC-XRD facility to Department of Chemistry, NITK Surathkal, under FIST program.

I am extending my gratitude to Prof. Parthasarathi Dastidar and Mr. Kaushik Sarkar from Indian Association for the Cultivation of Science (IACS) for extending the timely support of SC-XRD facility. I also thank Prof. Lokanath, department of physics, University of Mysore, and his students Dr. Naveen and Mr. Karthik Kumara for extending the SC-XRD facility during my research work.

I extend my appreciation to all the non-teaching staff of Chemistry Department namely, Mrs. Shamila Nandini, Mr. Prashant, Mrs. Sharmila, Mr. Pradeep, Mr. Harish and Mrs. Deepa for their support in the department.

I extend my sincere thanks to my friends and colleagues Dr. Manoj Kumar, Mr. Nimith, Mr. Mahendra, Mr. Brijesh, Mr. Ramesh Reddy, and Ms. Bindu from

Department of Physics, NITK Surathkal for their timely help and support. I thank Mr. Vishnu and Ms. Anjana from Chemical engineering department, NITK Surathkal for their timely help.

I am obliged to various research institutes and industries such as MIT Manipal, Apotex Pharmachem India Pvt Ltd, and STIC Kochi. I am thankful to Mr. Venkatesh Pilli, Balakonda Reddy, and Dr. Vasantha Kumar for their timely help and support.

I extend my sincere thanks to all the research colleagues from the chemistry department. My special thanks to Venkatadri Tekuri, Bharath Kumar, Srikala, Archana, Rajalakshmi, Vinaya kumara and Aranganathan for their help and support throughout my research work.

Finally, I extend my sincere thanks to my parents, brothers, sisters, and all my family members for their continuous support for my research activities and also for making me what I am today. I dedicate my thesis work to my parents for their support to achieve my Ph. D degree.

ABSTRACT

The pharmaceutical cocrystal of an active pharmaceutical ingredient with GRAS or non-GRAS compounds offers an opportunity to develop a new drug product with improved physicochemical properties. Pharmaceutical cocrystal exhibits better physicochemical properties such as solubility, stability, dissolution, melting point, crystal habit, compressibility, friability etc. without altering the biological activity of drug compounds. In the last two decades, numerous research activities have been carried out to develop the new drug products of BCS Class II and BCS Class IV drug ingredients by cocrystallization techniques. The result showed remarkable increment in the solubility and dissolution rate of BCS Class II and IV drug ingredients.

In this context, a series of active pharmaceutical ingredients have been chosen for the present work which is having poor or high aqueous solubility and permeability. All the active ingredients chosen in the study are screened for salt/cocrystallization experiments by crystal engineering approach with various GRAS and non-GRAS compounds. Solution crystallization and liquid-assisted grinding approach are followed for the cocrystallization experiments. The newly synthesized salts/cocrystals were characterized by various spectroscopic (FT-IR, NMR, and UV-Vis), thermal (DSC and TGA), and PXRD techniques. The crystal structure of the synthesized salts/cocrystals were determined by SC-XRD techniques. Aqueous solubility (equilibrium solubility) was measured for the cocrystal/salt of BCS class II drug by UV-Vis spectroscopy and compared the results with API alone. In all the five series, the stability of the synthesized salts/cocrystals were evaluated. In some cases, hygroscopicity study at accelerated humidity condition was performed to demonstrate the non-hygroscopicity of the synthesized cocrystal/salt. In few cases, isostructurality of the synthesized salt/cocrystal was described based on the SC-XRD analysis. Further, in one chapter DFT calculations were performed for the synthesized salt/cocrystal to support the crystal structure data determined from the SC-XRD analysis.

Keywords: Crystal Engineering, Pharmaceutical cocrystal, cocrystal, salts, supramolecular synthon, isostructurality, stability

CONTENTS

	Page No
DECLARATION.....	i
CERTIFICATE.....	ii
ACKNOWLEDGEMENT.....	iv-v
ABSTRACT.....	Vi
CONTENTS.....	vii-ix
LIST OF FIGURES AND TABLES.....	x-xviii
NOMENCLATURE.....	xix-xxi
1. INTRODUCTION.....	1
1.1 SUPRAMOLECULAR CHEMISTRY.....	1-3
1.2 CRYSTAL ENGINEERING.....	3-5
1.2.1 Special Role of Hydrogen Bond.....	5-7
1.2.2 Supramolecular Synthons.....	7-8
1.3 MOLECULAR ADDUCTS.....	9
1.3.1 Salt.....	9-10
1.3.2 Cocrystal.....	10-12
1.3.3 Multi-component Crystal.....	12-13
1.4 POLYMORPHISM.....	13-14
1.4.1 Factors Affecting the Formation of Polymorph.....	14-15
1.4.2 Challenges to Pharmaceutical Industry.....	15-17
1.5 PHARMACEUTICAL COCRYSTAL.....	17-19
1.5.1 Properties of Pharmaceutical Cocrystal.....	19-20
1.5.2 Synthesis of Pharmaceutical Cocrystal.....	21-23
1.5.3 Characterization of Pharmaceutical Cocrystal.....	23
1.5.4 Pharmaceutical cocrystal as Intellectual properties.....	23-24
1.6 BIOPHARMACEUTICAL CLASSIFICATION SYSTEM.....	25
1.7 CAMBRIDGE STRUCTURAL DATABASE.....	25-26
1.8 LITERATURE REVIEW.....	26-36
1.9 SCOPE AND OBJECTIVES OF THE WORK.....	36-39

CHAPTER 2.....	41
DESIGN, SYNTHESIS, CHARACTERIZATION, AND EVALUATION OF PHYSICOCHEMICAL PROPERTIES OF COCRYSTAL OF ANTI-INFLAMMATORY AND ANTI-VIRAL DRUGS	
2.1 INTRODUCTION.....	41-43
2.2 EXPERIMENTAL SECTION.....	43-46
2.3 RESULTS AND DISCUSSION.....	46-68
2.4 CONCLUSIONS.....	68-69
CHAPTER 3.....	71
DESIGN, SYNTHESIS, CHARACTERIZATION, AND EVALUATION OF PHYSICOCHEMICAL PROPERTIES OF SALT OF ANTI-TUBERCULOSIS DRUG ETHIONAMIDE	
3.1 INTRODUCTION.....	71-73
3.2 EXPERIMENTAL SECTION.....	73-74
3.3 RESULTS AND DISCUSSION.....	75-99
3.4 CONCLUSIONS.....	99-100
CHAPTER 4.....	101
DESIGN, SYNTHESIS, CHARACTERIZATION, AND EVALUATION OF PHYSICOCHEMICAL PROPERTIES OF SALTS OF COMMON ANTI-INFLAMMATORY DRUGS	
4.1 INTRODUCTION.....	101-102
4.2 EXPERIMENTAL SECTION.....	102-103
4.3 RESULTS AND DISCUSSION.....	103-130
4.4 CONCLUSIONS.....	130
CHAPTER 5.....	131
DESIGN, SYNTHESIS, CHARACTERIZATION, DFT, AND STABILITY STUDY OF COCRYSTAL/SALT OF ANTI- FIBRINOLYTIC HEMOSTATIC DRUG TRANEXAMIC ACID	
5.1 INTRODUCTION	131-132
5.2 EXPERIMENTAL SECTION.....	133-134

5.3 RESULTS AND DISCUSSION.....	134-178
5.4 CONCLUSIONS.....	178
CHAPTER 6.....	179
DESIGN, SYNTHESIS, CHARACTERIZATION, AND EVALUATION OF PHYSICOCHEMICAL PROPERTIES OF COCRYSTAL/SALT OF ANTI-FUNGAL DRUG FLUCYTOSINE	
6.1 INTRODUCTION	179-181
6.2 EXPERIMENTAL SECTION.....	181-182
6.3 RESULTS AND DISCUSSION.....	183-205
6.4 CONCLUSIONS.....	205-206
CHAPTER 7.....	207
SUMMARY AND CONCLUSIONS	
7.1 SUMMARY OF PRESENT WORK.....	207-208
7.2 CONCLUSIONS.....	208-210
7.3 SCOPE FOR FUTURE WORK.....	211
REFERENCES.....	211-236
LIST OF PUBLICATIONS.....	237-238
CURRICULUM VITAE.....	239-242

LIST OF FIGURES AND TABLES

LIST OF FIGURES

Figure No	Figure Description	Page No
Figure 1.1	Lock and key model.....	2
Figure 1.2	Photocycloaddition reaction of <i>Trans</i> -cinnamic acid.....	4
Figure 1.3	Hydrogen bonding in the water molecule.....	6
Figure 1.4	Supramolecular homosynthon and supramolecular	
& 1.5	heterosynthon representation.....	7,8
Figure 1.6	Commonly observed synthons.....	8
Figure 1.7	The formation of the pharmaceutical salt salbutamol	
	Sulfate.....	10
Figure 1.8	Cocrystal structure of quinhydrone.....	10
Figure 1.9	Comparison of different solid forms.....	11
Figure 1.10	An example of the host-guest system.....	13
Figure 1.11	Structure of ranitidine and ritonavir.....	16,17
& 1.12		
Figure 1.13	Structure of carbamazepine and BCS classification.....	19,25
& 1.14		
Figure 1.15	Number of entries to the CSD in recent years.....	26
Figure 1.16	Solvates of carbamazepine with (a) acetic acid, (b) formic	
	acid and (c) butyric acid.....	27
Figure 1.17	CBZ: Nicotinamide cocrystal (1:1)	28
Figure		
1.18, 1.21,	Structure of naproxen, isoniazid, dapsone, fluorouracil,	29,31,
1.23, 1.25	and ethenzamide.....	33,34 &
& 1.27		35
Figure 1.19	Supramolecular acid-pyridine hetero synthon observed in	
	naproxen/isonicotinamide cocrystal.....	30
Figure 1.20	Asymmetric unit in S-NPX/D-tyrosine cocrystal.....	31

Figure 1.22	Cocrystal of ISD/4-aminosalicylic acid with the partly ionic bond.....	32
Figure 1.24	Polymorphic forms of dapsone/flavone cocrystal.....	34
Figure 1.26	Two polymorphic forms of fluorouracil/4-hydroxybenzoic acid cocrystal.....	35
Figure 1.28	Trimorphic forms of ethenzamide/gentisic acid cocrystal...	36
Figure 2.1	Asymmetric unit (a) and tetrameric unit (b) of FFA-CNB cocrystal.....	47
Figure 2.2	Supramolecular 1D sheet stabilized by C-H...O hydrogen bond.....	48
Figure 2.3	3D Structure of FFA-CNB cocrystal stabilized via C-H...F and Cl...F interactions.....	48
Figure 2.4	Asymmetric unit (a) and tetrameric unit (b) in the FFA-ETZ cocrystal.....	49
Figure 2.5	3D representation of FFA-ETZ cocrystal.....	49
Figure 2.6	Asymmetric unit of ETZ-SNP cocrystal.....	50
Figure 2.7	1D representation of ETZ-SNP cocrystal.....	50
Figure 2.8	2D sheet-like structure of ETZ-SNP cocrystal.....	50
Figure 2.9	Asymmetric unit of CNB-SNP cocrystal.....	51
Figure 2.10	1D representation of CNB-SNP cocrystal.....	51
Figure 2.11	The 2D sheet-like structure of CNB-SNP cocrystal stabilized via C-H...O and C-H...Cl hydrogen bond.....	52
Figure 2.12	Comparison of FT-IR spectra of a) FFA-CNB b) FFA-ETZ, c) ETZ-SNP, and d) CNB-SNP cocrystal with respect to starting materials.....	54-56
Figure 2.13-2.16	¹ H NMR spectra of cocrystals (FFA-CNB, FFA-ETZ, ETZ-SNP, and CNB-SNP)	57-59
Figure 2.17 & 2.18	DSC thermograms and POM images of cocrystals.....	60-61
Figure 2.19-2.22	PXRD comparison plots of cocrystals.....	62-63

Figure 2.23-2.26	PXRD comparison plots of stability samples.....	65-66
Figure 2.27	Standard linearity curves of a) FFA, b) ETZ, and c) CNB drug molecules.....	68
Figure 3.1	Molecular diagram of ethionamide (ETH).....	71
Figure 3.2	Asymmetric unit in ETH-CNB salt/cocrystal.....	76
Figure 3.3	2D representation of ETH-CNB salt.....	77
Figure 3.4	Tetrameric unit of ETH-CNB cocrystal.....	77
Figure 3.5	2D propagation of ETH-CNB salt/cocrystal.....	77
Figure 3.6	Asymmetric unit in the molecular salt of ETH-2,6HBA salt	81
Figure 3.7	Six component supramolecular unit in ETH-2,6HBA salt...	81
Figure 3.8	1D tape-like structure of ETH-2,6HBA salt.....	81
Figure 3.9	Asymmetric unit in the molecular salt of ETH-2,3HBA....	82
Figure 3.10	1D tape-like structure of ETH-2,3HBA salt.....	82
Figure 3.11	2D structure of ETH-2,3HBA salt stabilized by thioamide dimer.....	83
Figure 3.12	Asymmetric unit in the molecular salt of ETH-DNB.....	84
Figure 3.13	Tetrameric unit of ETH-DNB salt interconnected through N-H...O and weak C-H...S hydrogen bond.....	84
Figure 3.14	Overlay of ETH molecule extracted from the crystal structure of neutral ETH and the molecular salts.....	85
Figure 3.15	Comparison of simulated and experimental PXRD patterns of a) ETH-CNB b) ETH-2,6HBA c) ETH-2,3HBA and d) ETH-DNB salts.....	86-87
Figure 3.16	FT-IR spectra of a) ETH-CNB b) ETH-2,6HBA c) ETH-2,3HBA and d) ETH-DNB salts.....	88-90
Figure 3.17	¹ H NMR plots of a) ETH-CNB b) ETH-2,6HBA c) ETH-2,3HBA and d) ETH-DNB salts.....	91-93
Figure 3.18	DSC plot of ETH salts in comparison with ETH.....	94

Figure 3.19	Comparison of PXRD patterns of initial and moisture exposed samples of a) ETH-CNB b) ETH-2,6HBA, c) ETH-2,3HBA salts.....	95-96
Figure 3.20	TGA plots of a) ETH-CNB, b) ETH-2,6HBA and c) ETH-2,3HBA salts after exposure to moisture.....	97
Figure 3.21	Standard linearity plot of ETH.....	98
Figure 4.1	Asymmetric unit (a) and tetrameric unit (b) of MFA-4AP salt hydrate.....	105
Figure 4.2	3D representation of MFA-4AP salt hydrate.....	105
Figure 4.3	Asymmetric unit (a) and tetrameric unit (b) in the molecular salt hydrate of MFA-DMAP.....	106
Figure 4.4	2D representation of MFA-DMAP salt hydrate.....	106
Figure 4.5	Asymmetric unit (a) and cyclic tetrameric unit of TFA-4AP salt hydrate.....	107
Figure 4.6	3D representation of TFA-4AP salt hydrate.....	107
Figure 4.7	Asymmetric unit (a) and tetrameric unit (b) of TFA-DMAP salt hydrate.....	108
Figure 4.8	2D representation of TFA-DMAP salt hydrate.....	108
Figure 4.9	Asymmetric unit (a) and tetrameric unit of (b) NPX-4AP salt hydrate.....	109
Figure 4.10	3D representation of NPX-4AP salt hydrate.....	110
Figure 4.11	Asymmetric unit of NPX-2AP molecular salt.....	110
Figure 4.12	2D representation of NPX-2AP molecular salt.....	111
Figure 4.13	3D representation of NPX-2AP molecular salt.....	111
Figure		
4.14-4.16	FT-IR comparison plots of salts.....	115-116
Figure 4.17	¹ H NMR spectra of salts.....	117-119
Figure		
4.18-4.23	PXRD Comparison plots of simulated and experimental....	120-122
Figure 4.24	Overlay of three different APIs (a-MFA, b-TFA and c-NPX) extracted from the crystal structure of binary solids..	124

Figure		
4.25-4.27	DSC thermogram of salts with starting materials.....	126-127
Figure 4.28	Comparison of PXRD patterns of molecular salts initial and moisture exposed samples.....	129
Figure 4.29	Comparison of PXRD patterns of molecular salts, initials and after six months.....	130
Figure 5.1	Asymmetric unit (b) 1D cyclic chain-like structure (c) 2D structure of the TXA-SAL salt.....	136
Figure 5.2	Asymmetric unit (b) 1D chain-like structure (c) 2D sheet-like structure of TXA-3HBA salt hydrate.....	137-138
Figure 5.3	Asymmetric unit (a) cyclic 1D structure (b) 2D network-like structure of TXA-2,4HBA salt (c).....	139
Figure 5.4	(a) Asymmetric unit (b) 1D tape-like structure (c) 3D structure of TXA-2,5HBA salt.....	140
Figure 5.5	(a) Asymmetric unit (b) cyclic 2D structure (c) 3D structure of TXA-2,6HBA salt.....	141
Figure 5.6	(a) Asymmetric unit (b) 2D sheet-like structure (c) 3D structure of TXA-GAA cocrystal.....	142-143
Figure 5.7	(a) Asymmetric unit (b) Cyclic six component supramolecular unit (c) 1D tape-like structure (d) 3D structure of TXA-OXA salt.....	143-144
Figure 5.8	(a) Asymmetric unit (b) 1D structure (c) 2D structure (d) 3D structure of TXA-TTA salt.....	145-146
Figure 5.9	(a) Asymmetric unit (b) cyclic 1D structure (c) 2D structure (d) 3D structure of TXA-FUM salt stabilized via N-H...O hydrogen bond.....	146-147
Figure 5.10	(a) Asymmetric unit (b) cyclic 1D structure (c) 3D structure of TXA-SUA salt stabilized via N-H...O hydrogen bond.....	148
Figure 5.11	(a) Asymmetric unit (b) 1D chain-like structure (c) 2D chain-like structure of TXA-CRA cocrystal.....	149

Figure 5.12	Comparison of FT-IR spectra of TXA salt/cocrystal with starting materials.....	156-161
Figure 5.13	DSC thermograms of TXA salt/cocrystal.....	163
Figure 5.14	POM images of salt/cocrystal of TXA	164-165
Figure 5.15	PXRD Comparison plots of Simulated and experimental patterns of TXA salt/cocrystal.....	168-173
Figure 5.16	The optimized hypothetical structures drawn for TXA-GAA and TXA- CRA cocrystal.....	175
Figure 5.17	The optimized structures of molecular salts of TXA.....	175
Figure 5.18-5.21	The PXRD comparison plots of (initial and after six months).....	176-178
Figure 6.1	Molecular structure of 5-fluorocytosine.....	179
Figure 6.2	Asymmetric unit of FLC-3HBA cocrystal.....	184
Figure 6.3	3D structure of FLC-3HBA cocrystal.....	184
Figure 6.4	Structure of FLC-3HBA cocrystal stabilized via C-H...O and C-H...F hydrogen bond.....	184
Figure 6.5	Asymmetric unit (a) and tetrameric unit (b) of FLC-2,5HBA cocrystal.....	185
Figure 6.6	1D chain like structure of FLC-2,5HBA cocrystal.....	185
Figure 6.7	2D sheet-like structure of FLC-2,5HBA cocrystal.....	186
Figure 6.8	Asymmetric unit of FLC-CNB cocrystal.....	187
Figure 6.9	2D sheet like structure of FLC-CNB cocrystal.....	187
Figure 6.10	Asymmetric unit of FLC-SAL salt.....	188
Figure 6.11	2D structure stabilized by N-H...O hydrogen bond.....	188
Figure 6.12	Asymmetric unit of FLC-GLA cocrystal.....	189
Figure 6.13	Cyclic 1D chain like structure of FLC-GLA cocrystal.....	189
Figure 6.14	Structure of FLC-GLA cocrystal stabilized by C-H...F hydrogen bond.....	189
Figure 6.15	FT-IR spectra of FLC cocrystal/salt with starting materials.....	193-195
Figure 6.16	DSC thermograms of FLC and FLC salt/cocrystal.....	196

Figure 6.17	POM images of salt/cocrystals of FLC.....	197
Figure 6.18	PXRD overlapping plots of simulated and experimental patterns.....	198-200
Figure 6.19	¹ H NMR spectra of FLC salt/cocrystals.....	201-203
Figure 6.20	TGA plots of FLC and the FLC cocrystal/salt.....	205

LIST OF TABLES

Table No	Table description	Page No
Table 1.1	Analogies between molecular and supramolecular chemistry.....	2
Table 1.2	Strength of different non-covalent interactions.....	3
Table 1.3	Hydrogen bonding distance of various X and Y elements.....	7
Table 2.1	Crystal structure details and the refinement parameters of FFA cocrystals.....	52
Table 2.2	Geometrical parameters of the intermolecular interactions in the cocrystals.....	53
Table 2.3	Comparison of stretching frequency of cocrystals with starting materials.....	56
Table 2.4	Melting point of FFA, coformers, and cocrystals.....	60
Table 2.5	Solubility of FFA and its co-crystal in Millipore water and in 0.1 N HCl solution (pH=1) at ~25 °C.....	67-68
Table 3.1	pKa & ΔpKa values of ETH and counter ions.....	75
Table 3.2	Crystal structure details and the refinement parameters of ETH salts.....	78
Table 3.3	Geometrical parameters of intermolecular interactions in ETH salts.....	79-80
Table 3.4	Torsion angles of ETH molecule in neutral ETH and in the molecular salts.....	85
Table 3.5	IR stretching frequencies of ETH, salt former and the salts.....	90

Table 3.6	Melting Point of ETH, counter ions and molecular salts	94
Table 3.7	Solubility of ETH and its molecular salts in purified water and 0.1 N HCl (pH=1) at room temperature (~25 °C).....	99
Table 3.8	Comparison of solubility profile of literature reported and the present work.....	99
Table 4.1	pKa and ΔpKa values of APIs and the salt formers.....	104
Table 4.2	Crystal structure and refinement details of molecular salts.....	112
Table 4.3	Hydrogen bond geometry of the synthesized salts.....	113-114
Table 4.4	Stretching frequencies of APIs and the molecular salts.....	114
Table 4.5	Isostructural parameters of molecular salts.....	124
Table 4.6	Torsion angle of APIs in molecular salts.....	125
Table 4.7	Melting point of APIs, salt former and the molecular salts.....	126
Table 5.1	The pKa and ΔpKa values of TXA and the cofomers used in the study.....	135
Table 5.2	The crystal structure details and the crystallographic parameters of TXA salt/cocrystal.....	150-151
Table 5.3	The geometrical parameters hydrogen bond interactions in the molecular salt/cocrystal of TXA.....	152-154
Table 5.4	FT-IR stretching frequencies of TXA, cofomers and the salt/cocrystals of TXA.....	155
Table 5.5	Melting point of TXA, cofomers and the salt/cocrystals of TXA.....	162
Table 5.6	The total energy, cofomer energy, and the IE value of the salt/cocrystals of TXA.....	174
Table 6.1	The pKa and ΔpKa values of FLC and the cofomers.....	183
Table 6.2	Crystallographic parameters and refinement details of FLC salt/cocrystal.....	190

Table 6.3	Geometrical parameters of hydrogen bond interactions in FLC salt/cocrystal.....	191-192
Table 6.4	Stretching frequency list of cocrystal/salt and starting materials.....	192
Table 6.5	Melting point of FLC, coformer, and the synthesized salt/cocrystal.....	196
Table 6.6	Percentage weight loss between 40 to 120 °C in the salt/cocrystal of FLC at 70-75% RH and at 90-95% RH....	204

NOMENCLATURE

ABBREVIATIONS

API	Active Pharmaceutical Ingredient
BCS	Biopharmaceutical Classification System
CSD	Cambridge Structural Database
CCDC	Cambridge Crystallographic Data Centre
LAG	Liquid Assisted Grinding Method
DSC	Differential Scanning Calorimetry
FT-IR	Fourier Transform Infrared
TGA	Thermogravimetric Analysis
POM	Polarized Optical Microscope
NMR	Nuclear Magnetic Resonance
SC-XRD	Single Crystal X-ray Diffraction
PXRD	Powder X-ray Diffraction
USFDA	United States Food and Drug Administration
UV-Vis	Ultraviolet-Visible
DFT	Density Functional Theory
DMSO-d ₆	Dimethyl Sulfoxide-deuterated
CDCl ₃	Chloroform-deuterated
IE	Interaction Energy
IP	Intellectual Property
mp	Melting point
FFA	Flufenamic acid
MFA	mefenamic acid
TFA	Tolfenamic acid
NPX	Naproxen
CBZ	Carbamazepine
ISD	Isoniazid
CNB	2-chloro-4-nitrobenzoic acid
ETZ	Ethenzamide

SNP	Sinapic acid
DNB	2,4-dinitrobenzoic acid
ETH	Ethionamide
2,3HBA	2,3-dihydroxybenzoic acid
2,6HBA	2,6-dihydroxybenzoic acid
2,5HBA	2,5-dihydroxybenzoic acid
2,4HBA	2,4-dihydroxybenzoic acid
3HBA	3-hydroxybenzoic acid
SAL	Salicylic acid
OXA	Oxalic acid
FUM	Fumaric acid
SUA	Succinic acid
TTA	Tartaric acid
CRA	Crotonic acid
GAA	Gallic acid
2AP	2-Aminopyridine
4AP	4-Aminopyridine
DMAP	4-Dimethylaminopyridine
DAP	Dapsone
mL	Millilitre
mmol	Millimole
nm	Nanometer
WHO	World Health Organization
pKa	Acid dissociation constant

SYMBOLS AND UNITS

α	Alpha
cm	Centimeter
nm	Nanometer
°	Degree
Å	Angstrom
°C	Degree Celsius
∠	Angle
mg	Milligram
>	Greater than
Hz	Hertz
\bar{i}	Inverse
λ	Lamda
<	Less than
L	Litre
MHz	Megahertz
μ	Mu
ppm	Parts per million
θ	Theta
π	Pi
V	Volume
kJ	Kilo joule
N	Normal

CHAPTER 1

INTRODUCTION AND LITERATURE REVIEW

In this chapter, a brief introduction to Supramolecular chemistry, Crystal engineering, and the concepts of Pharmaceutical cocrystal and its advantages are discussed. In addition, a detailed literature review on pharmaceutical cocrystal, scope, and objectives of the current research work have been incorporated in the present chapter.

1.1 SUPRAMOLECULAR CHEMISTRY

Supramolecular chemistry or chemistry beyond the molecule is the study of the chemistry of intermolecular bond and it is based on the mutual recognition of molecules. Organic molecules recognize each other through a complex combination of geometrical and chemical factors and the complementary relationship between interacting molecules is characteristic of the recognition process. Molecules interact with each other through their dissimilarities rather than their similarities. It was stated by the noted chemist Pauling. The complementary relationship between shapes and chemical functionalities are thus important in the area of supramolecular chemistry.

In the year 1806, Humphry Davy isolated crystals of chlorine hydrate and identified it as a loose addition compound of chlorine and water. It was probably the first multi-component crystal that was specifically characterized and thus the origin of supramolecular chemistry has begun at least 200 years back. In the year 1948 H.M. Powell described clathrates of hydroquinone in terms of their network structures. The supramolecular hypothesis is formally said to have begun in the year 1896 by Emil Fischer on the work of enzyme functioning. Fischer related the working of an enzyme to the action of a 'key in a lock'. The enzyme (lock) needs a small molecule (key) to make it work (open the lock). Hence only a particular key can be used to open the particular lock. A lock without a key is of no use and vice versa. This principle is called as the lock-and-key principle as shown in the **Figure 1.1**.

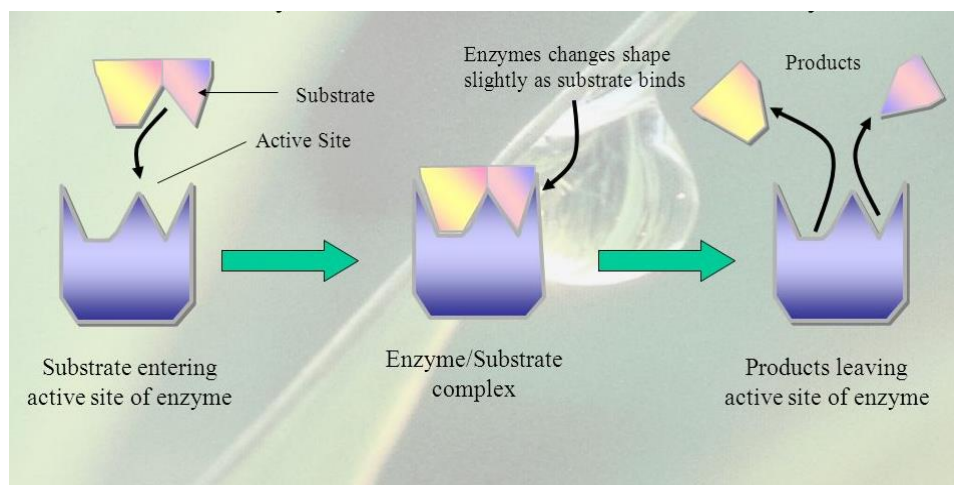


Figure 1.1: Lock and key model.

Supramolecular chemistry has been defined as ‘chemistry of molecular assemblies and of intermolecular bond’ by Jean-Marie Lehn and he received Nobel Prize for his work on supramolecular chemistry in the year 1987. Other definitions include the ‘chemistry of non-covalent’ and ‘non-molecular chemistry’. Originally supramolecular chemistry was defined in terms of the non-covalent interactions between a ‘host’ and a ‘guest’ molecule. J. D. Dunitz stated that a molecular crystal is the best example of a supramolecular entity. Accordingly, one can argue that crystal engineering, which is the design of crystalline solids is the supramolecular equivalent of organic synthesis. A polymorph can be taken as a supramolecular equivalent of a structural isomer, as supramolecular reaction involves crystallization. The table below gives the analogies between molecular and supramolecular chemistry (**Table 1.1**).

Table 1.1: Analogies between molecular and supramolecular chemistry.

Molecular chemistry	Supramolecular chemistry
Atom	Molecule
Covalent bond	Intermolecular bond
Molecule	Crystal
Synthesis	Crystal Engineering
Synthon	Supramolecular synthon
Isomer	Polymorph
Transition state	Nucleus
Reaction	Crystallization

Supramolecular chemistry extends beyond the field of atomic and molecular chemistry to afford highly complex and well defined supramolecular components. It emphasizes intermolecular interactions in the self-assembly of molecules governed by their geometrical and chemical factors. Intermolecular interactions include hydrogen bonding, π - π stacking, coordinative bonds, dipole-dipole interaction and van der Waals forces. These non-bonded interactions play a major role in the structure and function of biological systems such as protein folding and enzyme systems. A hydrogen bond is the most significant intermolecular interactions and is fundamental to the stability of double helix structure of DNA, which is the best-known self-assembly of supramolecular entity in nature. The table below (**Table 1.2**) is the strength of different non-covalent interactions in terms of kJ/mole.

Table 1.2: Strength of different non-covalent interactions.

Intermolecular interaction	Strength (kJ/mol)
Ion-ion	100-350
Ion-dipole	50-200
Hydrogen bond	4-120
Dipole-dipole	5-50
π - π stacking	<50
Van der Waals	<5

Supramolecular chemistry is one of the most vigorous and fast-growing fields of chemical endeavor in the last few decades. Its interdisciplinary nature has led to wide-ranging collaborations between physicists, theorists, computational modelers, crystallographers, inorganic and solid-state chemists, synthetic organic chemists, biochemists, and biologists.

1.2 CRYSTAL ENGINEERING

Crystal engineering can be defined as ‘the understanding of intermolecular interactions in the context of crystal packing and the utilization of such understanding in the design of new solids with desired physical and chemical properties’. This definition is now widely used was first given by Prof. Desiraju in his pioneering book on ‘Crystal Engineering’ (Desiraju et al. (2011)).

During the last three decades, the field of crystal engineering has attracted a varied group of scientists especially crystallographers and chemists. The concept of

crystal engineering was first introduced by Ray Pepinsky in the year 1955 and it was implemented by Gerhard M. J. Schmidt in the context of solid state photochemical reactions. He has clearly established the link between structure and reactivity in the solid-state structure for a series of photodimerizable alkenes. Consider an example of substituted *trans*-cinnamic acid (2+2) photocycloaddition reaction to cyclobutanes as shown in the figure (**Figure 1.2**). He found that crystal packing of the molecules within the crystal lattice provides an excellent spatial control on the initiation and progress of the solid-state organic reaction. Cinnamic acid does not undergo dimerization in a solution state, even if they do the overall conversion to dimer is low. In solid state reaction, conversion efficiencies are high and regioselectivities of the products are clear and decisive.

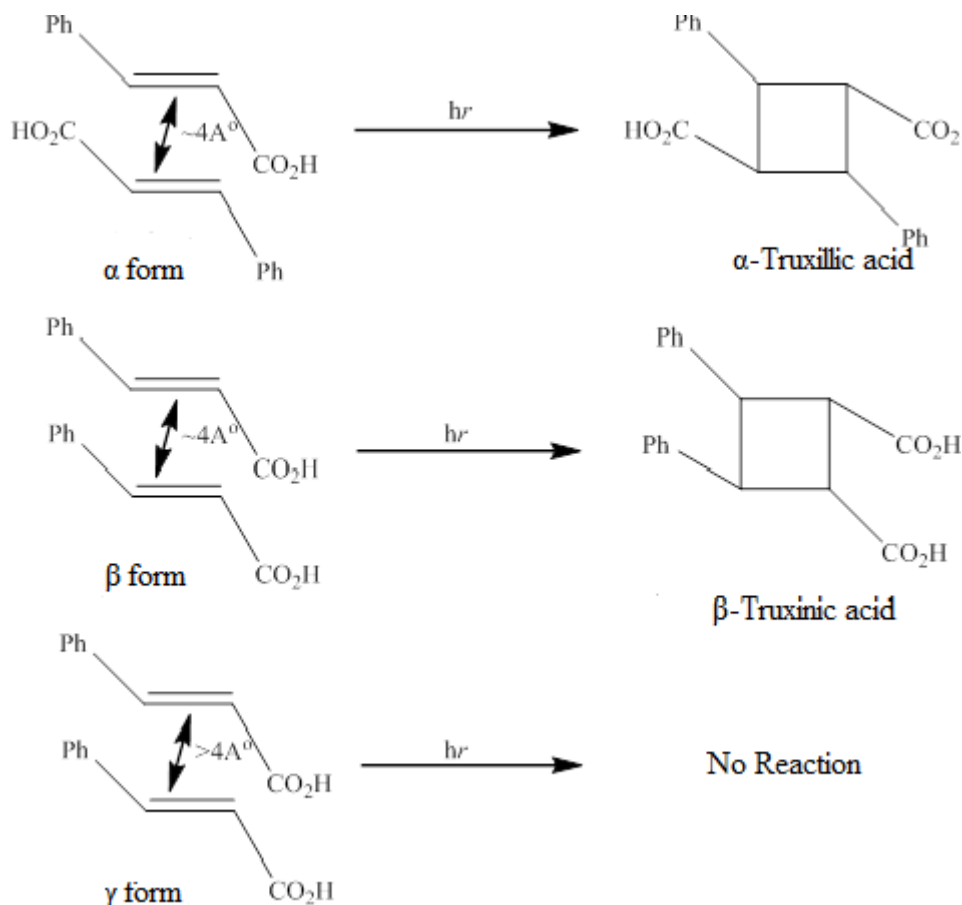


Figure 1.2: Photocycloaddition reaction of *Trans*-cinnamic acid.

Substituted cinnamic acid crystallizes in three forms namely α , β and γ forms. α and β forms react in a (2+2) manner to give cyclobutanes when irradiated in the solid state whereas γ form is photostable. Schmidt assumed that reactivity in the solid state takes place with a minimum of atomic and molecular movement, the topochemical

principle. Accordingly, the formation of mirror symmetry truxinic acid from β -cinnamic acid and the inversion symmetry truxillic acid from the α -cinnamic acid becomes intuitively obvious.

Schmidt's work revealed that physical and chemical properties of the crystalline material are dependent on the packing of the molecules within the crystal lattice. Thus, the ultimate aim of crystal engineering is to pre-design the solid-state components based on the knowledge of molecular structure. The field of crystal engineering has matured into an interdisciplinary scientific area with a wide range of applications in the area of, Drug design, Sol-Gel and inorganic polymers, Nanoparticles, Solid state chemical reactions, Monocrystalline thin films, Self-assembled thin films, Liquid crystals, Ionic liquids, Protein crystallization, Polymer chemistry, Co-ordination polymers, Photochromism, and Green chemistry applications.

Furthermore, the physicochemical properties that are associated with crystal engineered material can be exploited in many areas such as host-guest chemistry (Beatty, A.M (2003), organic semiconductor (Wurthner et al. (2006)), nonlinear optics (Lin et al. (2002)), Photographic materials (Hwang et al. (2003)), organo gels (Ghosh et al. (2005)) and solid-state organic chemistry (Zaworotko et al. (2007)).

1.2.1 Special role of hydrogen bond

Hydrogen bond is called as the master key interaction of molecular recognition and it is the most suitable toolkit for crystal engineer. It is having both strong and directional nature. As crystal engineering mainly concentrates on the non-bonded interactions, hydrogen bonding plays an important role in the design of new crystalline materials. George Jeffrey from the university of Pittsburg, USA has done a life time study of hydrogen bonding and classify them as a very strong, strong and weak hydrogen bonding according to the energy of interaction. Weaker hydrogen bonds play an important role in structure stabilization and it can be significant when large numbers are present. A typical example of hydrogen bonding is as shown below (**Figure 1.3**).

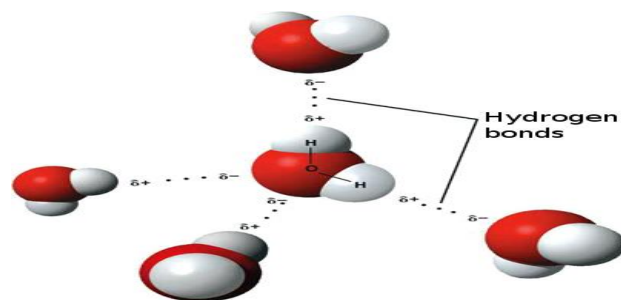


Figure 1.3: Hydrogen bonding in the water molecule.

A hydrogen bond can be represented as an interaction between a donor X-H and an acceptor Y-Z, the hydrogen bonding then represented as X-H \cdots Y-Z with three dots signifying the hydrogen bond. Where X and Y are electronegative non-metals like F, O and N. It was known that a small amount of covalent character exists in hydrogen bonding, due to the fact that a shifting of stretching frequency of the X-H bond to the lower frequency side was observed in the infrared spectrum. This bathochromic shift or the weakening of X-H bond can be taken as an indication of the covalent bond character in hydrogen bonding. Generally, it was observed that the hydrogen bond of the form X-H \cdots Y-Z, the distance between the elements X and Y are much shorter than their sum of the Van der Waals radii. The X-Y distance is referred as D and H to Y is taken as d. Hydrogen bonding is always tended towards linearity i.e., X-H \cdots Y bond angle tend towards 180°. However, this linear geometry is not always possible in crystal structures, as it's the result of a compromise between many intermolecular interactions of different strengths, bond angle and the distance dependence characteristics. Depending on the elements X and Y, various distance ranges were observed in hydrogen bonding as shown in the table (**Table 1.3**) with examples.

Very strong hydrogen bonding is formed between a strong acid and a good hydrogen bond acceptor as in the case of [HF₂]⁻, a strong hydrogen bond is formed between neutral donor molecules and neutral acceptor molecules via lone pairs. Strong hydrogen bonds do not have a linear geometry, they however found to be slightly bent. Weak hydrogen bonds are formed between unconventional donors and acceptors such as C-H groups, the π -systems of aromatic rings or alkynes or even transition metals and transition metal hydrides.

Table No 1.3: Hydrogen bonding distance of various X and Y elements.

Hydrogen bonds, X-H...Y-Z				
Strength	Examples	X-Y (D, Å)	H...Y (d, Å)	X-H...Y (θ°)
Very strong X-H~H...Y	[F-H-F] ⁻	2.2-2.5	1.2-1.5	175-180
Strong X-H<H...Y	O-H...O-H	2.6-3.0	1.6-2.2	145-180
	O-H...N-H	2.6-3.0	1.7-2.3	140-180
	N-H...O=C	2.8-3.0	1.8-2.3	150-180
	N-H...O-H	2.7-3.1	1.9-2.3	150-180
	N-H...N-H	2.8-3.1	2.0-2.5	135-180
Weak X-H<<H...Y	C-H...O	3.0-4.0	2.0-3.0	110-180

1.2.2 Supramolecular synthon

Prof. Gautam Desiraju in the year 1995 proposed the idea of supramolecular synthon, which plays a role similar to that played by Corey's synthon in organic synthesis. The pivotal idea was to define an organic crystal structure as a network. This network consists of nodes (molecules) and node connections (interactions). A simple example for a network like crystal structure is hydrogen cyanide (HCN). It consists of a linear sequence of HCN molecules linked with C-H...N≡C hydrogen bonds. Here the node is HCN molecules and the node connection is the H^{δ+}...N^{δ-} interaction. The C-H...N≡C hydrogen bond is called as supramolecular synthon and it may be dissected in the same way as a molecular synthon dissected in organic synthesis.

A supramolecular synthon was defined by Desiraju as "sub-structural unit in a molecular crystal that can be assembled with known or conceivable synthetic operations involving intermolecular interactions." The concept of supramolecular synthon was extended by Zaworotko into two distinct categories.

i. Supramolecular homosynthon

It is the result of intermolecular interactions between identical self-complementary functional groups such as carboxylic acid dimers and amide dimers as shown in the **Figure 1.4**.

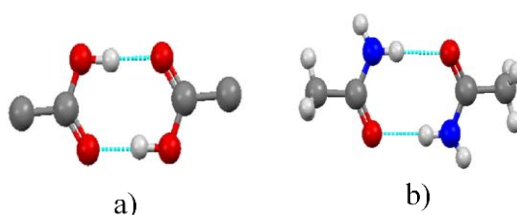


Figure 1.4: (a) Supramolecular acid-acid homosynthon (b) supramolecular amide-amide homosynthon.

ii. Supramolecular heterosynthon

It is the result of intermolecular interactions between two or more different but complementary functional groups such as carboxylic acid-amide and carboxylic acid-aromatic pyridine synthons as shown in the **Figure 1.5**.

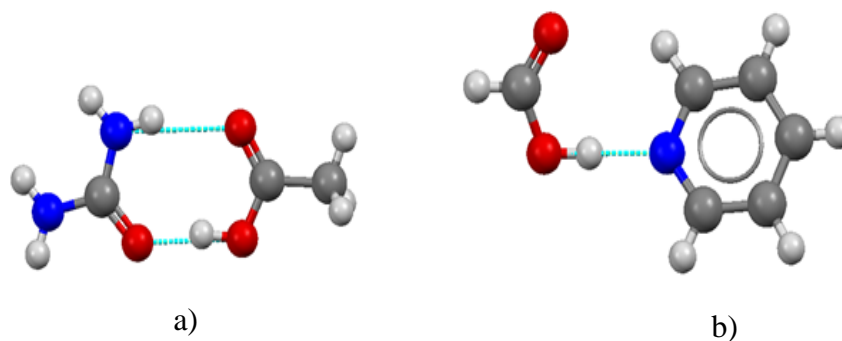


Figure 1.5: (a) Supramolecular amide-acid heterosynthon (b) supramolecular acid-pyridine heterosynthon.

The most commonly observed synthon consists of a few functional groups held together by strong and fairly directional interactions. Commonly observed synthons are shown in the **Figure 1.6**.

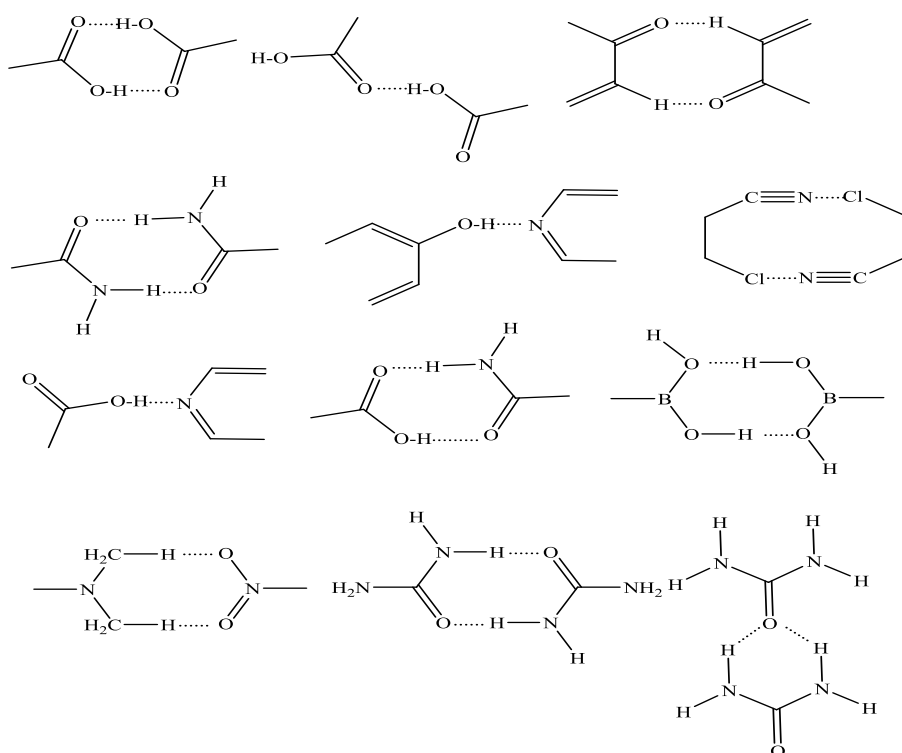


Figure 1.6: Commonly observed synthons in crystal engineering.

1.3 MOLECULAR ADDUCTS

A molecular adduct is defined as the product of direct addition of two or more different components, and the resulting single reaction products containing all the atoms of all the components added. The resultant product is considered as a distinct molecular species. Example include the formation of sodium percarbonate from hydrogen peroxide and sodium carbonate. Molecular adducts mainly classified into three different categories namely salt, cocrystal, and multi-component crystal.

1.3.1 Salt

Generally, salts are ionic compounds that are formed by the neutralization reaction between an acid and a base. It is composed of related numbers of cations (positively charged ions) and anions (negatively charged ions) so that the product is electrically neutral. These component ions can be inorganic (like chlorides and bromides) or organic (like acetate) and can be monoatomic (fluorides) and polyatomic (sulfates). In general, salt formation can be represented as,



The salt formation has been the primary aim to modify the physicochemical properties of an Active Pharmaceutical Ingredient (API). Approximately 50% of the drugs in the market is administered as salts. Its success and stability depend on the strength of acid or base and the acidity and basicity constant of the components involved. The general thumb rule for the formation of salt is that the acid ionization constant, pKa between acid and base should differ by at least two or three units. Salt formation of an API traditionally being used to improve the drug solubility and drug dissolution rates. Apart from this, the physical properties that can be altered by salt formation is,

- Melting point
- Thermal behavior
- Hygroscopicity
- Crystal habit
- Particle size
- Polymorphic behavior
- Stability and Purity

An example of the formation of pharmaceutical API salt is the formation of salbutamol sulfate (**Figure 1.7**). Salbutamol is a short-acting β_2 -adrenergic receptor agonist and has been used for the relief of bronchospasm in conditions such as asthma and chronic obstructive pulmonary disease since 1968 onwards.

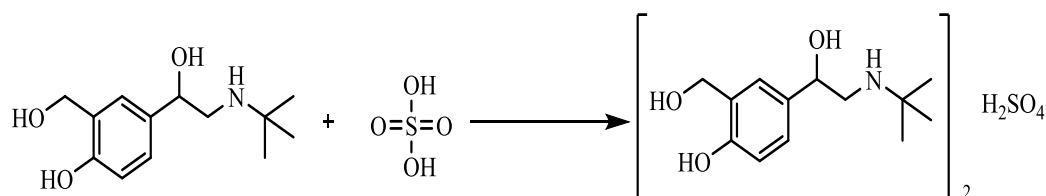


Figure 1.7: The formation of the pharmaceutical salt salbutamol Sulfate.

1.3.2 Cocrystal

The meaning of the term cocrystal has been debated in the crystallography field. A simple definition of cocrystal can be defined as,

- i. Compounds made from neutral molecules,
- ii. Constructed from reactants that are solids at ambient conditions,
- iii. Structurally homogenous crystalline materials that contain at least two different neutral building blocks with a well-defined stoichiometry.

In 1844 Friedrich Wohler reported first cocrystal ‘quinhydrone’, which is a cocrystal of quinone and hydroquinone. He found that the material was made up of a 1:1 molar combination of the components quinone and hydroquinone as shown in the figure below (**Figure 1.8**). Quinhydrone was analyzed by numerous research groups in next decades and synthesized several related cocrystals made from halogenated quinones. Many cocrystals were discovered in the late 1800 and throughout the 1900s, some were accidentally and others by screening methods.

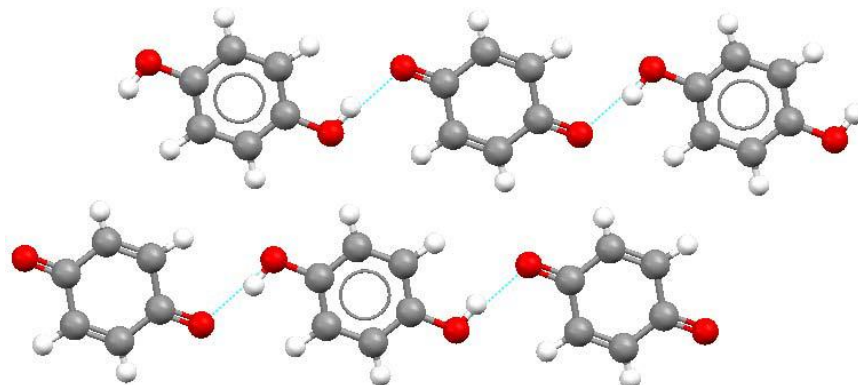


Figure 1.8: Cocrystal structure of quinhydrone (Cocrystal of quinone with hydroquinone).

In cocrystal, the components interact via non-bonded interactions such as hydrogen bonding, ionic interactions, Van der Waals interactions, and π -interactions. The cocrystal that is formed via intermolecular interactions can exhibit different physical and chemical properties that of properties of individual constituents. Properties include melting point, solubility, chemical stability and mechanical properties.

The major difference between salt and cocrystal is that in salt, there will be a transfer of protons whereas in cocrystal there is no proton transfer. The general rule for the formation of salt or cocrystal is based on ΔpK_a (pK_a (base)- pK_a (acid)) values of the constituent components. If the ΔpK_a value is less than -1, then there will be a negligible proton transfer and the resulting compound will be a cocrystal. If the ΔpK_a value greater than four, there will be a complete proton transfer and the resulting compound will be a salt (Sekhon B.S. (2009)). If the ΔpK_a value lies between -1 and 4, then there is a possibility of forming either salt or cocrystal. The figure below shows the distinction between the various solid forms of API (**Figure 1.9**).

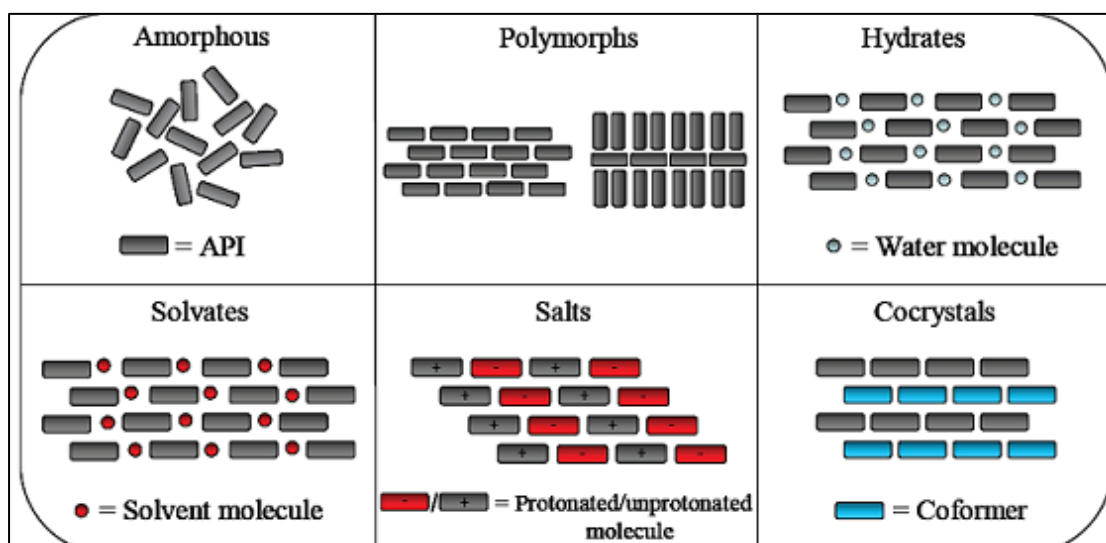


Figure 1.9: Comparison of different solid forms.

Cocrystal engineering is useful in the production of energetic materials, pharmaceuticals, and other materials. Off these, the most widely used and studied application is in the field of drug development. In the last few decades, research in the field of cocrystal has been enhancing mainly due to the application in the field of pharmaceutical industry. Changing the physical properties of API by cocrystal

formation can greatly influence the solubility and bioavailability of the drug. The principle idea for the preparation of cocrystal is to develop superior physicochemical properties of the API without changing the bioactivity of the molecules.

Prof. Desiraju and Dunitz had a debate for the term cocrystal and co-crystal. Desiraju considers co-crystal to be scientifically suspect whereas Dunitz notes that it is not perfect and it is irrevocably established. Later both of them agreed that cocrystal without a hyphen is undesirable. Subsequent to this Aakeröy and Salmon in *CrystEngComm* highlight posed a question ‘what is a co-crystal’? With characteristic features that are suitable for classifying these types of compounds. Amongst the vast set of multicomponent crystals, their overview considers only those that are “made from reactants that are solids at ambient conditions.” They also included a footnote that “one could make a case for including materials such as those prepared by co-condensation at reduced temperatures or elevated pressure”. In the same review, they also stated that there exists a need for distinguishing multi-component crystalline materials that are comprised of two or more solids versus those composed of one or more solids and a liquid.

1.3.3 Multi-component crystal

Crystals that contain more than one component (solid or liquid) in the crystal lattice is termed as multicomponent crystals (Desiraju et al. (2011)). It is impossible to classify and nomenclature for all multi-component crystal by a single specific system. There is no much difference between a multi-component crystal and a single component crystal at a fundamental level. The law that governs for the crystal packing for both single component and multi-component are same. However, there is some difference, the most important is the crystal growth formation. Since in multicomponent crystal, two distinct multi-components are involved, so one has to consider the relative solubilities, relative vapor pressure, and their intrinsic chemical nature.

Classification of multi-component crystals have varied from time to time, the term host-guest compound has used for over decades. Other terms include clathrate, intercalate and inclusion compound. In clathrate, host completely encapsulates the guest and in intercalate, the guest is sandwiched by the host in layers. Whereas, in the case of some inclusion compounds, the guest is located in a one-dimensional channel in host structure. In some type of guest–host compounds, guest can be removed to leave

the empty space for another guest molecule without disturbing the host structure. In other host-guest compounds, the removal of guest will completely collapse the host framework. These type of host networks actively require the guest presence and it is referred as guest induced host network (template effect). One of the best examples for the host-guest compound is crown ethers (eg. 18-crown-6) as shown in the **Figure 1.10**.

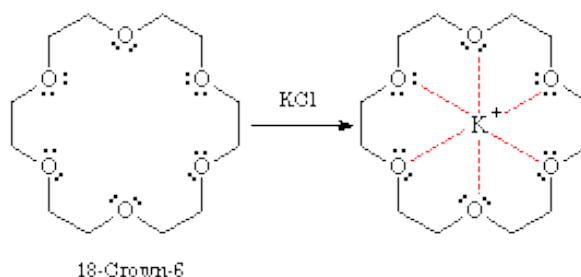


Figure 1.10: An example of the host-guest system.

Solid solutions are also considered as multi-component crystals and were first used by Kitaigorodskii as mixed crystals. However, this term is not in use today as the term molecular complexes arose in the 1960s and referred for molecular complexes in solutions. This term was popular for donor-acceptor (charge transfer) complexes between electron rich and electron poor complexes. Solvates and hydrates are also considered as multi-component crystals, wherein these cases there will be a presence of solvent or water molecules in the crystal lattice along with the solute molecules. Polar solvents like water are stabilized always in the crystal structure through directional interactions. The phenomenon of solvation or hydration is associated with polymorphism and is having industrial importance since the properties of many drugs and dyestuff are dependent on the properties whether or not solvent is included in the crystal lattice. The Cambridge Structural Database (CSD) contains at least 5000 molecules which include water in the crystal lattice. Methanol is the second most commonly found solvents in the crystal structure (Desiraju et al (2011)).

1.4 POLYMORPHISM

Polymorphism is the phenomenon wherein same chemical compound exist in different crystal structures or forms. These different crystal structures or forms are called as polymorphs. Polymorphism is therefore exclusively a solid-state phenomenon. Polymorphism is observed in all crystalline compounds including

molecular and non-molecular, organic, inorganic, organometallic and coordination complexes. In 1820, E. Mitscherlich was the first to recognize the polymorphism in sodium arsenate phosphate. Later in 1832, Friedrich Wohler and Justus Liebig discovered polymorphism in organic material benzamide (Brew et al. (2007)). Polymorphs have different crystal structures, thus all types of diffraction techniques of single crystal and powders are of great importance in identifying this phenomenon. Polymorphs in resorcinol were the first example of organic solids which were characterized by crystal structure determinations (Druzicki et al. (2005)).

Since polymorphs have different crystal structures, it is likely that they are having different morphologies. Some examples that find application in daily life are indigo, cocoa butter, sorbitol, lead tetraethyl and copper phthalocyanine. Polymorphism plays an important role in the pharmaceutical industry as the different crystal morphologies can affect processing properties like filtering, drying, flow, tableting, rate of dissolution, shelf life and bioavailability. Hence the process of crystallization and the crystal morphologies of the drug are of much importance in pharmaceutical industry. Polymorphs are classified as,

- i. Conformational polymorphs
- ii. Tautomeric polymorphs
- iii. Concomitant polymorphs
- iv. Disappearing polymorphs
- v. Pseudo polymorphs

1.4.1 Factors affecting the formation of polymorph

There are many factors that are responsible for the development of polymorphic forms. Various conditions such as,

- Solvent effects (The packing of the crystal may be different in polar and nonpolar solvents).
- Certain impurities inhibiting growth pattern and favor the growth of metastable polymorphs.
- The level of supersaturation from which material is crystallized (In which generally the higher the concentration above the solubility, the more likelihood of metastable formation).

- The temperature at which crystallization is carried out.
- The geometry of covalent bonds (Differences leading to conformational polymorphism).
- Change in stirring conditions.

1.4.2 Challenges to pharmaceutical industry

As the different polymorphs of a drug substance exhibit different physical properties including solubility, bioavailability, filtering, drying etc. it is important for a pharmaceutical industry to prepare and control the polymorphism in drug molecule. A significant number of molecules in the marketed drug exhibits polymorphism mainly because of two factors,

- i) Structural: As the drug molecule contains different functional groups that are capable of forming hydrogen bonds and are flexible. This combination of functional groups that contains rotatable bonds, which can also accept or donate hydrogen bonds can lead to different orientations in the crystal structures. Functional groups include OH, NH₂, NHCOCH₃, COOCH₃, and NHCH₃.
- ii) Thermodynamic: Due to high demand for yield and production rates, pharmaceutical industries forces crystallization to operate far from equilibrium. Under these conditions, there is a possibility to form polymorphs.

There are few examples from the pharmaceutical industry for the existence of polymorphs,

1) Ranitidine

It is a blockbuster anti-ulcer drug, developed by Glaxo and marketed in the form of hydrochloride of the free base under the brand name Zantac. The first patent was issued in the year 1977 for the drug. During the scale-up work, it was observed that a sample was obtained that is having different diffraction pattern from the other. Glaxo concluded that they got the new polymorphic form and they called it as form II. The material which was obtained in the first patent called as form I. In 1985 Glaxo filed a patent for form II also. Structure of ranitidine is shown in **Figure 1.11**.

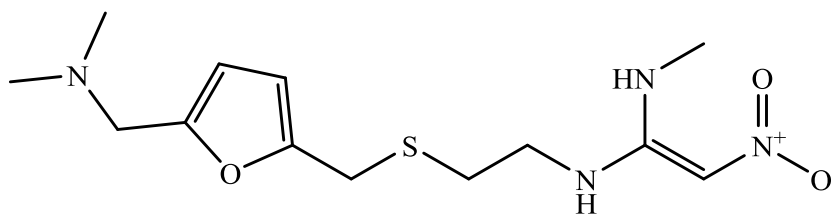


Figure 1.11: Structure of ranitidine.

As the patent on form I expected to expire by 1995 many generic companies prepared to go on the market with form I. One of the generic company Novopharm had a long intense legal battle with Glaxo, as they claimed that the first patent filed by Glaxo was inevitably produced form II instead of form I. Therefore, Novopharm claimed that the first patent was invalid and they sought to market form II. Glaxo successfully defended its patents and they proved that form I could indeed be prepared by the procedures given in the first patent. Novopharm lost to Glaxo in the first round of litigation. Later in 1994, Novopharm developed a method for the preparation of form I which are free from form II and sought to market the same. Now Glaxo sued against Novopharm claimed that Novopharm's form I contains form II which was again protected. However, Novopharm showed that their sample did not contain any detectable amount of form II. The court was stated that if the Novopharm's form I contains little of form II, then it can be treated as an impurity, and allowed to market the mixtures of form I and form II.

2) Ritonavir

It is an anti-HIV drug introduced in 1996 and sold by Abbot Laboratories under the trade name of Norvir (**Figure 1.12**). Originally it was dispensed as an ordinary capsule which did not require any refrigeration. It was not known that the drug was marketed the kinetic form of the drug molecule. The crystal description of the form was in the monoclinic system and it was referred as form I. In the year 1998 a second form was discovered as a result of the observation that several batches started failing for dissolution specification. Evaluation of the failed products suggested that the second form had precipitated from the formulation. It was a conformational and thermodynamically stable form.

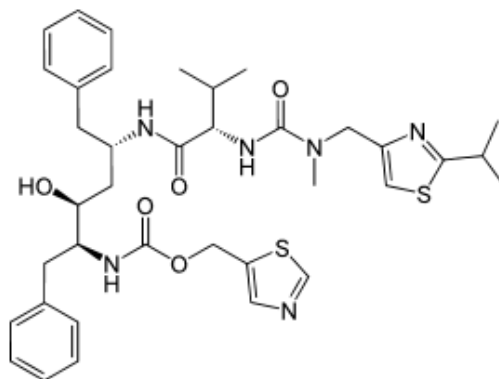


Figure 1.12: Structure of Ritonavir.

There are additional two factors that pertained to form II and it completely upset the production of a marketable form of the drug. The first factor was that the lower energy form II caused the therapeutically effective higher energy form I to convert to lower energy polymorph on contact. The second factor was that form II was pharmaceutically inactive as it was less soluble (~50%) than the kinetic form (form I). later Abbot was forced to remove the oral capsule from the market and it had serious implications for the marketed product and also for the patients taking the drug. After a substantial effort, Abbot was able to reproduce the kinetic form at considerable cost. They developed a new method for the formulation and launched the product as refrigerated filled gel capsules. The new formulation was very expensive than the original product.

These examples reveal the importance of polymorphs in pharmaceutical industries. Generic drug companies have been aware of the importance of crystal engineering activities in drug development in order to overcome the intellectual property (IP) issue related to polymorph and drug product.

1.5 PHARMACEUTICAL COCRYSTAL

Cocrystals are of special importance in the pharmaceutical industry in recent years due to their improved physicochemical properties of the drug substance. Pharmaceutical cocrystals have some advantageous property when compared with the original molecule in formulation stage when compared with the drugs of solvates or hydrates. This is because the number of acceptable solvents are limited, solvents tend

to be volatile and susceptible to desolvation leads to amorphization which may be undesirable.

Pharmaceutical cocrystal is defined as “Single-crystalline solids that incorporate two neutral molecules, one being a drug molecule and the other a cocrystal former (Sekhon B. S. (2009)).” A cocrystal former may be an excipient or neutral compounds that are listed from Generally Recognized As Safe (GRAS) compounds or another drug molecule. Pharmaceutical cocrystal offers potential improvement in solubility, dissolution rate, bioavailability, and physical stability of the drug molecules. Also, it helps to improve flowability, chemical stability, compressibility and hygroscopicity of drugs. Pharmaceutical cocrystal allows one to ease the patent liability unlike in the case of polymorphs. Three main criteria for patentability are novelty, non-obviousness, and utility. All three criteria satisfy pharmaceutical cocrystal. A Recent review on pharmaceutical cocrystal suggests that US food and drug administration (FDA) and European Medicines Agency (EMA) has approved a cocrystal hydrate of disodium valsartan and monosodium sacubitril developed by Novartis pharmaceuticals used in the treatment of chronic heart failures. Other drug-drug cocrystals with enhanced physicochemical properties which are under late stage development are a non-steroidal anti-inflammatory (NSAID) drug celecoxib and an opioid drug tramadol and a cocrystal of diabetic drug ertugliflozin with 5-oxo-proline.

Generally, there are two main approaches to synthesize a pharmaceutical cocrystal. The first approach is based on the retrosynthetic strategy and by identifying complementary hydrogen bonding sites in both API and coformer. For example, an anti-epileptic drug carbamazepine (**Figure 1.13**) phases many challenges in oral administration due to its low aqueous solubility and bioavailability. The molecule contains an amide functional group and the crystal structure of the drug contains amide-amide homosynthon. The retrosynthetic possibility suggests that the molecule contains an amide functional group and thus two possibilities are possible. One is amide-acid hetero synthon preparation and the second one retains the amide homosynthon but utilizes other hydrogen bond donor and acceptor sites in the drug molecule. These strategies enable carbamazepine to form a number of cocrystal with benzoic acid, acetic acid, formic acid, aspirin, succinic acid, saccharin, 4-aminobenzoic acid etc. with

superior dissolution properties, suspension stability and pharmacokinetics compared to the parent drug (Childs et al. (2008)).

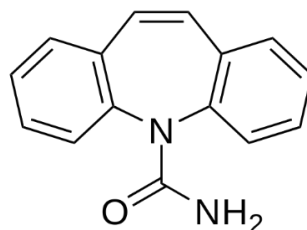


Figure 1.13: Structure of carbamazepine.

The second approach is based on the high throughput crystallization method. Solution based crystallization is preferred but the disadvantage is that poor efficiency and more time-consuming. The mechanochemical method provides an alternate path to prepare the cocrystal. A combination of the two approaches may be advantageous in cocrystal screening experiments.

1.5.1 Properties of pharmaceutical cocrystal

Success or failure of pharmaceutical formulation depends on its performance. There are many examples of pharmaceutical cocrystal which are having better solubility or stability compared to the pure drugs. Main properties of pharmaceutical cocrystals are as follows,

i. Melting point: It was observed that most of the pharmaceutical cocrystals (>50%) have their melting point intermediate to coformer and API (Walsh et al. (2003)). Higher the melting point of pharmaceutical cocrystal compared to API and coformer may lead to lower aqueous solubility and bioavailability compared to pure API (Schultheiss et al. (2009)).

ii. Stability: It is a heavily studied parameter for a pharmaceutical drug molecule during the development stage. Physical and chemical stability studies commonly studied at accelerated conditions to determine developability and shelf life. Water uptake is the major problem in handling and packaging point of view as this can lead to different forms. In pharmaceutical cocrystal or salt, solution stability is the most important one as the dissociation of material leads to the precipitation of less soluble parent compound or form. The major stability studies include,

- a) Relative humidity stress
- b) Thermal stress

c) Chemical stability

d) Solution stability

For example, caffeine is susceptible to hydration with change in humidity. Pharmaceutical cocrystal of caffeine with oxalic acid showed stability towards humidity for several weeks (Jones et al. (2005)).

iii. Solubility: One of the main aim to synthesize pharmaceutical cocrystal is to increase the solubility of a poorly soluble drugs. Cocrystallization can be performed either for free acid or free base and their salts to alter their solubility. Cocrystals of caffeine with glucuronic acid and norfloxacin with isonicotinamide showed higher solubility than pure drugs (Velaga et al. (2006)). Further, cocrystal formation exhibits decrease in the solubility of drug molecule as well (Zhang et al. (2009)).

iv. Intrinsic dissolution: Intrinsic dissolution is the measure of rate of dissolution without the effect of particle size. This is done by pressing a pellet or disk in dissolution medium. Concentration of the solution is measured over a period of time to check the solubility of drug molecule. For example, Cocrystals of Fluoxetine HCl with various acids are screened and it is observed that Fluoxetine HCl/succinic acid cocrystal showed 3-fold higher solubility than the pure drug (Childs et al. (2004)).

v. Bioavailability: It is the measure of rate and extent of active drug molecule that reaches systemic circulation. Only a limited number of bioavailability study have been reported with cocrystal. A 1:1 cocrystal of AMG 517/Sorbic acid showed increase in bioavailability compared to the pure drug (Schultheiss et al. (2009)). Even though the number of reports are limited for pharmaceutical cocrystal on bioavailability, it can greatly influence the bioavailability as the cocrystal formation can increase the solubility of drug molecule.

vi. Purification of APIs: APIs or intermediates can be purified by cocrystal formation. It is an alternate method for the purification of drugs or intermediates.

vii. Racemic resolution of APIs: Pharmaceutical cocrystallization can be employed for the purification of racemic mixture. Research has been carried on the racemic resolution of Naproxen, a non-steroidal anti-inflammatory drug (NSAID). It was observed that pure S-naproxen was observed from RS-naproxen by cocrystallization with bipyridine and piperazine (Manoj et al. (2014)).

1.5.2 Synthesis of pharmaceutical cocrystal

Traditional approach to do crystallization was by solvent evaporation, cooling or by anti-solvent addition. Even these methods can employ for the production of pharmaceutical cocrystal. The different methods to synthesize a pharmaceutical cocrystal are as follows,

i. Solution method

Solution method is one of the traditional methods for crystallization. Crystallization occurs from the solution with a proper supersaturation degree. The supersaturation can be achieved by different methods such as cooling, evaporation, the addition of a solvent that lowers the solubility of components. Among this, the solvent evaporation method is a most popular way of preparing pharmaceutical cocrystals. (Sekhon, B.S. 2012).

a) Solvent evaporation method

Two or more molecules in the stoichiometric ratio are dissolved in a single solvent or a mixture of solvents (inert) and left for slow evaporation. It can be done either under an atmospheric condition or under an inert atmosphere. It is considered as the best method if cofomers exhibit comparable degrees of solubility in the crystallizing solvent. The solution method is of great importance due to most of the cocrystals which qualify for single X-ray diffraction testing can only be prepared through this method. Limitation of slow evaporation method relates to issues with scale-up and use of the large volume of solvent.

b) Anti-solvent crystallization

This process is used for the cocrystallization of highly soluble substance. In this method, a solvent is added to the solution containing API and cofomer normally at the ambient condition to decrease the solubility of the desired substance. The solvent chosen should be inert so that it won't interact with desired substance or form a solvate (Desiraju, G. R. 2011)

ii. Melt crystallization (crystallization via melting and cooling)

This method is suitable for the cocrystallization of solids which shows comparatively low solubility. The cocrystal is achieved by the simple melting of two cocrystal formers together followed by cooling. The challenge includes in the melt

crystallization is the stability of solids on heating. The cofomers should not decompose on heating (Desiraju, G. R. 2011).

iii. Mechanochemical methods

a) Neat grinding method

Phase transformation from the physical mixture to cocrystal is obtained by grinding of the stoichiometric amount of API and cofomer in a pestle and mortar or ball mill. Heat generated during grinding can induce local melting at the interface between different reactant that causes the nucleation of a new phase. The main drawback of this method is that it is difficult to get a single crystal with good quality.

b) Solvent drop grinding method (Liquid Assisted Grinding Method)

Solvent drop grinding or Liquid Assisted Grinding (LAG) is one of the superior methods to produce cocrystal. In this method, cocrystal formers are ground together manually in the presence of catalytic amount of solvent, which enhances the cocrystallization process and enables the formation of cocrystals. It is an efficient method of screening for cocrystal hydrates. The LAG method has advantages over dry grinding method such as increased yield, ability to control polymorph production, better product crystallinity. It is highly cost-effective, efficient, green and reliable approach for the cocrystal synthesis.

iv. Supercritical fluid atomization technique

Different supercritical fluid techniques are used to produce cocrystal by taking advantage of different properties of the supercritical fluid (solvent, anti-solvent, or atomization enhancement). The supercritical atomization process is mainly based on the solubilization of controlled quantities of supercritical CO₂ in a liquid solution containing API and cofomer and subsequent atomization of the mixture through a nozzle thin wall. This method is helpful to synthesize amorphous as well as crystalline materials. The particle size of the materials can be controlled by careful selection of liquid solvent, processing temperature, nozzle diameter and concentration of the solution. It allows a single-step generation of cocrystal that is difficult or even impossible to obtain by traditional technique. Issues with scale up, low purity yield are limitations of supercritical fluid atomization method (Sekhon, B.S. 2012). Theophylline-saccharine cocrystal with 1:2 stoichiometry was obtained by supercritical

fluid enhanced atomization processes which was not previously reported by any other classical screening methods. (Sekhon, B.S. 2012).

1.5.3 Characterization of pharmaceutical cocrystal

Cocrystal can be characterized in a number of ways. Single crystal X-ray diffraction method (SC-XRD) is most commonly used method for the structural characterization. Powder diffraction method (PXRD) also can be used to characterize cocrystals, as each material gives its own distinct characteristic peaks. Solid state Nuclear Magnetic Resonance Spectroscopy (NMR) technique is recently introduced for the characterization of cocrystal. Here the advantage is that we can able to differentiate chiral and racemic cocrystals of similar structure. Other spectroscopic methods include Fourier Transform Infrared Spectroscopy (FT-IR) and Raman spectroscopy, by comparing the spectra of cocrystal with individual molecules. Another characterization method includes melting point apparatus, Differential Scanning Calorimetry (DSC), Polarized Optical microscope (POM) and Thermogravimetric Analysis (TGA) for the physical property studies.

1.5.4 Pharmaceutical cocrystal as intellectual properties

Compared to other classes of solid forms, cocrystals have particular scientific and regulatory advantages and alongside these advantages are intellectual property issues which confer cocrystal with unique opportunities and challenges. The protection of intellectual property of invented drug form is important to obtain patentability during the commercialization of the drug. There is a large number of acceptable cofomers are available and hence cocrystal can offer broad patent space. Therefore, it has great importance in the pharma industry. The investigation of cocrystal is important in a developing area of research in which scientific advances can afford legal advances. Patent help to promote good research for society's benefit and avoid others from practicing the invention of one inventor that contributes to commercial advantage. A number of areas have to be considered when patenting a pharmaceutical product such as the composition of matter (molecular structure, solid form or formulation), method of use (medical indication) and manufacturing process (chemical synthetic route). In order to obtain a patent coverage, the invented drug should satisfy three important criteria: novelty, utility, and non-obviousness.

i. Novelty

Cocrystal formation is a unique tool which enables the solid-state modification of API. The possibility to achieve distinct solid-state structures through cocrystallization satisfies the novelty requirement for patentability. It is clear that the cocrystals which have not been described before should satisfy the novelty requirement for patentability. The important investigation is that the product is apparently safe and acceptable for human ingestion. In that sense, the cocrystal is superior over salt due to the limited number of acceptable counter ions.

ii. Utility

The utility of an invention includes useful process, machine manufacture or any useful improvement. The cocrystal should possess useful therapeutic utility as parent API and it is worth enough to a patent if it possesses superior therapeutic utility over parent API. Cocrystal offers enhanced solubility and dissolution rate which influence the bioavailability of the drug molecule, and further, cocrystal offers physical and chemical stability to the API. These properties are superior for cocrystal over parent API. In addition to this, cocrystal shows potential improvement in properties like compressibility, hygroscopicity, and flowability etc.

iii. Non-obviousness

Obviousness can be analogized to the scientific notion of predictability. A cocrystal is a unique crystalline material with unpredictable structure and property. Numerous works are ongoing to predict the possible crystal structure from its molecular structure using advanced computational methods, but still, the prediction of actual crystal structure that forms in the laboratory is a challenging area of ongoing research. The prediction of cocrystal structure found a greater challenge, it includes (1) determining whether a given sets of molecular components will undergo crystallization, (2) identifying primary intermolecular interactions that will exist within the particular cocrystal structure, (3) envisioning the overall packing arrangement in the resulting cocrystal structure. The presence of multiple molecules in the crystal lattice and numerous stoichiometric possibilities make the task more complicated. Due to the challenges in predicting cocrystal structure and properties, the synthesis of cocrystal still follow trial-and-error method and it remains as a non-obvious form in a generally patentable perspective.

1.6 BIOPHARMACEUTICAL CLASSIFICATION SYSTEM (BCS)

It was primarily developed in the context of immediate release solid oral dosage forms. BCS is a scientific framework for classifying APIs based on their aqueous solubility and intestinal permeability. This system has been adopted worldwide by regulatory authorities as a means to establish technical standards for waiving bioavailability and bioequivalence testing requirements for oral drugs. According to BCS classification (**Figure 1.14**), drug substances are classified into four categories based on their solubility and permeability. (1) High permeability and high solubility (2) Low solubility and high permeability (3) High solubility and low permeability (4) Low solubility and low permeability. A drug substance is considered to be highly soluble if the highest dose strength is soluble in ≤ 250 ml of water over a pH range 1-7.5 and highly permeable when the extent of absorption is $\geq 90\%$ of the administered dose.

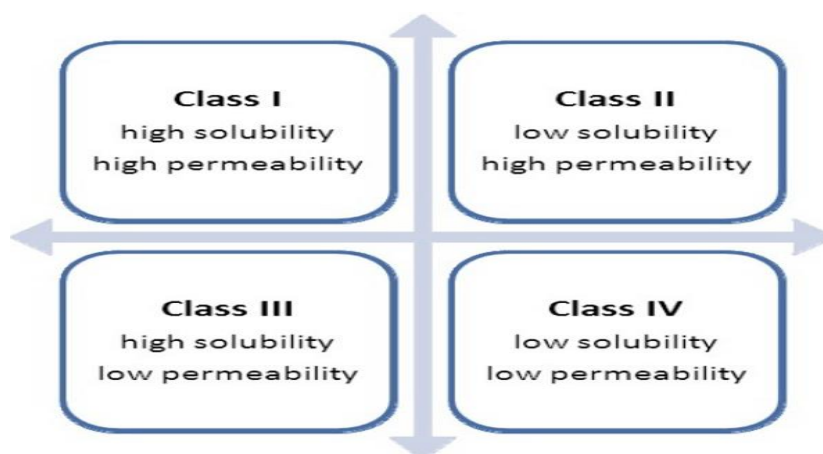


Figure 1.14: BCS Classification.

1.7 CAMBRIDGE STRUCTURAL DATABASE (CSD)

The Cambridge Structural Database (CSD) was established by the Cambridge Crystallographic Data Centre (CCDC), is a depository of X-ray and neutron data on organic and organometallic crystals. It was started in the year 1965 with only less than 2000 entries, today CSD comprises of over half million crystal structures making it a comprehensive and highly curated scientific resource for crystal engineering. Chemists and crystallographers have convenient access to a large amount of crystallographic data and structural information with the use of CSD.

The CSD may also be used to study interaction patterns other than individual intermolecular interactions. The CSD help chemists to fast visualization of crystal

structures and analysis of experimentally determined crystallographic data to further understand the behavior of molecules and the intermolecular forces within a crystal. It is also used to trace similarities between the directionality and interaction patterns of various hydrogen bonds and secondary bonds, namely p-block elements of heavy metal atoms and chloride ions. This knowledge is fundamental to crystal engineering as it gives information about intermolecular interactions, geometrical preferences, directionality and the type of supramolecular synthons involved. The figure below shows the growing number of entries to CSD in recent years (**Figure 1.15**).

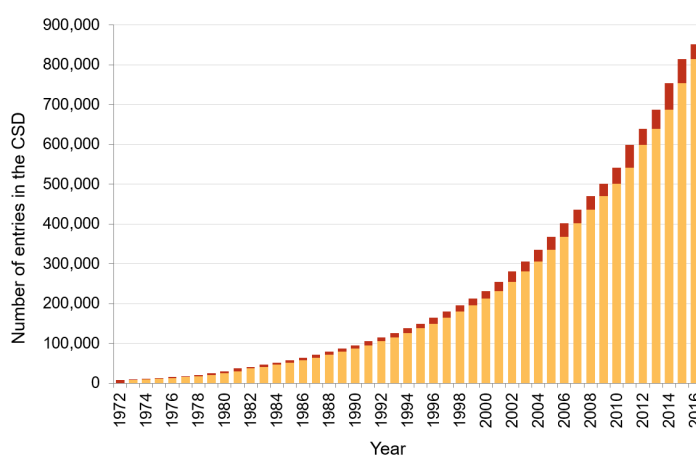


Figure 1.15: Number of entries to the CSD in recent years.

1.8 LITERATURE REVIEW

Pharmaceutical cocrystal can be prepared by crystal engineering approach based on the pKa value of the drug substance and the coformer used. There is a numerous number of cocrystals are reported yearly by various research groups with GRAS and non-GRAS substances as a coformer molecule. Few of the reported pharmaceutical cocrystals of various drug molecules are briefly explained below.

a) Carbamazepine

Carbamazepine (CBZ) is a medication used primarily in the treatment of epilepsy and neuropathic pain. It is not effective for absence seizures or myoclonic seizures. It may be used in schizophrenia along with other medications and as a second line agent in bipolar disorder. A controlled release formulation is available for which there is tentative evidence showing fewer side effects. Carbamazepine was discovered in 1953 by Swiss chemist Walter Schindler. It was first marketed in 1962 and is

currently available as a generic medication and is not very expensive. It is on the WHO Model List of Essential Medicines, the most important medications needed in a basic health system. Four polymorphs of carbamazepine are reported in the literature. CBZ drug falls under BCS Class II drug due to low aqueous solubility and high permeability. A large number of cocrystals of CBZ are found in the literature with various GRAS molecules.

Fleischman et al. (2003) synthesized solvates and cocrystal of carbamazepine with acetone, dimethyl sulfoxide, benzoquinone, terephthalaldehyde, saccharin, nicotinamide, formic acid, acetic acid, butyric acid, trimesic acid, 5-nitroisophthalic acid, adamantane-1,3,5,7-tetra carboxylic acid and formamide (**Figure 1.16**). Childs et al. (2008) reported 27 cocrystals with various carboxylic acid cofomers and they obtained higher solubility and stability compared to the pure drug. A drug-drug cocrystal of CBZ: indomethacin (1:1) is reported by Majumder et al. (2011) by milling method. Arora et al. (2011) synthesized cocrystal of CBZ: nicotinamide by water-mediated crystallization (which is released from the dehydration of dibasic calcium phosphate dihydrate) in intact tablets (**Figure 1.17**). They monitored the cocrystallization by powder X-ray diffractometer. They also studied the cocrystallization with aspirin as cofomer and found that water-mediated crystallization leads to the hydrolysis of aspirin and a new cocrystal CBZ: Salicylic acid is obtained instead of CBZ: Aspirin cocrystal.

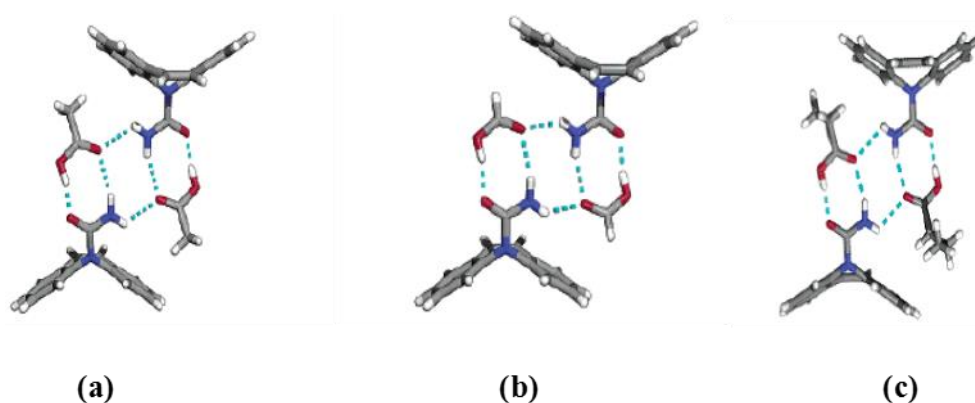


Figure 1.16: Solvates of carbamazepine with (a) acetic acid, (b) formic acid and (c) butyric acid.

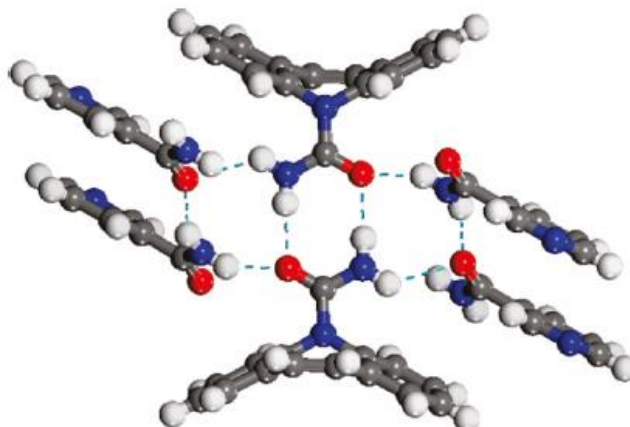


Figure 1.17: CBZ: Nicotinamide cocrystal (1:1).

Alhalaweh et al. (2012) prepared a cocrystal with saccharin as coformer and showed enhanced solubility (2-10 times) and impart pH sensitivity different from that of pure drug. A cocrystal polymorph of carbamazepine/malonic acid was reported by Limwikrant et al. (2012). They have used a vibrational rod mill for the production of new polymorph, where the known form was produced by a ball mill. Rahim et al. (2013) reported the synthesis of cocrystal of CBZ with various coformers like terephthalaldehyde, nicotinamide, trimesic acid, 5-nitro isophthalic acid, salicylic acid, adipic acid, fumaric acid, succinic acid, maleic acid, L-malic acid, malonic acid, glutaric acid, 4-amino benzoic acid, aspirin, 2,6 pyridine dicarboxylic acid and saccharin by employing various cocrystallization techniques like solvent evaporation, liquid-assisted grinding and dry grinding techniques. They have studied the cocrystallization with stoichiometric and non-stoichiometric ratios and found that 85% success rate achieved for non-stoichiometric ratios whereas only 61% success rate is observed for stoichiometric ratio by various methods.

Moradiya et al. (2014) synthesized carbamazepine/trans-cinnamic acid cocrystal by melt extrusion method and they obtained faster dissolution rate compared to bulk carbamazepine and the prototype cocrystal. Li and Matzger (2016) reported cocrystal of carbamazepine with different molar ratios of 4-aminobenzoic acid. However, in their study, no correlation of dissolution rate is observed with stoichiometry of cocrystals. Drozd et al. (2017) reported drug-drug cocrystal of carbamazepine with p-aminosalicylic acid with varying molar ratios and they achieved cocrystal, cocrystal hydrate and cocrystal solvate in their study.

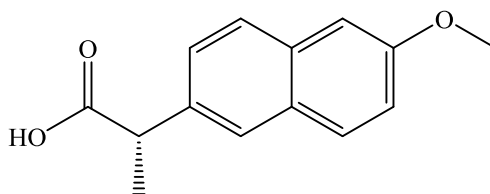
b) Naproxen

Figure 1.18: Structure of Naproxen.

Naproxen (NPX) usually sold as the sodium salt 'naproxen sodium,' is a non-steroidal anti-inflammatory drug (NSAID) of the propionic acid class (same class as ibuprofen) and is commonly used for the reduction of pain, fever, inflammation, and stiffness caused by conditions including migraine, osteoarthritis, kidney stones, rheumatoid arthritis, psoriatic arthritis, gout, ankylosing spondylitis, menstrual cramps, tendinitis, and bursitis, among others. It is also used for the treatment of primary dysmenorrhea. It is the preferred NSAID for long-term use in people with a high risk of cardiovascular (for example, heart attacks or strokes) complications, due to its relatively low risk of causing such complications. NPX has an intermediate risk of causing stomach ulcers as compared with ibuprofen, which is low risk, and indomethacin, which is of high risk. In order to reduce the risk of stomach ulceration, it is often combined with a proton-pump inhibitor (a medication that reduces the production of stomach acid) during long-term treatment, in those with pre-existing stomach ulcers, or a history of developing stomach ulcers while on NSAIDs. Four pseudo polymorphs and four hydrated polymorphs of naproxen are reported in the literature.

The cocrystal of NPX with pyridine carboxamide isomers (nicotinamide, isonicotinamide, and picolinamide) was synthesized by Castro et al. (2011) by cofler contact method and mechanochemistry (**Figure 1.19**). In all the three cocrystals, supramolecular acid-aromatic pyridine heterosynthon was observed regardless of the position of ring nitrogen.

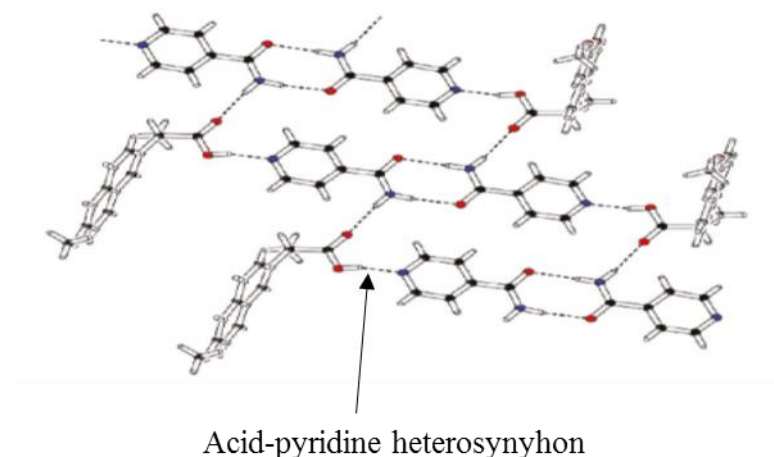


Figure 1.19: Supramolecular acid-pyridine heterosynthon observed in naproxen/isonicotinamide cocrystal.

A specific 2:1 cocrystal of NPX with nicotinamide was studied by Ando et al. (2011) and they found that the cocrystal showed faster dissolution and less water adsorption properties. Tilborg et al. (2013) synthesized naproxen cocrystal with zwitterionic coformer proline by liquid assisted grinding method. They synthesized cocrystal of S-naproxen with D and L-proline and RS-naproxen with D and L-proline hydrates. Manoj et al. (2014) synthesized cocrystal of racemic and specific S-NPX with bipyridine and piperazine as coformer. They also studied the preferential enrichment of s-NPX from racemic NPX. Efficient enrichment is not observed due to the lower solubility of enantiomers compared to the racemic mixture. Tumanova et al. (2014) synthesized cocrystal of S-NPX with a series of essential and nonessential amino acids (zwitterionic co-former) like L-alanine, D-alanine, D-tyrosine (**Figure 1.20**) and D-tryptophan monohydrate. All the synthesized cocrystal showed same structural motifs i.e. amino acids forms strong charge-assisted hydrogen bonding with S-NPX molecule. Kerr et al. (2017) evaluate the physicochemical properties of naproxen-picolinamide cocrystal, and they found that the intrinsic dissolution rate of NPX in the cocrystal was similar to that of NPX parent molecule.

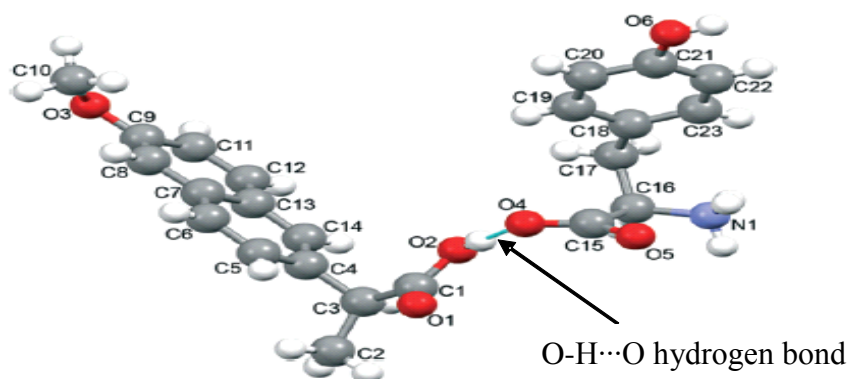


Figure 1.20: Asymmetric unit in S-NPX/D-tyrosine cocrystal.

c) **Isoniazid**

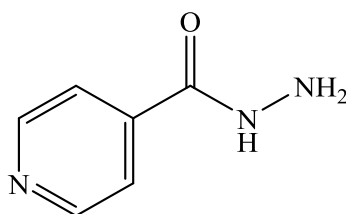


Figure 1.21: Structure of Isoniazid.

Isoniazid (ISD) is the first-line medication for prevention and treatment of tuberculosis. The compound was first synthesized in the early 20th century, but its activity against tuberculosis was first reported in the early 1950s. Isoniazid is available in tablet, syrup, and injectable forms (given intramuscularly or intravenously). It is available worldwide, is inexpensive, and is generally well tolerated. It is on the World Health Organization's List of Essential Medicines, a list of medicines that constitute the bare minimum for a basic health system.

Grobelny et al. (2011) synthesized ISD cocrystal with 4-aminosalicylic acid by the solvent drop grinding approach. Single crystal XRD revealed that simultaneous existence of pure hydrogen bonded and partially ionic character acid...nitrogen base dimer in the cocrystal (**Figure 1.22**). Lemmerer (2011) synthesized cocrystals of ISD with 2-hydroxybenzoic acid, succinic acid, 4-hydroxybenzoic acid and 2-chloro-4-nitrobenzoic acid as coformers. In all the cocrystals synthesized, he observed carboxylic acid...pyridine hetero synthon in the cocrystal structure. Ravikumar et al. (2013) synthesized ISD/p-coumaric acid cocrystal by slow evaporation method. Sarcevic et al. (2013) synthesized cocrystals with acid derivatives like benzoic acid, sebacic acid,

suberic acid and cinnamic acid as cofomers. They also observed polymorphism in ISD/suberic acid and ISD/cinnamic acid cocrystals. The solubility of the synthesized cocrystal showed that solubility increases with increase in solubility of carboxylic acids. Swapna et al. (2014) synthesized cocrystals of ISD with various GRAS cofomers like vanillic acid, ferulic acid, caffeic acid and resorcinol in order to enhance the physicochemical properties of ISD. All the cocrystals showed better stability towards accelerated humid conditions (40 °C, 70% RH) except ISD/resorcinol cocrystal. They have also studied the polymorphism in all the synthesized cocrystals.

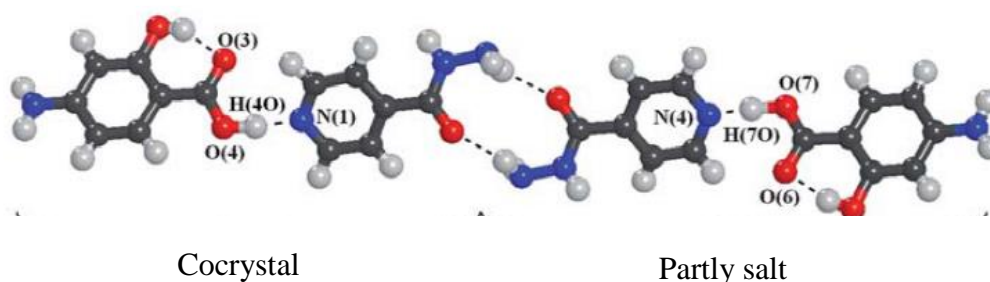


Figure 1.22: Cocrystal of ISD/4-aminosalicylic acid with the partly ionic bond.

Kaur et al. (2014) synthesized cocrystal of ISD with gallic acid as cofomer. They observed that cocrystal of ISD/gallic acid displays single crystal-to-single crystal transformation up on dehydration. Sarcevic et al. (2015) synthesized cocrystal of ISD with benzoic acid as cofomer. Mashhadi et al. (2014) synthesized cocrystals of ISD with hydroxybenzoic acid as cofomers (gallic acid, 2,3-dihydroxybenzoic acid, 3,5-dihydroxybenzoic acid and 3-hydroxybenzoic acid). Acid-pyridine hetero synthon is observed in all the cases except ISD/2,5-dihydroxybenzoic acid where hydroxyl-pyridine hetero synthon is observed. Sarcevic et al. (2016) studied the effect of chain length of dicarboxylic acid on the cocrystallization with ISD by vapochemical, mechanochemical, and thermal methods. Oruganti et al. (2016) studied the hierarchies of hydrogen bond in salt/cocrystals of ISD and its Schiff base. De Melo et al. (2016) synthesized pharmaceutically acceptable salts of ISD with HBr, H₂SO₄, and HNO₃. Mashhadi et al. (2016) reported cocrystal of ISD with 3,4-dihydroxybenzoic acid. Drozd et al. (2017) reported drug-drug cocrystal of ISD with p-aminosalicylic acid and performed solubility studies. Diniz et al. (2017) reported cocrystals of ISD with p-nitrobenzoic acid, p-cyanobenzoic acid, and p-aminobenzoic acid.

d) Dapsone

Dapsone (DAP) is an antibiotic commonly used in combination with rifampicin and clofazimine for the treatment of leprosy. It is a second-line medication for the treatment and prevention of *Pneumocystis pneumonia* and for the prevention of toxoplasmosis in those who have a poor immune function. Additionally, it has been used for acne as well as other skin conditions. DAP is available both topically and by mouth. It is on the World Health Organization's List of Essential Medicines, the most important medications needed in a basic health system. The oral form is available as a generic drug and not very expensive. DAP fall under BCS Class II drug due to poor aqueous solubility.

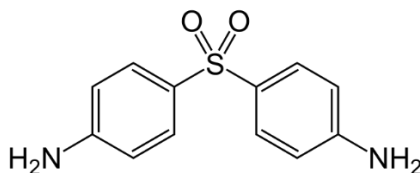


Figure 1.23: Structure of Dapsone.

Martins et al. (2013) synthesized two cocrystals of DAP with ϵ -caprolactam and 4, 4'-bipyridine by traditional crystallization techniques. In both the cases, $N_{NH_2}\cdots O_{SO_2}$ interactions are observed. Smith and Wermuth (2012) synthesized cocrystal of DAP with 1, 3, 5-trinitro benzene coformer. The cocrystal is formed through $-N-H\cdots O$ hydrogen bond associated with nitro O-atom acceptors.

Lemmer et al. (2012) synthesized three solvates of DAP such as dichloromethane, 1,4-dioxane, and tetrahydrofuran by solution crystallization method in respective solvents. Smith and Wermuth (2012) synthesized cocrystals of DPA with 3, 5-dinitrobenzoic acid as coformer. Six drug-drug cocrystals of DAP was reported by Jiang et al. (2014) with caffeine (1:1 and 1:2 ratio), flavone, luteolin, 2(3H)-benzothiazolone and sulfanilamide as coformer. They have also studied the equilibrium solubility of synthesized cocrystal and compared the results with parent drug. Further, He et al. (2016) studied the polymorphism of DAP/flavone cocrystal, which resulted in trimorphic forms of 1:1 dapsone/flavone cocrystal (**Figure 1.24**).

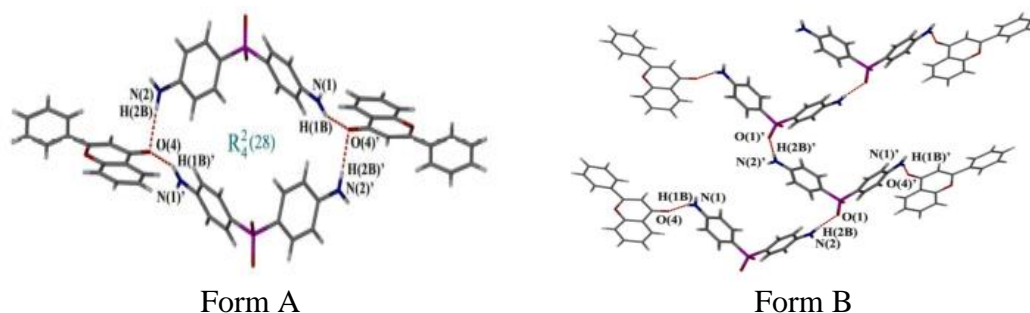


Figure 1.24: Polymorphic forms of dapstone/ flavone cocrystal.

e) **Fluorouracil**

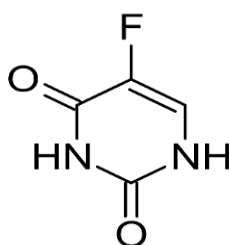


Figure 1.25: Structure of Fluorouracil.

Fluorouracil is a pyrimidine derivative drug which is used in the treatment of cancer. It is a suicide inhibitor and works through irreversible inhibition of thymidylate synthase. It belongs to antimetabolites family of drugs. It is on the World Health Organization's List of Essential Medicines, a list of the most important medications needed in a basic health system. Two polymorphs of Fluorouracil is reported in the literature.

Delori et al. (2013) synthesized three cocrystals of fluorouracil with acridine, phenazine and 4, 4-bispyridylethene as cofomer. Li et al. (2014) synthesized a 1:1 cocrystal of fluorouracil with 4-hydroxybenzoic acid as cofomer. They have studied polymorphism in the above-mentioned cocrystal and they found two new crystal forms of fluorouracil/4-hydroxybenzoic acid cocrystal (**Figure 1.26**). Dain et al. (2016) synthesized three cocrystals of fluorouracil with GRAS molecules such as 3-hydroxybenzoic acid, 4-aminobenzoic acid, and cinnamic acid. They have studied the permeability of these cocrystals and compared the results with fluorouracil. Increase in permeability was observed for all the cocrystals studied when compared to the fluorouracil as such in their study. Mohana et al. (2017) studied the supramolecular interactions in fluorouracil/5-bromothiophene-2-carboxylic acid and fluorouracil/

thiophene-2-carboxylic acid. In the same year, they have reported the hydrogen bond patterns in fluorouracil/4-methyl benzoic acid and fluorouracil/3-nitrobenzoic acid cocrystals.

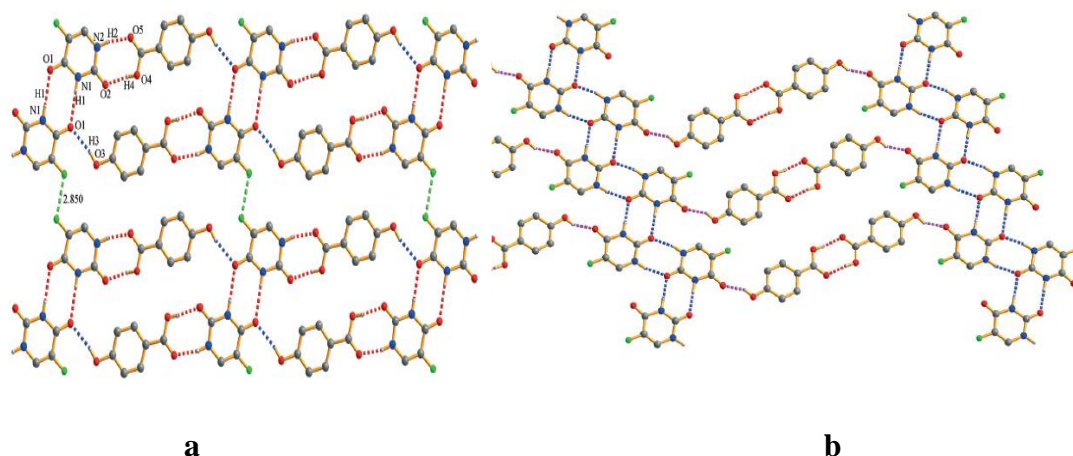


Figure 1.26: Two polymorphic forms of fluorouracil/4-hydroxybenzoic acid cocrystal (a and b).

f) Ethenzamide

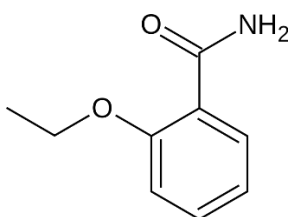


Figure 1.27: Structure of Ethenzamide.

Ethenzamide is an analgesic and anti-inflammatory drug that is used for the relief of fever, headaches, and other minor aches and pains. It is a common ingredient in numerous cold medications and many prescription analgesics.

Aitipamula et al. (2009) reported a trimorph of a pharmaceutical drug-drug cocrystal of ethenzamide with gentisic acid (**Figure 1.28**) and they found that the metastable polymorph formed is found to be converting to stable polymorph upon grinding. This was the first example of a trimorphic form of a cocrystal that contains two active molecules. In the same year, he has reported another polymorphic cocrystal of ethenzamide/saccharin cocrystal.

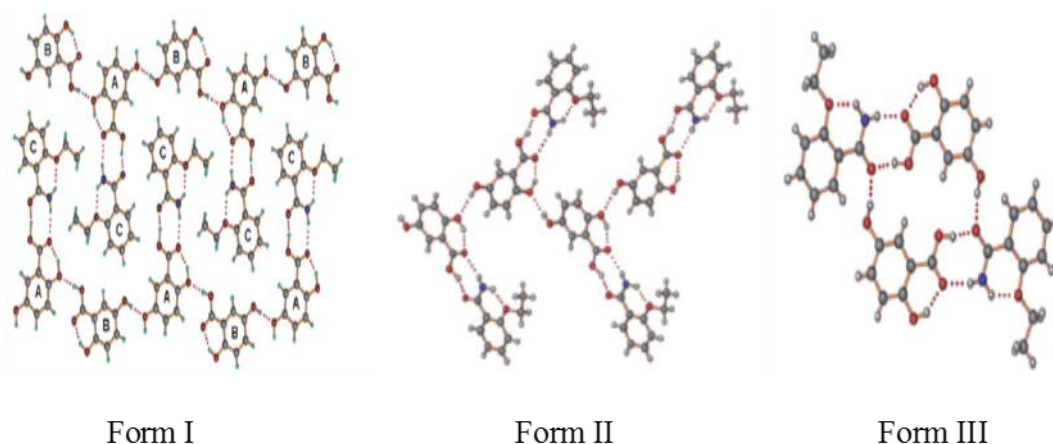


Figure 1.28: Trimorphic forms of ethenzamide/gentic acid cocrystal.

In the year 2010 Aitipamula et al. reported two polymorphic forms of a cocrystal ethenzamide/ethyl malonic acid. Cocrystal analysis suggests that ethenzamide molecule adopt different conformation but a common hydrogen bonding motif are observed. In the same year, he has reported a cocrystal of ethenzamide with 3,5-dinitrobenzoic acid with two polymorphic forms.

In the year 2012, Aitipamula et al. has reported six cocrystals of ethenzamide with salicylic acid, 2-chloro-4-nitrobenzoic acid, vanillic acid, 4-aminobenzoic acid, 4-hydroxybenzoic acid and fumaric acid. Solubility and dissolution study suggests that all the cocrystals were having faster dissolution rate and their equilibrium solubility is higher than the parent ethenzamide. Przybylek et al. (2016) reported cocrystals of ethenzamide with various benzoic acid derivatives and they studied the effect of substituent group on cocrystallization. Hariprasad et al. (2016) reported cocrystals of ethenzamide with gallic acid, nitrobenzoic acid isomers, and 3-toluic acid. Solubility study of ethenzamide/gallic acid cocrystal suggested the two-fold increment in the solubility of ethenzamide in the cocrystal when compared to ethenzamide as such. Sarmah et al. (2017) reported cocrystals of ethenzamide with hydroxybenzoic acid derivatives and studied the solubility of ethenzamide in ethenzamide cocrystals.

1.9 SCOPE AND OBJECTIVES OF PRESENT WORK

Pharmaceutical cocrystallization offers a considerable influence on the solid-state properties of a drug substance, particularly its stability, solubility, and bioavailability. Numerous research on pharmaceutical cocrystal proves that properties

like crystal habit, bulk density, solubility, compressibility, friability, melting point, hygroscopy, and dissolution rate of a drug substance can be improved without affecting the biological activity of the drug substance. Apart from this, pharmaceutical cocrystallization is an alternate way to purify a drug substance or drug intermediate with a GRAS or non-GRAS substances. Research showed that racemic resolution of a drug substance or intermediate can be achieved by pharmaceutical cocrystallization. Pharmaceutical cocrystallization/salt formation based on the ΔpK_a value of poorly water-soluble drug substance which comes under biopharmaceutical classification system, BCS class II or class IV can be of great importance in order to improve the performance of these classes of drug molecules. Further, cocrystallization technique can be employed for the drug molecules which does not have any ionization site in the molecular structure. This is one of the major advantages of cocrystallization technique. The formation of salt/cocrystal is generally guided by a thumb rule i.e., if the difference in the pKa value (pKa base-pKa acid), (ΔpK_a) < -1 , then there will not be any proton transfer, the resultant component will be a cocrystal. If the $\Delta pK_a > 4$, there will be a complete proton transfer results in the formation of molecular salts. If the value of ΔpK_a lies in between -1 to 4 then the prediction of proton transfer is ambiguous. The resultant product may be a salt or cocrystal. Like salt of two different APIs, cocrystals of two drug molecules with improved physicochemical properties can also be prepared by cocrystallization approach. Furthermore, Polymorphism of a drug molecule can be controlled by the application of cocrystallization and these are liable for patentability.

Based on the above scope and thorough literature survey, following objectives were proposed for the present research work,

- i. Selection APIs with poor/high aqueous solubility and permeability.
- ii. Selection of cofomer/salt former for a particular API based on the pKa values and also based on the presence of complementary functional groups.
- iii. Salt/cocrystal screening experiment by following any of the cocrystal synthesis methods.
- iv. Identifying the salt/cocrystal formation in the initial stages preferably by determining melting point.

- v. Characterization of synthesized salt/cocrystal by DSC, POM, TGA, FT-IR, ¹H NMR, UV-Vis, PXRD and SC-XRD techniques.
- vi. Comparison of synthesized salt/cocrystal structures with respect to crystal packing, crystal density, and the interactions involved in the crystal structures.
- vii. Evaluation of physicochemical properties such as solubility, hygroscopicity and long-term stability associated with synthesized salt/cocrystal.

To summarize, the thesis work on pharmaceutical cocrystal/salt covers five working chapters, which include design and synthesis of pharmaceutical cocrystals/salts of various drug molecules with GRAS and non-GRAS molecules followed by the evaluation of physicochemical properties such as stability and solubility associated with the synthesized cocrystal/salt. **Chapter 2** of the thesis work discusses pharmaceutical cocrystals of anti-inflammatory drugs (flufenamic acid and ethenzamide) and anti-viral drug (2-chloro-4-nitrobenzoic acid). The chapter confers a detailed structural, solubility and stability study of the synthesized cocrystal and compared the results with parent APIs. **Chapter 3** of the thesis work talks about the pharmaceutical salts of BCS Class II drug ethionamide with GRAS and non-GRAS compounds. Here again, the structural characterization, solubility, and stability of the synthesized salts were evaluated and compared the results with parent ETH. The two salts namely, ETH-CNB and ETH-2,3HBA in the work offer for the development of drug-drug salts with ETH molecule. **Chapter 4** describes the molecular salts of common anti-inflammatory drugs mefenamic acid, tolfenamic acid, and naproxen with aminopyridine derivatives. The detailed structural study and structural comparison based on SC-XRD analysis and stability study (including long-term and hygroscopicity) of drug-drug salts of these APIs with 4AP are reviewed in the work. **Chapter 5** of the thesis work discusses the cocrystal/salt of tranexamic acid, an anti-fibrinolytic hemostatic drug. Here, the benzoic and carboxylic acid derivatives were chosen for the salt/cocrystal screening. Eleven cocrystals/salt of TXA is reported in the work and all the crystal structures were determined by SC-XRD techniques. Further, Structural comparison and the stability study at room temperature is evaluated. Furthermore, DFT calculation was employed to support the crystal structures determined from SC-XRD analysis. **Chapter 6** describes the cocrystal/salt of anti-

fungal drug flucytosine with pharmaceutically acceptable coformers. A detailed structural study, a structural comparison based on SC-XRD analysis, and hygroscopicity study at accelerated humidity conditions are incorporated in the chapter. Towards the end of the thesis, **Chapter 7** describes the overall outcome of the entire research work carried out on pharmaceutical cocrystal/salt.

CHAPTER 2

***DESIGN, SYNTHESIS, CHARACTERIZATION, AND
EVALUATION OF PHYSICOCHEMICAL PROPERTIES
OF COCRYSTAL OF ANTI-INFLAMMATORY AND ANTI-
VIRAL DRUGS***

This chapter describes the design and synthesis of pharmaceutical cocrystals of flufenamic acid, ethebamide, and 2-chloro-4-nitrobenzoic acid drug molecules. The chapter discusses the detailed structural characterization followed by a study of physicochemical properties associated with the synthesized cocrystals.

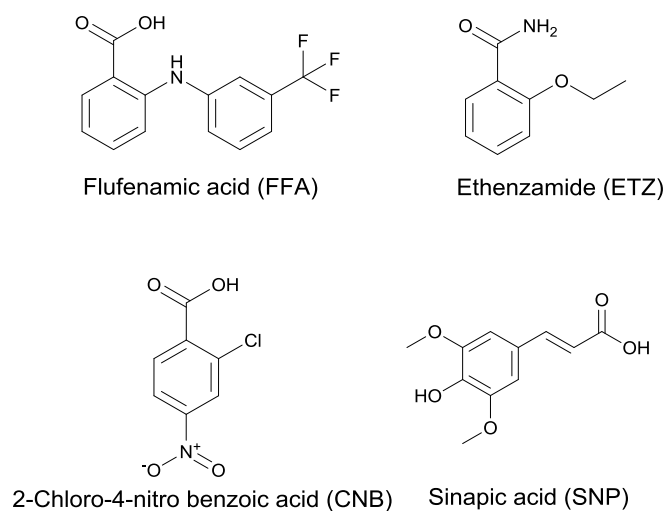
2.1 INTRODUCTION

Flufenamic acid (FFA) is an anthranilic acid derivative with analgesic, anti-inflammatory, and antipyretic properties. FFA along with meclofenamic acid are widely used drug for the treatment of lower back pain and are administered orally and topically. FFA belongs to biopharmaceutical classification system (BCS) Class II drug because of its low aqueous solubility (9.09 mg L^{-1}) and high permeability ($\log p=5.25$). Research has been carried out to increase the solubility of FFA drug by numerous techniques like amorphization using the inorganic carrier and forming a dispersion with polyvinyl pyrrolidone. FFA exists in nine polymorphic forms, out of which only form I and form III are commercially available. The report says that FFA displays an acute (oral) potency 16 times that of aspirin, 12 times that of aminopyrine, 3.2 times that of mefenamic acid, and 1.6 times that of phenylbutazone. Due to these harmful side effects, and weak benefits compared to other NSAIDs, the use of FFA in medicine remained somewhat limited. Ethebamide (ETZ) is a non-steroidal anti-inflammatory drug (NSAID) largely used as combination drug along with aspirin, dipyrone, allyl isopropyl acetyl urea, caffeine and ibuprofen for the treatment of mild to moderate pain. The main drawback of ETZ drug is the lower solubility and bioavailability which makes it a superior challenge to enhance its solubility behavior through cocrystallization. 2-chloro-4-nitrobenzoic acid (CNB) used as a novel potential therapy for the immunodeficiency diseases such as an anti-viral and anti-cancer agent. It exists as dimorphs in the solid state. CNB drug is recently released for administration in tablet or injectable solution form for the treatment of immunodeficiency diseases and HIV infections.

Pharmaceutical cocrystals of FFA, ETZ, and CNB have been reported recently with GRAS and non-GRAS molecules. The reported cocrystals of FFA include nicotinamide, theophylline, 2-pyridone and 4, 4'-bipyridine. The remarkable increment in the solubility of FFA was observed in FFA-nicotinamide and FFA-

theophylline cocrystal. In all the reported cocrystal robust supramolecular acid-pyridine heterosynthon was observed. A 1:1 cocrystal of ETZ and thiourea have been reported in the literature. Aitipamula et al. synthesized various polymorphic cocrystals of ethenzamide with saccharin, gentisic acid, ethylmalonic acid and 3, 5-dinitro benzoic acid. They also synthesized pharmaceutical cocrystals with salicylic acid, 2-chloro-4-nitrobenzoic acid, vanillic acid, 4-aminobenzoic acid, 4-hydroxybenzoic acid and fumaric acid with enhanced solubility and dissolution rate. Przybylek et al. synthesized cocrystals of ethenzamide with benzoic acid, 2-fluoro benzoic acid, 2-iodo benzoic acid, salicylic acid, 2,4-dihydroxybenzoic acid, 2,5-dihydroxybenzoic acid, 2,6-dihydroxybenzoic acid, 3,4-dihydroxybenzoic acid and 3,5-dihydroxybenzoic acid. Several cocrystals and salts of CNB drug molecule are reported in the literature with various amide and pyridine derivatives. Further, few solvates of CNB are also reported in the literature.

In continuation of research on the development of new crystal forms of FFA, ETZ, and CNB with improved physical properties, cocrystallization experiment has been carried out and resulted in two drug-drug cocrystals of FFA with ETZ and CNB and a cocrystal of ETZ and CNB with sinapic acid (SNP). The cocrystal of FFA with SNP is not obtained in the crystallization process. Molecular diagrams of APIs and the cofomers are shown in **Scheme 2.1**. SNP used as a cofomer is a nutraceutical compound, a member of hydroxycinnamic acid family which occurs as a free acid and in the form of an ester. It is found more commonly in the human diet as it is prevalent in many fruits, medicinal plants, oilseed crops, vegetables, and cereals. SNP and its derivatives exhibit a bundle of biological functions such as anti-inflammatory, antioxidant, anti-anxiety and anti-carcinogenic activities which are beneficial to human health. It also exhibits an antimicrobial activity which is vital for food preservation. Thus, it has gained considerable interest in food, cosmetic and pharmaceutical industries. In the present chapter, structural characterization, and physicochemical properties of the synthesized cocrystals such as solubility and stability (hygroscopicity and long-term stability) are evaluated and compared the result with the parent APIs.



Scheme 2.1: Molecular diagram of APIs and the cofomers.

2.2 EXPERIMENTAL SECTION

2.2.1 Material and methods

Flufenamic acid, 2-chloro-4-nitrobenzoic acid, and sinapic acid were purchased from Sigma-Aldrich were used as such without any further purification. Ethenzamide was purchased from Alfa Aesar. Analytical grade solvents were used for all the cocrystallization experiments. Purified distilled water is used for the solubility study.

2.2.2 Solvent evaporation method for cocrystallization

Pure cocrystals were synthesized by solvent evaporation method at room temperature. Experiments were performed with various solvents ranging from most polar to non-polar solvents.

FFA-CNB Cocrystal: FFA (100 mg, 0.355 mmol) and CNB (71.55 mg, 0.355 mmol) were taken in equimolar ratio and dissolved in 10 mL ethyl acetate solvent at room temperature and left for slow evaporation at ambient conditions. Flake shaped orange-colored crystals were obtained after 7 days with 1:1 stoichiometry in the cocrystal. Other solvents like methanol, ethanol, dichloromethane, acetonitrile, acetone, chloroform and tetrahydrofuran did not yield cocrystal.

FFA-ETZ Cocrystal: FFA (100 mg, 0.355 mmol) and ETZ (58.64 mg, 0.355 mmol) were taken in equimolar ratio and dissolved in 10 mL ethanol solvent at 60 °C and left for slow evaporation at ambient conditions. Flake shaped colorless crystals were

obtained after 4 days with 1:1 stoichiometry in the cocrystal. Other solvents like methanol, isopropanol/water yielded cocrystal with 1:1 stoichiometry.

ETZ-SNP Cocrystal: ETZ (100 mg, 0.6054 mmol) and SNP (135.73 mg, 0.6054 mmol) were taken in equimolar ratio and dissolved in 10 mL of ethanol solvent at 80 °C and left for slow evaporation at ambient conditions. Block-shaped orange-colored crystals were obtained after 5 days with 1:1 stoichiometry in the cocrystal. The cocrystal was obtained in methanol solvent as well.

CNB-SNP Cocrystal: The equimolar ratio of CNB (100 mg, 0.4961 mmol) and SNP (111.24 mg, 0.49610mmol) was dissolved in 10 mL of ethanol solvent at 80 °C and left for slow evaporation at ambient conditions. Flake shaped orange-colored crystals were obtained after 5 days with 1:1 stoichiometry in the cocrystal. The cocrystal was obtained in methanol solvent as well.

2.2.3 Solvent drop assisted grinding method

This method was carried out for the synthesis of the cocrystal in order to show a different approach for the cocrystallization. This method again yielded good quality crystals. In this method, equimolar amounts were ground with a few drop addition of particular solvents (same solvent used for solvent evaporation method). This pasty mixture is then dissolved completely in a particular solvent and then allowed for the crystals to grow in ambient conditions. Since grinding is the particle size reduction process, the solvent evaporation method is followed after grinding in order to get the crystals.

2.2.4 Single crystal X-ray diffraction (SC-XRD): Single crystal X-ray diffraction data for the cocrystals were collected on a Bruker Apex II duo diffractometer with CCD detector. Monochromatic Molybdenum (Mo) K α radiation ($\lambda=0.7107 \text{ \AA}$) was used as a source of radiation. Data collection was done at ambient conditions (296 K). All the structures were solved by the direct method using SHELXL-2007/2014 software and refinement was carried out by full-matrix least squares technique. Anisotropic displacement parameters were calculated for all non-hydrogen atoms except for disordered atoms. H atoms attached to the O/N atoms were located in a difference Fourier density map and refined anisotropically. In some cases, hydrogen atoms were fixed geometrically. All the diagrams were prepared using mercury 3.5.1/3.8 software.

2.2.5 Powder X-ray diffraction (PXRD): PXRD analysis was carried out using Joel (JDX-8P) powder X-ray diffractometer with Cu K α radiation ($\lambda=1.54059$ Å). The voltage and current applied were 40 kV and 30 mA. For a typical experiment, samples were placed on the standard sample holder and then scanned continuously with a scan rate of 2 °min⁻¹. The diffraction patterns obtained from the cocrystal screening experiments were compared with that of parent API. The cocrystal formation was confirmed by the appearance of new peaks in the diffraction patterns.

2.2.6 ¹H NMR spectroscopy (NMR): ¹H NMR Spectrum was recorded on a Bruker Biospin 400 MHz Spectrometer (Bruker, Germany). ¹H NMR was recorded in a DMSO-d₆/CDCl₃ solvent with TMS as the internal reference standard. For the analysis, approximately 5-10 mg of the samples were dissolved in a DMSO-d₆/CDCl₃ solvent and the spectrum was recorded with 16 numbers of the scan.

2.2.7 Fourier-Transform infrared spectroscopy (FT-IR): FT-IR Spectrum was recorded on a Bruker Alpha Fourier Transform Infrared Spectrophotometer (FT-IR) equipped with silicon carbide IR source. For the data acquisition, an attenuated total reflectance accessory with a zinc selenide (ZnSe) crystal is used. All the samples were recorded with 16 scans with a sample resolution of 4 cm⁻¹. Background data set was measured with a clean ZnSe crystal.

2.2.8 Differential scanning calorimetry (DSC): DSC analysis was performed on a DSC60 Differential Scanning Calorimetry (SHIMADZU, Japan) which was calibrated for temperature and enthalpy using the tin standard material. In a typical experiment, 2-5 mg of samples were placed into an aluminum pan, and it was covered with a crimped lid. This weighed, crimped aluminum pan was kept in the sample reference cell and scanned from 30 °C to 250 °C at a heating rate of 10 °C/min under a continuously purged dry nitrogen atmosphere.

2.2.9. Polarized optical microscopy (POM): INSTEC MK 2000 instrument was used for recording the images of the synthesized salt/cocrystal at various temperatures. CCD DSP color camera attached to the instrument is used for the photographs of the crystal images. The instrument is operated at a heating rate of 10 °C/min and the samples were heated continuously from 30 °C to 250 °C.

2.2.10 Solubility measurement: Solubility measurements were performed on a UV-Vis (Analytikjena Specord S600) Spectrometer in standard 3.5 mL quartz cells (2 optical windows) with a 10 mm path length. Individual linearity was performed for all the APIs. For FFA, two absorption maxima were observed at 286 nm and 340 nm, for ETZ absorption maxima were observed at 233 nm and 290 nm, and for CNB absorption maxima was observed at 260 nm. For quantification of FFA in FFA-CNB, 286 nm was chosen as the peak separation was observed in the cocrystal. In the FFA-ETZ cocrystal, both FFA and ETZ maxima were merged together at 290 nm, and hence for quantification of FFA 340 nm was chosen. SNP absorption maxima were observed at 235 nm, 302 nm, and 329 nm respectively. Clear separation of absorption maxima was observed for CNB-SNP cocrystal, however, the peak was not separated properly in ETZ-SNP cocrystal. Therefore, approximate solubility of ETZ is measured in ETZ-SNP cocrystal. The Solubility measurement was done in Millipore water and in 0.1N HCl (pH=1) at ambient temperature (~25 °C). In a typical experiment, an excess quantity of each synthesized cocrystal was taken in 10 mL of Millipore water/0.1 N HCl (pH=1) solution and it was stirred for 24 hours at ambient temperature. Upon equilibrium, the sample was filtered through a 0.2 µm syringe filter and the concentration of the sample was determined by UV-Vis spectroscopy. Solubility is calculated based on the equation, $y = m*x + c$

Where, m = slope, x = concentration, c = constant and y = absorbance

In all the subsequent chapters, the experimental techniques (instruments) used were same. Therefore, instrumentation part under experimental condition is not shown in subsequent chapters.

2.3 RESULTS AND DISCUSSION

The cocrystal formation was initially confirmed by DSC and IR spectroscopy. The as-synthesized cocrystals exhibited a difference in melting point in the DSC analysis and the shift of the carbonyl stretching frequency in the FT-IR spectrum when compared to that of precursor materials confirms the formation of cocrystal. Subsequently, all the cocrystals were characterized further by SC-XRD, PXRD and ^1H NMR analysis.

2.3.1 X-ray crystal structure of cocrystals

FFA-CNB: A 1:1 cocrystal of FFA and CNB was obtained by the solvent drop grinding method as well as solvent evaporation method in ethyl acetate solvent. Crystal structure details and the refinement parameters are listed in **Table 2.1**, the geometry of intermolecular interactions in cocrystals are shown in **Table 2.2**. The asymmetric unit in the cocrystal consists of one molecule each of FFA and CNB which belongs to monoclinic crystal system with $P 2_1/c$ space group (**Figure 2.1a**). Two point acid-acid homosynthon between FFA and CNB with O-H \cdots O bond distance of 2.572 Å and 2.701 Å ($\angle 173.4^\circ$ and $\angle 166.65^\circ$) was observed in the cocrystal. The primary supramolecular adduct is interconnected to the neighboring component through a weak self-complementary C-H \cdots O hydrogen bond (3.480 Å and 3.459 Å) of FFA and CNB (C12H5 \cdots O2 and C18H8 \cdots O6) resulting in a tetrameric unit as shown in the figure (**Figure 2.1b**). Each tetrameric unit is interconnected to the adjoining units through a C-H \cdots O (3.518 Å, $\angle 156^\circ$) hydrogen bond of FFA and CNB (C-H of FFA and O of CNB) to form one dimensional (1D) sheet (**Figure 2.2**). The resultant 1D sheet is further connected to the neighboring sheets through a weak halogen bond interaction of F \cdots Cl (3.150 Å) involving fluorine atom of FFA and chlorine atom of CNB and weak C-H \cdots F (3.335 Å, $\angle 170.02^\circ$) hydrogen bond between CNB and FFA molecules to form a 2D sheet-like structure. The stacking interaction between FFA and CNB molecule was observed with centroid to centroid bond distance of 3.821 Å. Overall F \cdots Cl and C-H \cdots F secondary bond interactions are accountable for the crystal stabilization and the sheet-like structure of FFA-CNB cocrystal (**Figure 2.3**). Color code for the atoms are, gray: carbon; off-white: hydrogen; red: oxygen; blue: nitrogen; green: chlorine; green: fluorine.

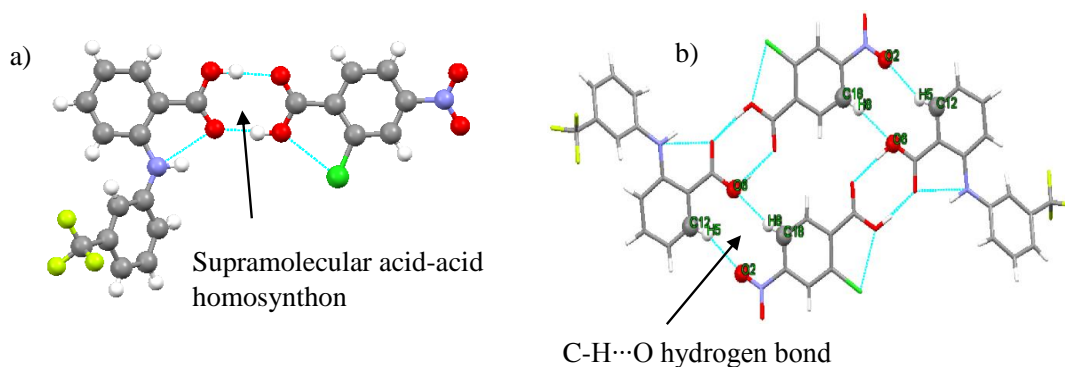


Figure 2.1: Asymmetric unit (a) and tetrameric unit (b) of FFA-CNB cocrystal.

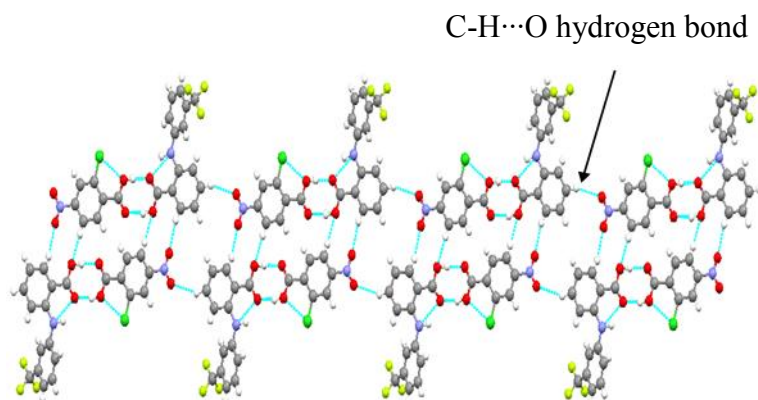


Figure 2.2: Supramolecular 1D sheet stabilized by C-H...O hydrogen bond.

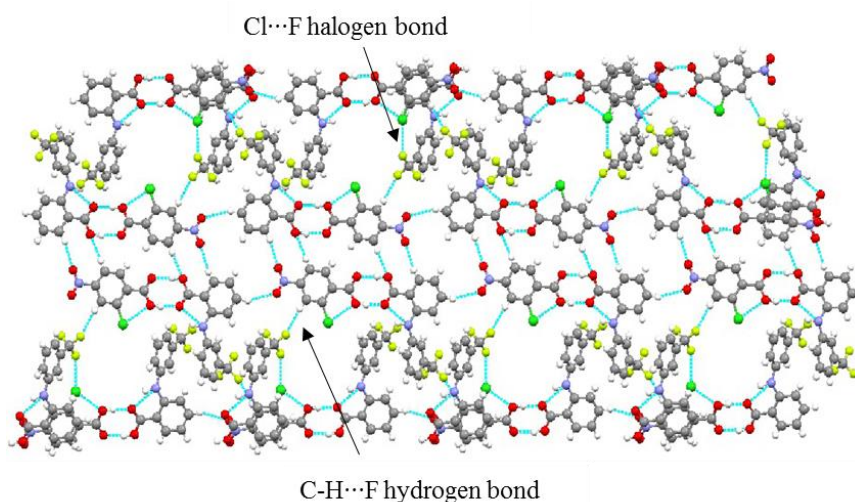


Figure 2.3: 3D Structure of FFA-CNB cocrystal stabilized via C-H...F and Cl...F interactions.

FFA-ETZ: A 1:1 cocrystal of FFA and ETZ was obtained by solvent evaporation/solvent drop grinding method in an ethanol solvent. The asymmetric unit in the cocrystal consists of one molecule each of FFA and ETZ which belongs to triclinic crystal system with $P\bar{1}$ space group (**Figure 2.4a**). Two point Robust supramolecular acid-amide heterosynthon (N-H...O distance of 2.983 Å and O-H...O distance of 2.566 Å) was observed in the crystal structure with $R_2^2(8)$ ring motifs. In the crystal structure, two adjacent supramolecular units were interconnected through weak C-H...O (3.396 Å, $\angle 172.89^\circ$ and 3.486 Å, $\angle 134.62^\circ$) hydrogen bond of FFA and ETZ, which is resulting in a tetrameric unit of FFA-ETZ cocrystal (**Figure 2.4b**). Each tetrameric unit connected to the neighboring unit through weak C-H... π interaction (2.895 Å) involving C-H of FFA and π system of ETZ, C-H... π interaction (2.738 Å)

involving C-H of CH₂ group of ETZ and π system of FFA and π - π interaction between FFA and ETZ molecule with centroid to centroid distance of 3.355 Å respectively (**Figure 2.5**).

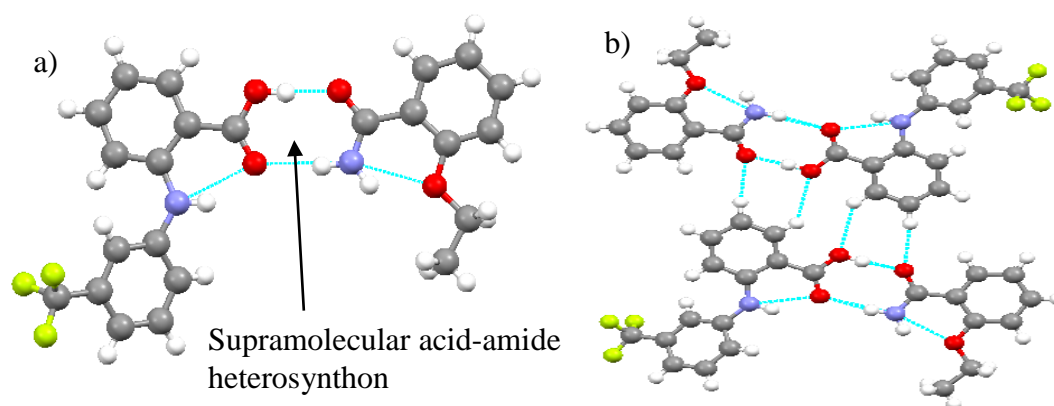


Figure 2.4: Asymmetric unit (a) and tetrameric unit (b) in the FFA-ETZ cocrystal.

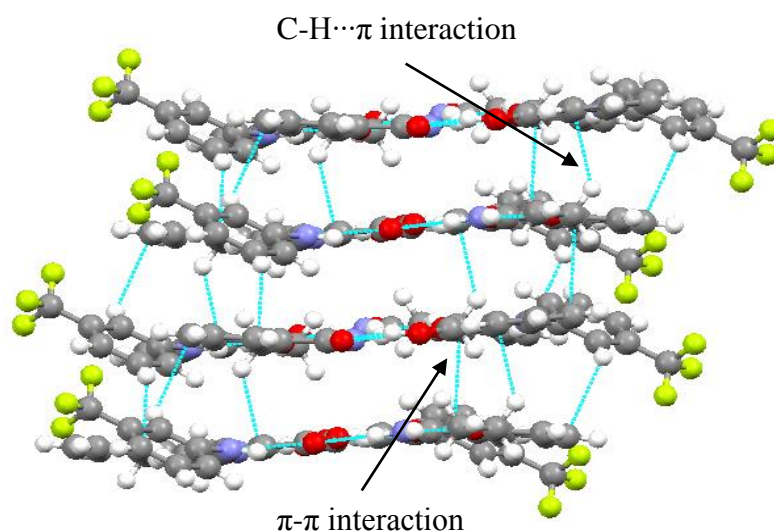


Figure 2.5: 3D representation of FFA-ETZ cocrystal.

ETZ-SNP: The cocrystal was crystallized in monoclinic crystal system with space group $P 2_1/c$. The asymmetric unit consists of one molecule each of ETZ and SNP, and the molecules in the crystal structure interacted through robust acid-amide heterosynthon with O-H \cdots O and N-H \cdots O bond distance of 2.571 Å and 2.941 Å respectively (**Figure 2.6**). The two neighboring supramolecular units were interconnected through O-H \cdots O hydrogen bond (2.775 Å) between SNP molecules (4-hydroxy group and carbonyl group), which further continues forming a 1D structure of SNP-ETZ cocrystal (**Figure 2.7**). The 1D structure converts to the 2D structure by

utilizing weak C-H \cdots O hydrogen bond (3.458 Å) between ETZ and SNP molecule (Figure 2.8). The 2D structure further converts to the 3D structure using C-H \cdots π interaction (3.633 Å) between SNP molecule.

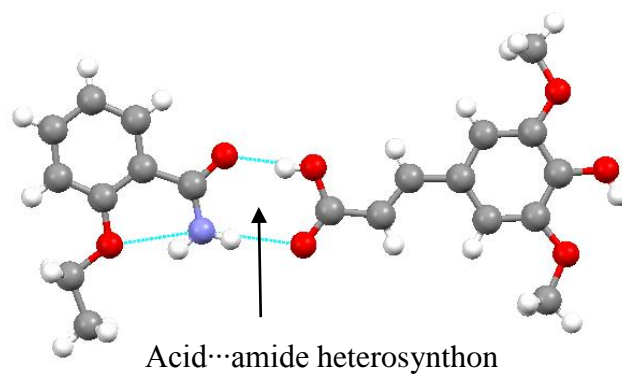


Figure 2.6: Asymmetric unit of ETZ-SNP cocrystal.

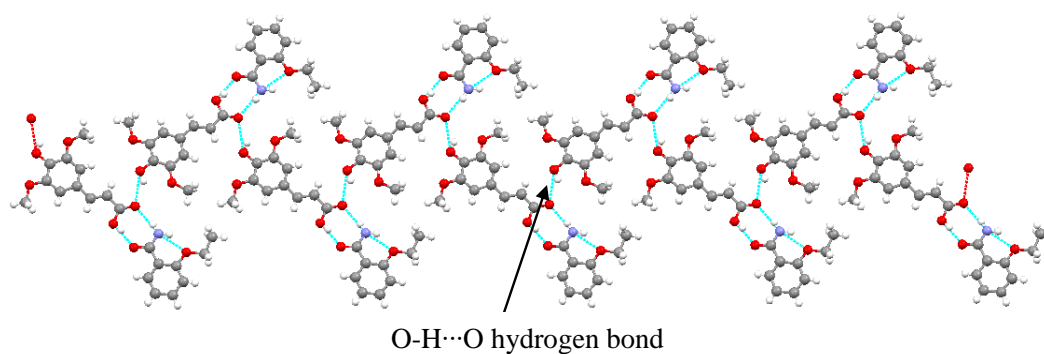


Figure 2.7: 1D representation of ETZ-SNP cocrystal.

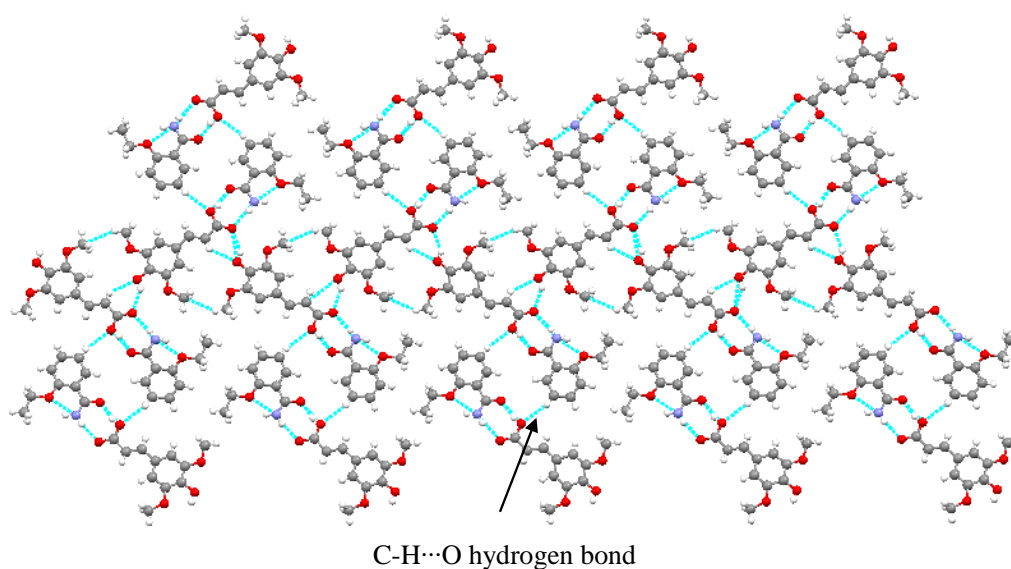


Figure 2.8: 2D sheet-like structure of ETZ-SNP cocrystal.

CNB-SNP: It was crystallized in monoclinic crystal system with space group P 21/c. The asymmetric unit in the crystal structure consists of two molecules each of SNP and CNB, where, the molecules interacted through robust acid-acid homomorphism. Two different interaction distances were observed for the acid-acid homomorphism between SNP and CNB (**Figure 2.9**). In the first instance, the O-H \cdots O bond distance is 2.631 Å and 2.632 Å, and in the second instance, the O-H \cdots O bond distance is 2.648 Å and 2.670 Å. These two dimers were interconnected through O-H \cdots O hydrogen bond (2.895 Å) between the hydroxyl group of SNP and acid group of SNP. The supramolecular units were further connected through O \cdots O chalcogen bond (2.888 Å) resulting in a 1D structure of SNP-CNB cocrystal (**Figure 2.10**). The 1D structure of SNP-CNB cocrystal expands to 2D using C-H \cdots Cl and C-H \cdots O hydrogen bond between SNP and CNB molecules. This further converted to the 3D structure by utilizing weak C-H \cdots Cl hydrogen bond (3.784 Å) and π - π interaction between SNP and CNB molecule with centroid to centroid distance of 3.289 Å. The overall crystal structure of SNP-CNB features weak C-H \cdots O hydrogen bond between a nitro group of CNB and C-H group of SNP, C-H \cdots O hydrogen bond between C-H group of CNB and carbonyl group of SNP, and C-H \cdots O hydrogen bond between two SNP molecules (**Figure 2.11**).

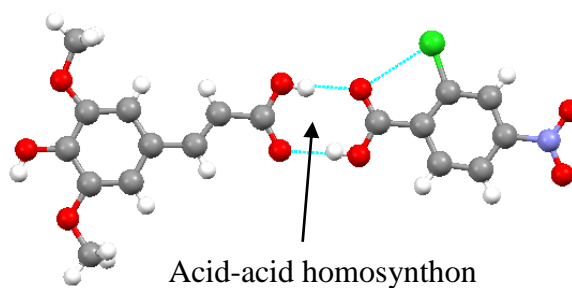


Figure 2.9: Asymmetric unit of CNB-SNP cocrystal.

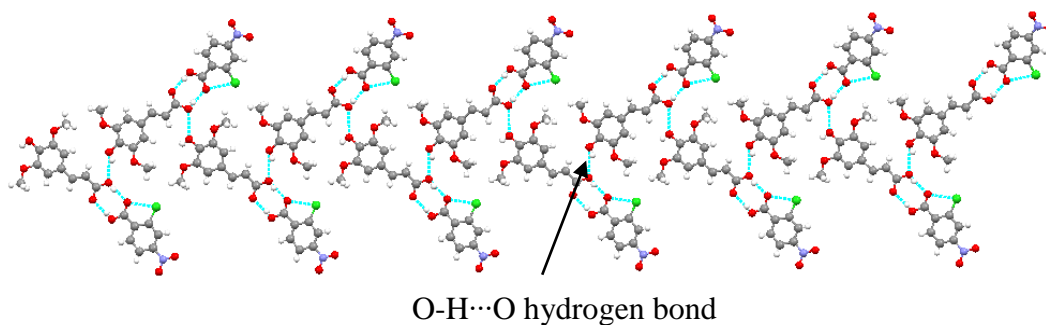


Figure 2.10: 1D representation of CNB-SNP cocrystal.

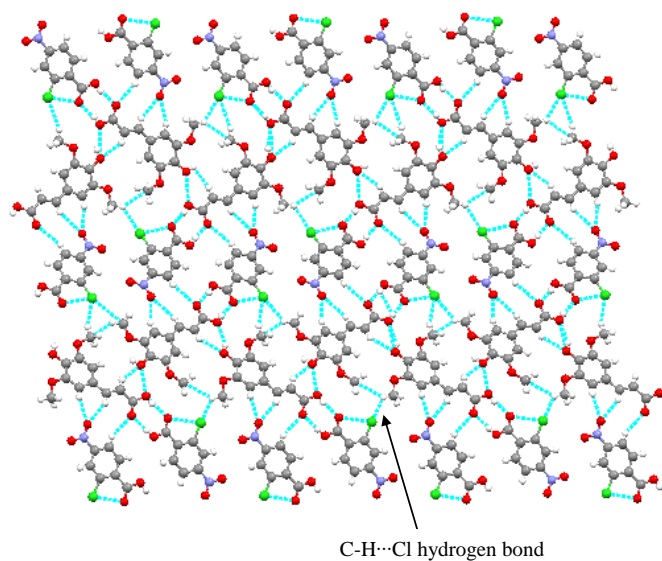


Figure 2.11: The 2D sheet-like structure of CNB-SNP cocrystal stabilized via C-H...O and C-H...Cl hydrogen bond.

Table 2.1: Crystal structure details and the refinement parameters of FFA cocrystals.

Crystal structure details	FFA-CNB	FFA-ETZ	ETZ-SNP	CNB-SNP
CCDC number	1448785	1448786	1581650	1581652
Mol. formula	C ₂₁ H ₁₄ ClF ₃ N ₂ O ₆	C ₂₃ H ₂₁ F ₃ N ₂ O ₄	C ₂₀ H ₂₃ NO ₇	C ₁₈ H ₁₆ ClNO ₉
Molar mass	482.79	446.42	389.39	425.77
crystal system	Monoclinic	Triclinic	monoclinic	Monoclinic
Space group	P 21/c	P $\bar{1}$	P 21/c	P 21/c
a / Å	7.6335(2)	7.6281(3)	14.055(2)	11.3470(6)
b / Å	32.1379(9)	8.8078(3)	16.2149(18)	35.018(2)
c / Å	8.4402(3)	17.4273(6)	8.6090(12)	9.3902(5)
α / °	90	103.788(2)	90	90
β / °	95.1710(10)	94.744(2)	97.404(6)	97.673(3)
γ / °	90	102.941(2)	90	90
Volume/ Å ³	2062.16(11)	1096.75(7)	1945.7(4)	3697.8(4)
Z	4	2	4	8
Density [g/cm ³]	1.513	1.352	1.329	1.530
μ (MoK α) [mm ⁻¹]	0.253	0.110	0.101	0.261
T/K	296 (2)	296 (2)	296(2)	296(2)
Reflns collected	4069	3845	4670	7421
Unique rflns	3573	3042	3036	4517
Parameter refined	354	373	266	535
R1(I > 2 σ)	0.0670	0.0667	0.0642	0.0594
wR 2 (I > 2 σ)	0.2139	0.1858	0.1723	0.1644
GOF	1.452	1.098	0.951	1.025

Table 2.2: Geometrical parameters of the intermolecular interactions in the cocrystals.

Cocrystal	D-H...A ^a	H...A/ Å	D...A/ Å	<D-H...A/ °	Symmetry code
FFA-CNB	C6-H1...C11	2.988	3.887	164.41	x-1, y, z
	C20-H6...F3	2.398	3.335	170.04	x+1, -y+1/2, z+1/2
	N1-H1...O5	1.878	2.650	137.90	x, y, z
	O3-H12...O5	1.664	2.572	173.33	x, y, z-1
	O6-H14...O4	1.743	2.702	166.72	x, y, z+1
FFA-ETZ	N1-H2...O1	2.067	2.983	170.37	x, y, z
	N1-H1...O001	2.001	2.658	130.02	x, y, z
	N2-H9...O1	1.929	2.665	140.03	x, y, z
	O2-H18...O3	1.677	2.566	168.67	x, y, z
ETZ-SNP	C10-H10...O3	2.521	3.202	130.27	-x, y-1/2, -z+1/2
	O3-H10...O3	2.230	2.660	112.98	x, y, z
	O3-H10...O4	2.078	2.775	142.71	-x, y+1/2, -z+1/2
	O5-H5A...O6	1.766	2.571	166.84	x, y-1, z
	N1-H2...O8	1.955	2.646	137.68	x, y, z
	N1-H1...O4	2.088	2.940	167.79	x, y+1, z
CNB-SNP	C9-H9...O17	2.434	3.214	140.93	x-1, y, z+1
	C16-H16...O11	2.424	3.299	156.85	-x, y+1/2, -z+3/2
	C17-H17A...C12	2.939	3.785	147.64	-x, -y, -z+2
	C17-H17B...C12	2.891	3.788	155.82	x, y, z
	C18-H18B...C11	2.732	3.432	130.28	x, y, z
	C22-H22...O5	2.629	3.476	151.75	-x, y-1/2, -z+3/2
	C27-H27...O8	2.430	3.213	141.83	x, y, z
	C30-H30...O1	2.425	3.313	159.72	-x+1, y-1/2, -z+1/2
	C35-H35B...C11	2.962	3.831	151.29	x, y, z
	C36-H36B...C12	2.965	3.428	133.64	x+1, y, z-1
	O6-H6A...O4	1.856	2.671	172.04	x-1, y, z+1
	O8-H8...O9	2.156	2.614	115.37	x, y, z
	O8-H8...O14	2.156	2.895	149.93	x, y, z
	O12-H12A...O15	1.819	2.632	170.95	x, y, z
	O14-H14...O13	1.819	2.631	170.30	x, y, z
O17-H17...O16	2.237	2.678	114.08	x, y, z	
O3-H10...O5	1.827	2.648	166.80	x+1, y, z-1	

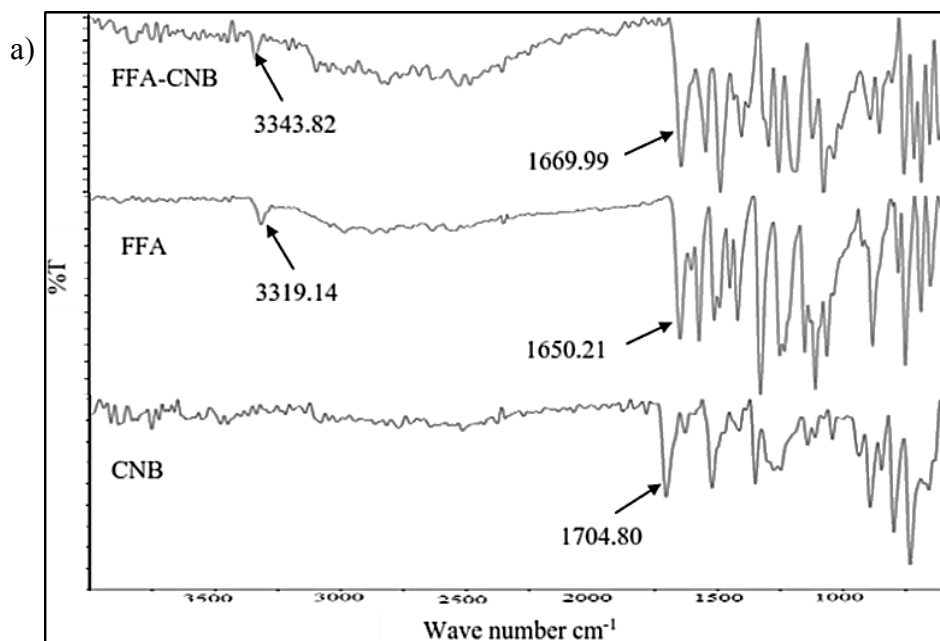
^aD-donor, A-acceptor

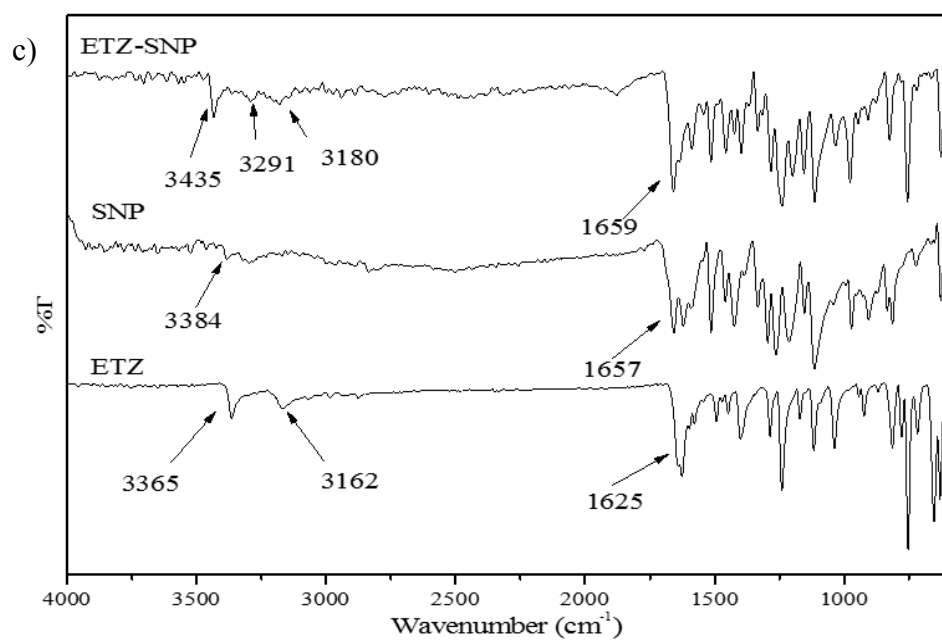
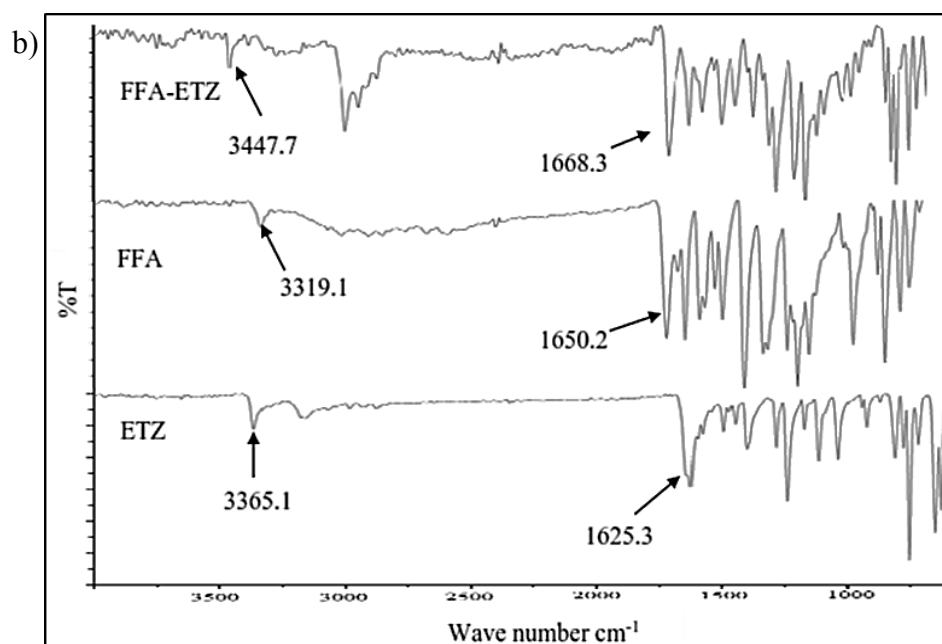
2.3.2 Spectroscopic analysis of cocrystals

2.3.2.1 FT-IR spectroscopy

Synthesized cocrystals were analyzed by FT-IR spectroscopy to confirm the cocrystal formation by comparing the spectrum with their respective starting materials. In pure FFA, CNB, ETZ, and SNP the carbonyl stretching frequencies were observed

at 1650 cm^{-1} , 1705 cm^{-1} , 1625 cm^{-1} , and 1657 cm^{-1} respectively. Considerable changes in the stretching frequencies were observed for cocrystals compared with starting materials. The synthesized cocrystals exhibited $\text{C}=\text{O}$ stretching frequency at 1670 cm^{-1} for FFA-CNB, 1668 cm^{-1} in the case of FFA-ETZ cocrystal, 1659 cm^{-1} for ETZ-SNP, and 1684 cm^{-1} for CNB-SNP cocrystal. Blue shift in carbonyl stretching frequency was observed in FFA-ETZ cocrystal. This is probably due to the fact that carbonyl group of ethenzamide is involved in a bifurcated hydrogen bond with FFA molecule. Apart from the carbonyl stretching frequency, a shift in hydroxyl (OH) stretching frequency was observed for the cocrystals. The shift in stretching frequencies are displayed in **Table 2.3**. Comparison plot of FT-IR spectra is shown in **Figure 2.12**.





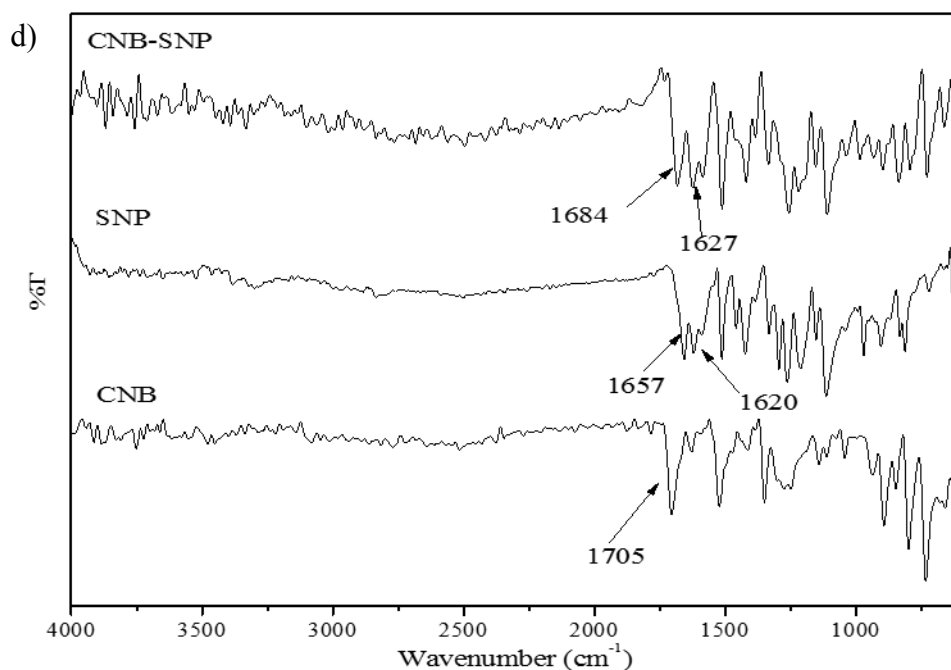


Figure 2.12: Comparison of FT-IR spectra of a) FFA-CNB b) FFA-ETZ, c) ETZ-SNP, and d) CNB-SNP cocrystal with respect to starting materials.

Table 2.3: Comparison of stretching frequency of cocrystals with starting materials.

Crystal forms	-C=O stretch (cm ⁻¹)	-OH stretch (cm ⁻¹)
FFA	1650	3319
CNB	1705	-
ETZ	1625	-
DNB	1700	-
SNP	1657	-
FFA-CNB	1670	3344
FFA-ETZ	1668	3448
ETZ-SNP	1659	3435, 3291
CNB-SNP	1684	-

2.3.2.2 ¹H NMR spectroscopy

¹H NMR spectroscopy was carried out to confirm the molecular stoichiometry of the synthesized cocrystals. The analysis was carried out in DMSO-d₆ as a solvent with TMS as internal reference standard. ETZ-SNP analysis is performed in a CDCl₃ solvent. All the cocrystals showed a 1:1 molecular stoichiometry in the asymmetric unit. The chemical shift (δ) and the coupling constant (J) value in the cocrystal is

described below. The ^1H NMR spectrum of cocrystals is shown in **Figure 2.13-Figure 2.16**.

FFA-CNB (DMSO- d_6 , δ ppm): 14.0 (1H, s), 13.2 (1H, s), 9.67 (1H, s), 8.361-8.356 (1H, d (J=24 Hz)), 8.259-8.233 (1H, m), 8.015-7.993 (1H, d (J=8.8 Hz)), 7.948-7.923 (1H, dd (J=16 Hz)), 7.552-7.481 (3H, m), 7.466-7.442 (1H, t), 7.350-7.296 (2H, m), 6.918-6.877 (1H, t (J=4 Hz)).

FFA-ETZ (DMSO- d_6 , δ ppm): 13.22 (1H, s), 9.691 (1H, s), 7.94 (1H, s), 7.82 (1H, s), 7.594-7.549 (5H, m), 7.462 (2H, s), 7.348-7.316 (2H, m), 7.124 (1H, s), 7.028-7.013 (1H, d (J=6 Hz)), 6.910-6.895 (1H, d (J=6 Hz)), 4.17 (2H, t), 1.402-1.387 (3H, t (J=6 Hz)).

ETZ-SNP (400 MHz, CDCl_3 , δ ppm): 8.22-8.20 (1H, d (J=8 Hz)), 7.93 (1H, s), 7.68-7.64 (1H, d (J=16 Hz)), 7.47-7.43 (1H, t (J=8 Hz)), 7.08-7.04 (1H, t (J=8 Hz)), 6.97-6.95 (1H, d (J=8 Hz)), 6.79 (1H, s), 6.58 (1H, s), 6.34-6.30 (1H, d (J=16 Hz)), 4.23-4.18 (2H, q (J=8 Hz)), 3.92 (6H, s), 1.53-1.49 (3H, t (J=8 Hz)).

CNB-SNP (400 MHz, DMSO- d_6 , δ ppm): 8.92 (1H, s), 8.36-8.35 (1H, d (J=4 Hz)), 8.26-8.23 (1H, dd (J=8 Hz)), 8.01-7.99 (1H, d (J=8 Hz)), 7.51-7.47 (1H, d (J=16 Hz)), 6.98 (2H, s), 6.43-6.39 (1H, d (J=16 Hz)), 3.80 (6H, s).

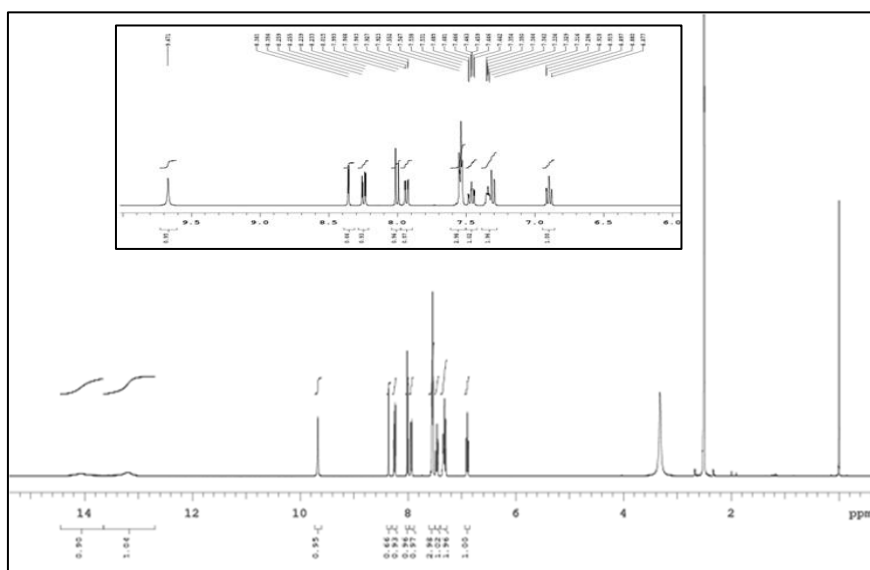


Figure 2.13: ^1H NMR spectrum of FFA-CNB cocrystal.

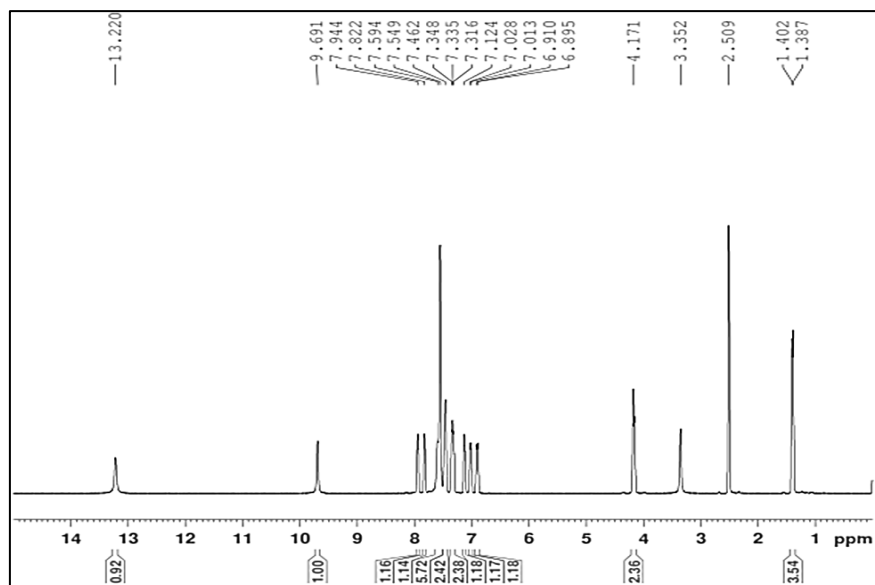


Figure 2.14: ^1H NMR spectrum of FFA-ETZ cocrystal.

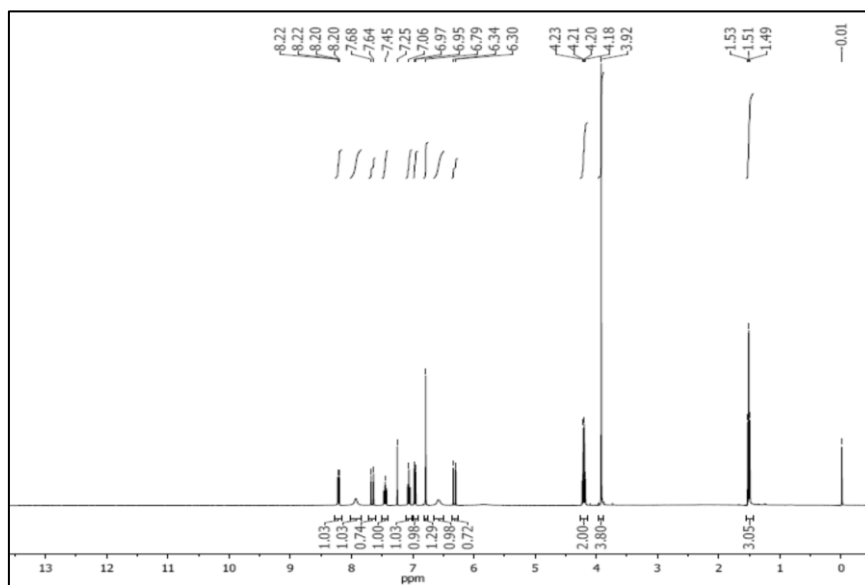


Figure 2.15: ^1H NMR spectrum of ETZ-SNP cocrystal.

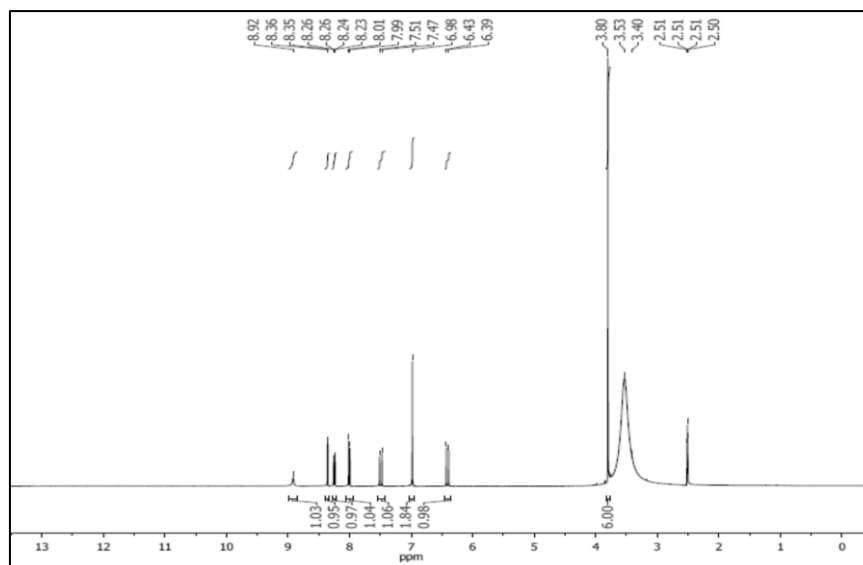


Figure 2.16: ^1H NMR spectrum of CNB-SNP cocrystal.

2.3.3 DSC and POM analysis

In the present study, DSC analysis was performed to determine the melting point of the synthesized cocrystals and to study the thermal behavior of synthesized cocrystals. The melting temperature for the cocrystal FFA-CNB, FFA-ETZ, ETZ-SNP, and CNB-SNP were observed at 136.81 °C, 89.46 °C, 148.94 °C, and 188.42 °C respectively. The melting point of APIs, coformer and cocrystals are displayed in **Table 2.4**. FFA-CNB, ETZ-SNP, and CNB-SNP cocrystals melt exactly in between the melting point of its constituent starting materials, whereas FFA-ETZ cocrystal melts at lower temperature compared to its starting materials. This is probably due to the loose crystal packing of FFA-ETZ cocrystal when compared to other cocrystals, which is reflected in the low crystal density of the cocrystal. However, ETZ-SNP crystal density was slightly lower than FFA-ETZ cocrystal. In FFA-ETZ cocrystal the secondary interactions were found to be fewer, whereas in ETZ-SNP O-H \cdots O hydrogen bond associated with hydroxy group of SNP is observed, and due to this stronger hydrogen bond melting temperature was found to be more compared to FFA-ETZ. Single endothermic peak was observed for all the cocrystals in the DSC analysis suggests that there is no phase transformation in the cocrystal and it is thermally stable (**Figure 2.17**).

Apart from DSC analysis, POM analysis was carried out for the cocrystals to demonstrate the thermal stability. The images of the cocrystals at different temperature were taken during heating to check the morphological changes in the

cocrystals. It is found that all the four cocrystals exhibited thermal stability during heating till the cocrystal melts. The POM images of the cocrystals are shown in **Figure 2.18**.

Table 2.4: Melting point of FFA, cofomers and cocrystals.

API (°C)	Cofomer (°C)	Cocrystal (°C)
(FFA) 135.45	(SNP) 202.00	(FFA-CNB) 136.81
(CNB) 141.00		(FFA-ETZ) 89.46
(ETZ) 129.03		(ETZ-SNP) 148.94
		(CNB-SNP) 188.42

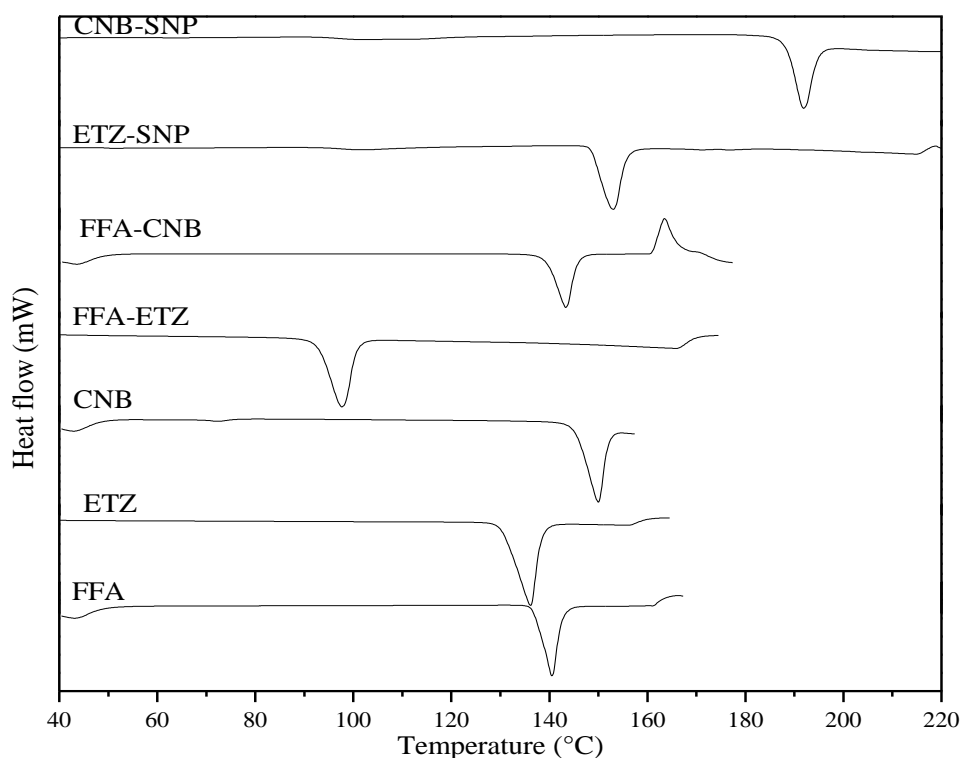


Figure 2.17: DSC plots of APIs and the cocrystals.

2.3.4 Crystal structure comparison between cocrystals

FFA-CNB and CNB-SNP cocrystal have formed via supramolecular acid···acid homosynthon, whereas FFA-ETZ and ETZ-SNP cocrystal uses supramolecular acid···amide heterosynthon. Off all these cocrystals, the density of ETZ-SNP was found to be least, however, the melting temperature was found to be higher than that of FFA-ETZ cocrystal though the crystal density is higher for FFA-ETZ cocrystal. This is probably due to the interactions associated with the crystal structure. In ETZ-SNP

cocrystal, in addition to acid-made heterosynthon, strong O-H \cdots O hydrogen bond between a hydroxy group of SNP molecule and the carbonyl group of SNP is observed. The higher melting is probably attributed to this O-H \cdots O hydrogen bond which was not observed in FFA-ETZ cocrystal. In the case of FFA-CNB cocrystal, Cl \cdots F halogen bond and C-H \cdots F hydrogen bond secondary interactions were observed. Whereas in CNB-SNP cocrystal, halogen bond was not observed, however, weak C-H \cdots F hydrogen bond is observed. The crystal density was found to be higher for CNB-SNP cocrystal, and therefore the melting temperature too was higher for this cocrystal.

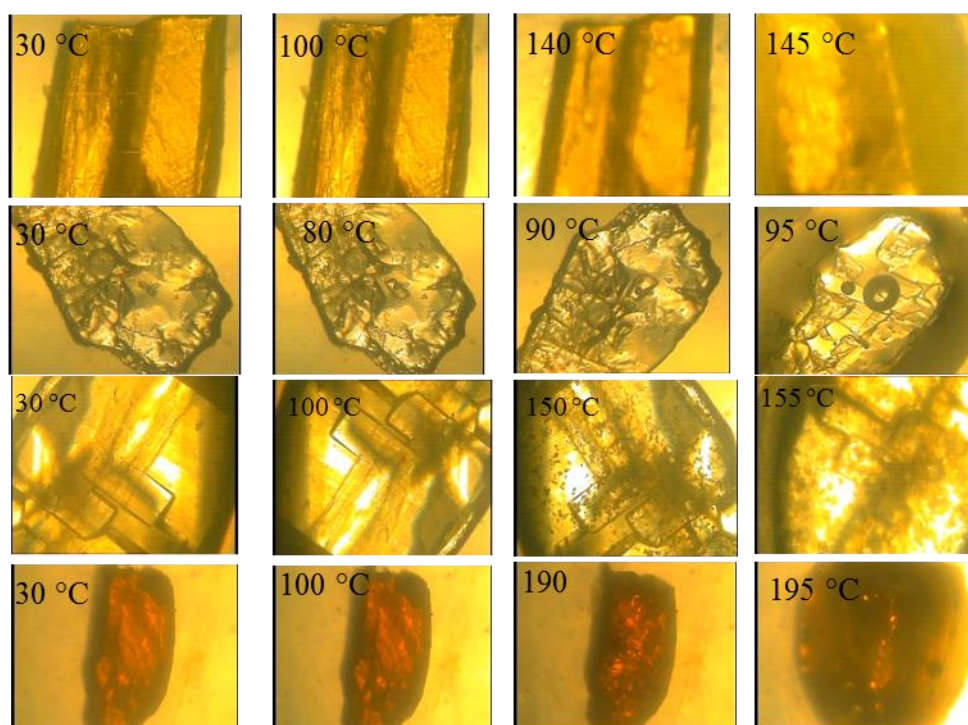


Figure 2.18: POM images of cocrystal at various temperature (1st row (from top): FFA-CNB, 2nd row: FFA-ETZ, 3rd row: ETZ-SNP, and 4th row: CNB-SNP).

2.3.5 PXRD analysis

The PXRD analysis was carried out to check the bulk purity of the synthesized cocrystals. Experimentally observed PXRD pattern was compared with the simulated PXRD pattern obtained from SC-XRD analysis and it substantiates the bulk purity of the synthesized cocrystal (**Figure 2.19-2.22**).

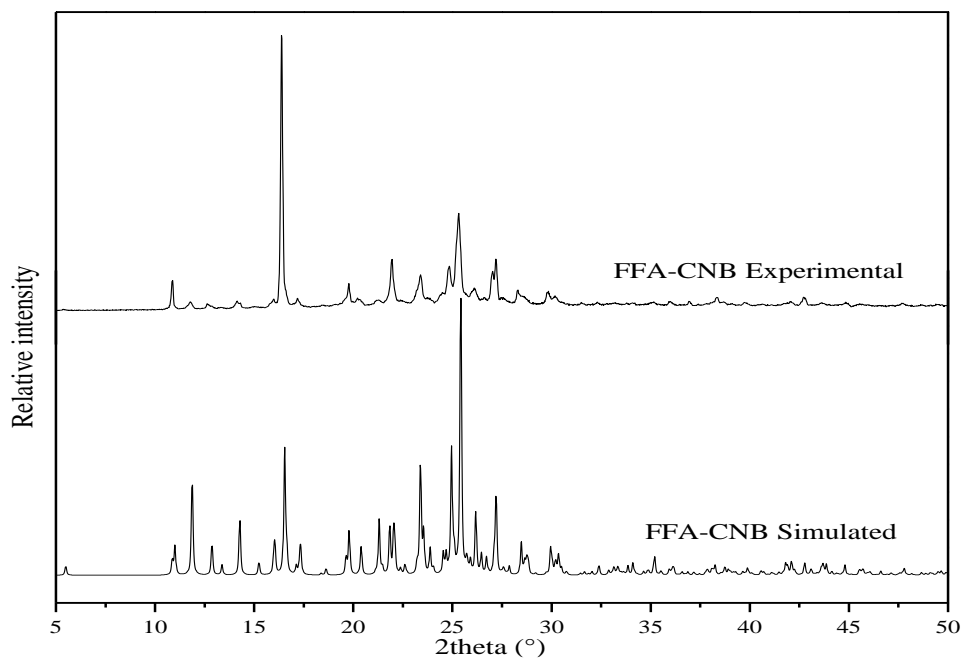


Figure 2.19: Comparison of experimental and simulated PXRD pattern of FFA-CNB cocrystal.

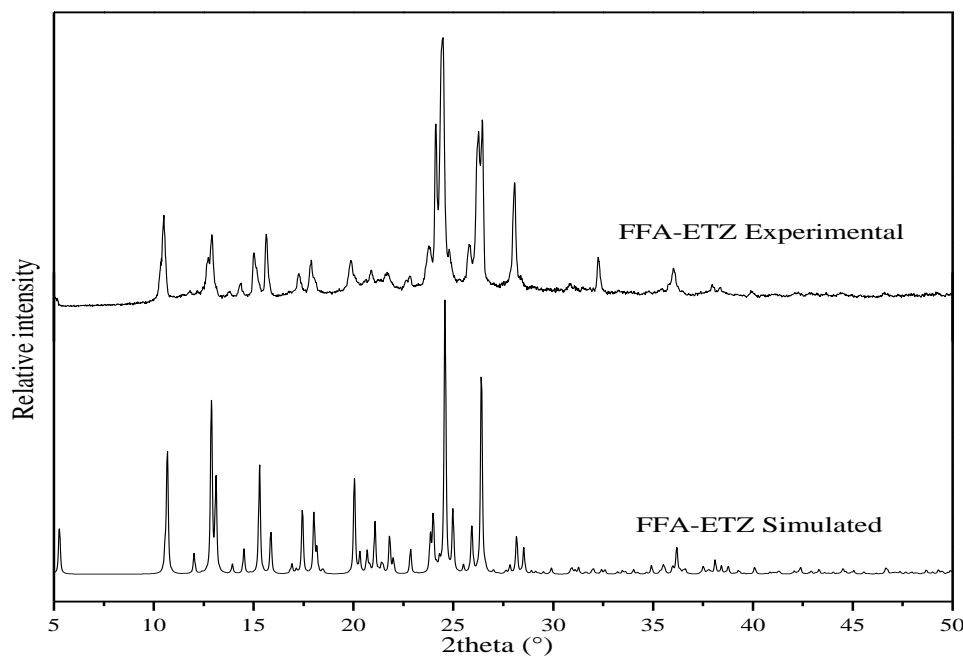


Figure 2.20: Comparison of experimental and simulated PXRD pattern of FFA-ETZ cocrystal.

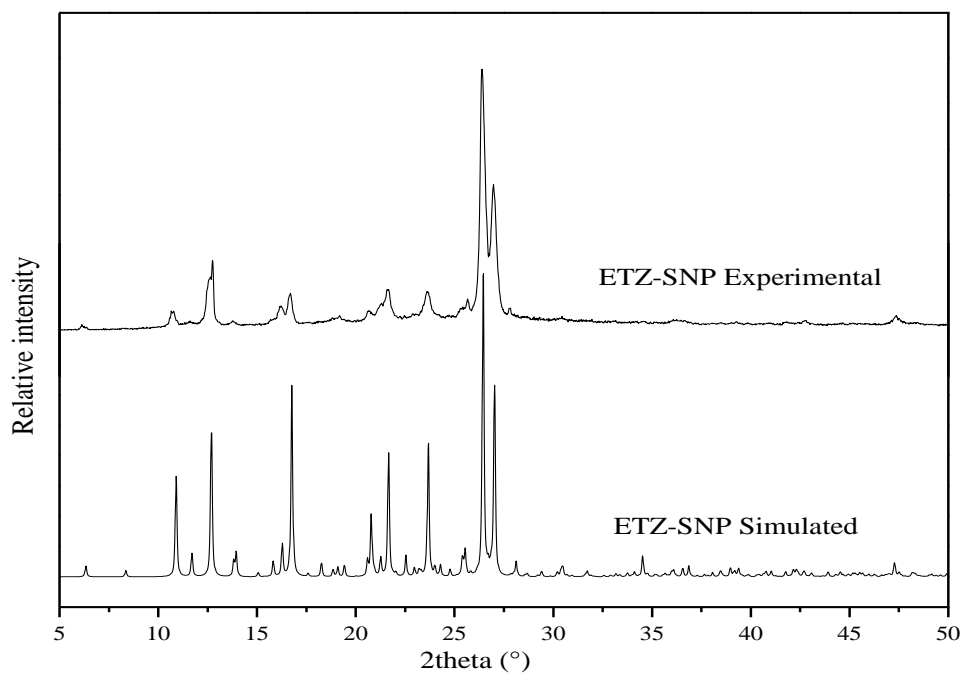


Figure 2.21: Comparison of experimental and simulated PXRD pattern of ETZ-SNP cocrystal.

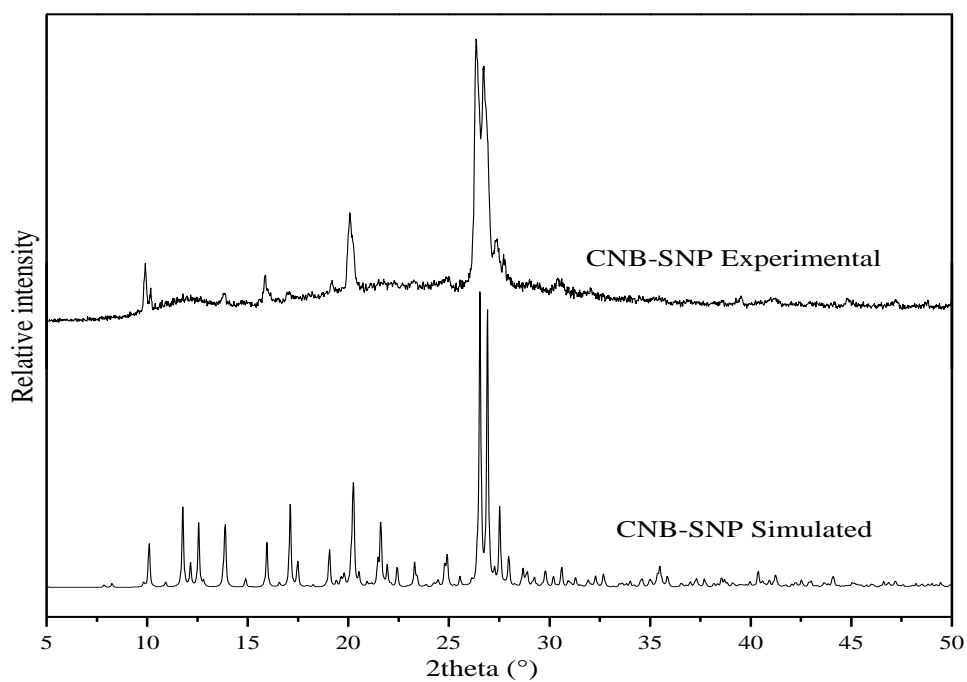


Figure 2.22: Comparison of experimental and simulated PXRD pattern of CNB-SNP cocrystal.

2.3.6 Stability study of cocrystals

Hygroscopicity study and long-term stability:

The hygroscopicity of the synthesized cocrystals was evaluated in the present study by a conventional method at accelerated conditions. FFA, ETZ, and CNB are found to be non-hygroscopic, however, upon heating and storage condition, polymorphic phase transformation in FFA was reported in the literature. In the conventional method, a known quantity of the sample (cocrystal) was kept in a desiccator which was filled with saturated sodium chloride solution to maintain the humidity of ~75% RH. The weight of the samples was recorded periodically (every 24 hours) for a time period of 7 days to check the absorbance of a water molecule. All the synthesized cocrystals in the present study were found to be non-hygroscopic as there was no change in the weight of the sample and it was further confirmed by analyzing PXRD analysis (**Figure 2.23 & Figure 2.24**). No changes in the diffraction patterns were observed before and after hygroscopic study in the PXRD analysis. From the above-studied data (weight loss method and PXRD analysis) it was concluded that the cocrystals are non-hygroscopic at ~75% RH at ambient temperature (~25 °C).

Long-term stability study was performed for the synthesized cocrystals at ambient temperature (~25 °C) for a time period of six months. A known quantity of the synthesized cocrystals was kept at room temperature for a period of six months. The phase purity of the stability sample was confirmed by PXRD analysis (**Figure 2.25 & Figure 2.26**). It was observed that the synthesized cocrystals are stable for about six months at ambient conditions.

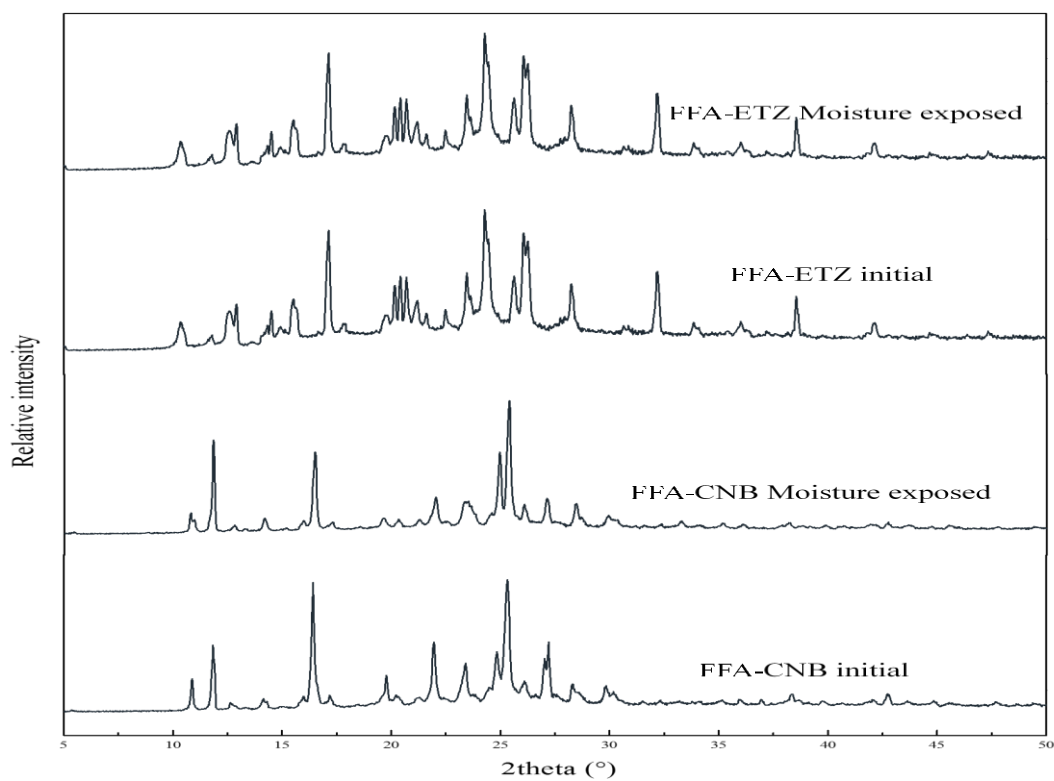


Figure 2.23: PXR D comparison pattern of FFA-CNB and FFA-ETZ cocrystal initial and after moisture exposure.

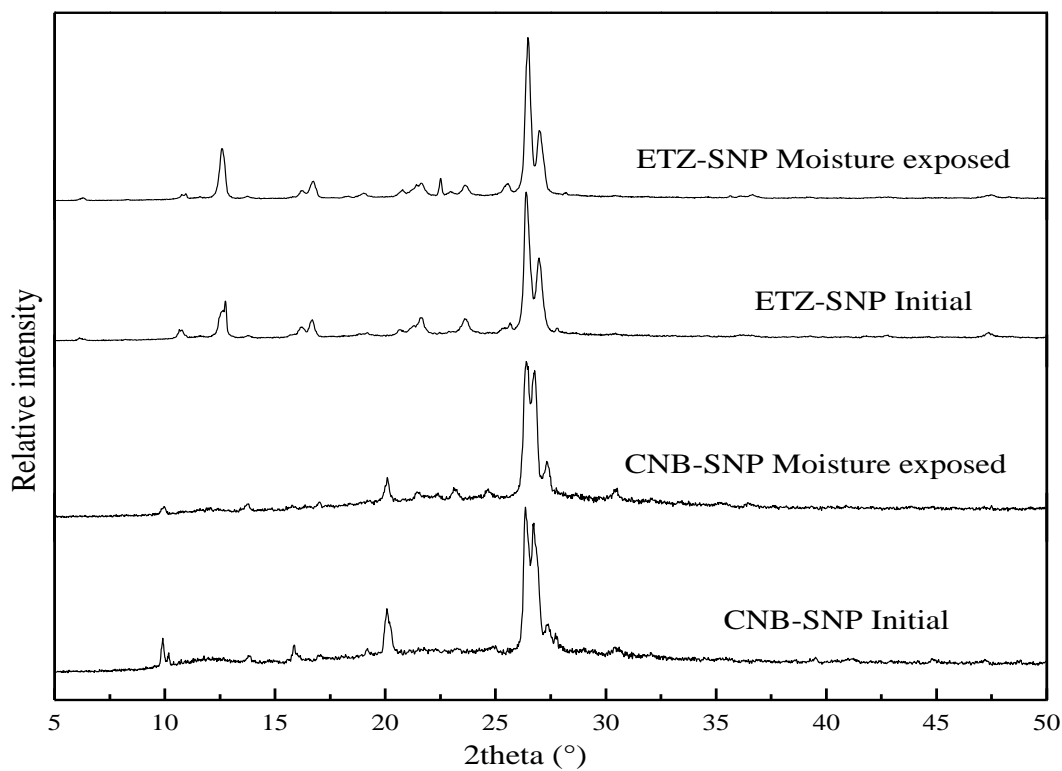


Figure 2.24: PXR D comparison pattern of ETZ-SNP and CNB-SNP cocrystal initial and after moisture exposure.

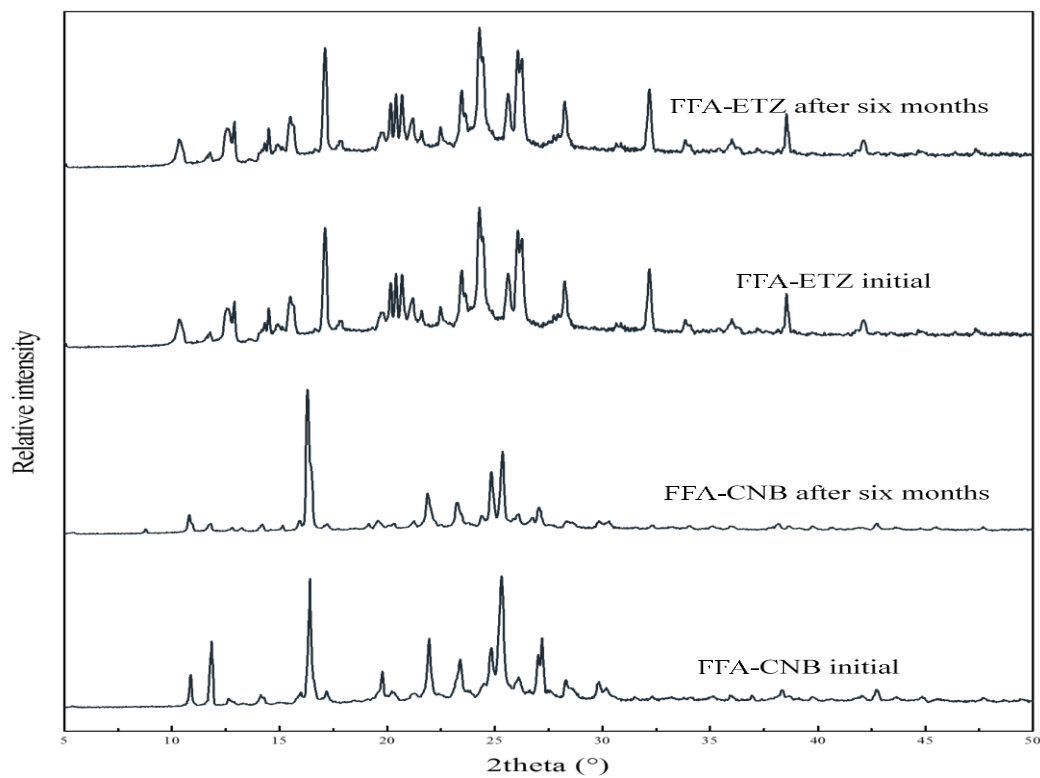


Figure 2.25: Comparison of PXRD pattern of FFA-CNB and FFA-ETZ cocrystal initial and after six months.

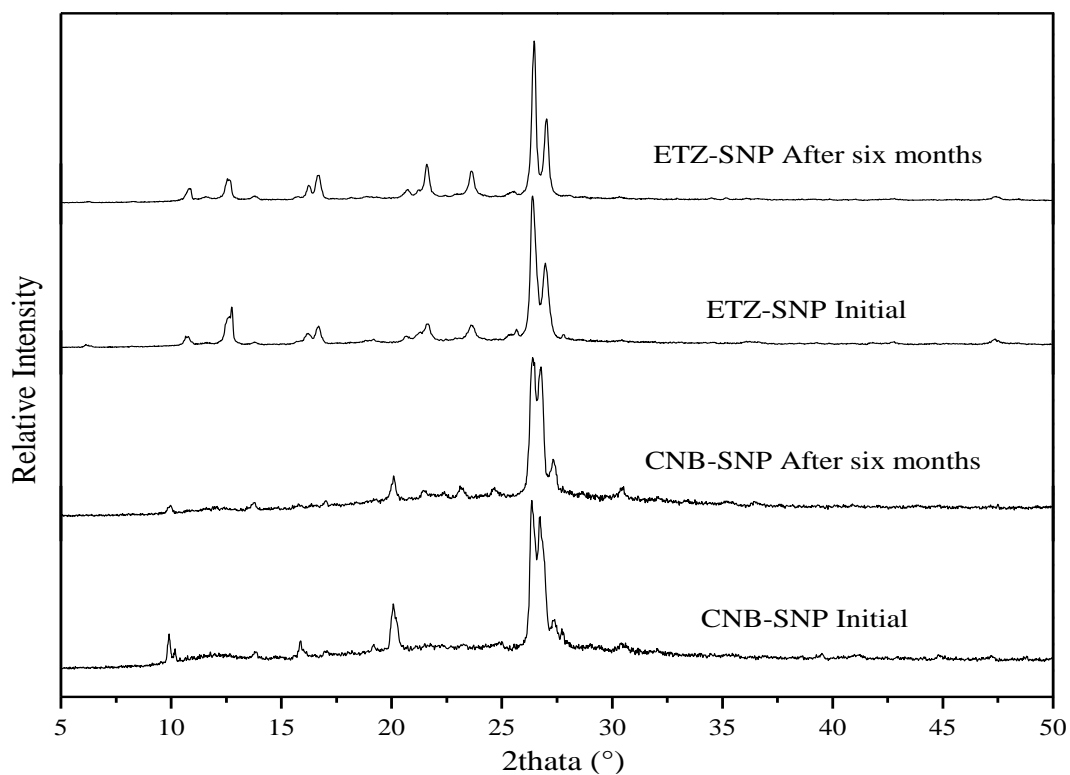


Figure 2.26: Comparison of PXRD pattern of ETZ-SNP and CNB-SNP cocrystal initial and after six months.

2.3.7 Solubility study

The APIs drug solubility and the synthesized cocrystals drug solubility were measured in purified water as well as in 0.1 N HCl solution (pH=1) at ambient condition (~25 °C). In a typical experimentation, excess powder samples of FFA, ETZ, CNB and the cocrystals were taken in the minimum quantity of water/0.1N HCl solution (pH=1) separately and stirred for 24 hours at ambient temperature. Aliquots were taken out and filtered through a syringe filter (0.2 µm) and upon dilution with water, drug content was quantified by UV-Vis spectroscopy. The standard linearity curve of the drug molecules are shown in **Figure 2.27**. The solubility data are summarized in **Table 2.5**. Dilution correction has been included in the calculation part. From the solubility data, it was observed that FFA solubility was increased by two-fold when it is in FFA-CNB cocrystal and the solubility was comparable with FFA (as such) in FFA-ETZ cocrystal in Millipore water. However, the solubility of ETZ and CNB in the cocrystal is slightly lower when compared with parent drugs. The solubility experiment in 0.1 N HCl (pH=1) showed good improvement in the solubility of FFA in the cocrystals, as both the cocrystal exhibited about 5 times more solubility when compared to FFA as such. The solubility of ETZ and CNB in the cocrystals in 0.1N HCl solution is drastically decreased. This may probably due to the drug-coformer interactions in the cocrystal.

Table 2.5: Solubility of APIs and cocrystals in water and in 0.1 N HCl solution (pH=1) at ~25 °C.

Solubility in water	
Solid form	Equilibrium solubility of APIs (mg/L)*
FFA	52.00
ETZ	1156
CNB	2745
FFA-CNB	105.5 (×2.03)
FFA-ETZ	50.80
ETZ-SNP	1070
CNB-SNP	1077
Solubility in 0.1 N HCl solution (pH=1)	
FFA	48.6
ETZ	1784
CNB	2490
FFA-CNB	266.0 (×5.47)

FFA-ETZ	253.0 ($\times 5.21$)
ETZ-SNP	1090
CNB-SNP	264

* Values in the parenthesis indicates the extent of increment in the solubility of FFA in FFA-CNB and FFA-ETZ cocystal.

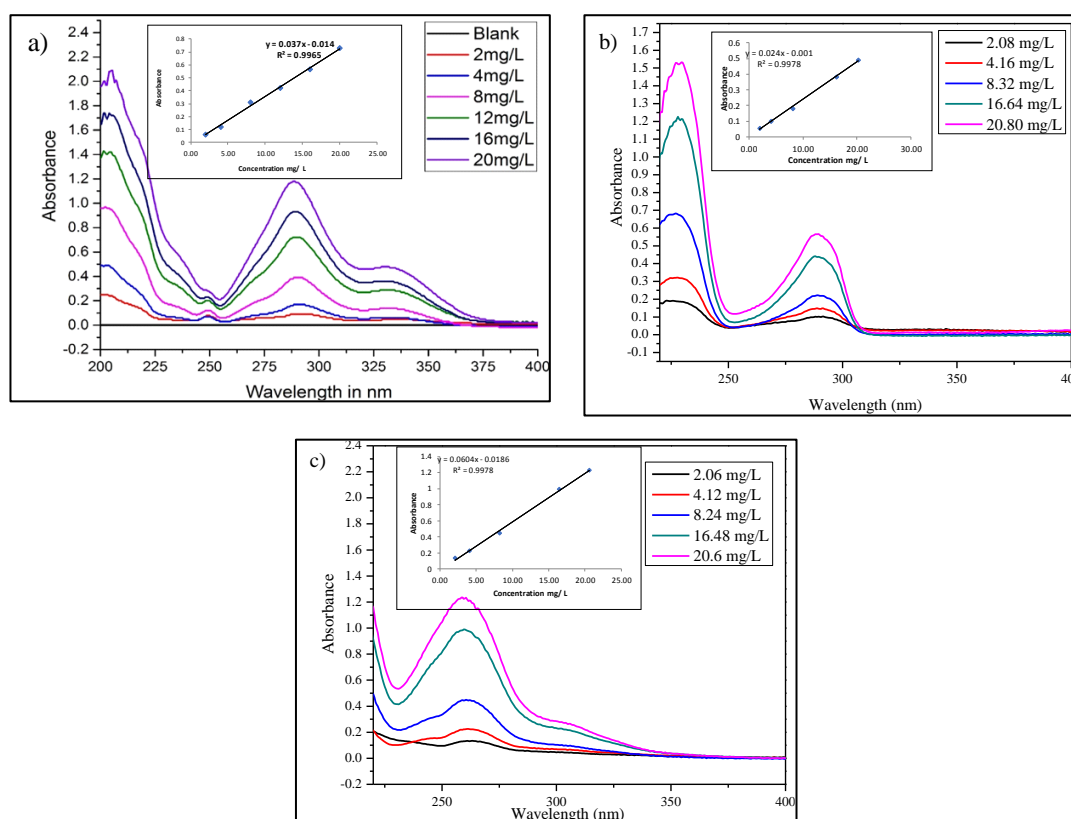


Figure 2.27: Standard linearity curves of a) FFA, b) ETZ, and c) CNB drug molecules.

2.4 CONCLUSIONS

In conclusion, four novel pharmaceutical cocystals of anti-inflammatory and anti-viral drugs have been synthesized by crystal engineering approach and characterized by various spectroscopic and thermal techniques. The crystal structures of the synthesized cocystals were determined by SC-XRD analysis. FFA-CNB cocystal and CNB-SNP cocystal was formed via supramolecular acid-acid homosynthon and in FFA-ETZ and ETZ-SNP cocystals, two point supramolecular acid-amide heterosynthon was observed. The synthesized cocystals were found to be non-hygroscopic at accelerated humid conditions ($\sim 75\%$ RH). The solubility study in purified water suggested that FFA solubility is increased by two-fold when it is in the

form of FFA-CNB cocrystal and the solubility of FFA in FFA-ETZ cocrystal is found to be nearly same as that of FFA. The greater extent (~5 fold) of increment in the solubility of FFA was observed in FFA-CNB and FFA-ETZ cocrystal in 0.1 N HCl (pH=1) solution. There was no increment in the solubility of ETZ and CNB in the cocrystal was observed in both purified water and in 0.1N HCl solution. Further, all the synthesized cocrystals were found to be stable for a period of six months at ambient temperature (~25 °C) and accordingly, these cocrystals offer an opportunity to develop the new drug product with FFA, CNB, and ETZ drug molecules.

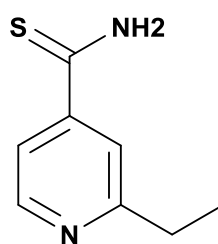
CHAPTER 3

***DESIGN, SYNTHESIS, CHARACTERIZATION, AND
EVALUATION OF PHYSICOCHEMICAL PROPERTIES
OF SALT OF ANTI-TUBERCULOSIS DRUG
ETHIONAMIDE***

This chapter describes the design and synthesis followed by structural characterization and study of physicochemical properties of ethionamide salt/cocrystal with GRAS counter ions. Physicochemical properties such as solubility and hygroscopicity study were performed and compared the results with parent ethionamide API.

3.1 INTRODUCTION

Ethionamide (ETH) (**Figure 3.1**) is an antibiotic used for the treatment of Tuberculosis (TB). ETH belongs to BCS Class II drug having poor aqueous solubility and high permeability. The solubility of ETH was estimated as 0.84 mg/mL in water media (drug bank). ETH is a second line anti-tuberculosis drug, an analog of isoniazid sold in the market under the brand name of Trecator or Trecator SC. The pharmacokinetic profile of the ETH hydrochloride salt (250 mg dosage) in humans shows a C_{max} value of 1.94 $\mu\text{g/mL}$ at T_{max} of 1.75 h. In another study, pharmacokinetics were reported upon administration with food, orange juice or antacids in healthy human volunteers (ETH free base, 500 mg dosage) and exhibited C_{max} 2.3 $\mu\text{g/mL}$ at T_{max} 1.70 h. However, in all these studies much differences were not observed in the administration of ETH drug.



Ethionamide (ETH)

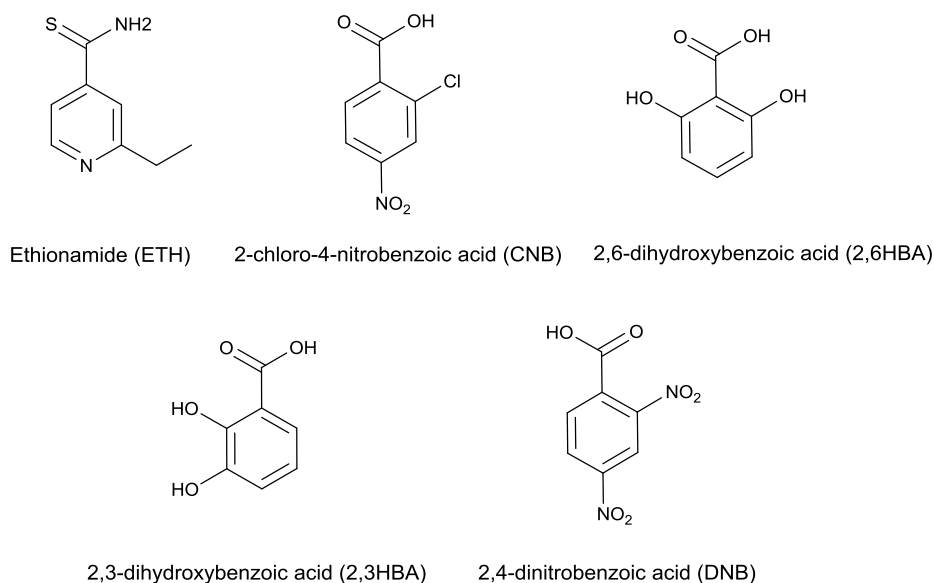
Figure 3.1: Molecular diagram of ethionamide (ETH).

ETH is used for the treatment of multi-drug resistant TB in combination with drugs like aminoglycoside, fluoroquinolone, isoniazid, pyrazinamide, rifampicin, ethambutol, and cycloserine to minimize the drug resistance. A combination of ETH and gatifloxacin, an antibiotic drug has also been proposed. Only one reformulation of ETH was developed in 2005 since the discovery in 1956, where a sugar-coated tablet

was replaced by a film-coated tablet. ETH is included in the list of WHO's most essential medicines needed in a basic health system.

Pharmaceutical salts and cocrystals of ETH drug molecule with various carboxylic acid cofomers have been reported in the literature. Cristiane et al. synthesized three molecular salts of ETH with saccharin, maleic acid, and oxalic acid. It was reported that ETH-maleate was highly soluble though it was less stable compared to pure ETH. Mannava et al. synthesized five cocrystals of ETH with glutaric acid, adipic acid, suberic acid, sebacic acid, fumaric acid and a salt of oxalic acid. The remarkable increment in the solubility of ETH was observed in ETH-oxalate salt. In all the reported molecular salt/cocrystal supramolecular neutral/charge assisted acid...pyridine heterosynthion was observed. Apart from neutral ETH structure, hexafluorosilicate, hydrochloride, nitrate and hydrobromide salts were reported. Though few cocrystal/salts of ETH are reported in the literature, however, a study on salt/cocrystal formation with benzoic acid derivatives were not witnessed in the literature. Thus, benzoic acid derivatives have chosen in the present work with the intention to increase the solubility of ETH drug molecule as hydroxybenzoic acids are more soluble than ETH in aqueous media.

In the present chapter, four molecular salts of ETH are reported. Molecular diagrams of ETH and the counter ions namely, 2-chloro-4-nitrobenzoic acid (CNB), 2,6-dihydroxybenzoic acid (2,6HBA), 2,3-dihydroxybenzoic acid (2,3HBA) and 2,4-dinitro benzoic acid (DNB) are shown in the **Scheme 3.1**. The counter ions are selected in the present study is based on their pKa values, further, these molecules are considered as GRAS molecules except DNB. CNB counter ion used in the present study is a potential anti-viral and anti-cancer agent exists as dimorph in the solid state. 2,3HBA and 2,6HBA are substituted hydroxybenzoic acids. 2,3HBA found in phyllanthus acidus fruit and in aquatic fern salvinia molesta. It is an iron-chelating drug and also has antimicrobial properties. It is also a product of human aspirin metabolism.



Scheme 3.1: Molecular diagrams of ETH and counter ions.

3.2 EXPERIMENTAL SECTION

3.2.1 Materials

Ethionamide was purchased from TCI Chemicals, Japan. 2-chloro-4-nitrobenzoic acid, 2,3-dihydroxybenzoic acid, 2,6-dihydroxybenzoic acid, and 2,4-dinitrobenzoic acid were purchased from Sigma-Aldrich. All the chemicals were used as such without any further purification. Analytical grade/HPLC grade solvents were used for the crystallization experiment. Deionized purified water was used in the experiments.

3.2.2 Synthesis by solvent evaporation method

All the molecular salts reported in the present study were synthesized by a solvent evaporation method in various solvents.

ETH-CNB salt: ETH (50 mg, 0.301 mmol) and CNB (60.62 mg, 0.301 mmol) were taken in 25 mL beaker and dissolved in 5 mL of methanol solvent at room temperature. This clear orange colored solution was then allowed for slow evaporation at room temperature. Block-shaped orange colored crystal was obtained in 1:1 molecular stoichiometry after 2 days.

ETH-2,6HBA salt: ETH (50 mg, 0.301 mmol) and 2,6HBA (46.39 mg, 0.301 mmol) were taken in 25 mL beaker, dissolved in 10 mL of methanol solvent at room

temperature. It was left for slow evaporation at ambient temperature. Block-shaped orange colored crystal was obtained after 4 days with 1:1 stoichiometry in the molecular salt.

ETH-2,3HBA salt: ETH (50 mg, 0.301 mmol) and 2,3HBA (46.39 mg, 0.301 mmol) were taken in 25 mL beaker, dissolved in 10 mL of methanol solvent at room temperature. This clear solution was then left for slow evaporation at ambient temperature. Block-shaped orange colored crystal was obtained after 4 days with 1:1 stoichiometry in the molecular salt.

ETH-DNB salt: ETH (50 mg, 0.301 mmol) and DNB (63.85 mg, 0.301 mmol) were taken in 25 mL beaker, dissolved in 10 mL of 5% water in ethanol solvent at 60 °C temperature. This clear solution was allowed for slow evaporation at room temperature. Block-shaped yellow colored crystal was obtained after 6 days with 1:1 stoichiometry in the molecular salt.

3.2.3 Thermogravimetric analysis (TGA): TGA analysis was performed on a PerkinElmer (TGA4000/Pyris6) instrument in a temperature range of 40 °C to 350 °C with a scan rate of 10 °C/minute under a continuously purged nitrogen atmosphere. For the analysis, weighed sample was kept on a ceramic crucible and scanned continuously from 40 °C to 350 °C.

3.2.4 Solubility study: Solubility measurements for ETH and the synthesized salts were performed on UV-Vis (Analytikjena Specord S600) Spectrometer in standard 3.5 mL quartz cells (2 optical windows) with a path length of 10 mm. The linearity of ETH drug molecule is performed in ACN solvent. Absorption maximum for ETH was observed at 291 nm. All the cofomer absorption maxima were clearly separating from the ETH maxima. Solubility measurement was done in 0.1 N HCl solution and in purified distilled water at ambient condition (~25 °C). For the experiment, an excess quantity of synthesized salt was taken in 2 mL of respective dissolution media (0.1 N HCl and water) and it was shaken for 40 hours in a mechanical shaker (ORBITEK, Scigenics biotech) at ambient temperature. Upon equilibrium, the sample was filtered through a 0.2 µm syringe filter, diluted sufficiently with acetonitrile solvent (using standard volumetric flask) and then the concentration of the sample was determined by UV-Vis spectroscopy. Dilution correction has been included in the calculation part.

3.3 RESULTS AND DISCUSSION

ETH is a weak base having pKa value of 5.0 (for pyridyl N). The difference in the pKa values for all the chosen counter ions was found to be above 3, thus it was expected that salt formation is favorable over cocrystal formation except for 2,3HBA salt former where the ΔpK_a value was found to be in between 0-3. The resultant product may be a salt or cocrystal. The prediction of salt/cocrystal is ambiguous in this case. The pKa and ΔpK_a values of ETH and the counter ions are listed in **Table 3.1**. Synthesized molecular salts in the present study were initially confirmed by determining their melting points and compared with their respective starting materials. All the synthesized salts were further characterized by FT-IR, PXRD, ^1H NMR and SC-XRD techniques.

Table 3.1: pKa & ΔpK_a values of ETH and counter ions.

API pKa1	Counter ion pKa2	ΔpK_a (pKa1-pKa2)	Molecular adducts formed
Ethionamide (ETH)- 5.0	CNB-1.96	3.04	Salt/cocrystal
	2,6HBA-1.30	3.70	Salt
	2,3HBA-2.91	2.09	Salt
	DNB-1.43	3.57	Salt

3.3.1 X-ray crystal structure of molecular salts

ETH-CNB: A 1:1 molecular salt/cocrystal of ETH-CNB was obtained in methanol solvent, which was crystallized in monoclinic crystal system with $P 2_1/n$ space group. Both charge assisted and neutral two point supramolecular heterosynthon was observed in this molecular components. This was further confirmed by the shift in CNC bond angle ($\angle 122.17^\circ$ for ionic and 119.83° for neutral supramolecular units). Primary synthon consists of one molecule each of neutral and charge assisted acid...pyridine heterosynthon with N-H...O bond distance of 2.573 Å, $\angle 171.96^\circ$ and 2.562 Å, $\angle 172.90^\circ$ respectively (**Figure 3.2**). Supramolecular unit of charge assisted acid...pyridine heterosynthon propagate in a 2D manner through N-H...O hydrogen bond (2.848 Å, $\angle 177.20^\circ$) involving -NH of thioamide group of ETH and O of a carboxylic acid group of CNB (**Figure 3.3**). Two neighboring neutral acid...pyridine supramolecular units interconnected through strong complementary N-H...O hydrogen bond (2.883 Å,

$\angle 171.20^\circ$) involving $-\text{NH}$ of thioamide group of ETH and O of a carboxyl group of CNB and weak $\text{C-H}\cdots\text{O}$ hydrogen bond between ETH and CNB (3.216 Å) resulted in a cyclic tetrameric unit (**Figure 3.4**). This neutral tetrameric unit is connected to the charge assisted supramolecular units through thionamide homo dimer ($\text{N-H}\cdots\text{S}$ distance of 3.379 Å, $\angle 156.60^\circ$ and 3.612 Å, 174.11°), $\text{C-H}\cdots\text{O}$ hydrogen bond (3.511 Å) between aromatic C-H of ETH and O of nitro group of CNB and two unlike $\text{C-H}\cdots\text{O}$ hydrogen bond between nitro group of CNB with aromatic C-H of ETH (3.386 Å) and methyl C-H of ETH (3.431 Å) (**Figure 3.5**). The overall crystal structure features weak interactions involved with methyl group of ETH and sulfur atom of an amide group. The unusual behavior of the salt/cocrystal continuum may be explained based on the hydrogen bond associated with ETH molecules. It was observed that in the cocrystal adduct secondary interactions associated with 6th C-H proton of ETH experiences only weak hydrogen bond with O of nitro group (3.511 Å), however in salt adduct both 5th and 6th C-H protons of ETH are involved in hydrogen bond formation (3.264 Å, 3.489 Å and 3.386 Å) comparatively stronger than the previous one which makes the electronic environment of the pyridine nitrogen to be more polar leading to a state of ionic and molecular character for these type of interactions. Crystal structure details and the geometrical parameters of intermolecular interactions are displayed in **Table 3.2** and **Table 3.3** respectively. Color code for the atoms are gray: carbon; off-white: hydrogen; red: oxygen; blue: nitrogen; yellow: sulfur, green: chlorine.

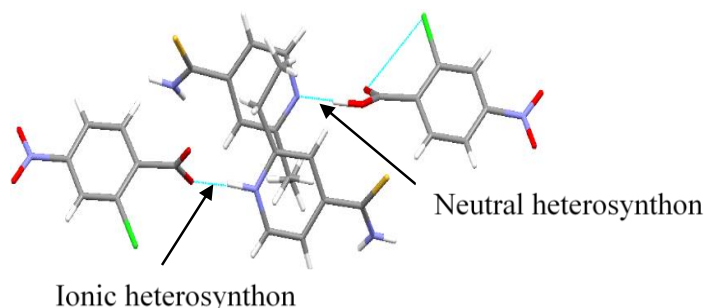


Figure 3.2: Asymmetric unit in ETH-CN B salt/cocrystal.

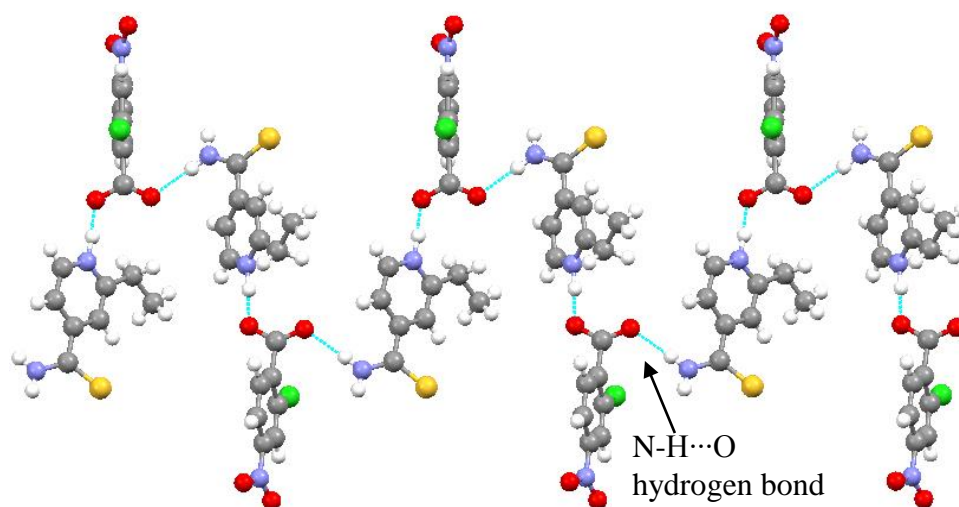


Figure 3.3: 2D representation of ETH-CNB salt.

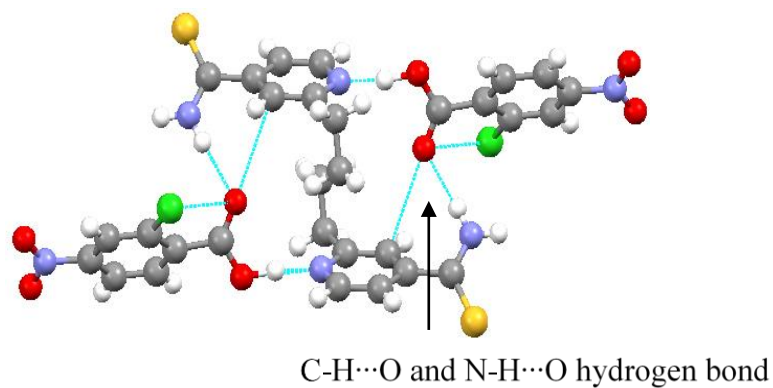


Figure 3.4: Tetrameric unit of ETH-CNB cocrystal.

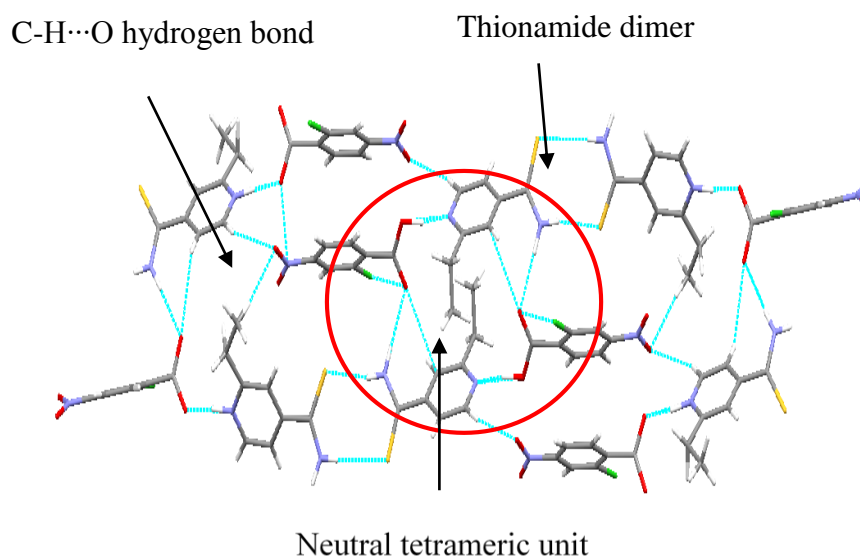


Figure 3.5: 2D propagation of ETH-CNB salt/cocrystal.

Table 3.2: Crystal structure details and the refinement parameters of ETH salts.

structure details	ETH-CNB	ETH-2,6HBA	ETH-2,3HBA	ETH-DNB
CCDC number	1477880	1477881	1477884	1477889
Mol. formula	C ₁₅ H ₁₄ ClN ₃ O ₄ S	C ₁₅ H ₁₆ N ₂ O ₄ S	C ₁₅ H ₁₆ N ₂ O ₄ S	C ₁₅ H ₁₄ N ₄ O ₆ S
Molar mass	367.80	320.36	320.36	378.36
crystal system	Monoclinic	Triclinic	Triclinic	Triclinic
Space group	P 2 ₁ /n	P $\bar{1}$	P $\bar{1}$	P $\bar{1}$
a / Å	14.1353(4)	7.3114(3)	7.2867(9)	11.0451(17)
b / Å	13.1242(4)	9.9448(3)	8.1683(9)	12.9511(19)
c / Å	18.4453(6)	11.5288(3)	13.3084(17)	12.9889(18)
α / °	90	70.7830(10)	99.587(6)	68.582(7)
β / °	102.334(2)	85.1230(10)	94.081(6)	81.187(7)
γ / °	90	70.4330(10)	103.911(6)	86.584(7)
Volume/ Å ³	3342.89(18)	745.54(4)	753.01(16)	1709.3(4)
Z	8	2	2	4
Density [g/cm ³]	1.462	1.427	1.413	1.470
μ (MoK α) [mm ⁻¹]	0.378	0.237	0.235	0.231
T/K	296 (2)	296 (2)	296 (2)	296 (2)
Reflns collected	5883	2911	2918	6556
Unique rflns	5223	2670	2450	5080
Parameter refined	515	263	252	551
R ₁ (I > 2 σ)	0.0369	0.0360	0.1163	0.0595
wR ₂ (I > 2 σ)	0.1149	0.0983	0.3412	0.1719
GOF	0.836	0.669	1.135	1.218

Table 3.3: Geometrical parameters of intermolecular interactions in ETH salts.

Salt	D-H...A ^a	H...A/ Å	D...A/ Å	<D-H...A/ °	Symmetry code
ETH-CNB	N4-H2...O1	1.985	2.883	171.05	-x+1, -y+1, -z+1
	N4-H1...S1	2.529	3.379	156.53	x+1/2, -y+1/2, z-1/2
	C15-H5...O4	2.555	3.511	160.79	x-1, y, z
	N3-H10...O5	1.977	2.848	177.30	-x+1/2, y+1/2, -z+3/2
	N3-H9...S2	2.763	3.612	174.16	x-1/2, -y+1/2, z+1/2
	C7-H7...O4	2.657	3.464	144.38	x-1/2, -y+1/2, z+1/2
	C8-H8...O7	2.569	3.386	148.63	x, y, z
	N1-H11...O6	1.515	2.562	172.37	x, y, z
	C20-H14...S1	2.891	3.756	155.78	x+1, y, z
	C27-H16...S2	3.025	3.816	146.19	x+1/2, -y+1/2, z+1/2
O2-H19...N2	1.480	2.573	171.53	x+1, y, z	
ETH- 2,6HBA	N2-H1...O3	2.088	2.837	143.66	x, y, z-1
	C3-H3...O4	2.441	3.376	164.79	x, y-1, z
	C4-H4...O1	2.619	3.280	128.10	x, y, z
	N2-H2...S1	2.665	3.457	156.70	-x+1, -y, -z
	O3-H12...O1	1.601	2.480	160.52	x, y, z
	N1-H5...O1	2.549	3.223	125.37	x, y, z
	N1-H5...O2	1.656	2.642	175.52	x, y, z
O4-H13...O2	1.727	2.557	150.55	x, y, z	
ETH- 2,3HBA	C12-H11...O3	2.416	3.120	128.52	x, y-1, z
	C12-H11...O1	2.250	2.984	130.93	x, y, z
	N1-H12...O2	2.017	2.845	155.43	x, y, z
	N1-H12...O1	2.413	3.052	129.46	x, y, z
	C14-H6...O2	2.550	3.290	146.88	x, y, z
	O2-H16...O3	1.613	2.475	152.85	x, y, z
	O1-H13...O4	1.800	2.637	177.55	x, y-1, z
	N2-H9...O4	1.825	2.835	176.72	-x+1, -y+1, -z+1
	N2-H8...S1	2.719	3.401	148.33	-x+1, -y, -z+2

ETH-DNB	C9-H4...O00D	2.657	3.401	133.74	-x+2, -y+1, -z+1
	C19-H21...O5	2.521	3.384	150.45	x, y+1, z-1
	C26-H6...S2	2.893	3.771	155.11	-x+1, -y+1, -z+2
	N8-H9...S2	2.546	3.462	170.33	-x+1, -y+1, -z+2
	N8-H8...O10	1.949	2.809	176.80	-x+1, -y+1, -z+1
	C15-H14...O9	2.447	3.189	135.21	x, y, z
	C16-H22...O9	2.536	3.269	140.54	-x+2, -y+1, -z+1
	C16-H22...O3	2.648	3.365	138.69	x+1, y, z
	C14-H12...O2	2.457	3.407	174.31	-x+1, -y+2, -z
	N2-H13...O10	2.427	3.060	121.43	x, y, z
	N2-H13...O11	1.715	2.680	164.60	x, y, z
	N1-H15...O8	1.508	2.549	175.30	x, y, z
	C21-H17...O5	2.527	3.340	142.40	-x+2, -y+1, -z+2
	N7-H23...O11	2.068	2.911	155.32	x, y, z
N7-H24...S1	2.592	3.415	172.31	-x+2, -y+2, -z	

^a D-donor, A-acceptor

ETH-2,6HBA: A 1:1 molecular salt of ETH and 2,6HBA resulted in methanol solvent at ambient temperature by solvent evaporation method which belongs to triclinic crystal system with space group $P\bar{1}$. Primary synthon in the molecular salt consists of four point supramolecular synthon in which proton transfer from 2,6HBA to ETH was observed (**Figure 3.6**). Ion pairs are linked through strong N-H...O hydrogen bond (2.642 Å, $\angle 175.63^\circ$ and 3.223 Å, $\angle 125.29^\circ$) and weak C-H...O hydrogen bond (3.280 Å, $\angle 128.41^\circ$ and 3.302 Å, $\angle 128.34^\circ$). Intramolecular O-H...O hydrogen bond is observed in 2,6HBA. Neighboring supramolecular units are interconnected through strong N-H...O hydrogen bond (2.837 Å) and weak C-H...O hydrogen bond (3.376 Å) resulted in a cyclic six components supramolecular unit (**Figure 3.7**) which further extends to give 1D sheet-like structure of ETH-2,6HBA molecular salt (**Figure 3.8**). The 1D sheet further extends to the 3D sheet through thionamide homo dimer with complementary N-H...S interaction with a bond distance of 3.457 Å. The crystal structure features π - π interaction between ETH and 2,6HBA with centroid to centroid distance of 3.705 Å.

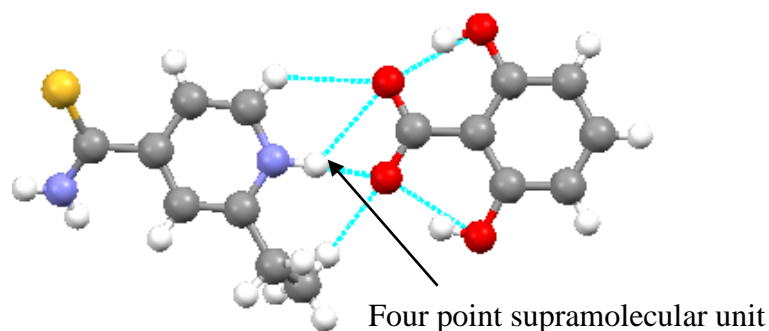


Figure 3.6: Asymmetric unit in the molecular salt of ETH-2,6HBA salt.

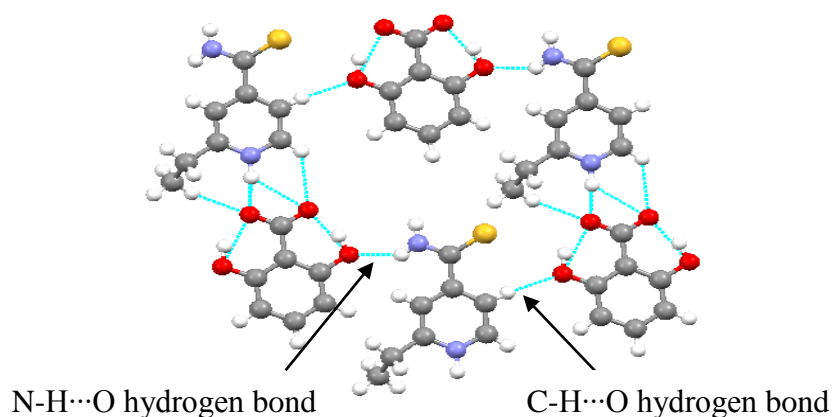


Figure 3.7: Six component supramolecular unit in ETH-2,6HBA salt.

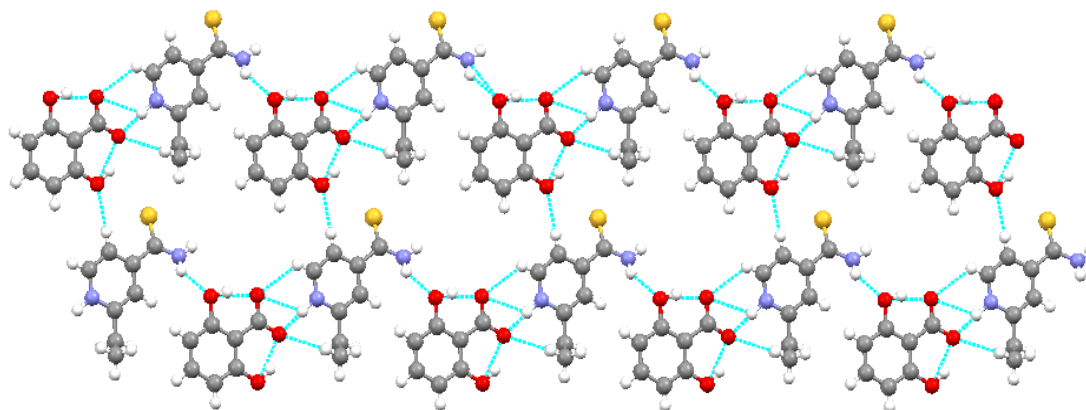


Figure 3.8: 1D tape-like structure of ETH-2,6HBA salt.

ETH-2,3HBA: A 1:1 molecular salt of ETH-2,3HBA was obtained in methanol solvent by a solvent evaporation method, which belongs to triclinic crystal system with space group $P\bar{1}$. Primary synthon in the molecular salt consists of one molecule each of ETH and 2,3HBA in which four point supramolecular synthon between ETH and 2,3HBA was observed (**Figure 3.9**). The ion pairs are connected through strong N-H...O

hydrogen bond (N1-H12...O2 distance 2.845 Å, $\angle 155.90^\circ$ and N1-H12...O1 distance of 3.051 Å, $\angle 129.22^\circ$) between the hydroxyl group of 2,3HBA and pyridyl N of ETH and weak C-H...O hydrogen bonds (C12H11...O1 bond distance of 2.983 Å and C14H6...O2 bond distance of 3.290 Å). Two neighboring molecular adducts interconnected through strong O-H...O hydrogen bond (2.636 Å, $\angle 177.22^\circ$) involving hydroxyl group of 2,3HBA and carboxylic acid group of 2,3HBA resulted in a linear 1D tape-like structure of ETH-2,3HBA salt (**Figure 3.10**). The 1D tape is further extended to 2D tape through weak complementary supramolecular thionamide-thionamide homosynthon (N-H...S distance of 3.400 Å) of ETH (**Figure 3.11**). 2D tape extends to 3D tape through strong N-H...O hydrogen bond (2.835 Å, $\angle 176.17^\circ$) involving amide -NH and carboxylic acid group of 2,3HBA. The crystal structure also features weak C-H...O hydrogen bond (3.290 Å) between a -CH₂ group of ETH and Oxygen of ortho hydroxyl group of 2,3HBA & π - π interaction between ETH and 2,3HBA (3.389 Å).

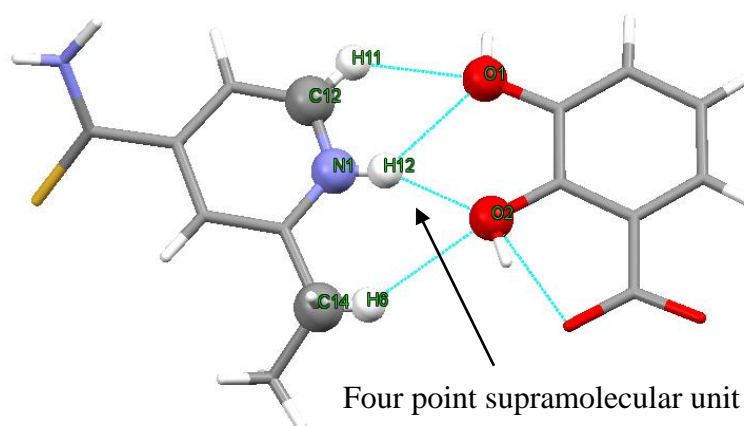


Figure 3.9: Asymmetric unit in the molecular salt of ETH-2,3HBA.

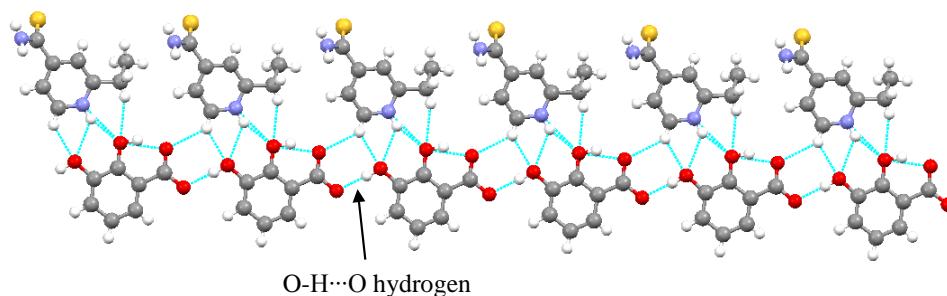


Figure 3.10: 1D tape-like structure of ETH-2,3HBA salt.

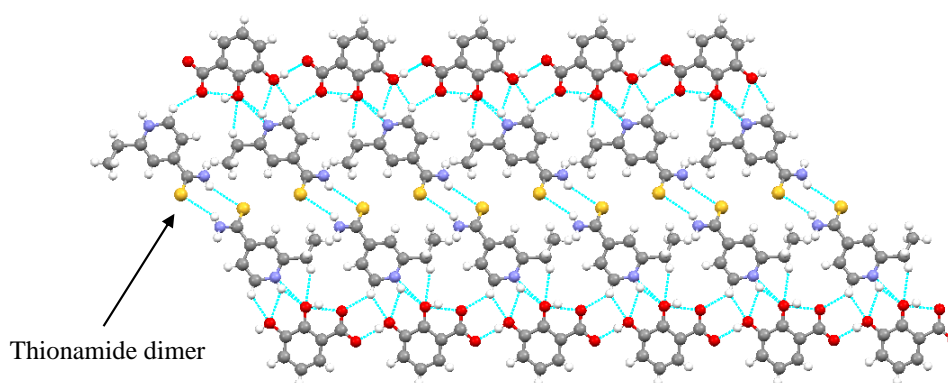


Figure 3.11: 2D structure of ETH-2,3HBA salt stabilized by thioamide dimer.

ETH-DNB: A 1:1 molecular salt of ETH-DNB was yielded by a solvent evaporation method in 5% water in ethanol solvent, which belongs to triclinic crystal system with $P\bar{1}$ space group. The molecular salt exhibited 1:1 stoichiometry in the asymmetric unit. Two distinct hydrogen bond ring motifs are observed in this molecular salt. i.e., both partial and complete proton transfer was observed in this molecular salt which was reflected in the two different N-H \cdots O hydrogen bond distance. A change in C-N-C bond angle ($\angle 122.87^\circ$ and $\angle 120.93^\circ$) was observed when compared to neutral ETH molecule (118.24°) further substantiates the existence of partial and complete proton transfer. The primary synthon consists of both two point and three point supramolecular synthon in which proton transfer from DNB to ETH was observed. The ion pairs are linked through charge assisted N-H \cdots O hydrogen bond (N-H \cdots O bond distance of 2.680 Å, $\angle 164.33^\circ$ & 3.060 Å, $\angle 121.19^\circ$ and 2.549 Å, $\angle 175.45^\circ$ & 3.360 Å, $\angle 120.62^\circ$) (**Figure 3.12**). Adjacent supramolecular units are interconnected through weak complementary C-H \cdots O hydrogen bond (3.340 Å) between ETH (-CH₂ group) and DNB (O of 4-nitro group) for partially ionic supramolecular unit and for completely ionic supramolecular unit, adjoining molecular adducts are interconnected through complementary C-H \cdots O hydrogen bond (3.407 Å) between aromatic C-H of ETH and 4-nitro group of DNB. These supramolecular units are further connected through strong N-H \cdots O hydrogen bond (2.912 Å) and weak C-H \cdots S hydrogen bond (3.804 Å) (**Figure 3.13**). The molecular units extend in 3D supramolecular architect through thioamide \cdots thioamide homo dimer (N-H \cdots S distance of 3.462 Å for completely ionic and 3.415 Å for partially ionic). The crystal structure features weak interactions involved with both nitro group

of DNB and C-H group of ETH. The π - π interaction between DNB was observed with centroid to centroid distance of 3.375 Å.

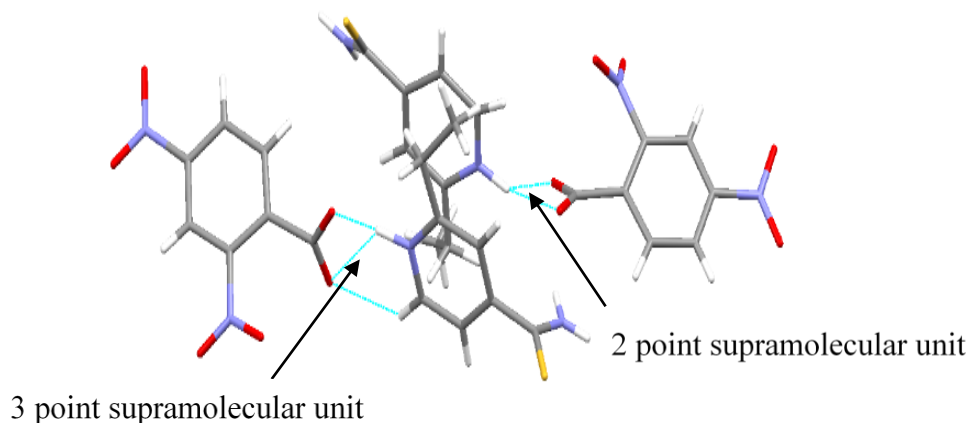


Figure 3.12: Asymmetric unit in the molecular salt of ETH-DNB.

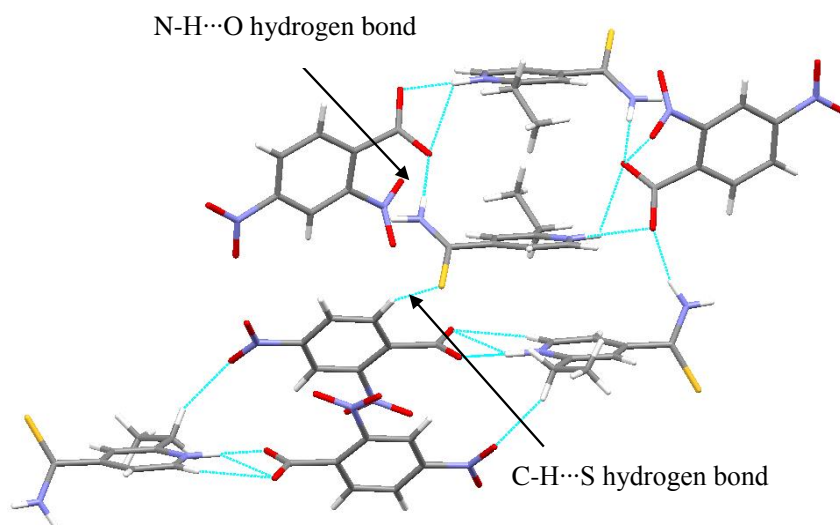


Figure 3.13: Tetrameric unit of ETH-DNB salt interconnected through N-H...O and weak C-H...S hydrogen bond.

3.3.2 Conformational analysis of molecular salts

Drug molecules are generally flexible and it can adopt different orientations or conformations based on the interactions (hydrogen bond), steric effect and the crystal packing of the molecule. These conformational changes can greatly influence the physicochemical properties of the crystal. Conformational changes were observed in all the molecular salts (**Figure 3.14**). Similar kind of conformational changes was observed for ETH-2,6HBA and ETH-DNB. However, different conformations were

observed for ETH-CNB and ETH-2,3HBA when compared to ETH drug conformation (Torsion angles are displayed in **Table 3.4**).

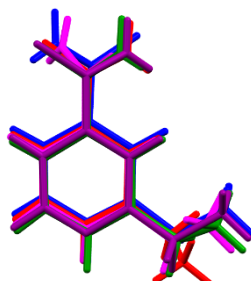


Figure 3.14: Overlay of ETH molecule extracted from the crystal structure of neutral ETH and the molecular salts. Purple= ETH, Blue=ETH-CNB, Red=ETH-2,6HBA, Magenta=ETH-2,3HBA and Green=ETH-DNB.

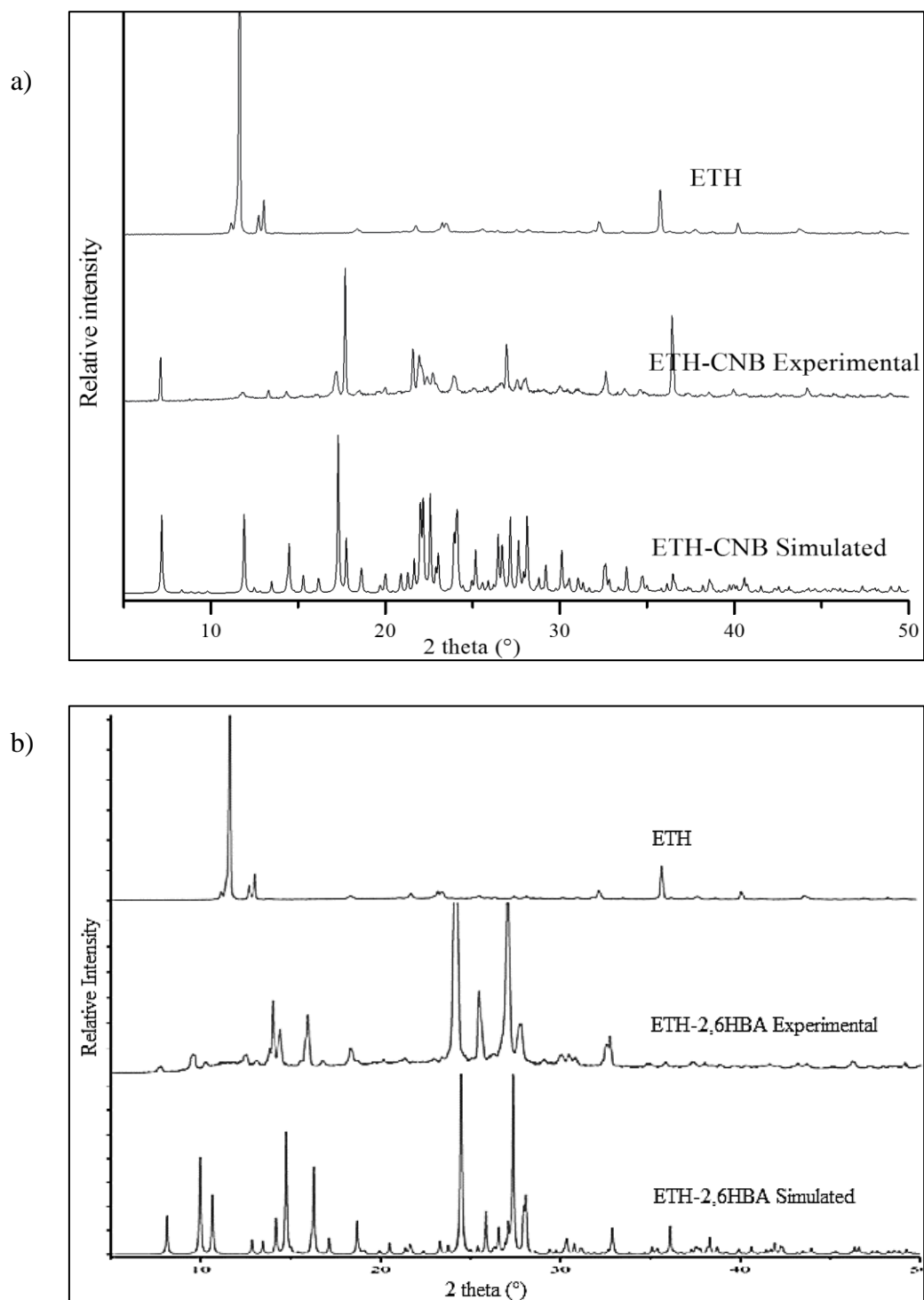
Table 3.4: Torsion angles of ETH molecule in neutral ETH and in the molecular salts.

τ_1 N1-C2-C10-C11, τ_2 C11-C10-C2-C3, τ_3 C3-C4-C5-S8, τ_4 C3-C4-C5-N9				
Molecular components	τ_1	τ_2	τ_3	τ_4
ETH	177.78	-3.35	164.11	-159.66
ETH-CNB	179.14	-0.80	-144.50	165.89
ETH-2,6HBA	-70.84	110.65	-161.40	157.55
ETH-2,3HBA	-145.01	34.47	140.72	-160.91
ETH-DNB	-127.72	51.84	-157.15	150.04

3.3.3 PXRD analysis

The PXRD analysis is generally used for the identification of new crystalline phase/polymorphic form of a crystalline material. In the present study, PXRD analysis

was carried out to confirm the formation of new crystalline adducts as well as to confirm the bulk purity of the synthesized molecular salts. All the molecular salts synthesized in the present study displayed diffraction patterns which are in good agreement with the simulated diffraction patterns obtained single crystal XRD analysis demonstrating the bulk purity of the molecular salts (**Figure 3.15**).



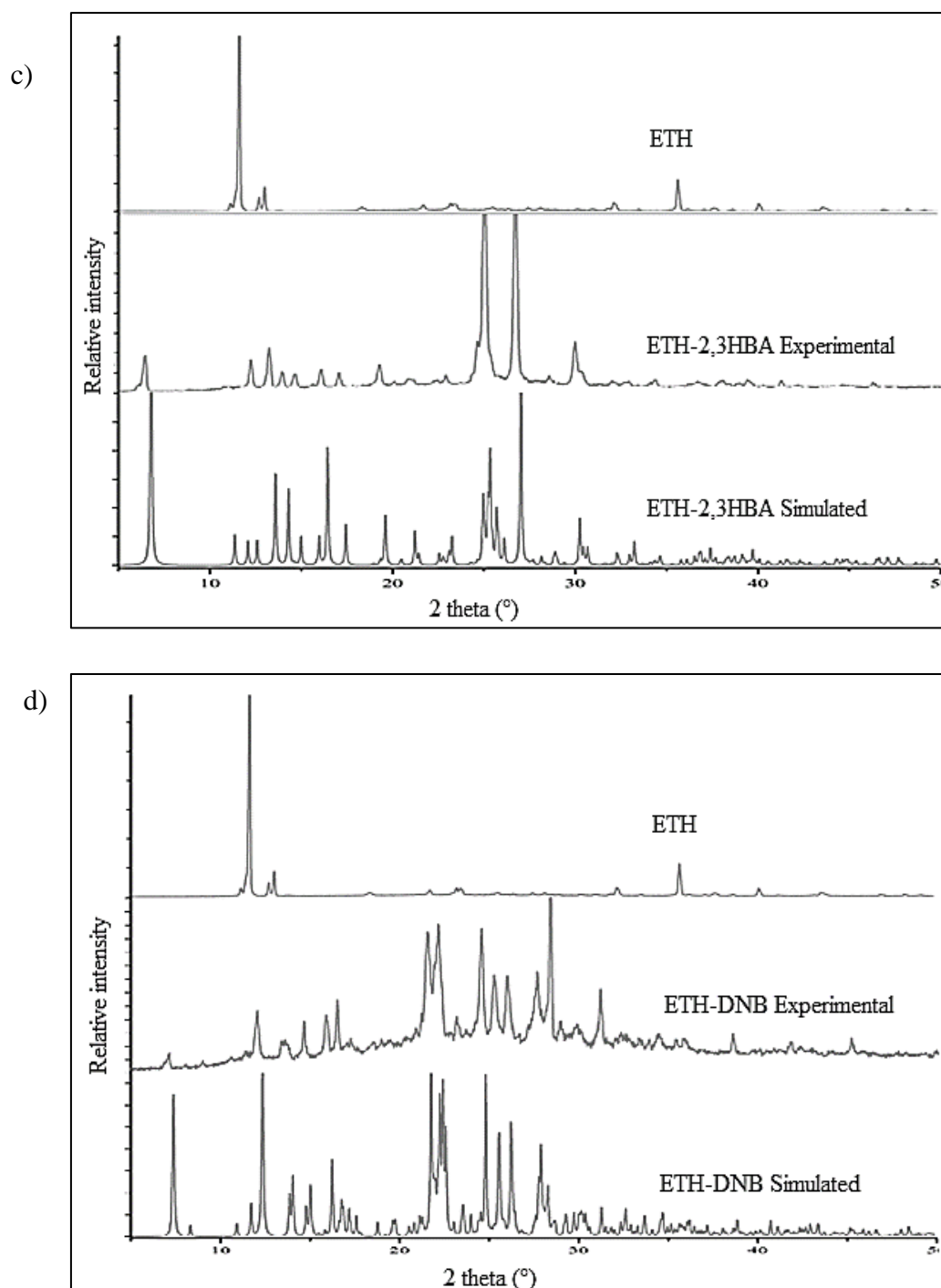
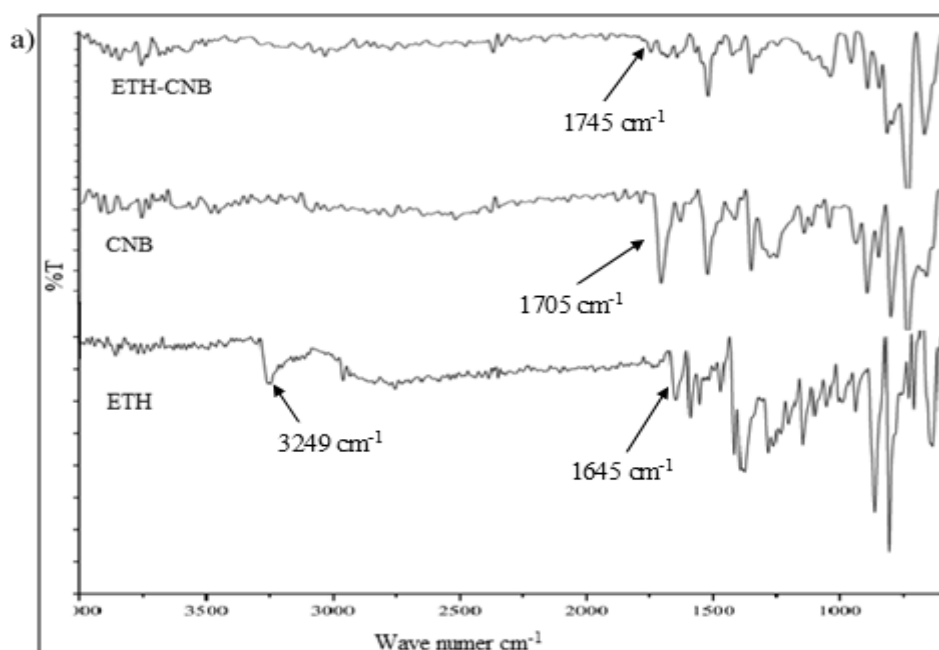


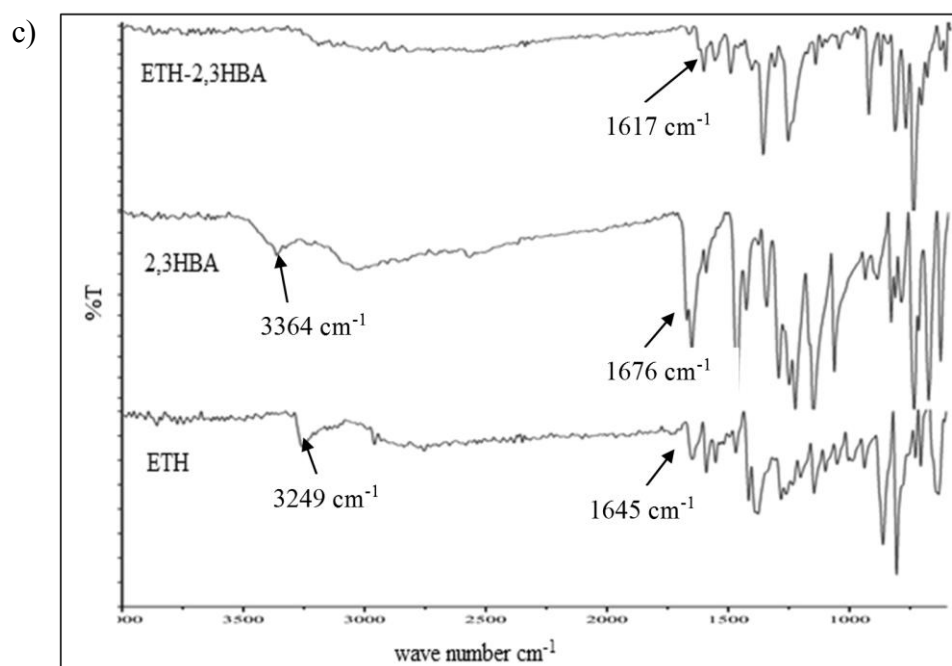
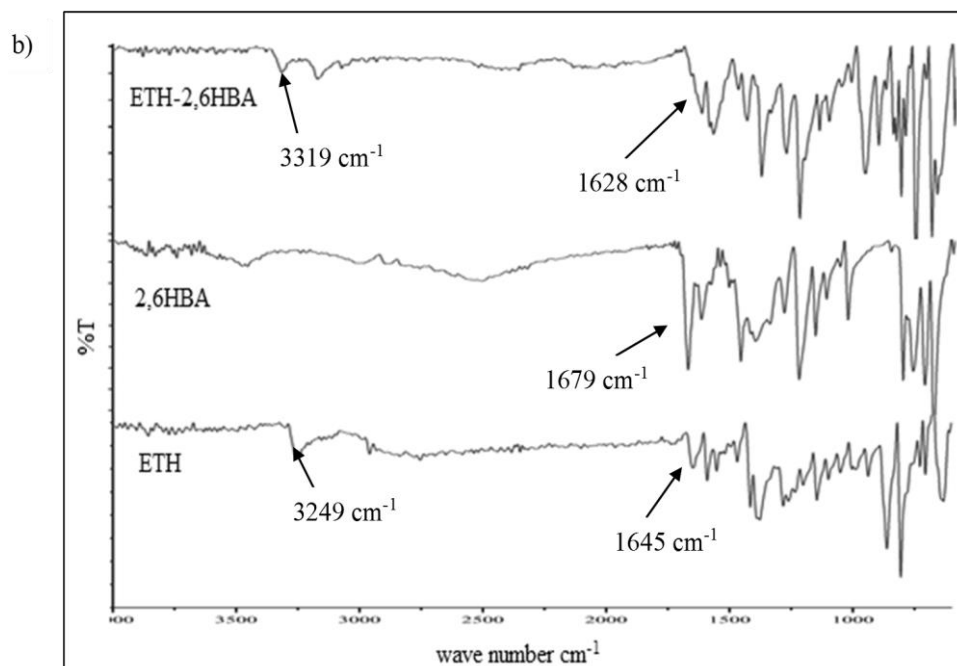
Figure 3.15: Comparison of simulated and experimental PXRD patterns of a) ETH-CNB b) ETH-2,6HBA c) ETH-2,3HBA and d) ETH-DNB salts.

3.3.4 Spectroscopic analysis of molecular salts

3.3.4.1 FT-IR spectroscopy

All the synthesized molecular salts were analyzed by FT-IR spectroscopy in order to confirm the formation of molecular salts. FT-IR spectra of molecular salts were compared with their respective starting materials in order to confirm the salt formation. All the molecular salts exhibited a change in carbonyl stretching frequency of acid group with respect to their starting material. Thionamide functional group of ETH appeared at 1648 cm^{-1} , -NH stretching frequency appeared at 3249 cm^{-1} . In all the synthesized molecular salts, a significant shift of carbonyl (-C=O) stretching frequency was observed except for ETH-CNB where both salt/cocrystal was observed. In ETH-CNB carbonyl stretching frequency was appeared at 1745 cm^{-1} and for ETH-2,6HBA, ETH-2,3HBA & ETH-DNB molecular salts carboxylate stretching frequency appeared at 1628 cm^{-1} , 1617 cm^{-1} and 1633 cm^{-1} respectively (FT-IR spectra with stretching frequencies are displayed in **Figure 3.16** & **Table 3.5**).





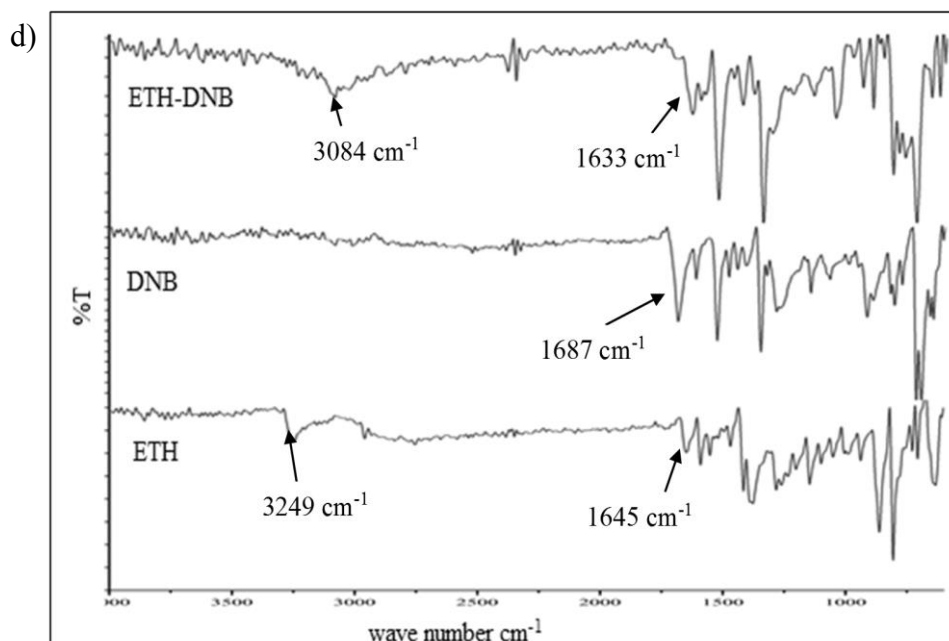


Figure 3.16: FT-IR comparison spectra of a) ETH-CNB b) ETH-2,6HBA c) ETH-2,3HBA and d) ETH-DNB salts.

Table 3.5: FT-IR stretching frequencies of ETH, salt former and the salts.

Crystal forms	-C=S amide stretch (cm ⁻¹)	-NH/-OH stretch (cm ⁻¹)	-C=O stretching of acid (cm ⁻¹)
ETH	1645	3249	
ETH-CNB	1642	-	1745
ETH-2,6HBA	1599	3319	1628
ETH-2,3HBA	1570		1617
ETH-DNB	-	3084	1633
CNB	-	-	1705
2,6HBA	-	-	1679
2,3HBA	-	3364	1676
DNB	-	-	1687

3.3.4.2 ¹H NMR spectroscopy

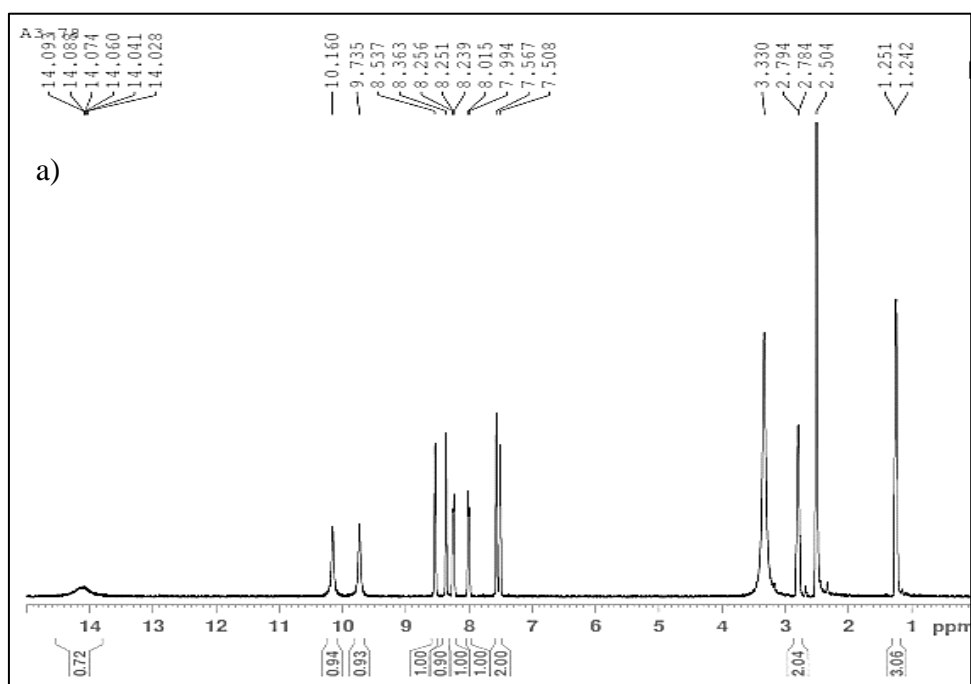
¹H NMR spectrum of synthesized molecular salts revealed that all the molecular salts demonstrated 1:1 molecular stoichiometry in the asymmetric unit. The chemical shift δ and the coupling constant J values of the molecular salts are displayed below. ¹H NMR spectrum of molecular salts are displayed in **Figure 3.17**.

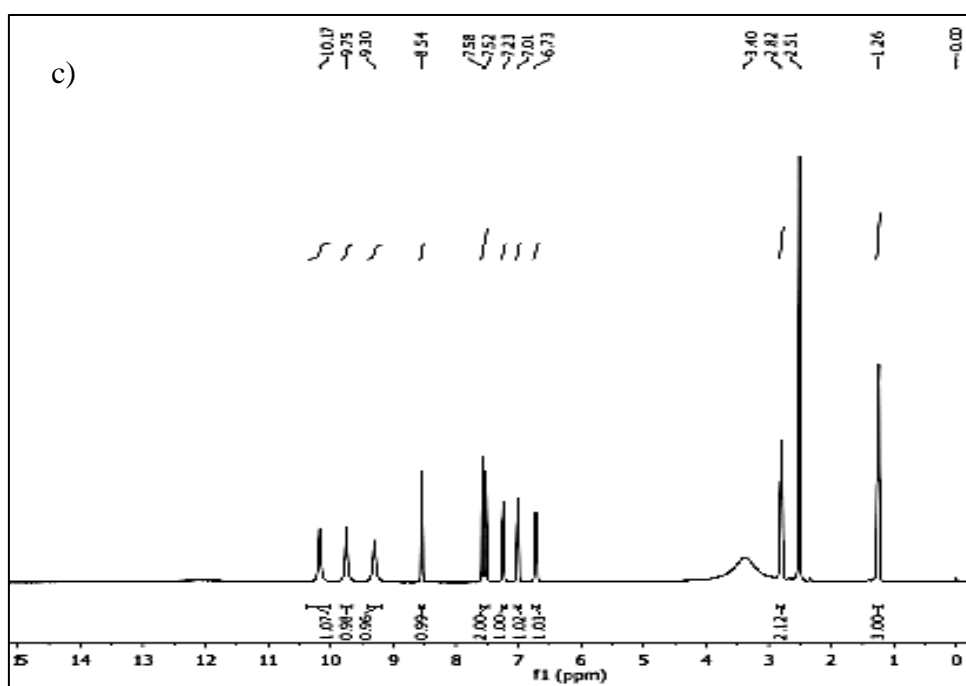
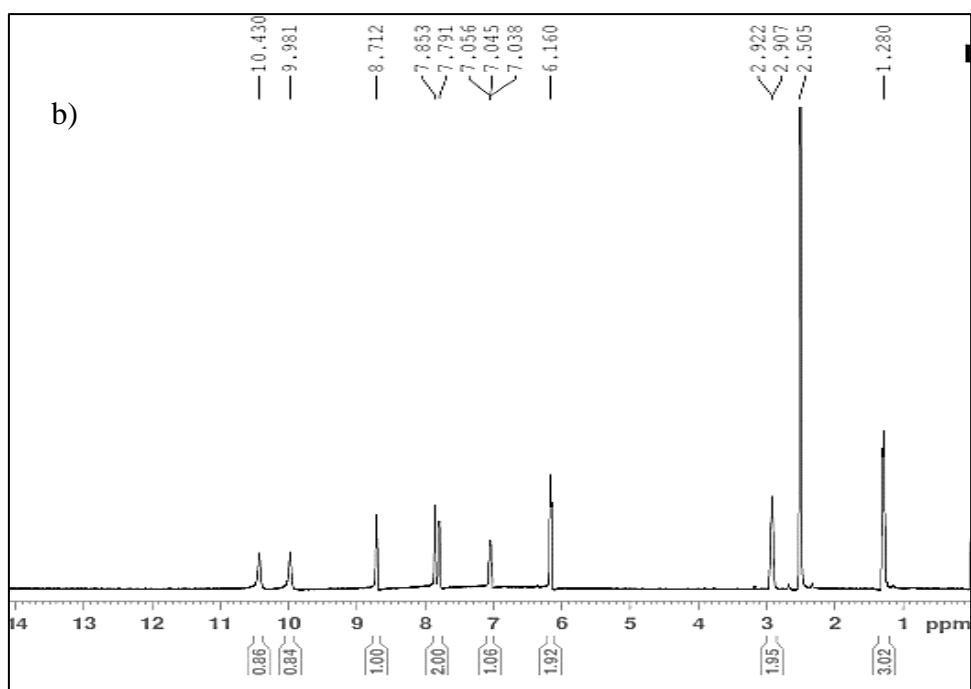
ETH-CNB (DMSO-d₆, 400 MHz, δ ppm): 14.09 (1H, s), 10.160 (1H, s), 9.735 (1H, s), 8.537 (1H, s), 8.363(1H, s), 8.256-8.239 (1H, t), 8.015-7.994 (1H, d (J=8.4 Hz)), 7.567 (1H, s), 7.508 (1H, s), 2.794-2.784 (2H, q) 1.251-1.242 (3H, t).

ETZ-2,6HBA (DMSO-d₆, 400 MHz, δ ppm): 10.43 (1H, s), 9.981 (1H, s), 8.712 (1H, s), 7.853 (1H, s), 7.791 (1H, s), 7.056-7.038 (1H, t), 6.160 (2H, s), 2.922-2.907 (2H, q), 1.280 (3H, s).

ETH-2,3HBA (DMSO-d₆, 400 MHz, δ ppm): 10.17 (1H, s), 9.74 (1H, s), 9.30 (1H, s), 7.58-7.52 (2H, d), 7.21 (1H, s), 7.08 (1H, s), 6.73 (1H, s), 2.84 (2H, s), 1.26 (3H, s).

ETH-DNB (DMSO-d₆, 300 MHz, δ ppm): 10.18 (1H, s), 9.75 (1H, s), 8.79 (1H, s), 8.60-8.53 (2H, m), 8.13-8.10 (1H, d (J=9 Hz)), 7.57 (1H, s), 7.52-7.51 (1H, d (J=3 Hz)), 2.83-2.76 (2H, q (J=6 Hz)), 1.27-1.22 (3H, t (J=6 Hz)).





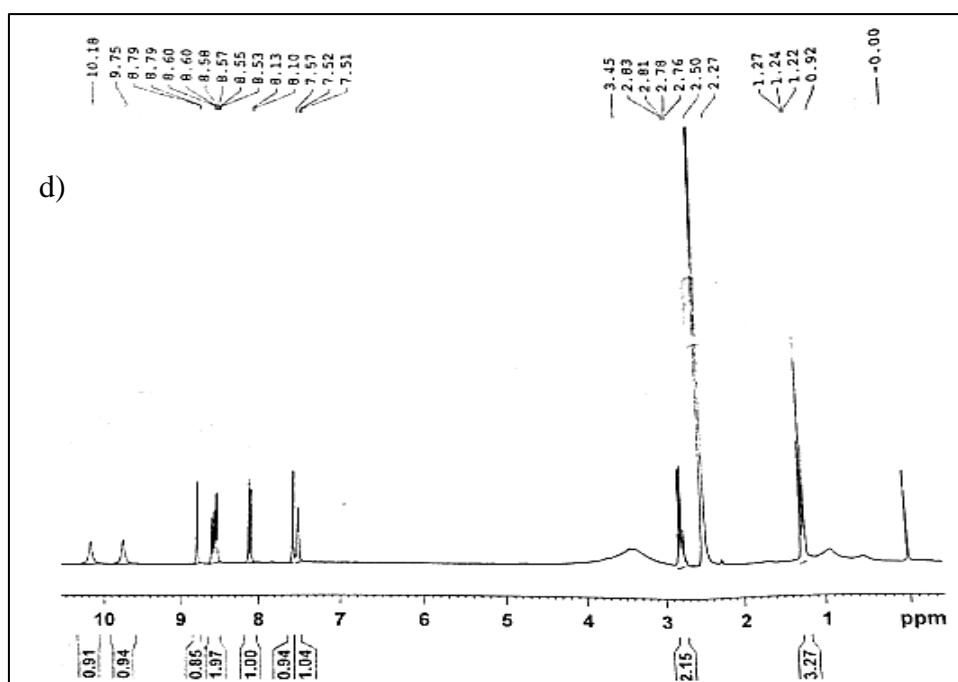


Figure 3.17: ^1H NMR spectra of a) ETH-CNB b) ETH-2,6HBA c) ETH-2,3HBA and d) ETH-DNB salts.

3.3.5 Thermal analysis

DSC technique is useful for the observation of fusion and recrystallization events. In the present study, DSC analysis was carried out to study the thermal behavior of the molecular salts. The melting point of ETH, synthesized molecular salts and the counter ions are displayed in **Table 3.6**. ETH exhibited two sharp melting point at 163.26°C and 165.17°C , however, the phase purity of ETH was confirmed with the reported single crystal structure of ETH. ETH-2,6HBA and ETH-2,3HBA melt near to the melting point of ETH whereas ETH-CNB melts just below the melting temperature of CNB. It was unexpected that the melting point of ETH-DNB salt was well below the melting of their respective starting materials even though a greater number of secondary interactions are involved in crystal formation. This lower melting of ETH-DNB salt is correlated with primary and secondary interactions involved in the molecular salts. It was observed that when compared to ETH-CNB and ETH-2,6HBA primary interactions were found to be weak, further, secondary interactions associated with ETH-DNB salt was found to be weaker as well. This may be the reason for lower melting of ETH-DNB salt. ETH-2,3HBA salt is not taken for comparison as it is formed through hydroxyl \cdots pyridine heterosynthon. ETH-2,6HBA and ETH-2,3HBA salt was

found to be dissociating after the melting of salts, whereas ETH-CNB and ETH-DNB were found to be stable at a temperature of 200 °C. In all the synthesized salts single endothermic peak was observed, which was confirmed the phase purity and homogeneity of the molecular salts (DSC plot is displayed in **Figure 3.18**).

Table 3.6: Melting point of ETH, counter ions and molecular salts.

API mp (°C)	Counter ion mp (°C)	Salt mp (°C)	Primary N-H...O bond distance (Å)
ETH (163.26 and 165.17)	CNB (148.04)	146.59	2.573, 2.562
	2,6HBA (171.75)	160.17	2.642
	2,3HBA (212.68)	163.19	2.845, 3.051
	DNB (187.90)	128.75	2.680, 3.060

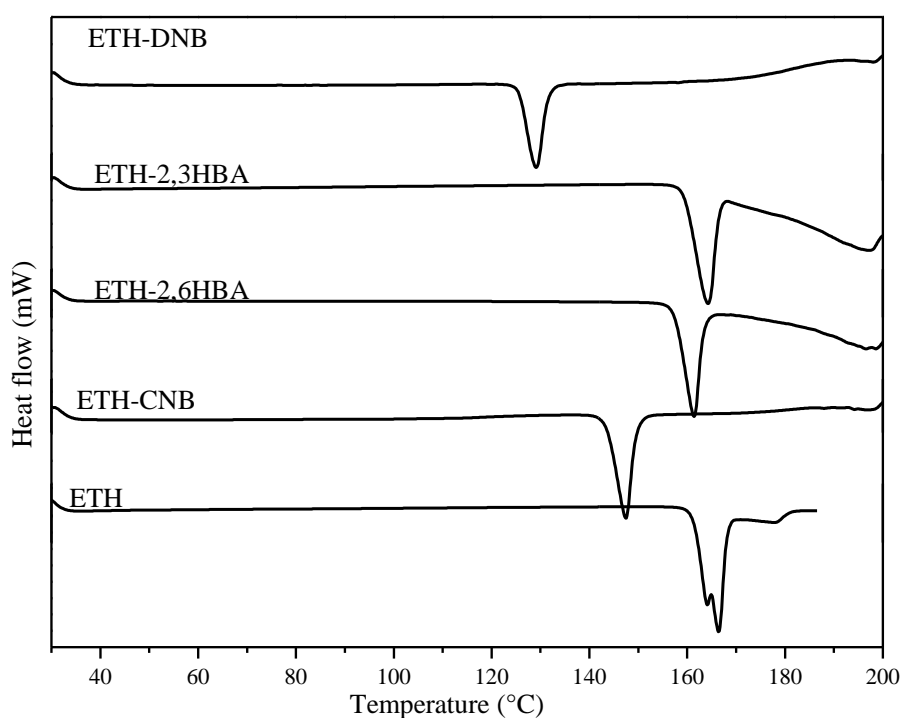
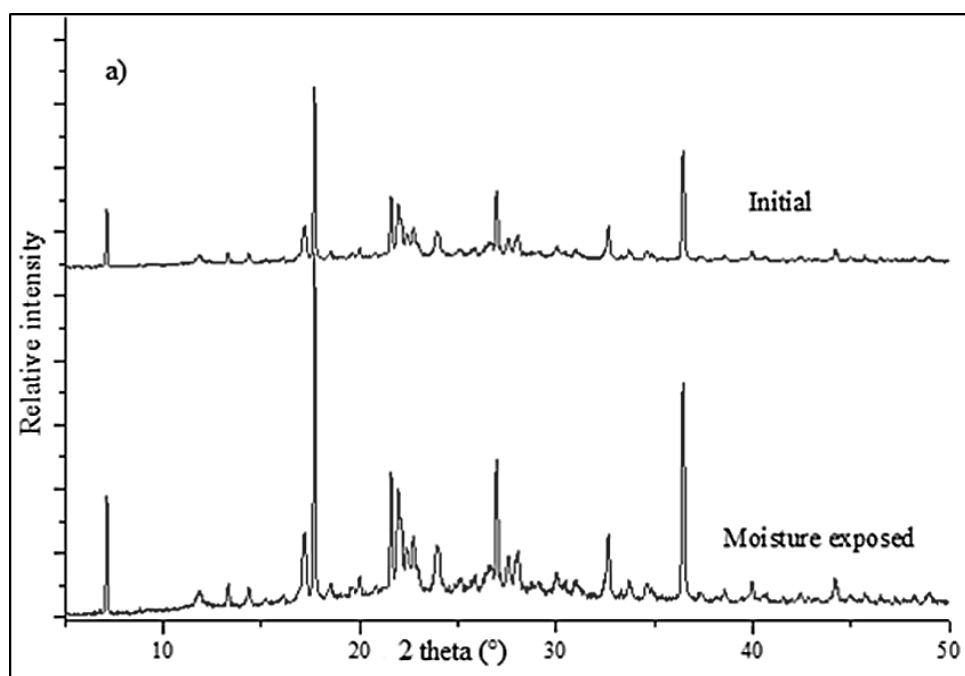


Figure 3.18: DSC plots of ETH salts in comparison with ETH.

3.3.6 Hygroscopicity study

Owing to the pharmaceutical importance of synthesized molecular salts, the hygroscopicity of the salts were determined in the present study by conventional weight loss method at the accelerated condition. i.e., a known quality of the sample was kept in a desiccator which was filled with saturated sodium chloride solution in order to

attain the relative humidity of ~75% for a period of seven days. The weight of the sample was monitored periodically and finally, the hygroscopicity was measured based on the gain in weight of the sample. In the present study ETH-CNB, ETH-2,6HBA and ETH-2,3HBA hygroscopicity were measured and it was found that all the three salts were non-hygroscopic at ~75% RH. It was further confirmed by PXRD and TGA analysis. In PXRD analysis, there was no variation/changes in the diffraction pattern was observed (**Figure 3.19**). TGA analysis further confirmed the non-hygroscopicity of synthesized salts as there was no steepness curve observed around 100 °C (**Figure 3.20**).



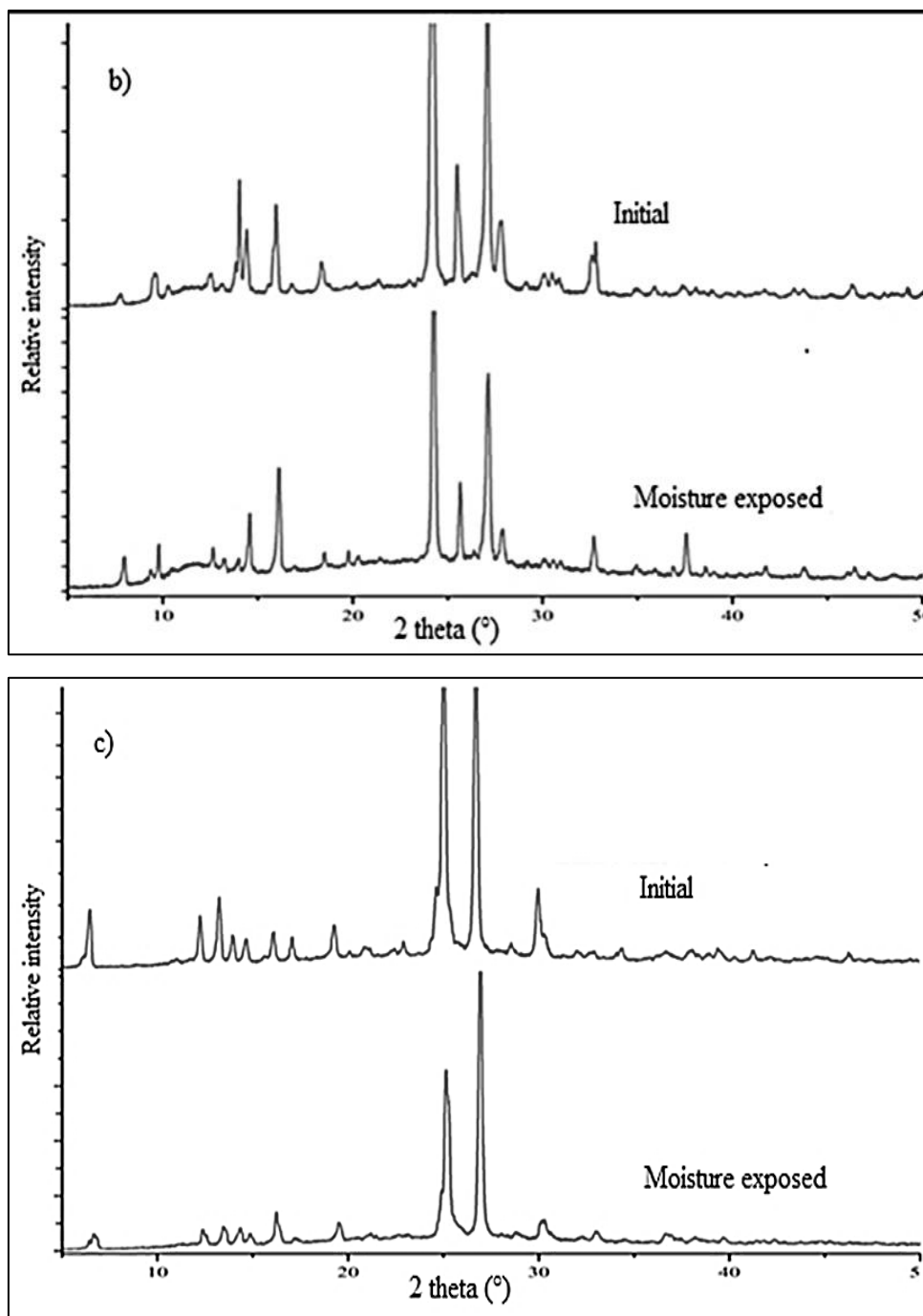


Figure 3.19: Comparison of PXRD patterns of initial and moisture exposed samples of a) ETH-CNB b) ETH-2,6HBA, c) ETH-2,3HBA salts.

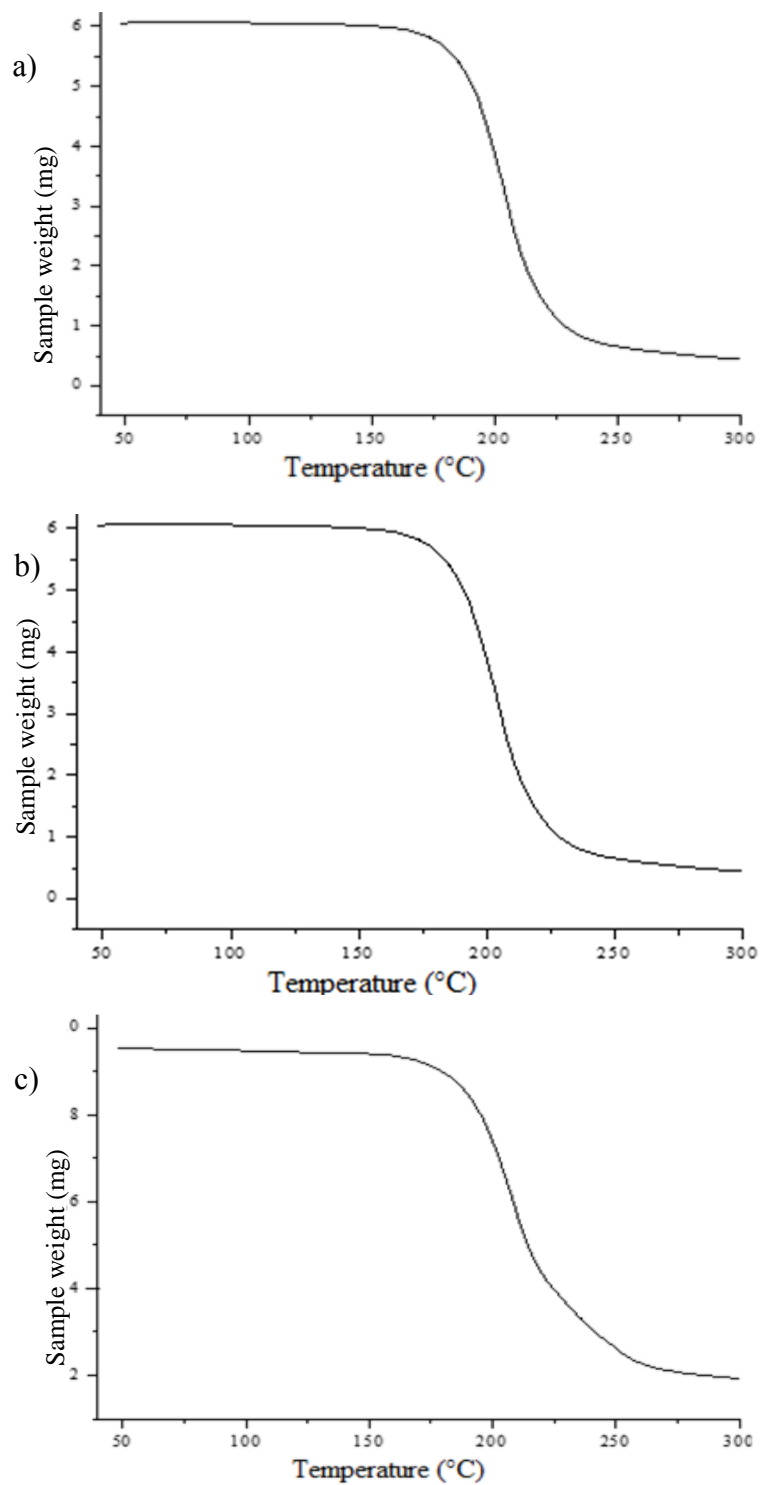


Figure 3.20: TGA plots of a) ETH-CNB, b) ETH-2,6HBA and c) ETH-2,3HBA salts after exposure to moisture.

3.3.7 Solubility study

Aqueous solubility is the major concern with respect to pharmaceutical products when it comes to the formulation of the new chemical entity as well as for the generic drug development. The solubility of a drug molecule basically depends on the physical and chemical properties of the solute and solvent used. It also depends on the pressure, temperature, and pH of the dissolution media. ETH used in the present study belongs to BCS class II drug with poor aqueous solubility. Solubility experiment was performed in 0.1 N HCl solution and in purified distilled water for ETH-CNB, ETH-2,6HBA and ETH-2,3HBA salts. Standard linearity plot of ETH is shown in **Figure 3.21**. Equilibrium solubility of ETH in 0.1 N HCl obtained in the present study was 12.27 mg/mL, which was about 26 times higher solubility compared to the pure drug (0.487 mg/mL) due to the formation of the hydrochloride salt. The solubility of the synthesized salts in 0.1 N HCl media was found to be less when compared to ETH drug. However, when compared to aqueous media, all the salts exhibited increased solubility than neutral ETH. In purified water, all the molecular salts were found to be more soluble than pure ETH (solubility data are displayed in **Table 3.7**). ETH-CNB salt displayed highest solubility (7.5 fold) followed by ETH-2,6HBA (3.4 fold) and ETH-2,3HBA (2.9 fold) in purified water. Therefore, it is concluded that solubility study of the synthesized molecular salts suggests that ionic compounds are more soluble than neutral compounds, where these can alter crystal lattice energy as well as the degree of solvation.

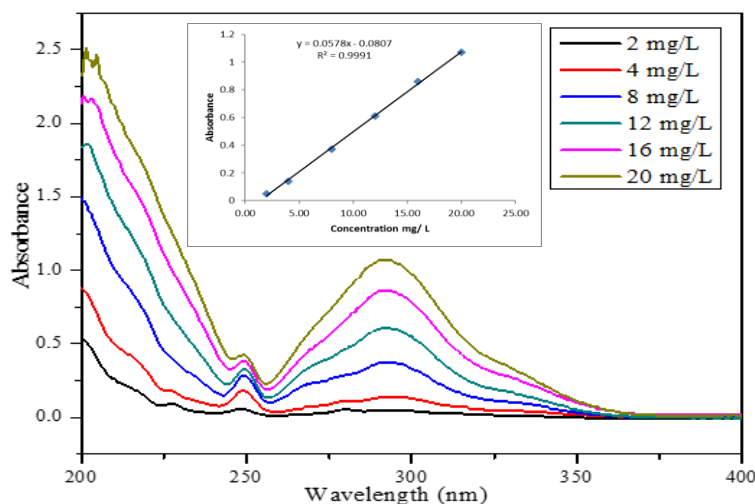


Figure 3.21: Standard linearity plot of ETH.

Table 3.7: Solubility of ETH and its molecular salts in purified water and 0.1 N HCl (pH=1) at room temperature (~25 °C).

Solid forms	Equilibrium solubility of ETH in purified water (mg/mL)*	Equilibrium solubility of ETH in 0.1 N HCl (pH=1) (mg/mL)
ETH	0.487	12.28
ETH-CNB	3.64 (×7.47)	10.08
ETH-2,6HBA	1.65 (×3.38)	10.00
ETH-2,3HBA	1.39 (×2.85)	9.96

*The values in the parenthesis specifies the extent of increase in solubility of ETH drug molecule in molecular salts relative to the pure ETH

A comparison of literature reported solubility study on cocrystal/salt of ETH with present study is tabulated in **Table 3.8**. The reported salt of ETH with maleate and oxalate exhibited about 35 and 25-fold increment in the solubility when compared with ETH alone.

Table 3.8: Comparison of solubility profile of literature reported and the present work.

Salt/cocrystal	Extent of increase in solubility in folds in comparison with ETH	Reference
ETH-maleate	35.0	De Melo et al. (2015)
ETH-oxalate	24.6	Mannava et al. (2016)
ETH-glutaric acid	10.2	
ETH-Adipic acid	2.6	
ETH-suberic acid	3.2	
ETH-sebacic acid	2.1	
ETH-fumaric acid	6.2	
ETH-CNB	7.47	Present work
ETH-2,6HBA	3.38	
ETH-2,3HBA	2.85	

3.4 CONCLUSIONS

Four molecular salts of anti-tuberculosis drug ethionamide have been synthesized by crystal engineering approach and it was characterized by various spectroscopic, thermal and X-ray diffraction techniques. In all the synthesized

molecular salts charge assisted acid···pyridine heterosynthion was observed except for ETH-2,3HBA salts, where molecules interacted through hydroxyl···pyridine heterosynthion. ETH-CNB molecular adduct reveals the presence of both salt and cocrystal in the asymmetric unit, whereas in ETH-DNB both partial and complete proton transfer was observed. Solubility study associated with three of the synthesized molecular salts were determined in 0.1 N HCl and in purified water, it was observed that all the salts exhibited an increase in the solubility of ETH in purified water compared to pure drug. The solubility of synthesized salt follows the order of ETH-CNB>ETH-2,6HBA>ETH-2,3HBA>ETH. The hygroscopic study revealed that synthesized salts were non-hygroscopic in accelerated humid condition (~75% RH). In summary, ETH salt with GRAS counter ions have demonstrated a greater improvement in the solubility of ETH drug molecule in aqueous media and the salts namely, ETH-CNB and ETH-2,3HBA offer the development of combination drug with ETH API.

CHAPTER 4

***DESIGN, SYNTHESIS, CHARACTERIZATION, AND
EVALUATION OF PHYSICOCHEMICAL
PROPERTIES OF SALTS OF COMMON ANTI-
INFLAMMATORY DRUGS***

This chapter describes the synthesis and characterization of pyridine derivative salts of common anti-inflammatory drugs namely, mefenamic acid, tolfenamic acid and naproxen. Further, this chapter talks about the structural comparison of molecular salts based on SC-XRD analysis and the physicochemical properties involved with drug-drug salts.

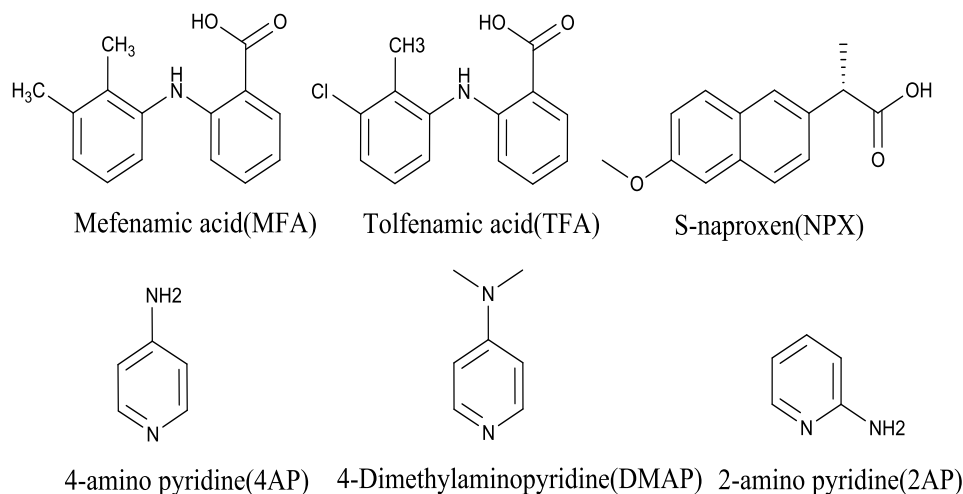
4.1 INTRODUCTION

The three active pharmaceutical ingredients (API) chosen in the present study namely, mefenamic acid (MFA), tolfenamic acid (TFA) and naproxen (NPX) are non-steroidal anti-inflammatory drugs. All the APIs falls under the BCS class II drug due to their poor aqueous solubility and high permeability. MFA and TFA are anthranilic acid derivatives used to treat mild to moderate pain and furthermore these drugs used to prevent migraines associated with menstruation. NPX is a propionic acid class of drug used to treat fever, pain, swellings, and stiffness.

Various reports are available in the literature on cocrystal/salts of naproxen API. However, a few cocrystal/salts are reported for MFA and TFA APIs. Reported cocrystals of MFA and TFA include nicotinamide and 4, 4'-bipyridine. A drug-drug cocrystal of MFA with paracetamol was reported by Chirag et al in the year 2013. Dixit et al. prepared microparticle of MFA with β -cyclodextrin to enhance the solubility of MFA drug. Cocrystals/salts of NPX include nicotinamide, isonicotinamide, picolinamide, bipyridine, piperazine, proline, S-arginine, L-alanine, D-alanine, D-tyrosine, and D-tryptophan. Although numerous reports are available, the salt/cocrystal screening experiment with aminopyridine derivatives was not witnessed in the literature. Therefore, in the present chapter, salt/cocrystal screening experiment was carried out with pyridyl derivative as the salt former based on the pKa values of APIs and the salt former.

Salt formers used in the study are 4-aminopyridine (4AP), 4-dimethylaminopyridine (DMAP) and 2-aminopyridine (2AP). Molecular diagrams APIs and the salt formers are shown in **Scheme 4.1**. 4AP used in the present study as a salt former is a drug molecule used for the treatment of multiple sclerosis by blocking the potassium channel. This is the first drug that was specifically approved to help with mobility in multiple sclerosis patients and it is approved by U.S Food and Drug

Administration (FDA) in the year 2010. Salt/cocrystal screening experiment resulted in two molecular salt hydrate of MFA with 4AP and DMAP, two molecular salt hydrate of TFA with 4AP and DMAP and two molecular salts of NPX with 4AP and 2AP, where NPX-4AP is a salt hydrate. DMAP salt of NPX and 2AP salt of MFA and TFA were not obtained in the salt screening experiment.



Scheme 4.1: Molecular diagrams of APIs and the salt former.

4.2 EXPERIMENTAL SECTION

4.2.1 Materials and methods

Mefenamic acid, tolfenamic acid, and naproxen APIs were purchased from TCI Chemicals and used as such without any further purification. Salt formers 4-amino pyridine, 4-dimethylaminopyridine and 2-amino pyridine were purchased from various vendors and used as such. All the crystallization experiments were carried out with analytical grade solvents.

4.2.2 Synthesis of molecular salts

All the molecular salts synthesized in the present study followed solvent evaporation method and pure crystals were obtained in all the cases.

MFA-4AP: The equimolar ratio of MFA (100 mg, 0.414 mmol) and 4AP (39.0 mg, 0.414 mmol) were dissolved in 10 mL of ethanol solvent at 60 °C and left for slow evaporation at room temperature. Block shaped colorless crystals were obtained after 4 days with 1:1 stoichiometry in the molecular salt. Salt formation observed in methanol solvent as well, however, good quality crystal was not obtained in this solvent.

MFA-DMAP: The equimolar ratio of MFA (100 mg, 0.414 mmol) and DMAP (50.58 mg, 0.414 mmol) were dissolved in 10 mL of ethanol solvent at 60 °C and left for slow evaporation at room temperature. Block shaped colorless crystals were obtained after 4 days with 1:1 stoichiometry in the molecular salt.

TFA-4AP: The equimolar ratio of TFA (100 mg, 0.382 mmol) and 4AP (35.96 mg, 0.382 mmol) were dissolved in 10 mL of methanol solvent at 60 °C and left for slow evaporation at room temperature. Block shaped colorless crystals were obtained after 4 days with 1:1 stoichiometry in the molecular salt. Salt formation and good quality crystal were obtained in ethanol as well as toluene solvents.

TFA-DMAP: The equimolar ratio of TFA (100 mg, 0.382 mmol) and DMAP (46.67 mg, 0.382 mmol) were dissolved in 10 mL of ethanol solvent at 60 °C and left for slow evaporation at room temperature. Block shaped colorless crystals were obtained after 4 days with 1:1 stoichiometry in the molecular salt.

NPX-4AP: The equimolar ratio of NPX (100 mg, 0.434 mmol) and 4AP (40.87 mg, 0.434 mmol) were dissolved in 10 mL of methanol solvent at 60 °C and left for crystallization at room temperature. Needle-shaped colorless crystal was obtained after 4 days with 1:1 stoichiometry in the molecular salt. Ethanol solvent too yielded good quality crystals.

NPX-2AP: The equimolar ratio of NPX (100 mg, 0.434 mmol) and 2AP (40.87 mg, 0.434 mmol) were dissolved in 10 mL of ethanol solvent at 60 °C and left for crystallization at room temperature. Needle-shaped colorless crystals were obtained after 4 days with 1:1 stoichiometry in the molecular salt.

4.3 RESULTS AND DISCUSSION

Based on the pK_a values, the salt formation was expected for all the salt formers chosen except 2AP cofomer. The salt/cocrystal formation was unpredictable in the case of NPX-2AP, where Δ pK_a values lie in between 0-3 range. The pK_a and Δ pK_a values of APIs and the salt formers are displayed in **Table 4.1**.

Table 4.1: pKa and ΔpK_a values of APIs and the salt formers.

API/ Salt former	pKa	ΔpK_a	Salt/cocrystal
Mefenamic acid	4.2	-	-
4AP	8.59	4.39	1:1 Salt hydrate
DMAP	9.6	5.4	1:1 Salt hydrate
Tolfenamic acid	3.66	-	-
4AP	8.59	4.93	1:1 Salt hydrate
DMAP	9.6	5.94	1:1 Salt hydrate
Naproxen	4.15	-	-
4AP	8.59	4.44	1:1 Salt hydrate
2AP	6.68	2.53	1:1 Salt

4.3.1 SC-XRD analysis

MFA-4AP salt hydrate: A molecular salt hydrate of MFA was obtained with 4AP in a 1:1 stoichiometric ratio in ethanol solvent by solvent evaporation method. Crystal structure details are depicted in **Table 4.2** and the geometries of intermolecular interactions are shown in **Table 4.3**. Asymmetric unit in the molecular salt consists of one molecule each of MFA, 4AP, and H₂O which was crystallized in monoclinic crystal system with P 2₁/n space group. Proton transfer from a carboxylic acid group of MFA to 4AP was observed, however, the molecule interacted each other mediated by a water molecule with O-H...O (O-H of water and O of MFA) bond distance of 2.640 Å ($\angle 164.45^\circ$) and N-H...O (N-H of 4AP and O of water) bond distance 2.773 Å ($\angle 159.64^\circ$) (**Figure 4.1a**). The water molecule in the crystal lattice acts as a bridge between two MFA molecule resulting in a cyclic tetrameric unit with R₄⁴(12) graph sets (**Figure 4.1b**). This tetrameric structure further self-assembled through different N-H...O (N-H of the amino group of 4AP and O of water & N-H of pyridyl nitrogen and O of water) hydrogen bond with a bond distance of 2.843 Å ($\angle 175.22^\circ$) and 2.773 Å ($\angle 159.64^\circ$) respectively resulting in a 2D ladder-like structure of MFA-4AP salt hydrate. 2D structure expands to the 3D structure via weak secondary interactions such as two different hydrogen bond between C-H of 4AP and O of the carboxyl group of MFA (C-H...O distance 3.339 Å and 3.364 Å) and N-H...O hydrogen bond (3.130 Å) between N-H of the amine group of 4AP and O of the carboxyl group of MFA. The crystal structure features stacking interaction between MFA and 4AP molecule with

centroid to centroid bond distance of 3.622 Å (**Figure 4.2**). Color code for the atoms are gray: carbon; off-white: hydrogen; red: oxygen; blue: nitrogen; green: chlorine.

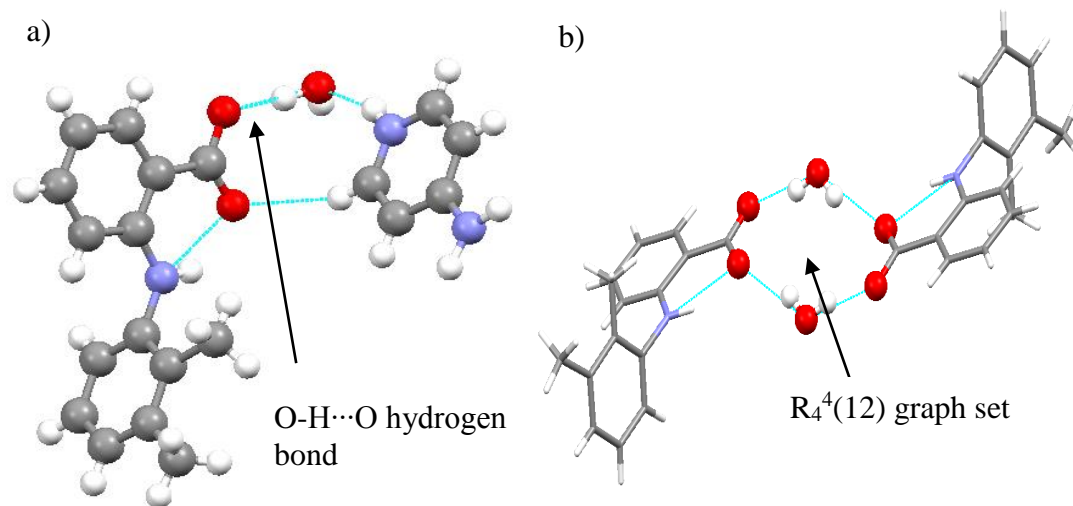


Figure 4.1: Asymmetric unit (a) and tetrameric unit (b) of MFA-4AP salt hydrate.

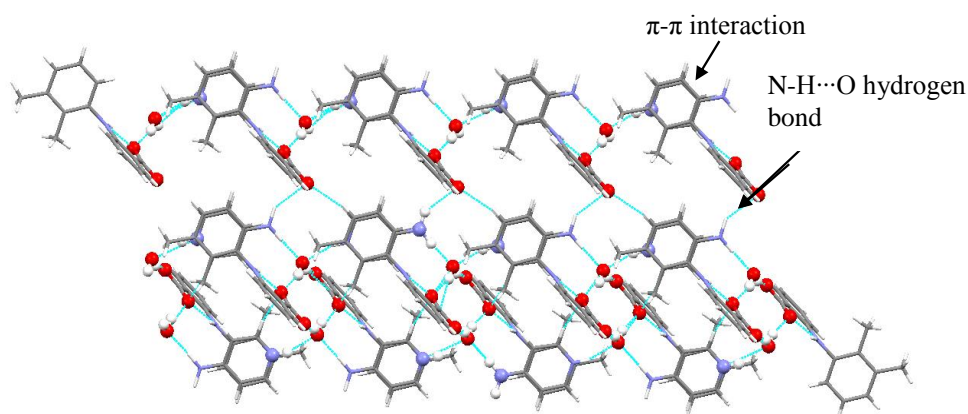


Figure 4.2: 3D representation of MFA-4AP salt hydrate.

MFA-DMAP salt hydrate: A 1:1 molecular salt hydrate of MFA with DMAP resulted in ethanol solvent by solvent evaporation method. The molecular salt was crystallized in triclinic crystal system with $P\bar{1}$ space group. Primary synthon in the molecular salt hydrate was a charge assisted acid...pyridine (N-H...O distance 2.713 Å, $\angle 171.92^\circ$) heterosynthon between MFA and DMAP and a hydrogen bond between O of MFA and O-H of a water molecule (O-H...O distance 2.874 Å, $\angle 165.07^\circ$) respectively (**Figure 4.3a**). The water molecule in the crystal lattice leads to the formation of the cyclic tetrameric unit between two MFA molecule with $R_4^4(12)$ ring motifs (**Figure 4.3b**).

The tetrameric structure expands in a 2D ladder-like structure by utilizing weak hydrogen bonds such as C-H \cdots O (C-H of methyl group of DMAP and O of MFA), C-H \cdots C (C-H of methyl group of DMAP and C of MFA) and C-H \cdots O (aromatic C-H of DMAP and O of a water molecule) hydrogen bond with distance 3.491 Å, 3.550 Å and 3.297 Å respectively (**Figure 4.4**). 2D structure converts to the 3D structure using weak C-H \cdots O hydrogen bond (3.211 Å) between C-H of DMAP and O of MFA molecule.

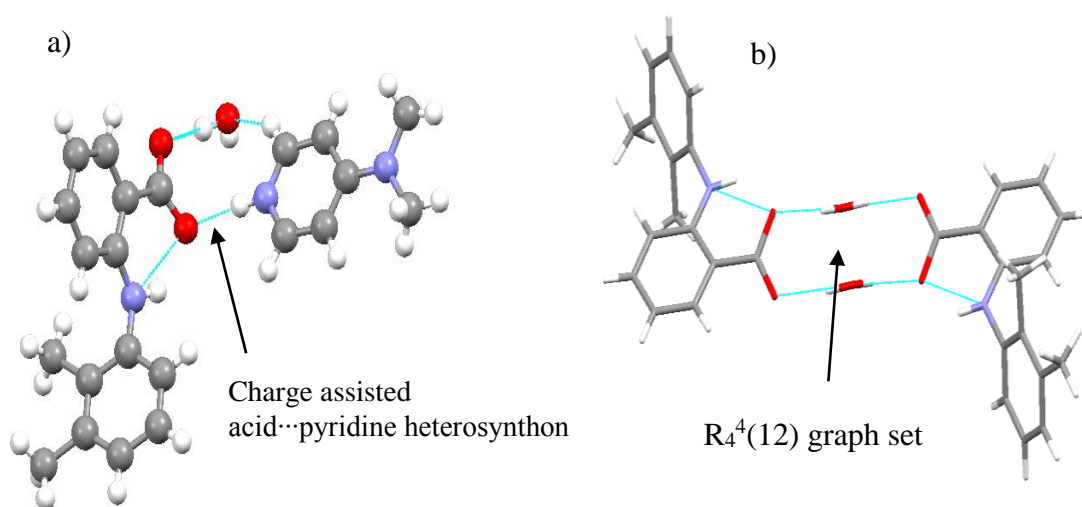


Figure 4.3: Asymmetric unit (a) and tetrameric unit (b) in the molecular salt hydrate of MFA-DMAP.

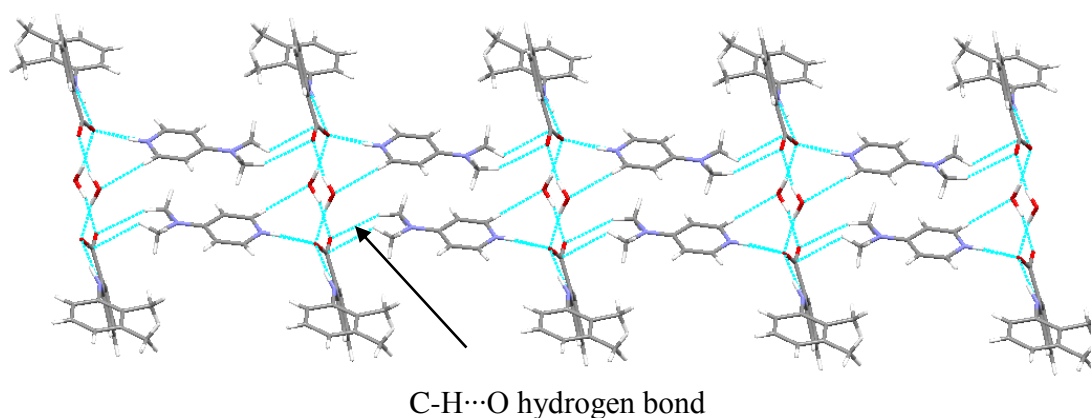


Figure 4.4: 2D representation of MFA-DMAP salt hydrate.

TFA-4AP salt hydrate: A 1:1 molecular salt hydrate of TFA with 4AP was obtained in methanol solvent by solvent evaporation method. The molecule was crystallized in monoclinic crystal system with $P 2_1/n$ space group. Proton transfer from TFA to 4AP was observed, however, the molecules interacted through water molecule with N-H \cdots O and O-H \cdots O bond distance of 2.748 Å and 2.640 Å (angle $\angle 149.54^\circ$ and $\angle 171.03^\circ$)

respectively (**Figure 4.5a**). Here again, water molecule acts as a bridge between two TFA molecule, which is resulting in a tetrameric structure with $R_4^4(12)$ ring motifs (**Figure 4.5b**). This tetrameric structure converts to the 3D structure by utilizing N-H \cdots O hydrogen bond (N-H of the amine group of 4AP and O of a water molecule) with distance 2.844 Å, angle $\angle 173.73^\circ$ and stacking interaction between TFA and 4AP with centroid to centroid distance of 3.671 Å. The overall crystal structure features weak C-H \cdots O (C-H of 4AP and O of TFA) and N-H \cdots O hydrogen bond (N-H of the amine group of 4AP and O of TFA) (**Figure 4.6**).

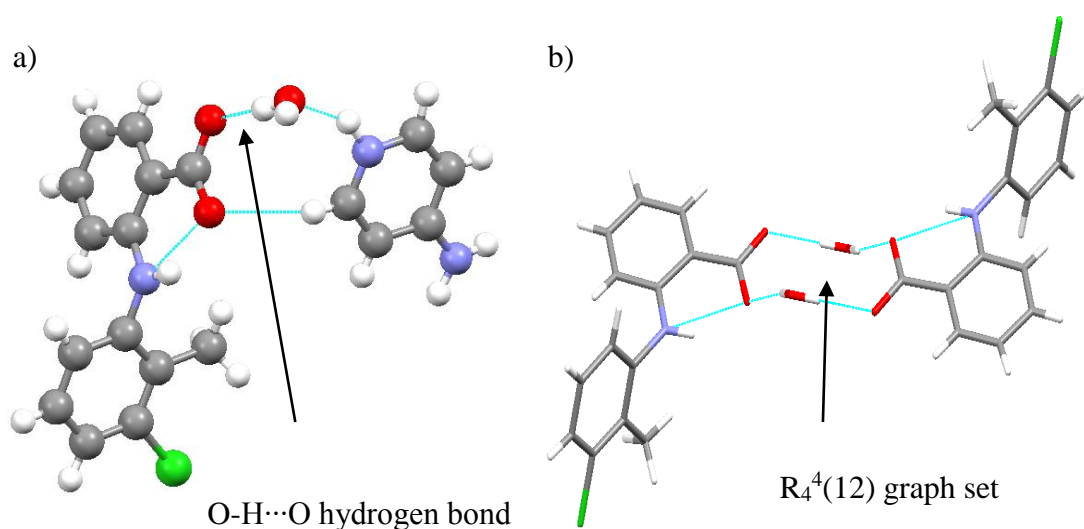


Figure 4.5: Asymmetric unit (a) and cyclic tetrameric unit of TFA-4AP salt hydrate.

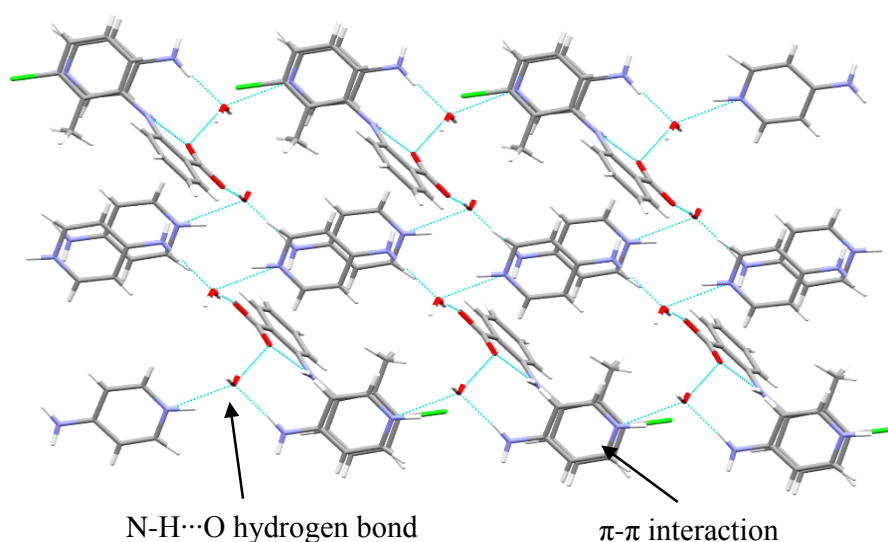


Figure 4.6: 3D representation of TFA-4AP salt hydrate.

TFA-DMAP salt hydrate: A 1:1 molecular salt hydrate of TFA with DMAP was obtained in ethanol solvent by solvent evaporation method which was crystallized in triclinic crystal system with $P\bar{1}$ space group. Charge assisted two point heterosynthon between TFA and DMAP was observed with N-H \cdots O bond distance of 2.716 Å ($\angle 171.89^\circ$). The water molecule in the asymmetric unit forms a hydrogen bond with the carboxyl group of TFA with O-H \cdots O bond distance of 2.773 Å ($\angle 164.66^\circ$) (**Figure 4.7a**). The water molecule in the crystal lattice resulting in the formation of cyclic tetrameric structure between two TFA molecule with $R_4^4(12)$ ring motifs (**Figure 4.7b**). This tetrameric structure extends to 2D ladder-like structure via C-H \cdots O hydrogen bond (C-H of the methyl group of DMAP and O of TFA) and C-H \cdots O hydrogen bond between aromatic C-H of DMAP and O of a water molecule (**Figure 4.8**). This further convert to the 3D structure by utilizing C-H \cdots O (3.306Å) hydrogen bond between DMAP and TFA.

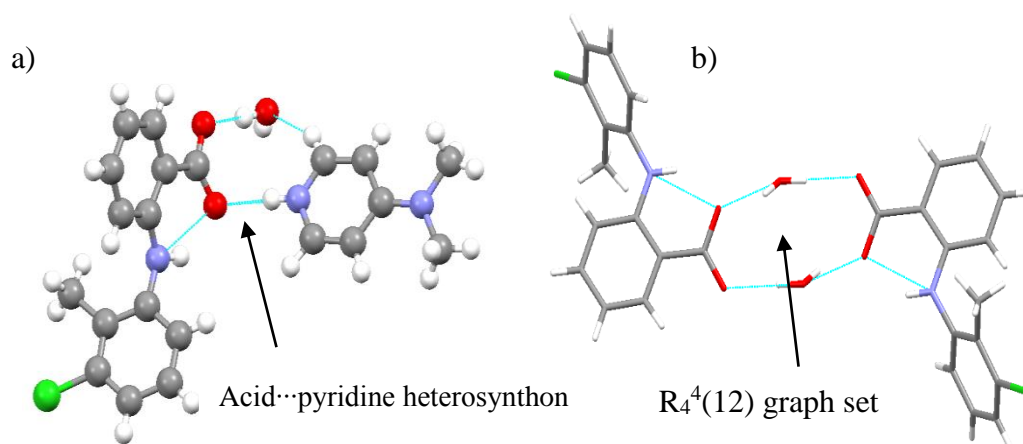


Figure 4.7: Asymmetric unit (a) and tetrameric unit (b) of TFA-DMAP salt hydrate.

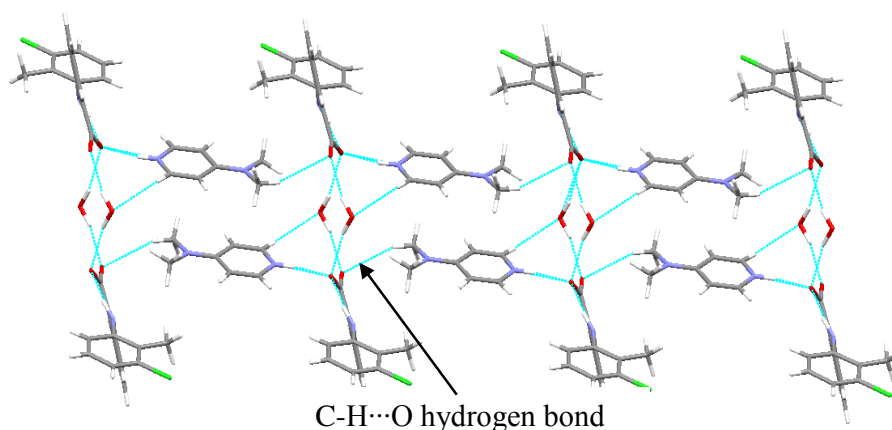


Figure 4.8: 2D representation of TFA-DMAP salt hydrate.

NPX-4AP salt hydrate: A molecular salt hydrate of NPX with 4AP resulted in methanol solvent, which was crystallized in monoclinic crystal system with $P 2_1$ space group. Primary synthon in the molecular salt consists of charge assisted acid...pyridine heterosynthon between NPX and 4AP with N-H...O bond distance 2.612 Å ($\angle 160.53^\circ$) (**Figure 4.9a**). The water molecule in the asymmetric unit forms a hydrogen bond with NPX and 4AP resulting in cyclic $R_3^3(9)$ ring motifs. The presence of water molecule interconnects two NPX molecule resulting in cyclic pentamer structure (O-H...O distance of 2.763 Å and 2.784 Å, N-H...O distance 2.899 Å and 2.894 Å) (**Figure 4.9b**). Two neighboring pentamer unit interconnected through $N^+ \cdots H \cdots O$, N-H...O and C-H...O hydrogen bond between NPX and 4AP molecules resulting in a 2D layer like structure of NPX-4AP salt hydrate. The molecule in the crystal lattice aggregates in AAAA... manner resulting in the 3D structure of NPX-4AP salt hydrate (**Figure 4.10**). The overall crystal structure features weak C-H... π interaction (3.786 Å) between 4AP and NPX, π - π interaction between 4AP-4AP and NPX-NPX with centroid to centroid distance of 5.951 Å and 5.952 Å respectively.

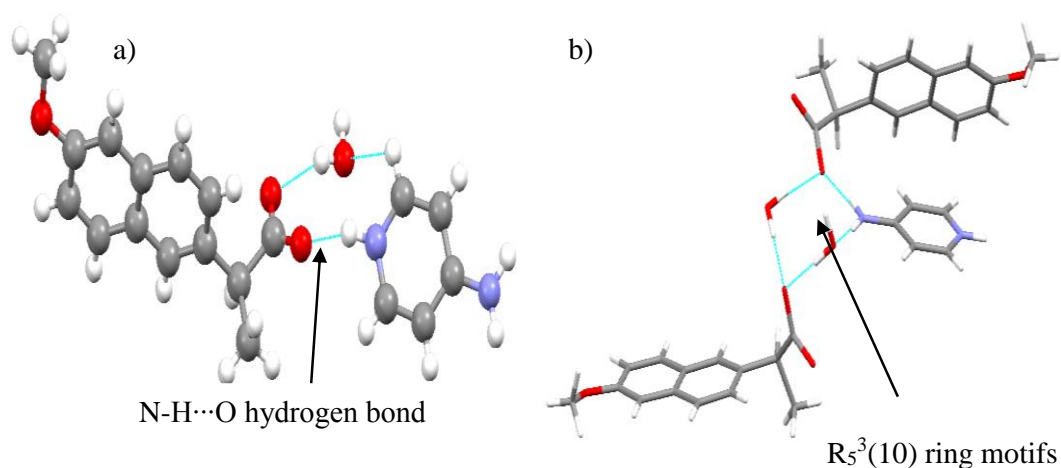


Figure 4.9: Asymmetric unit (a) and tetrameric unit (b) of NPX-4AP salt hydrate.

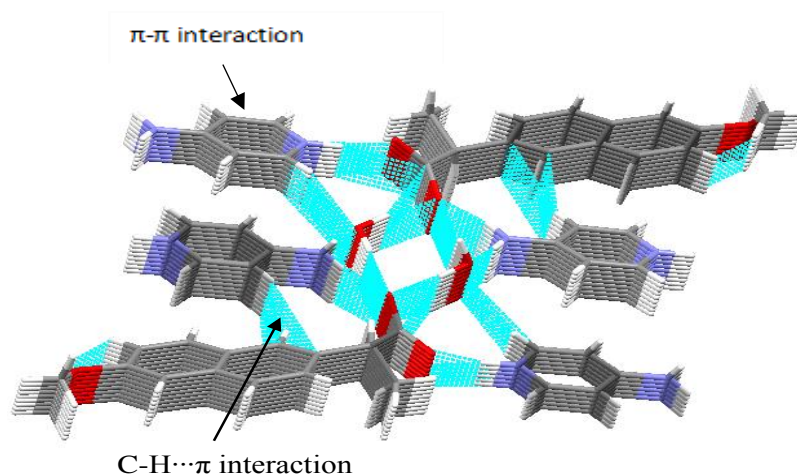


Figure 4.10: 3D representation of NPX-4AP salt hydrate.

NPX-2AP salt: A 1:1 molecular salt of NPX with 2AP was yielded in ethanol solvent by solvent evaporation method. The salt was crystallized in monoclinic crystal system with $P 2_1$ space group. The primary synthon in the molecular salt consists of two point supramolecular unit in which, charge assisted acid...pyridine heterosynthon was observed ($N^+-H\cdots O$ distance 2.580 Å, $\angle 167.99^\circ$ and $N-H\cdots O$ distance 2.875 Å, $\angle 170.93^\circ$) (**Figure 4.11**). This supramolecular unit further self-assembled to give a 2D tape-like structure by utilizing strong $N-H\cdots O$ (2.893 Å, $\angle 154.82^\circ$) and weak $C-H\cdots O$ (3.268 Å, $\angle 132.41^\circ$) hydrogen bond between 2AP and NPX molecule (**Figure 4.12**). This 2D tape converts to the 3D structure via $C-H\cdots O$ hydrogen bond (3.382 Å) between C-H of 2AP and O of methoxy group of NPX. The molecules in the crystal lattice are arranged in AAAA...manner where molecules of 2AP and NPX are stacked one by one individually with the π - π interaction between 2AP-2AP and NPX-NPX molecules with centroid to centroid distance of 6.110 Å and 6.110 Å respectively (**Figure 4.13**).

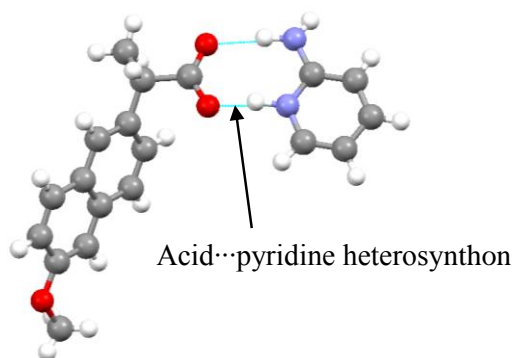


Figure 4.11: Asymmetric unit of NPX-2AP molecular salt.

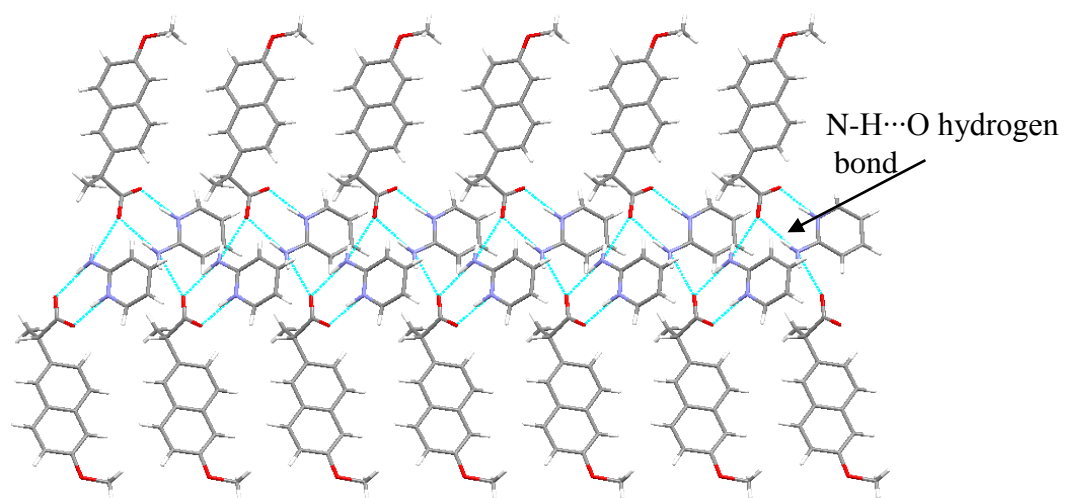


Figure 4.12: 2D representation of NPX-2AP molecular salt.

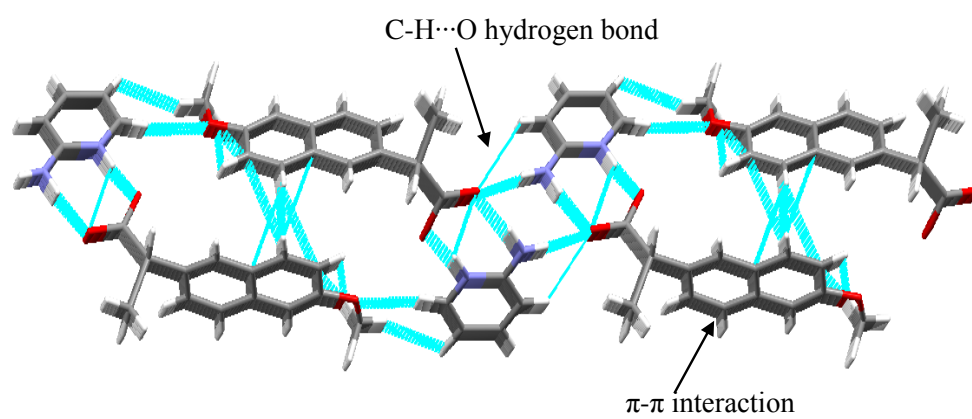


Figure 4.13: 3D representation of NPX-2AP molecular salt.

Table 4.2: Crystal structure and refinement details of molecular salts.

Crystal structure details	MFA-4AP	MFA-DMAP	TFA-4AP	TFA-DMAP	NPX-4AP	NPX-2AP
CCDC number	1496328	1496333	1496334	1496335	1496336	1496337
Mol. formula	C ₂₀ H ₂₃ N ₃ O ₃	C ₂₂ H ₂₇ N ₃ O ₃	C ₁₉ H ₂₀ ClN ₃ O ₃	C ₂₁ H ₂₄ ClN ₃ O ₃	C ₁₉ H ₂₂ N ₂ O ₄	C ₁₉ H ₂₀ N ₂ O ₃
Molar mass	353.41	381.46	373.83	401.88	342.39	324.37
crystal system	Monoclinic	Triclinic	Monoclinic	Triclinic	Monoclinic	Monoclinic
Space group	P 2 ₁ /n	P $\bar{1}$	P 2 ₁ /n	P $\bar{1}$	P 2 ₁	P 2 ₁
a / Å	7.7601(3)	7.8149(4)	7.7749(3)	7.8481(3)	10.0057(3)	9.7396(3)
b / Å	8.3522(4)	8.1357(4)	8.3263(3)	8.1034(3)	5.9515(2)	6.1100(2)
c / Å	28.6233(12)	16.3674(8)	28.3693(11)	16.3092(5)	15.3212(4)	14.6168(4)
α / °	90	79.589(2)	90	100.5870(10)	90	90
β / °	95.315(2)	81.330(2)	95.172(2)	98.0310(10)	99.3890(10)	95.3830(10)
γ / °	90	89.955(2)	90	90.3870(10)	90	90
Volume/ Å ³	1847.21(14)	1011.43(9)	1829.04(12)	1008.99(6)	900.14(5)	865.99(5)
Z	4	2	4	2	2	2
Density [g/cm ³]	1.271	1.253	1.358	1.323	1.263	1.244
μ (MoK α) [mm ⁻¹]	0.087	0.084	0.233	0.216	0.089	0.085
T/K	296(2)	296(2)	296(2)	296(2)	296(2)	296(2)
Reflns collected	3638	3929	3598	3922	3495	3358
Unique rflns	3220	3496	3261	3456	3325	3151
Parameter refined	257	317	304	349	303	297
R ₁ (I > 2 σ)	0.0665	0.0448	0.0475	0.0471	0.0313	0.0301
wR ₂ (I > 2 σ)	0.1565	0.1203	0.1513	0.1304	0.0862	0.0827
GOF	1.105	1.050	1.047	0.786	1.026	1.048

Table 4.3: Hydrogen bond geometry of the synthesized salts.

Salt	D-H...A ^a	H...A/ Å	D...A/ Å	∠D-H...A/ °	Symmetry code
MFA-4AP	N3-H25...O1	1.950	2.772	159.56	x, y+1, z
	C16H18...O3	2.502	3.364	154.17	x, y, z
	C20H17...O2	2.524	3.339	146.45	-x, -y+2, -z+1
	O1-H21...O3	1.912	2.697	158.08	-x+1, -y+1, -z+1
	O1-H20...O2	1.767	2.640	164.67	x, y-1, z
	N1-H14...O1	1.807	2.843	174.97	x, y, z
	N1-H15...O2	2.343	3.129	133.97	-x, -y+1, -z+1
	N2-H23...O3	1.955	2.656	139.88	x, y, z
MFA- DMAP	C21-H17...O2	2.658	3.550	154.73	x, y, z
	N1-H13...O1	1.944	2.673	138.57	x, y, z
	C17-H3...O2	2.490	3.211	129.41	x, y-1, z
	C19-H4...O3	2.440	3.337	162.86	-x+2, -y+1, -z+1
	C20-H5...O3	2.494	3.297	144.41	x+1, y-1, z
	N3-H1...O1	1.836	2.713	171.74	x+1, y-1, z
	O3-H26...O1	1.980	2.874	165.13	-x+1, -y+1, -z+1
	O3-H28...O2	1.881	2.774	163.89	x, y, z
TFA-4AP	N3-H5...O2	1.933	2.645	141.05	x, y, z
	C3-H9...O2	2.484	3.350	156.06	x, y, z
	C1-H12...O3	2.372	3.306	148.97	-x, -y, -z+1
	O1-H13...O3	1.840	2.640	171.03	x, y+1, z
	O1-H14...O2	1.917	2.705	163.70	-x+1, -y+1, -z+1
	N2-H15...O1	1.907	2.845	173.82	x, y, z
	N2-H16...O3	2.527	3.173	132.26	-x, -y+1, -z+1
	N1-H17...O1	1.840	2.748	149.39	x, y-1, z
TFA- DMAP	C4-H1...O1	2.450	3.333	166.26	-x+1, -y+1, -z+1
	C7-H5...O2	2.490	3.187	129.03	x+1, y+1, z
	C5-H2...O1	2.552	3.306	146.69	x, y+1, z
	N3-H3...O3	1.839	2.716	172.03	x, y+1, z
	N1-H15...O3	1.948	2.668	140.19	x, y, z
	O1-H17...O2	1.903	2.773	164.36	x, y, z
	O1-H16...O3	2.008	2.878	160.14	-x+1, -y+1, -z+1
NPX-4AP	O1-H1...O2	1.951	2.763	154.68	x, y, z
	O1-H2...O2	1.876	2.783	177.98	-x+1, y-1/2, -z+1
	N2-H7...O3	1.691	2.612	160.73	x+1, y, z
	N1-H17...O2	1.971	2.894	171.24	x, y, z
	N1-H16...O1	1.934	2.899	177.21	-x+1, y-1/2, -z+1
NPX-2AP	N2-H12...O2	1.902	2.874	170.81	x+1, y, z
	N2-H13...O2	2.089	2.893	154.55	-x+1, y-1/2, -z+2
	N1-H11...O1	1.553	2.580	168.47	x+1, y, z
	N1-H11...O2	2.640	3.441	133.63	x+1, y, z

	C4-H17...O2	2.567	3.268	132.65	-x+1, y-1/2, -z+2
	C1-H14...O3	2.508	3.383	149.77	-x+2, y-1/2, -z+1

^aD-donor, A-acceptor

4.3.3 Spectroscopic analysis of molecular salts

4.3.3.1 FT-IR analysis

The FT-IR spectra of all the molecular salts were recorded and compared the spectra with their respective starting materials in order to confirm the product formation in the initial stages of salt screening experiments. Shifts in carbonyl/acid/amine stretching frequencies were accounted for the product confirmation. In pure MFA, TFA and NPX, carbonyl stretching frequency was observed at 1647 cm⁻¹, 1654 cm⁻¹ and 1724 cm⁻¹ respectively. A detailed stretching frequency of molecular salts and the starting materials are displayed in **Table 4.4** MFA-4AP, MFA-DMAP, TFA-4AP, TFA-DMAP, NPX-4AP and NPX-2AP molecular salts exhibited carbonyl stretching frequencies at 1650 cm⁻¹, 1639 cm⁻¹, 1649 cm⁻¹, 1639 cm⁻¹, 1644 cm⁻¹ and 1654 cm⁻¹ respectively. A slight increase in the stretching frequency was observed in the case of MFA-4AP probably due to the hydrogen bond acceptor character of both oxygen atoms of the carbonyl group, thereby restricting the resonance and thus increasing the bond strength of carbonyl group. In TFA-4AP, same was observed however, carbonyl stretching frequency was slightly lower than neutral TFA molecule. In the case of NPX salts, ionization caused a large shift in the carbonyl stretching frequency (FT-IR spectra are displayed in **Figure 4.14-4.16**).

Table 4.4: Stretching frequencies of APIs and the molecular salts.

Solid forms	-C=O stretching frequency (cm ⁻¹)	-NH/-OH stretching frequency (cm ⁻¹)
MFA	1647	-
TFA	1654	3337
NPX	1724	-
MFA-4AP	1650	-
MFA-DMAP	1639	-
TFA-4AP	1649	3424
TFA-DMAP	1639	3478
NPX-4AP	1644	3535, 3275
NPX-2AP	1654	3332

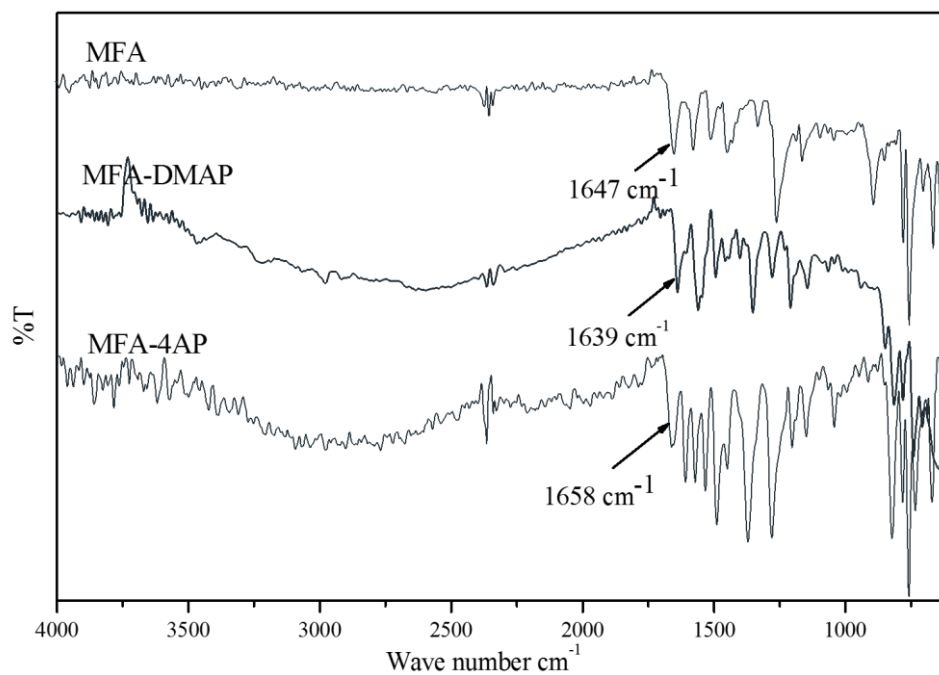


Figure 4.14: Comparison of FT-IR spectra of MFA salts with MFA.

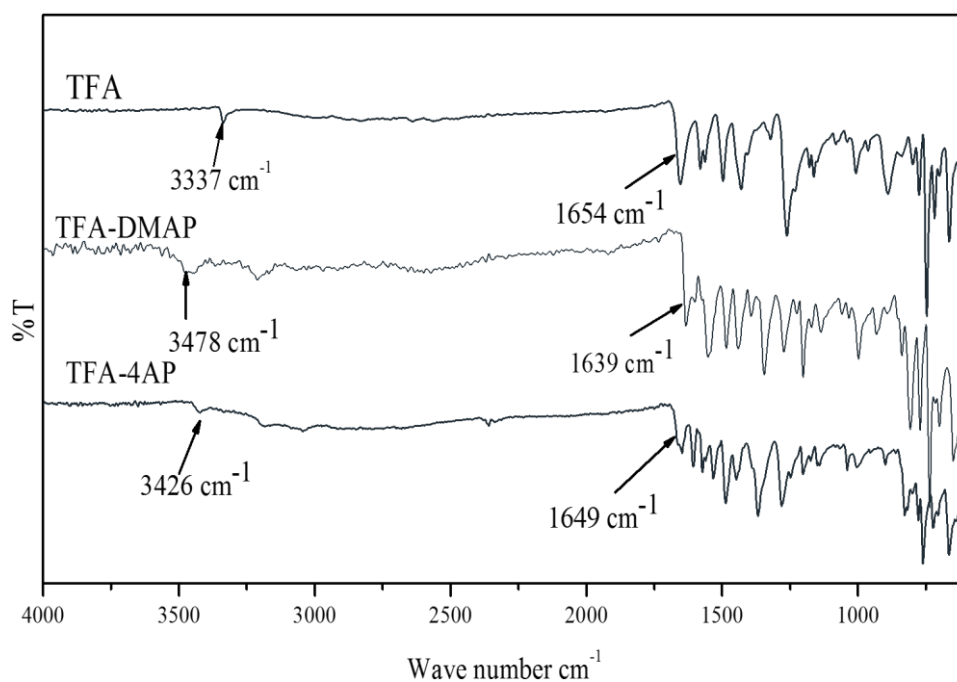


Figure 4.15: Comparison of FT-IR spectra of TFA salts with TFA.

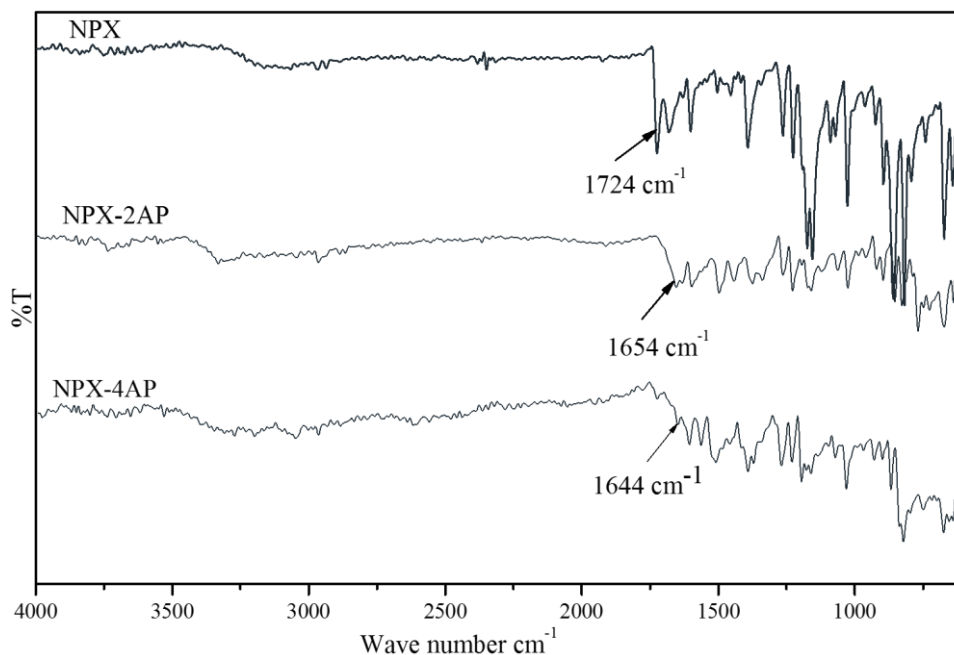


Figure 4.16: Comparison of FT-IR spectra of NPX salts with NPX.

4.3.3.2 ^1H NMR analysis

^1H NMR spectra of all the molecular salt confirm the 1:1 molecular stoichiometry of synthesized salts. Spectral details are given below.

MFA-4AP salt hydrate: (400 MHz, DMSO- d_6 , δ ppm): 10.5 (1H, s), 8.05-8.03 (2H, d), 7.91-7.89 (1H, dd), 7.239-7.196 (1H, t), 7.141-7.123 (1H, d), 7.092-7.055 (1H, t), 6.951-6.932 (1H, d), 6.760-6.739 (1H, d), 6.683-6.629 (3H, m), 6.584-6.568 (2H, d), 2.275 (3H, s), 2.113 (3H, s).

MFA-DMAP salt hydrate: (400 MHz, DMSO- d_6 , δ ppm): 9.82 (1H, s), 8.15 (2H, s), 7.89 (1H, s), 7.26 (1H, s), 7.12 (2H, s), 6.99 (1H, s), 6.70 (4H, s), 3.01 (6H, s), 2.28 (3H, s), 2.10 (3H, s).

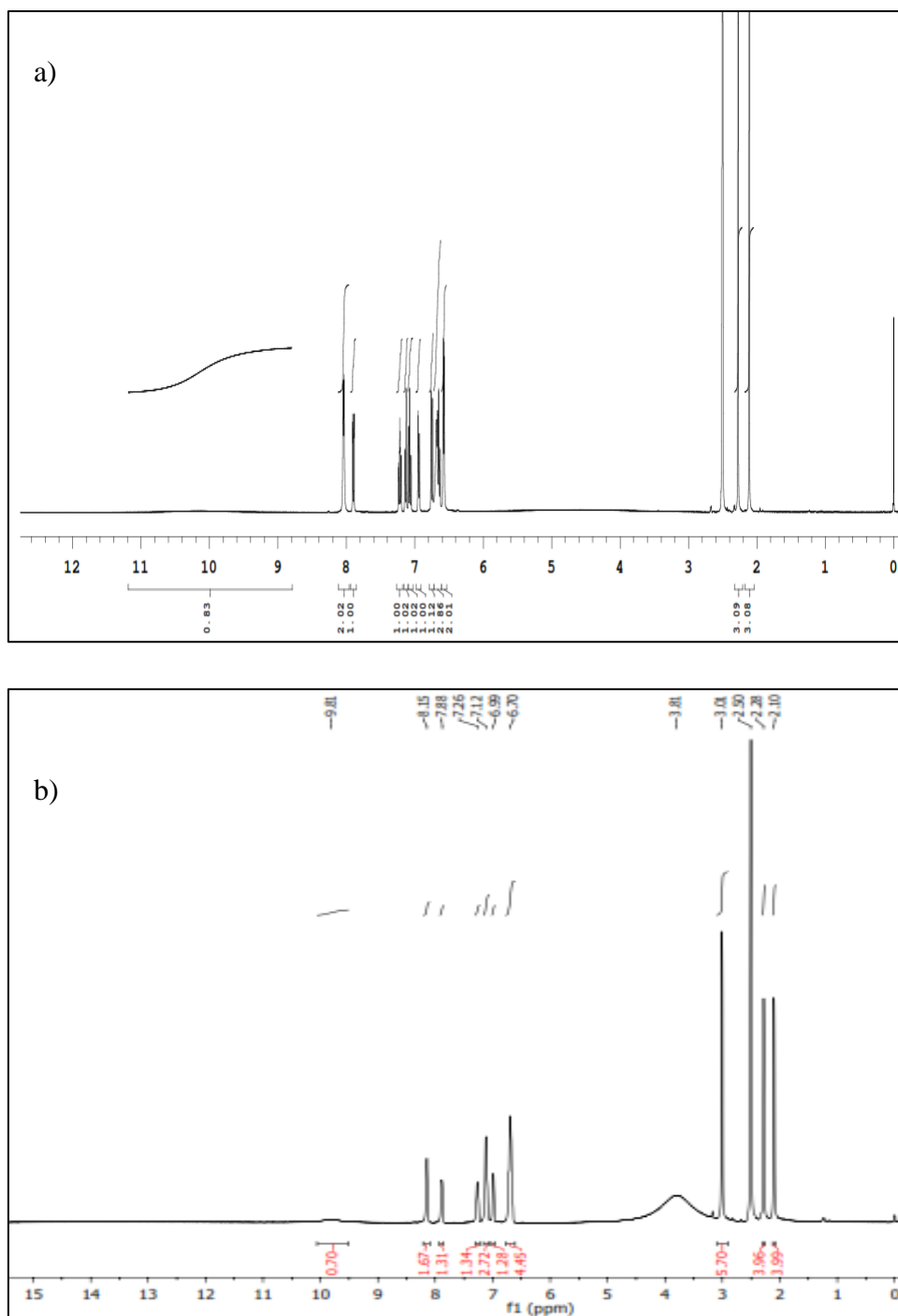
TFA-4AP salt hydrate: (400 MHz, DMSO- d_6 , δ ppm): 10.84 (1H, s), 8.09 (2H, s), 7.95 (1H, s), 7.32 (1H, s), 7.25 (1H, s), 7.16-7.12 (4H, s), 6.97-6.95 (1H, d), 6.74-6.73 (1H, d), 6.66 (2H, s), 2.29 (3H, s).

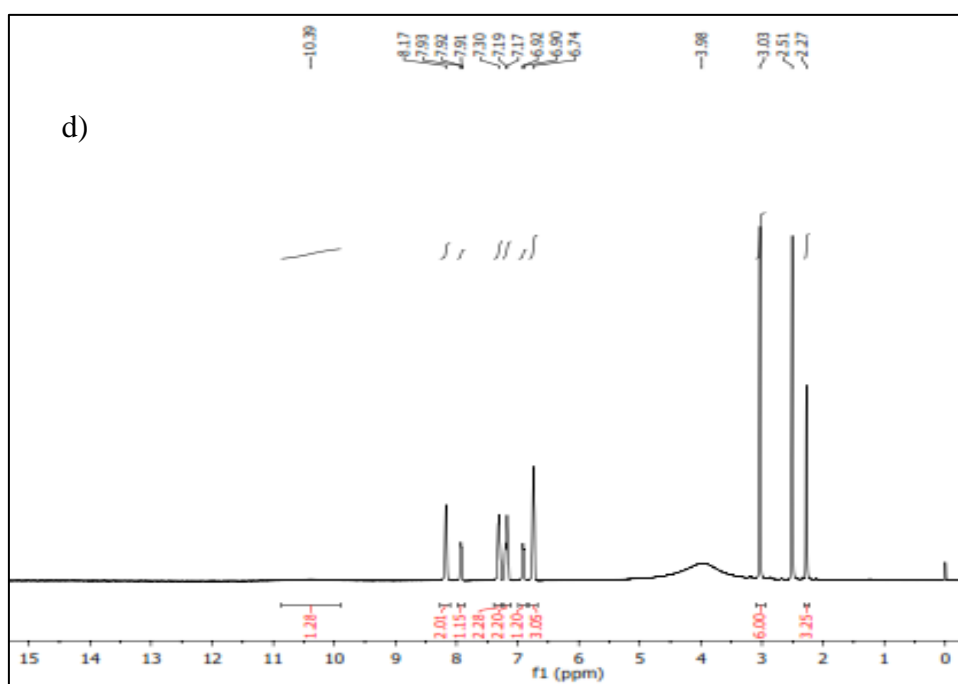
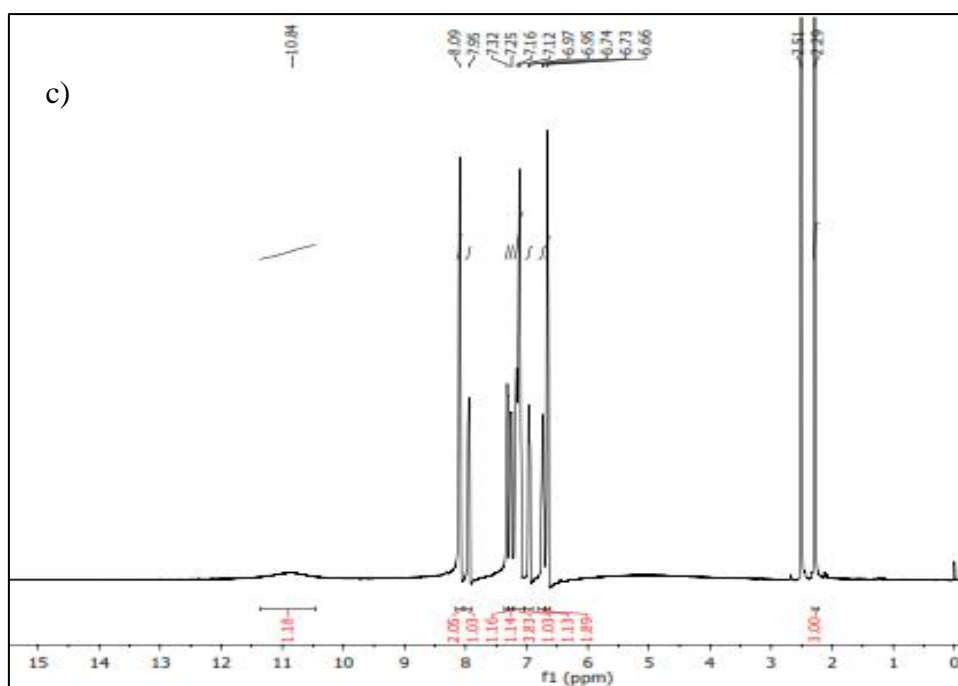
TFA-DMAP salt hydrate: (400 MHz, DMSO- d_6 , δ ppm): 10.39 (1H, s), 8.17 (2H, s), 7.93-7.91 (1H, t), 7.30 (2H, s), 7.19-7.17 (2H, s), 6.92-6.90 (1H, d), 6.74 (3H, s), 3.03 (6H, s), 2.27 (3H, s).

NPX-4AP salt hydrate: (400 MHz, DMSO- d_6 , δ ppm): 7.97 (2H, s), 7.78 (2H, s), 7.71 (1H, s), 7.41-7.42 (1H, d), 7.29 (1H), 7.15-7.16 (1H, d), 6.47 (2H, s), 6.12 (2H, s), 3.80 (3H, s), 3.79 (1H, s), 1.44 (3H, s).

NPX-2AP: (400 MHz, DMSO- d_6 , δ ppm): 7.88 (1H, s), 7.81-7.71 (3H, m), 7.41-7.29 (3H, m), 7.16-7.14 (1H, d), 6.46-6.41 (2H, q), 5.86 (2H, s), 3.86 (3H, s), 3.79 (1H, s), 1.44 (3H, s).

^1H NMR spectra of the molecular salts are displayed in the **Figure 4.17**





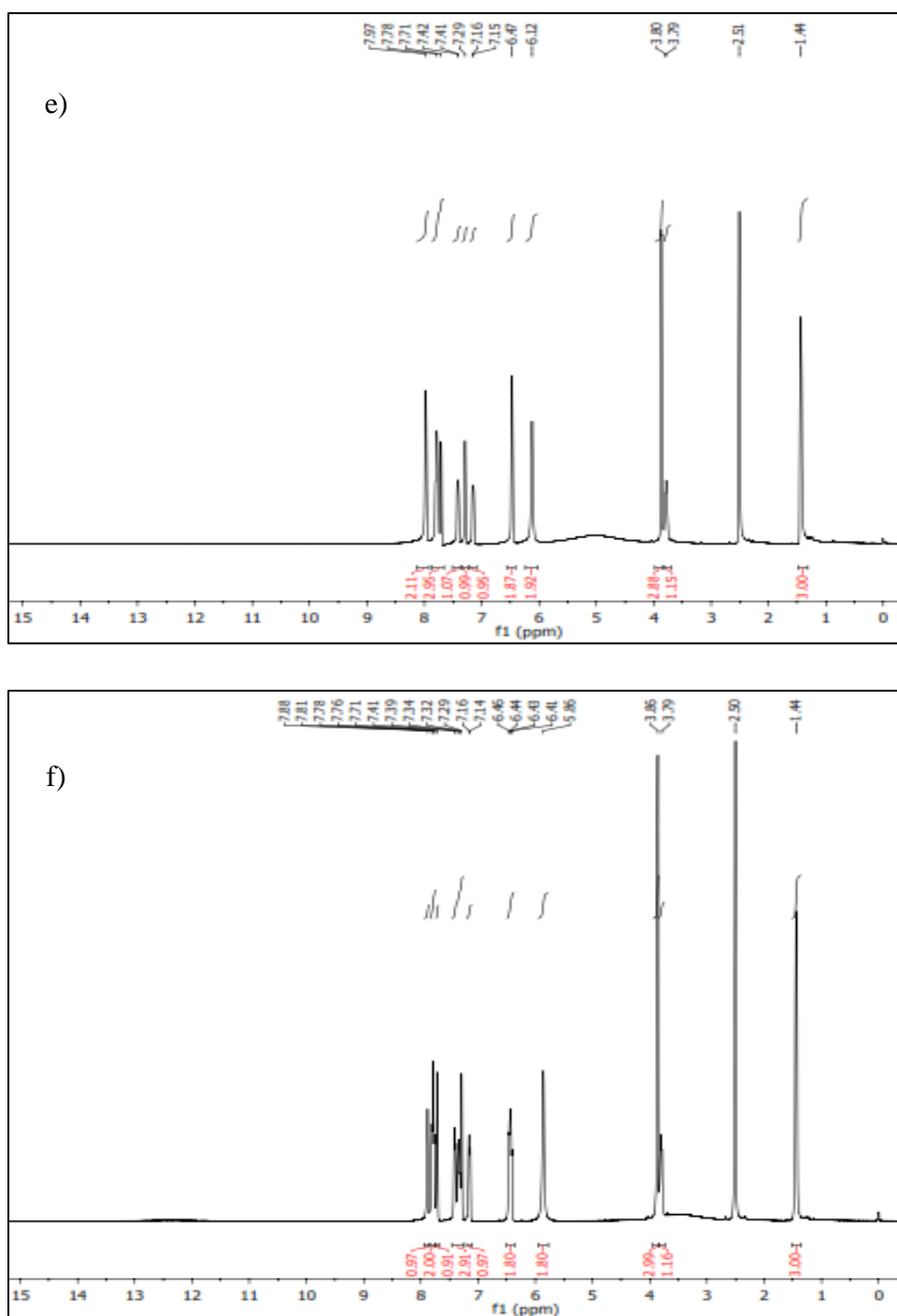


Figure 4.17: ^1H NMR spectra of a) MFA-4AP, b) MFA-DMAP, c) TFA-4AP, d) TFA-DMAP, e) NPX-4AP and f) NPX-2AP molecular salts.

4.3.4 PXRD analysis

PXRD analysis of all the molecular salts was performed and compared the pattern with their respective precursors. All the synthesized molecular salts were exhibited different diffraction patterns when compared to precursors and the pattern

was found to be well in agreement with the calculated PXRD pattern obtained from SCXRD analysis, which proves the bulk purity of the synthesized molecular salts. PXRD comparison plot of simulated and the experimental patterns are displayed in **Figure 4.18-4.23**.

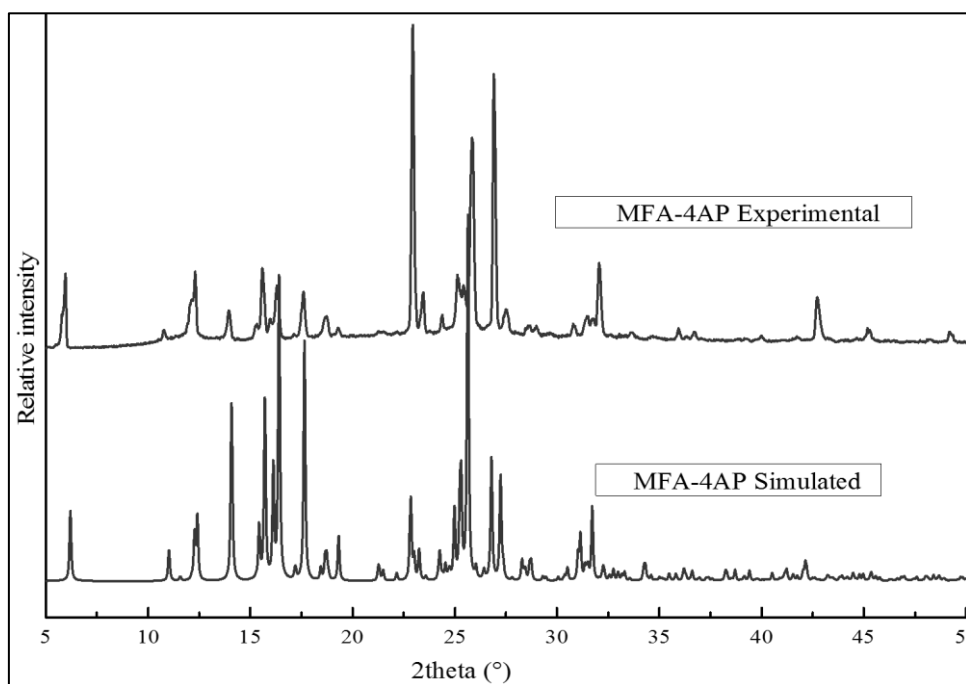


Figure 4.18: Experimental and simulated PXRD patterns of MFA-4AP salt.

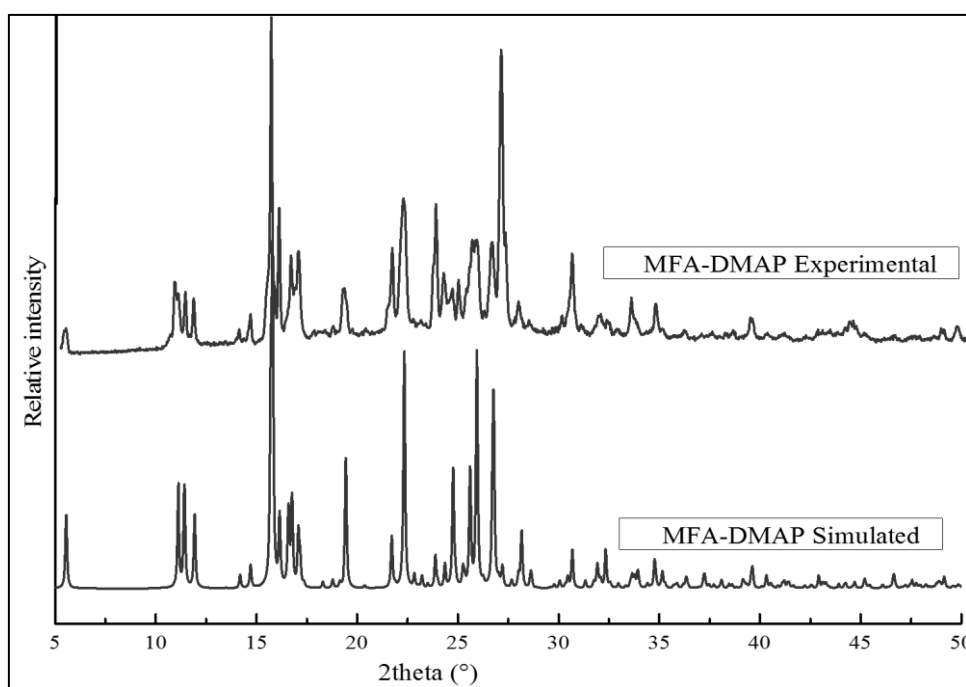


Figure 4.19: Experimental and simulated PXRD patterns of MFA-DMAP salt.

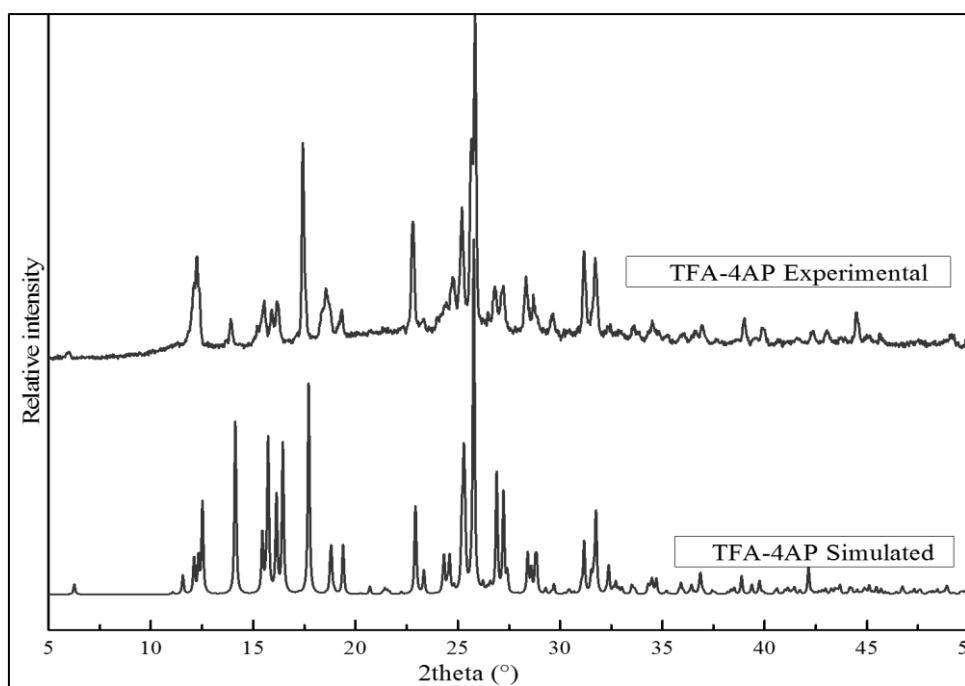


Figure 4.20: Experimental and simulated PXRD patterns of TFA-4AP salt.

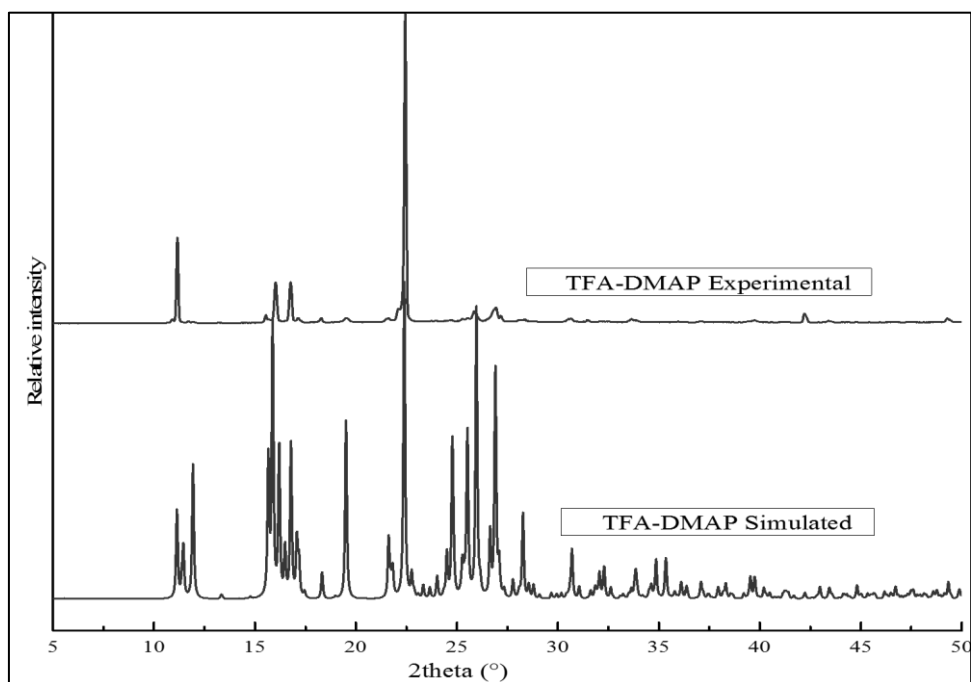


Figure 4.21: Experimental and simulated PXRD patterns of TFA-DMAP salt.

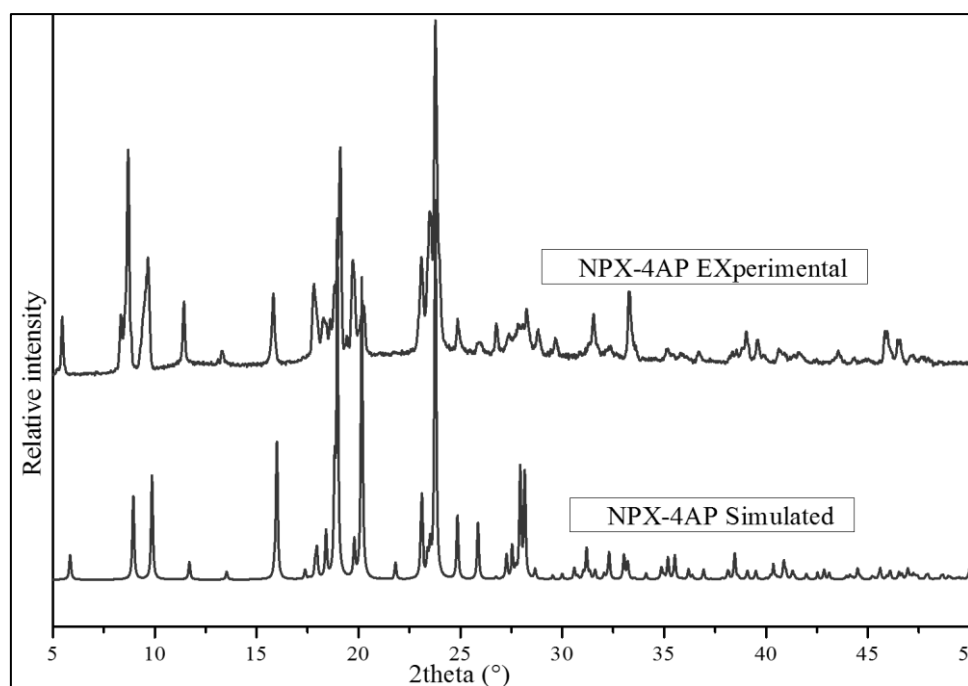


Figure 4.22: Experimental and simulated PXRD patterns of NPX-4AP salt.

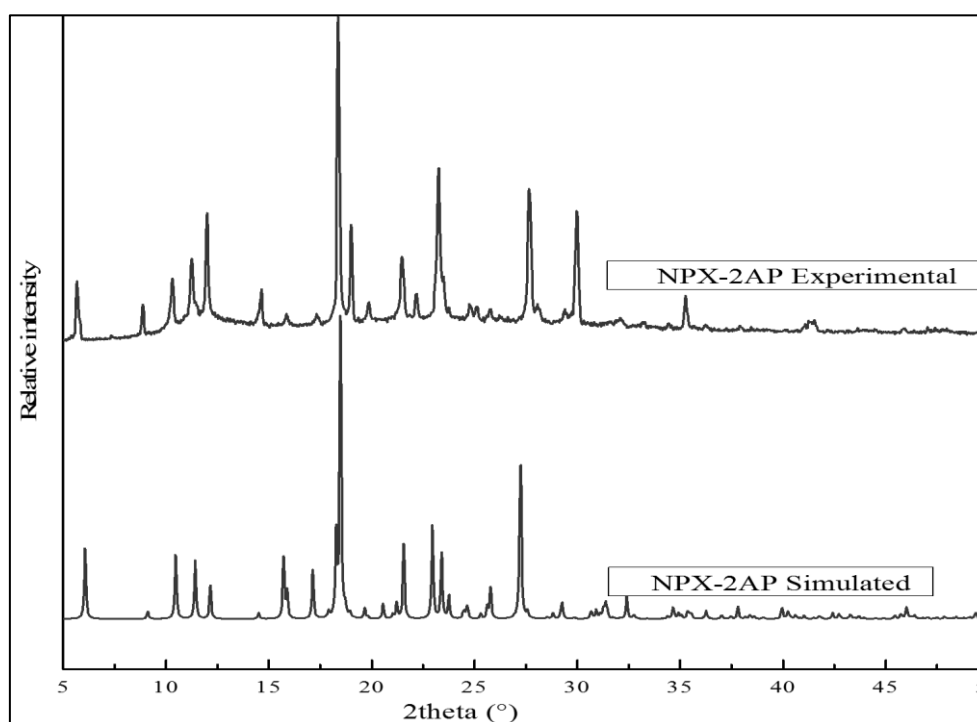


Figure 4.23: Experimental and simulated PXRD patterns of NPX-2AP salt.

4.3.5 Structural comparison of molecular salts

The crystal packing in salt hydrate of MFA-4AP and TFA-4AP were found to be isostructural with similar bond lengths and bond angles. These salt hydrates were exhibited 1:1 molecular stoichiometry in the crystal lattice and the acid...pyridine interactions were mediated by a water molecule. In both the salt hydrates stacking interaction between 4AP and the respective APIs were observed. The isostructurality of both the salts is compared using the isostructural index. The similarity index of the unit cell parameter is based on the equation π , where

$$\pi = ((a + b + c) / (a' + b' + c')) - 1, \text{ for } a + b + c > a' + b' + c'$$

Where, a , b , c and a' , b' , c' are the orthogonal lattices parameters of the respective molecular salts. The values obtained from the above equation is found to be close to zero indicating the isostructurality of molecules.

Another criterion for comparing isostructurality was given by Rutherford by defining a new parameter ϵ , where

$$\epsilon = (V' / V)^{1/3} - 1, \text{ such that } V' > V$$

Where V and V' are the volumes of the unit cell corresponding to the respective salts. Isostructural parameter values π and ϵ for the molecular salts are shown in **Table 4.5**.

The molecular salt hydrate of MFA-DMAP and TFA-DMAP were found to be isostructural. Unit cell length and cell angles of both the salts are found to have a close resemblance. Molecular salts were crystallized in triclinic crystal system with space group $P\bar{1}$. Charge assisted acid...pyridine heterosynthon observed in both cases unlike in 4AP salts of MFA and TFA, where molecules interacted through a water molecule. In MFA-DMAP both the methyl group associated with DMAP forms a hydrogen bond with the carboxyl group of MFA via C-H...O and C-H...C hydrogen bond whereas in TFA-DMAP, only one methyl group of DMAP molecule was found to form a hydrogen bond with TFA molecule. Isostructurality index π and ϵ are found to be close to zero indicating the close resemblance in crystal packing.

Table 4.5: Isostructural parameters of molecular salts.

Molecular salts	Parameter	
	π	ξ
MFA-4AP and TFA-4AP	0.00596	0.00330
MFA-DMAP and TFA-DMAP	0.001776	0.00081

4.3.6 Conformational analysis of molecular salts

Owing to the influence of steric effect, hydrogen bonding and the packing of molecules in the solid state, molecules can take different orientations or conformations. These conformational changes of molecules (drug molecules) can impact the physical properties such as solubility, stability and thermal behavior. In the molecular salts of three different APIs, conventional acid···acid homosynthon was replaced by charge assisted acid···pyridine heterosynthon. In the case of MFA salts, molecule takes two different conformations for 4AP and DMAP salts. Due to the presence of two methyl group in DMAP molecule, the conformation of MFA was twisted at C-N-C bond angle. In TFA salts as well, the different conformations of TFA molecule were observed in TFA-4AP and TFA-DMAP salts. Conformational changes observed for NPX API as well, in NPX-4AP salt, due to the presence of water molecule, crystal structure follows $R_3^3(9)$ graph set. However, in anhydrous NPX-2AP, crystal structure follows $R_2^2(8)$ ring motifs (**Figure 4.24**) (torsion angles for all the salts are displayed in **Table 4.6**).

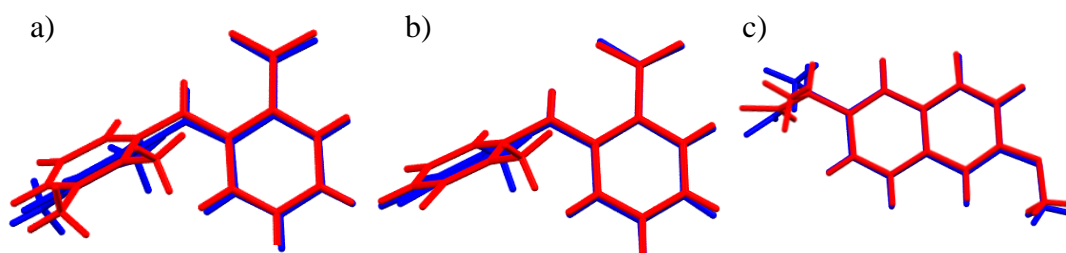


Figure 4.24: Overlay of three different APIs (a-MFA, b-TFA and c-NPX) extracted from the crystal structure of binary solids. Blue=MFA-4AP, TFA-4AP and NPX-4AP and Red=MFA-DMAP, TFA-DMAP and NPX-2AP.

Table 4.6: Torsion angle of APIs in molecular salts.

MFA salts	TFA salts	NPX salts
τ_1 N7-C8-C9-C15 τ_2 C6-N7-C8-C13 τ_3 C1-C6-N7-C13 τ_4 C8-C9-C10-C14 τ_5 C1-C6-N7-C15	τ_1 N7-C8-C9-C15 τ_2 C6-N7-C8-C13 τ_3 C1-C6-N7-C13 τ_4 C8-C9-C10-C14 τ_5 C1-C6-N7-C15	τ_1 C14-C5-C3-C4 τ_2 C4-C3-C5-C6 τ_3 O1-C2-C3-C4 τ_4 C7-C6-C5-C4 τ_5 C7-C6-C5-C3

Molecular components	τ_1	τ_2	τ_3	τ_4	τ_5
MFA-4AP	2.24	-93.16	-144.84	178.61	114.25
MFA-DMAP	1.47	-104.53	135.76	179.38	-128.28
TFA-4AP	-35.18	-89.08	147.16	-177.77	-118.61
TFA-DMAP	0.39	-105.74	134.08	-179.54	-129.96
NPX-4AP	-92.52	85.97	-15.10	-142.67	179.52
NPX-2AP	-103.81	73.69	-158.11	-144.17	-178.32

4.3.7 DSC analysis

DSC analysis was performed to analyze the thermal stability and to determine the melting point of synthesized molecular salts. Any changes in the melting point of a compound is an indicative of the formation of new crystalline phase. The melting point of starting materials and the molecular salts are displayed in **Table 4.7**. All the synthesized molecular salts exhibited different melting points when compared to their respective starting materials. All the salts melt at a lower temperature compared to starting material is probably due to the presence of water molecule in the salts. 4AP salt of MFA was found to have three different endothermic peaks. This is perhaps due to the phase transformation of molecular crystal, and it further substantiates the possibility of polymorphism in this molecular salt. 4AP salt of TFA and NPX is found to have single endothermic peak indicating the thermal stability of the salts. DMAP salt of MFA and TFA found to exhibit two endothermic peaks where initial endothermic peak

corresponds to the release of the water molecule and then follows the melting of molecular salt. Due to the isostructurality, DSC thermogram was found to be similar for the isostructural molecular salts (DSC plot is displayed in **Figure 4.25-4.27**).

Table 4.7: Melting points of APIs, salt former and the molecular salts.

API (°C)	Salt former (°C)	Molecular salt (°C)
MFA (235.52)	4AP (164.43) DMAP (117.64)	MFA-4AP (124.46) MFA-DMAP (165.03)
TFA (221.45)	2AP (52.63)	TFA-4AP (102.08) TFA-DMAP (158.90)
NPX (161.04)		NPX-4AP (110.93) NPX-2AP (96.02 & 106.60)

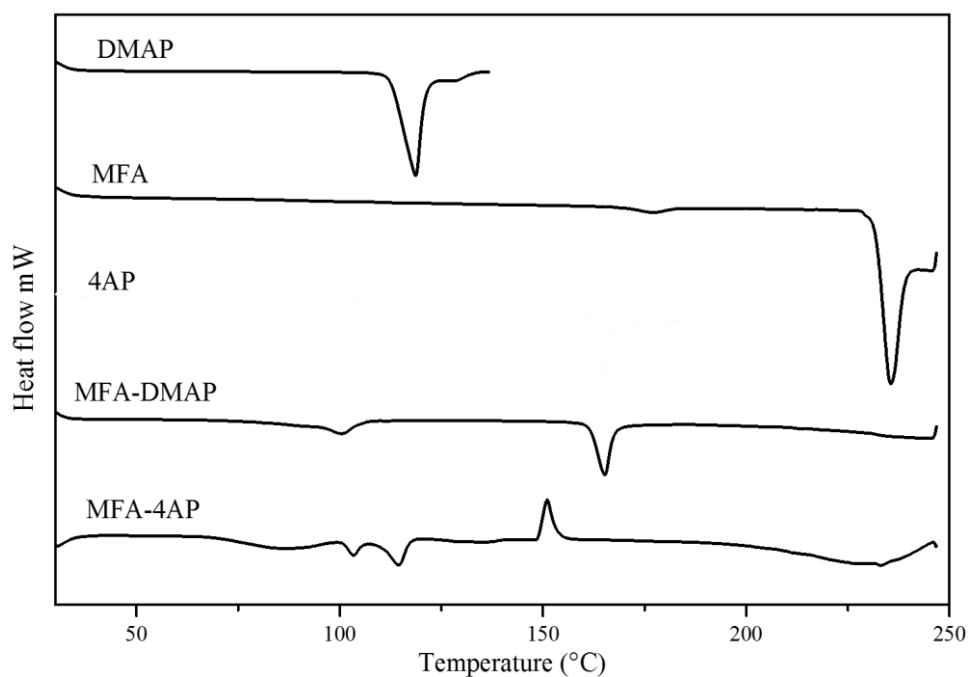


Figure 4.25: Comparison of DSC plots of MFA salts with respect to starting materials.

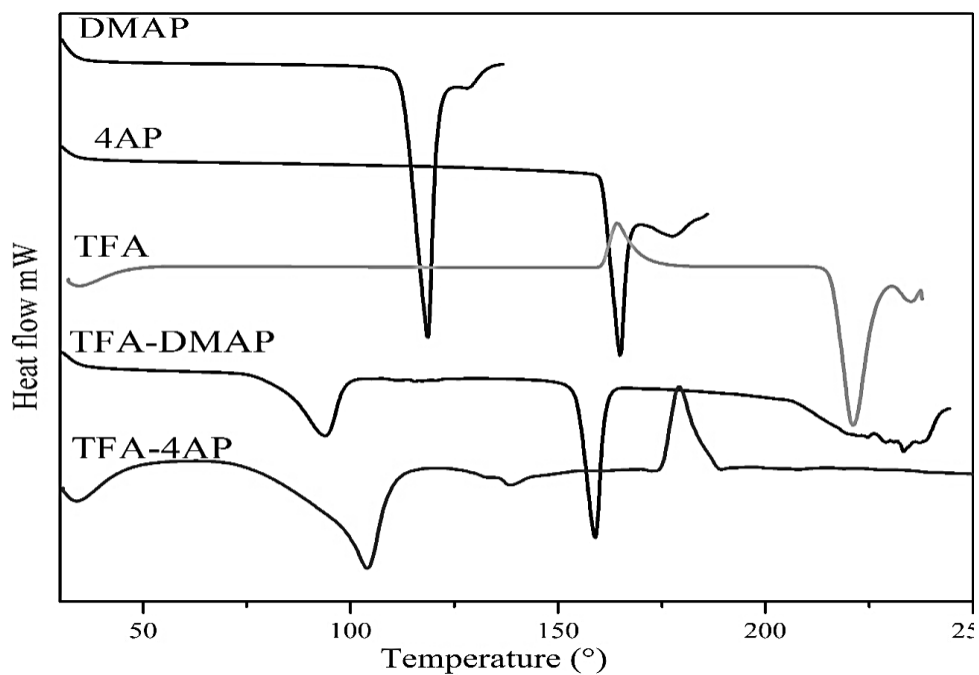


Figure 4.26: Comparison of DSC plots of TFA salts with respect to starting materials.

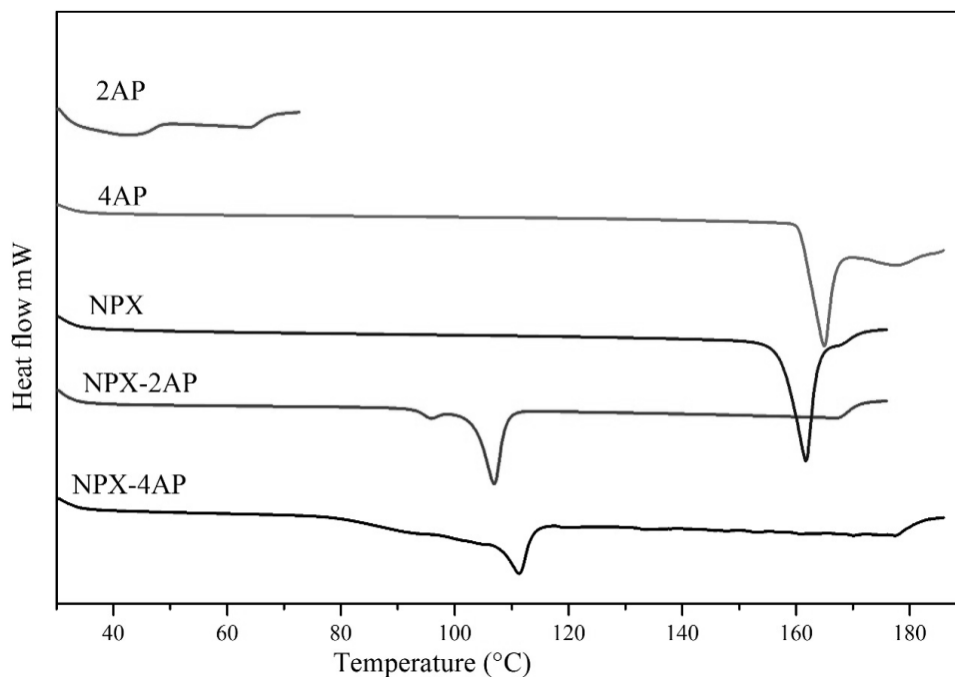


Figure 4.27: Comparison of DSC plots of NPX salts with respect to starting materials.

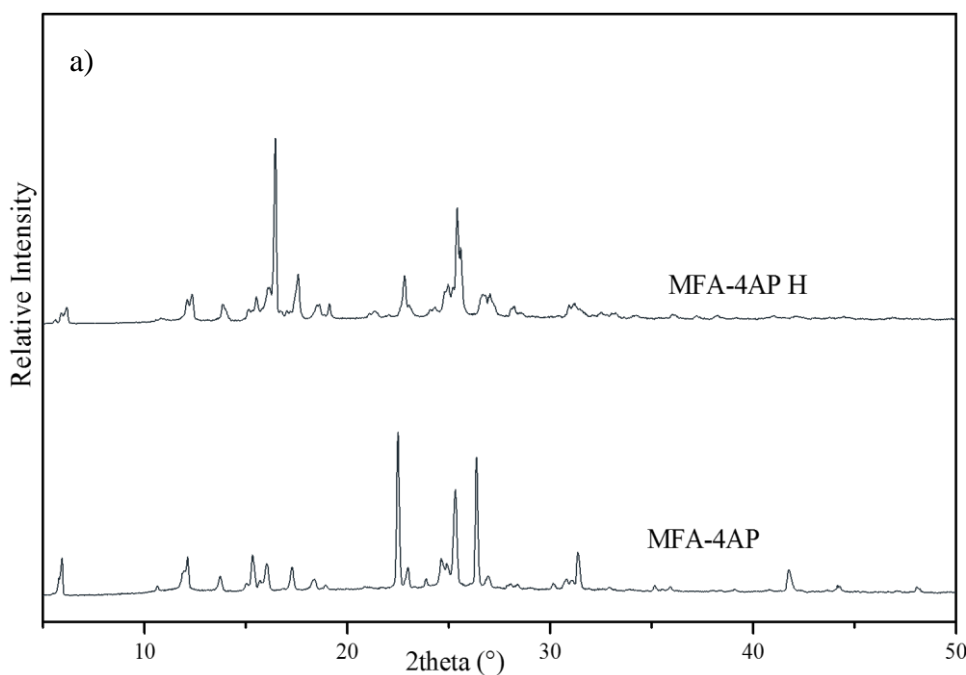
4.3.8 Stability study of molecular salts

Hygroscopicity and long-term stability

Hygroscopicity and long-term stability of 4AP salts of MFA, TFA and NPX have been carried out. The hygroscopicity study was done at accelerated humid

condition (~75% RH) by conventional weight loss method, wherein a known quantity of sample was kept in a desiccator in which relative humidity of ~75% RH was maintained by saturated sodium chloride solution. Weight sample under experimentation was monitored regularly for a period of seven days in order to measure the hygroscopicity. For the experiment, weight was monitored regularly and then phase purity was finally confirmed by PXRD analysis. It was found that further hydration of these molecular salts was not observed under these experimental conditions (**Figure 4.28**).

Long-term stability of these molecular salt was performed at ambient condition for a period of six months. For the experimentation, a known quantity of the sample was kept at room temperature for a period of six months, phase purity of the sample was monitored by PXRD analysis at the end of the experiment. It was found that all the three molecular salts were found to be stable for about six months at room temperature (**Figure 4.29**).



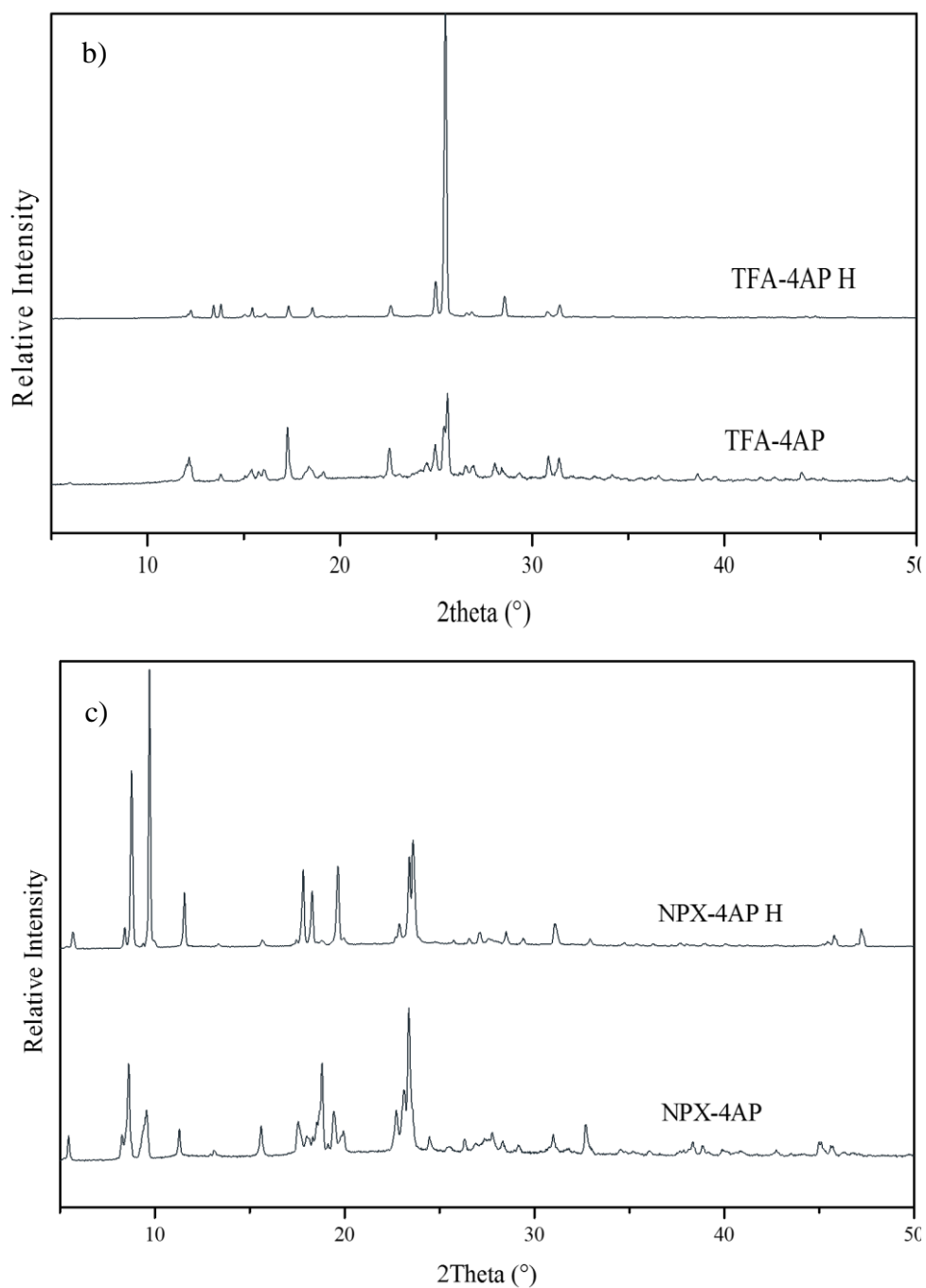


Figure 4.28: Comparison of PXRD patterns of molecular salts of initial and moisture exposed samples: a) MFA-4AP, b) TFA-4AP, and c) TFA-4AP. “H” represents the PXRD pattern of moisture exposed samples.

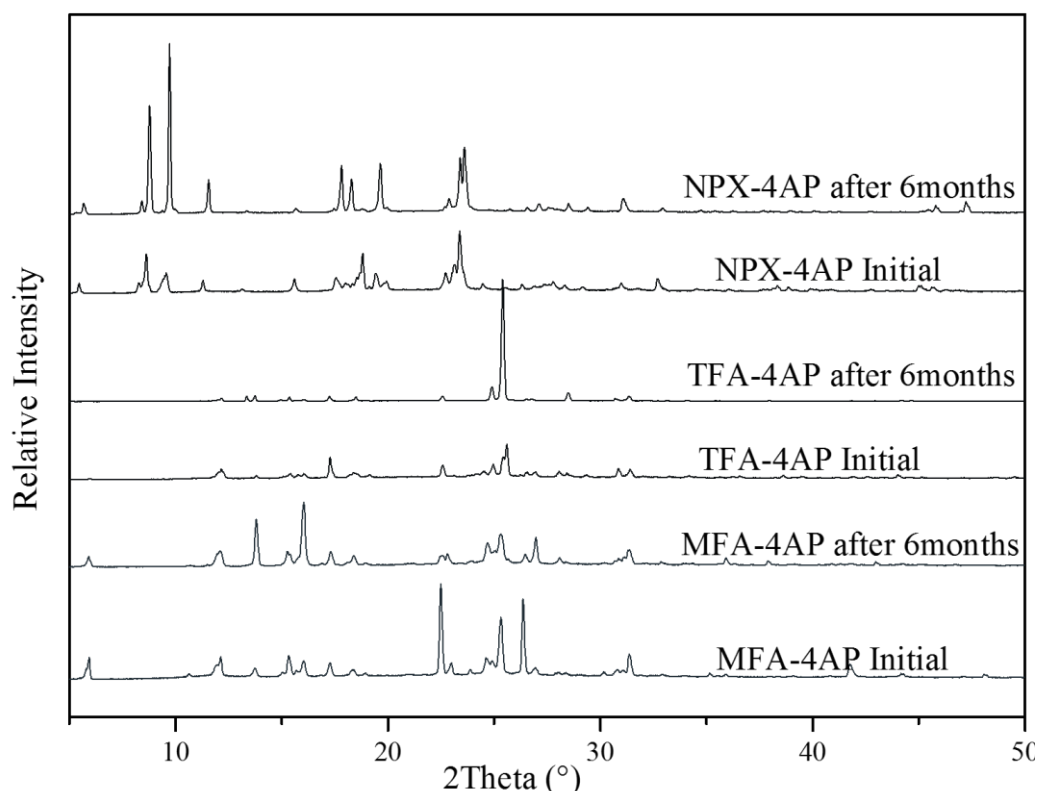


Fig 4.29: Comparison of PXRD patterns correspond to molecular salts recorded at initial stage and after six months.

4.4 CONCLUSIONS

A series of six molecular salts of three different APIs namely MFA, TFA and NPX were synthesized by crystal engineering approach with different pyridyl derivatives. Two molecular salt hydrate of MFA with 4AP and DMAP, two molecular salt hydrate of TFA with 4AP and DMAP and two molecular salts of NPX with 4AP and 2AP were synthesized by a simple solvent evaporation method and the crystal structures of all the salts were determined by SCXRD analysis. Crystal structure data revealed that in all the synthesized salts, charge assisted acid···pyridine heterosynthon was observed. All the molecular salts except NPX-2AP includes a water molecule in the crystal lattice. Further, 4AP salts of MFA and TFA and DMAP salts of MFA and TFA were found to be isostructural based on the isostructural parameters π and ϵ . Stability studies associated with three drug-drug molecular salts (MFA-4AP, TFA-4AP, and NPX-4AP) revealed that these salts were found to be stable for a time period of six months at ambient condition and further hydration of the molecular salts was not observed even at accelerated humid conditions (~75% RH).

CHAPTER 5

***DESIGN, SYNTHESIS, CHARACTERIZATION, DFT,
AND STABILITY STUDY OF COCRYSTAL/SALT OF
ANTI-FIBRINOLYTIC HEMOSTATIC DRUG
TRANEXAMIC ACID***

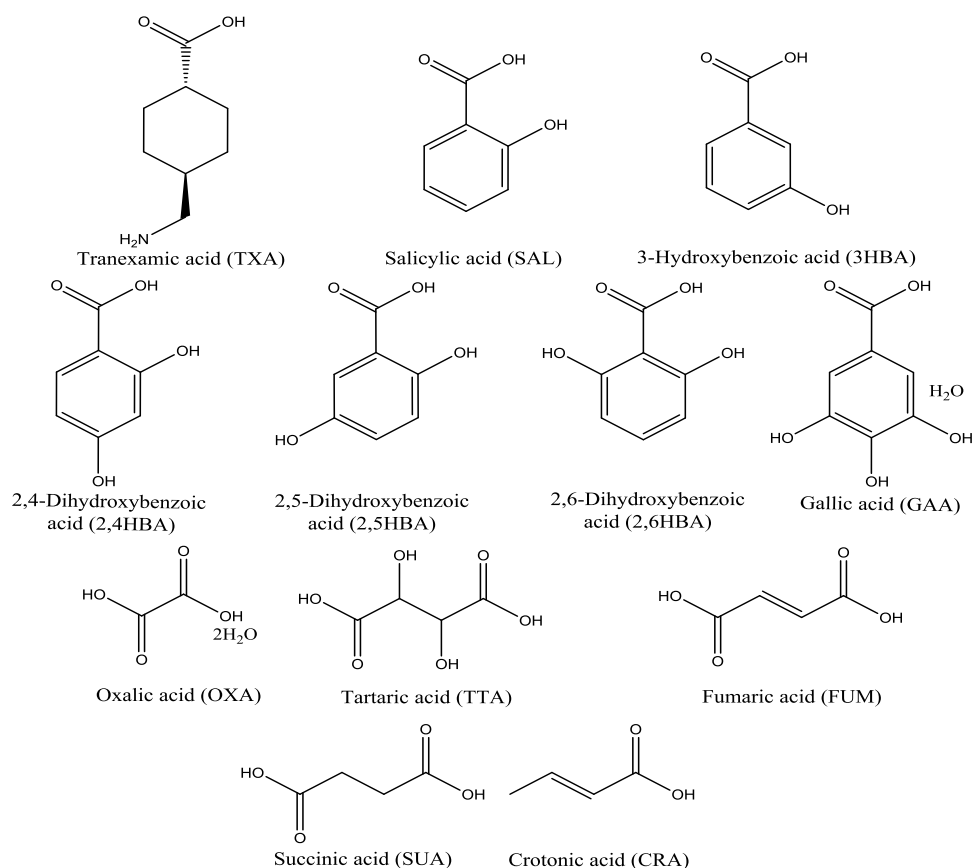
This chapter briefly describes the molecular salt/cocrystal of anti-fibrinolytic hemostatic drug tranexamic acid with GRAS coformers. A detailed structural characterization based on SC-XRD analysis and the stability study of the synthesized salt/cocrystal at room temperature were concisely studied in the present chapter. DFT study was performed to support the salt/cocrystal formation of TXA.

5.1 INTRODUCTION

Tranexamic acid (TXA) is one of the important medication being used extensively worldwide for the treatment of excessive blood loss from trauma, surgery and various medical conditions including hemophilia and heavy menstrual bleeding. Further, TXA is used for the treatments like dental extractions, tonsillectomy, cardiac surgery and prostate surgery. In the year 1986, US FDA approved this drug as intravenous administration for the short-term use in hemophiliac patients undergoing tooth extraction. Presently, the TXA drug is available in both oral and intravenous forms. This drug is on the list of World Health Organization's Essential Medicines, the most important medications needed in a basic health system. TXA is a lysine analog, functions by inhibiting plasminogen activation. The trans-isomer is found to be biologically active, while the cis-isomer is found to be biologically inactive. TXA is found to be highly soluble in water. The main disadvantage of TXA drug is that it's of low absorption (~35-40%) in the gastrointestinal tract possibly due to its amphoteric nature. It has a very short half-life of about 2-3 hours after administration and it is excreted rapidly through kidneys.

Various derivatives of TXA drug molecule have been developed by various research groups in order to increase the absorption in the gastrointestinal tract by varying the side chain of TXA and also by varying the composition of excipients. However, the crystal engineering approach has not been applied to this drug molecule. The CSD contains a guest free form of TXA, exists as zwitter ion. The HBr salt of TXA and two complexes with bismuthate too reported in the literature. No reports on cocrystal/salts of TXA is found in the literature. Therefore, in the present work, we describe the pharmaceutical cocrystal/salt of TXA with carboxylic acid derivatives, mono hydroxy, dihydroxy and tri hydroxybenzoic acid derivatives by a simple solvent evaporation method. The detailed structural and the stability study associated with these

drug products are evaluated in the present study. Further, the Density Functional Theory (DFT) calculations were carried out to better understand the geometric structure of the molecules presented in our study. The interaction energy of the molecular salts and cocrystals were calculated to support the reported structure of the crystalline adducts. The molecular structure of TXA and the cofomers are displayed in **Scheme 5.1**. The cofomers used are salicylic acid (SAL), 3-hydroxybenzoic acid (3HBA), 2,4-dihydroxybenzoic acid (2,4HBA), 2,5-dihydroxybenzoic acid (2,5HBA), 2,6-dihydroxybenzoic acid (2,6HBA), gallic acid (GAA), oxalic acid (TXA), tartaric acid (TTA), fumaric acid (FUM), succinic acid (SUA) and crotonic acid (CRA). The salicylic acid used in the present study is a well-known drug for the treatment of aches and pains and reduce the fever. Further, it is used for the treatment of anti-inflammatory diseases. 2,5HBA is a NSAID drug and it's also known for anti-ageing properties. Remaining hydroxybenzoic acids used in the study are GRAS molecules and all the derivatives exhibit antioxidant properties. All the carboxylic acids used are considered as GRAS molecules according to US FDA.



Scheme 5.1: Molecular diagram of TXA and the cofomers.

5.2 EXPERIMENTAL SECTION

TXA, carboxylic acids, and hydroxybenzoic acid derivatives were purchased from various suppliers and used as such for the synthesis of salt/cocrystals. Analytical reagents grade solvents and purified distilled water were used for the synthesis. Solvent evaporation method is followed for the synthesis of salt/cocrystal.

TXA-SAL: TXA (100 mg, 0.636 mmol) and SAL (87.86 mg, 0.636 mmol) were dissolved in water (10 mL) at 80 °C in a 25 mL beaker, and then allowed this clear solution to crystallize at room temperature. Block shaped pale brown colored crystals were obtained after 2 weeks with 1:1 molecular stoichiometry in the asymmetric unit.

TXA-3HBA: TXA (100 mg, 0.636 mmol) and 3HBA (87.86 mg, 0.636 mmol) were taken in a 25 mL beaker, dissolved in 1:1 methanol/water solvent (10 mL) at 80 °C. The resulting clear solution is then allowed to crystallize at room temperature. Block shaped colorless crystals were obtained after 2 weeks with 1:1 molecular stoichiometry, and a molecule of water in the asymmetric unit.

TXA-2,4HBA: TXA (100 mg, 0.636 mmol) and 2,4HBA (98 mg, 0.636 mmol) were dissolved in purified water (10 mL) at 80 °C temperature. The resultant clear solution is then allowed for slow evaporation at ambient temperature to yield block shaped colorless crystals of TXA-2,4HBA salt in 1:1 stoichiometric ratio.

TXA-2,5HBA: TXA (100 mg, 0.636 mmol) and 2,5HBA (98 mg, 0.636 mmol) were dissolved in 1:1 ethanol/water (10 mL) at 80 °C, followed by slow evaporation of the solvent resulted in TXA-2,5HBA salt in 1:1 ratio after 2 weeks.

TXA-2,6HBA: In a 25 mL beaker, TXA (100 mg, 0.636 mmol) and 2,6HBA (98 mg, 0.636 mmol) were taken in purified water (10 mL), dissolved at 80 °C and then allowed to crystallize slowly at room temperature. After 2 weeks colorless block-shaped crystals were obtained in 1:1 stoichiometric ratio of TXA and 2,6HBA in the asymmetric unit.

TXA-GAA: In a 25 mL beaker, TXA (100 mg, 0.636 mmol) and GAA (119.6 mg, 0.636 mmol) were taken in purified water (10 mL), dissolved at 80 °C and then allowed to crystallize slowly at room temperature. After 2 weeks light brown colored block-shaped

crystals were obtained in 1:1 stoichiometric ratio of TXA and GAA in the asymmetric unit.

TXA-OXA: A 1:1 ratio of TXA (100 mg, 0.636 mmol) and OXA (80.17 mg, 0.636 mmol) were taken in 10 mL of purified water, dissolved completely at 80 °C. This clear solution is then allowed to crystallize slowly at room temperature for about 2 weeks. Colorless block-shaped crystals were obtained in 2:1 molecular ratio in the asymmetric unit after 2 weeks by filtration.

TXA-TTA: A 1:1 ratio of TXA (100 mg, 0.636 mmol) and TTA (95.45 mg, 0.636 mmol) were taken in 10 mL of 1:1 ethanol/water solvent media, dissolved completely at 80 °C, followed by slow crystallization at room temperature yielded 1:1 salt of TXA-TTA after 2 weeks as colorless crystals.

TXA-FUMA 1:1 ratio of TXA (100 mg, 0.636 mmol) and FUM (73.82 mg, 0.636 mmol) were taken in 10 mL of 1:1 methanol/water solvent media, dissolved at 80 °C. 1 mL of dimethylformamide solvent is added in order to get the complete clear solution. This clear solution is then allowed for slow evaporation at room temperature resulted in 2:1 block shaped colorless crystals of TXA-FUM salt after 2 weeks by filtration.

TXA-SUA: A 1:1 stoichiometric ratio of TXA (100 mg, 0.636 mmol) and SUA (75.11 mg, 0.636 mmol) were taken in 10 mL of 1:1 methanol/water solvent media, dissolved completely at 80 °C. This clear solution allowed to evaporate completely at room temperature yielded colorless crystals of TXA-SUA salt in 2:1 stoichiometric ratio in the asymmetric unit after 2 weeks by filtration.

TXA-CRA: TXA (100 mg, 0.636 mmol) and CRA (54.75, 0.636 mmol) were dissolved in 10 mL of 1:1 methanol/water media at 80 °C, followed by slow evaporation at room temperature yielded 1:1 cocrystal of TXA-CRA after 2 weeks as colorless crystals.

5.3 RESULTS AND DISCUSSION

Tranexamic acid exists as a zwitter ion in the solid state and it has a pka value of 4.56 & 10.2 (for acid and amino group). Since the molecule exists as zwitter ion, the prediction of salt or cocrystal formation in the experiment is difficult. Nevertheless, the ΔpK_a comparison has been done for the chosen cofomers. It was observed that all the

ΔpK_a (pK_a base- pK_a acid) values for the coformers chosen in the present study lie above 4 units, which indicate the salt formation is favored over cocrystal formation. However, in the synthesized crystalline materials, except TXA-GAA and TXA-CRA, proton transfer is observed from acid group of coformer to amino group of TXA, and the carboxylate group of TXA exists as the carboxylic acid in the newly formed crystalline materials. TXA-GAA and TXA-CRA crystallized as cocrystal where no proton transfer observed. The pK_a and ΔpK_a values of TXA and the coformers are shown in **Table 5.1**.

Table 5.1: The pK_a and ΔpK_a values of TXA and the coformers used in the study.

API pK_a (pK_{a1})	Coformer/counter ion pK_a (pK_{a2})	ΔpK_a (pK_{a1} - pK_{a2})	Crystalline adducts formed
TXA (10.2)	SAL (2.97)	7.23	Salt
	3HBA (4.08)	6.12	Salt
	2,4HBA (3.1)	7.1	Salt
	2,5HBA (2.95)	7.25	Salt
	2,6HBA (1.6)	8.6	Salt
	GAA (4.5)	5.7	Cocrystal
	OXA (1.25 & 4.14)	8.95 & 6.06	Salt
	TTA (2.89 & 4.40)	7.31 & 5.80	Salt
	FUM (3.03 & 4.44)	7.17 & 5.76	Salt
	SUA (4.2 & 5.6)	6.0 & 4.6	Salt
	CRA (4.69)	5.51	cocrystal

5.3.1 SC-XRD analysis of salt/cocrystal of TXA

TXA-SAL

It was crystallized in monoclinic crystal system with space group $P 2_1/n$, the proton transfer from acid group of SAL to amino group of TXA was observed and the molecules in the asymmetric unit interacted through O-H \cdots O hydrogen bond (2.647 Å, $\angle 177.68^\circ$) between acid group of TXA and carbonyl group of SAL (**Figure 5.1a**). The neighboring molecular units were interconnected through two different complementary -N-H \cdots O hydrogen bond (3.053 Å & 3.001 Å) between the amino group of TXA and carboxyl group of SAL and C-H \cdots O hydrogen bond (3.225 Å) between C-H of TXA and oxygen of SAL resulting in a cyclic four component supramolecular unit. These interactions further continue resulting in 1 Dimensional (1D) and 2D cyclic chain like structure of TXA-SAL salt (**Figure 5.1b** & **Figure 5.1c**). This further converts to the 3D structure by utilizing two different C-H \cdots π interactions between TXA and SAL with

bond distances 3.731 Å and 3.761 Å respectively. The crystal structure details and the refinement parameters are displayed in **Table 5.2a** & **Table 5.2b**. The geometrical parameters of intermolecular interactions in the salt/cocrystal of TXA is displayed in supplementary material **Table 5.3**. Color code for the atoms are gray: carbon, off-white: hydrogen, red: oxygen, blue: nitrogen.

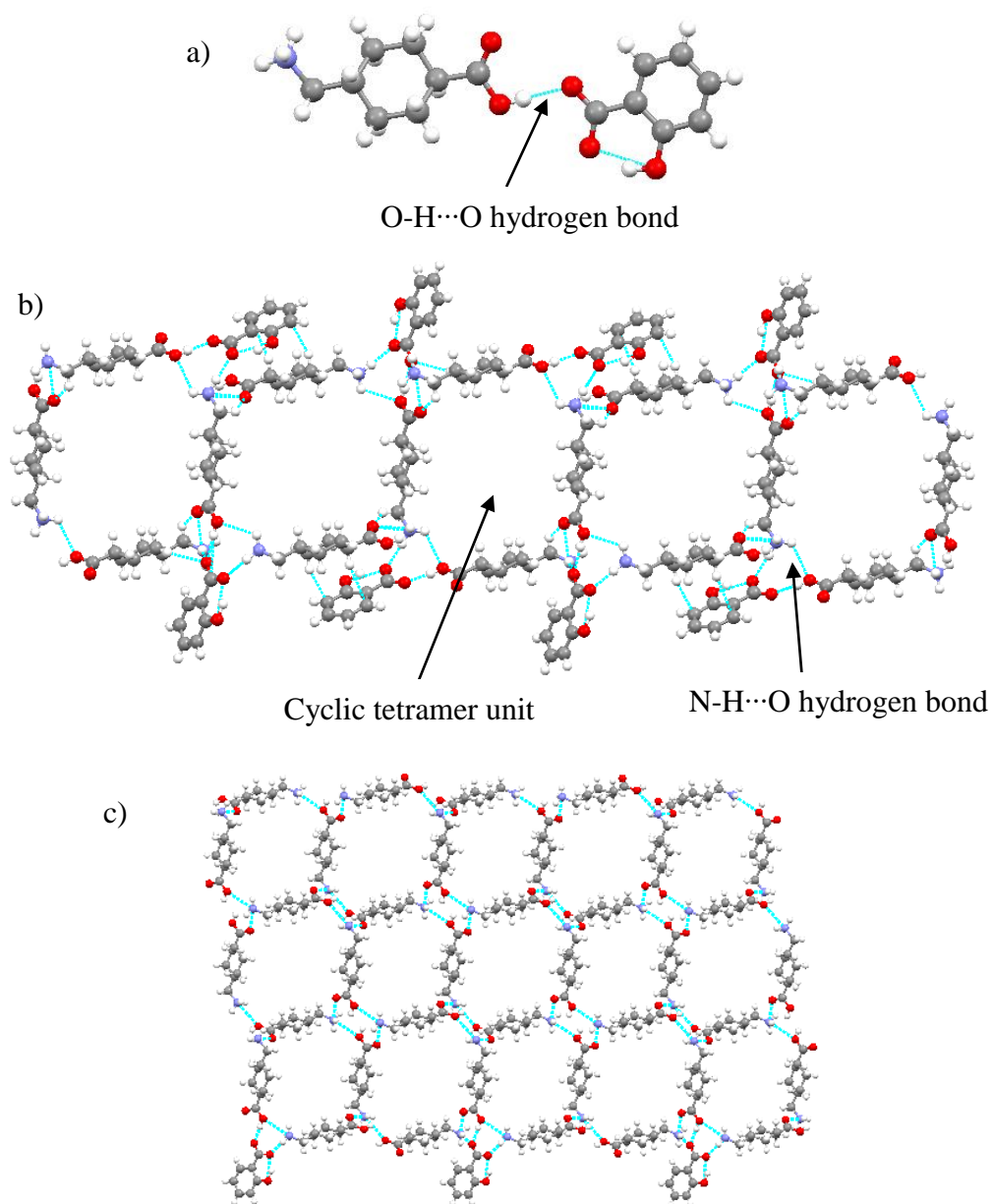
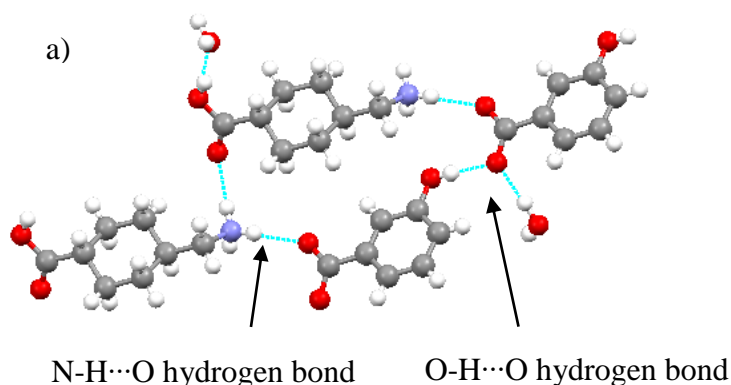


Figure 5.1: (a) Asymmetric unit (b) 1D cyclic chain-like structure (c) 2D structure of the TXA-SAL salt.

TXA-3HBA

It was crystallized as a monohydrate salt and the asymmetric unit consists of two molecules each of TXA, 3HBA, and water. It was crystallized in triclinic crystal system with space group $P\bar{1}$. The molecules were interconnected through N-H \cdots O hydrogen bond (2.861 Å and 2.917 Å) between TXA and 3HBA molecules (**Figure 5.2a**). 3-hydroxy group of 3HBA forms hydrogen bond with carbonyl group of another 3HBA molecule. Water molecule in the crystal structure forms hydrogen bond with acid group of TXA and carbonyl group of 3HBA molecules. In the crystalline structure, molecules form a cyclic six component supramolecular unit by utilizing O-H \cdots O and N-H \cdots O hydrogen bond involving TXA, 3HBA and water molecule, and this further continues resulting in a cyclic 1D tape-like structure of TXA-3HBA salt hydrate (**Figure 5.2b**). This cyclic 1D structure connected to the neighboring cyclic six component supramolecular units via N-H \cdots O hydrogen bond (2.861 Å & 2.858 Å) which in turn inter connected to the neighboring unit resulting in a 2D sheet-like structure of TXA-3HBA salt hydrate (**Figure 5.2c**). This converts to the 3D structure by utilizing N-H \cdots O and O-H \cdots O hydrogen bond between TXA, 3HBA and water molecules. The overall crystal structure features weak C-H \cdots O hydrogen bond and C-H \cdots π interactions between TXA and 3HBA molecules.



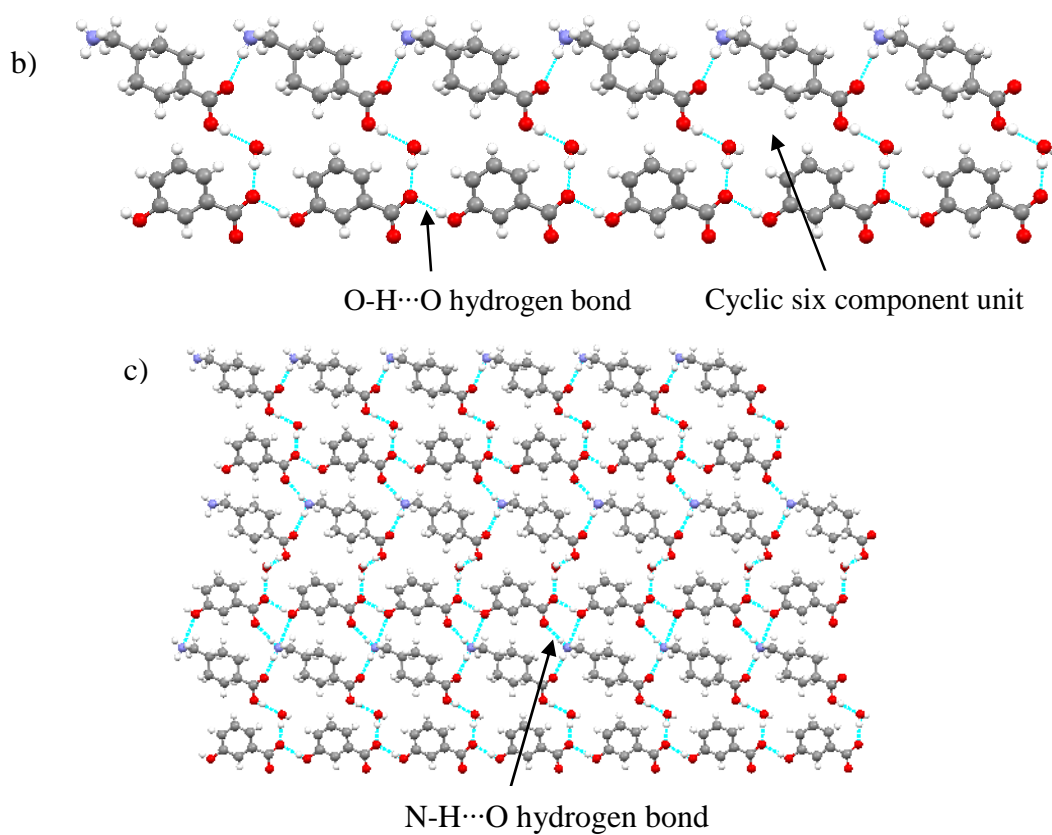


Figure 5.2: (a) Asymmetric unit (b) 1D chain-like structure (c) 2D sheet-like structure of TXA-3HBA salt hydrate.

TXA-2,4HBA

This salt was crystallized in monoclinic crystal system with $P 2_1/n$ space group. The primary synthon involves acid...carbonyl heterosynthon between TXA and 2,4HBA with bond distance 2.627 Å ($\angle 173.48^\circ$) (**Figure 5.3a**). The neighboring supramolecular units were interconnected through two different N-H...O hydrogen bond (2.762 Å & 2.954 Å) involving N-H of TXA and oxygen of carboxyl group of 2,4HBA, O-H...O hydrogen bond (2.840 Å) between 4-hydroxy group of 2,4HBA and the carboxyl group of TXA resulting in a cyclic pentamer unit. This further continues to give a cyclic 1D and 2D structure of TXA-2,4HBA salt (**Figure 5.3b** & **Figure 5.3c**). The 2D structure converts to the 3D structure by utilizing weak C-H... π interaction between TXA and 2,4HBA (bond distance 3.563 Å). The overall crystal structure featured weak C-H...O hydrogen bond between TXA and 2,4HBA.

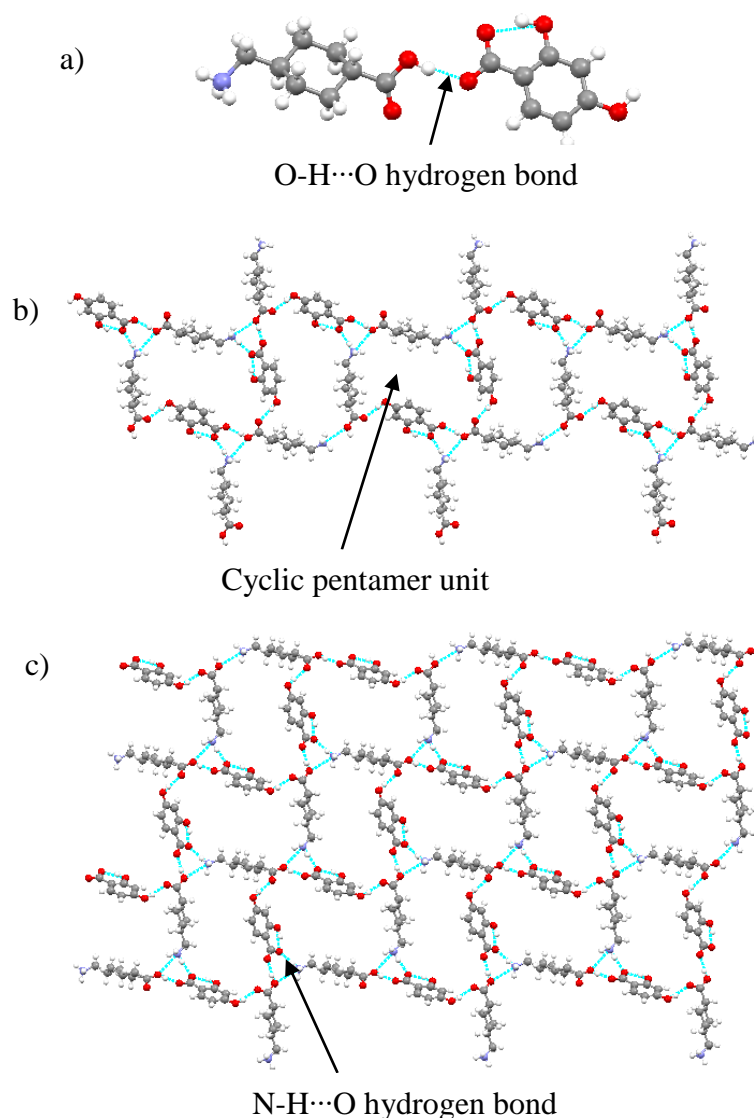


Figure 5.3: (a) Asymmetric unit (b) cyclic 1D structure (c) 2D network-like structure of TXA-2,4HBA salt.

TXA-2,5HBA

This salt was crystallized in monoclinic crystal system with space group $P 2_1/n$. The charge assisted acid...amine heterosynthon was observed in the asymmetric unit with N-H...O bond distance of 2.783 Å ($\angle 174.36^\circ$) (**Figure 5.4a**). The neighboring supramolecular adducts were interconnected through two different O-H...O hydrogen bond (2.756 Å & 2.716 Å) between hydroxy group of 2,5HBA and the carboxyl group of TXA resulting in a cyclic six component supramolecular unit. This further continues to give a 1D tape-like structure of TXA-2,5HBA salt (**Figure 5.4b**). This further converts to the 3D structure by utilizing two different N-H...O hydrogen bond (2.854

Å & 2.871 Å) between N-H of TXA and O of TXA and 2,5HBA respectively (**Figure 5.4c**). The overall crystal structure features weak C-H \cdots O hydrogen bond between TXA molecules and TXA & 2,5HBA molecules.

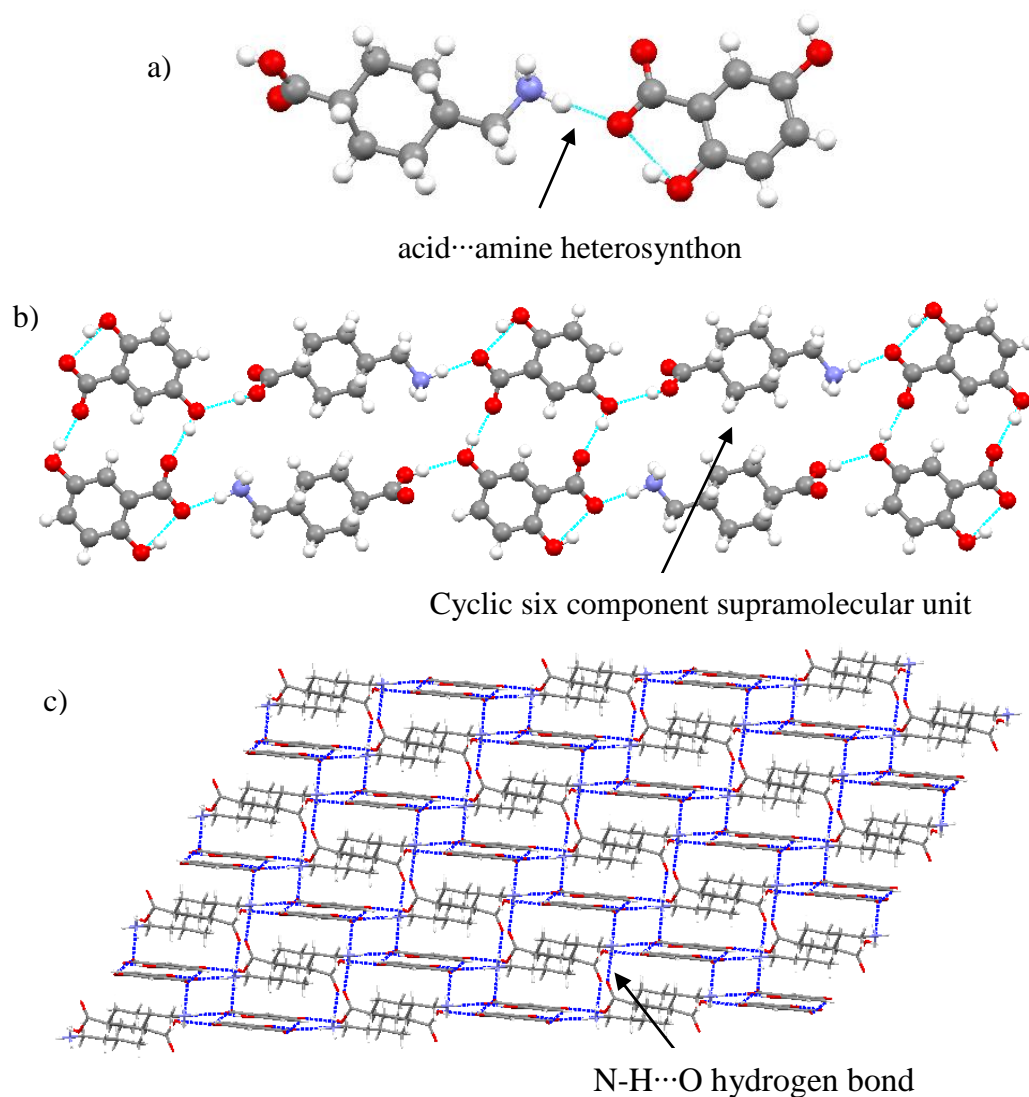


Figure 5.4: (a) Asymmetric unit (b) 1D tape-like structure (c) 3D structure of TXA-2,5HBA salt.

TXA-2,6HBA

A 1:1 molecular salt was obtained which was crystallized in triclinic crystal system with $P\bar{1}$ space group. Primary supramolecular interaction involves the charge assisted acid \cdots amine heterosynthon between 2,6HBA and TXA with N-H \cdots O bond distances 2.854 Å and 3.013 Å (**Figure 5.5a**). The acid group of TXA forms dimer with another TXA molecule with O-H \cdots O bond distance 2.652 Å. These molecular units further self-

assembled through N-H \cdots O hydrogen bond (2.973 Å) involving N-H group of TXA and oxygen of 2,6HBA resulting in a six component cyclic supramolecular unit and this further continues in a diagonal manner resulting in giving a 2D structure of TXA-2,6HBA salt (**Figure 5.5b**). The 2D structure converts to 3D using N-H \cdots O hydrogen bond between N-H of TXA and oxygen of 2,6HBA. The stacking between 2,6HBA molecules is observed in the crystal structure, and the overall crystal structure features weak C-H \cdots O hydrogen bond between TXA and 2,6HBA molecules (**Figure 5.5c**).

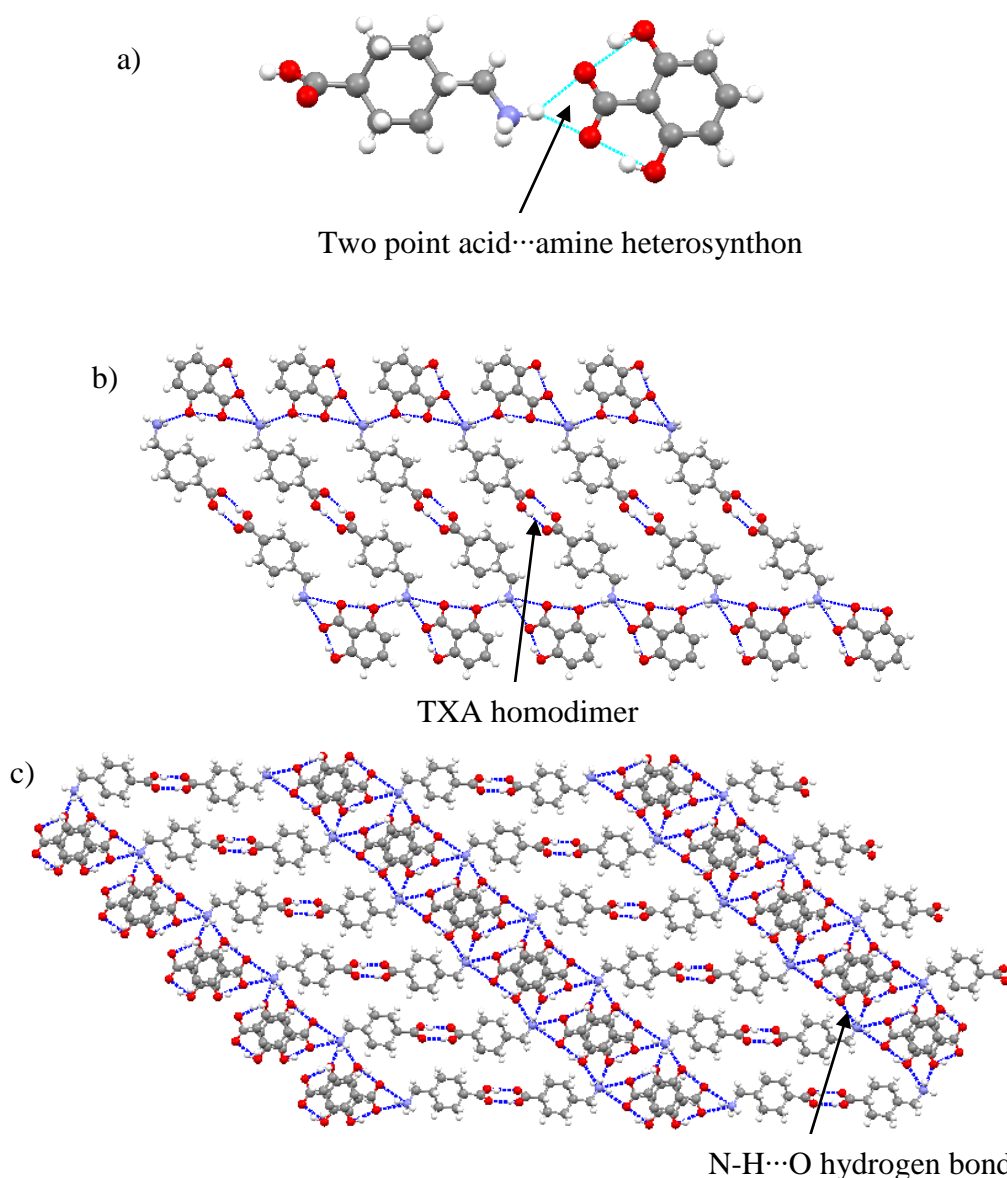
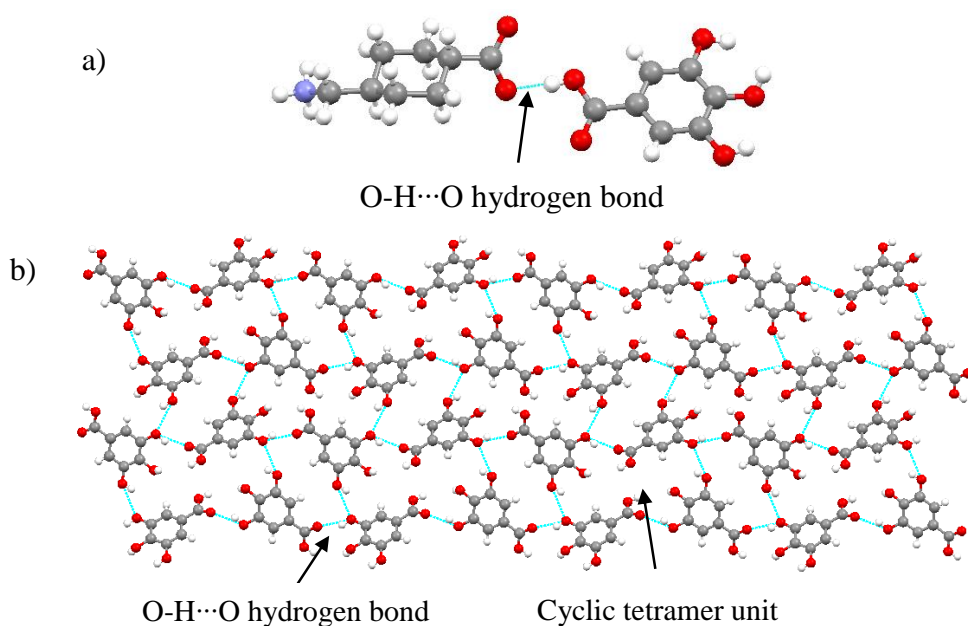


Figure 5.5: (a) Asymmetric unit (b) cyclic 2D structure (c) 3D structure of TXA-2,6HBA salt.

TXA-GAA

A 1:1 cocrystal of TXA and GAA was obtained, which was crystallized in monoclinic crystal system with $P 2_1/n$ space group. TXA molecule in the crystalline material exists as zwitter ion. The primary interaction involves the O-H \cdots O hydrogen bond (2.511 Å, $\angle 174.90^\circ$) between acid group of GAA and carboxylate group of TXA (**Figure 5.6a**). The GAA molecule in the crystalline material forms a cyclic tetramer unit via O-H \cdots O hydrogen bond (2.745 Å & 2.907 Å) which further self-assembled to give a 2D sheet-like structure of GAA in TXA-GAA cocrystal (**Figure 5.6b**). The 2D structure further converts to the 3D structure via O-H \cdots O hydrogen bond (2.690 Å) and N-H \cdots O hydrogen bond (2.930 Å) between TXA and GAA. Further, the TXA molecule in the crystalline structure forms a tetramer unit via N-H \cdots O hydrogen bond (2.765 Å & 2.814 Å) which further interconnected through N-H \cdots O hydrogen bond resulting in a 2D structure of TXA molecule in TXA-GAA cocrystal (**Figure 5.6c**). The overall crystal structure features weak C-H \cdots π (3.785 Å) and C-H \cdots O hydrogen bond between TXA and GAA.



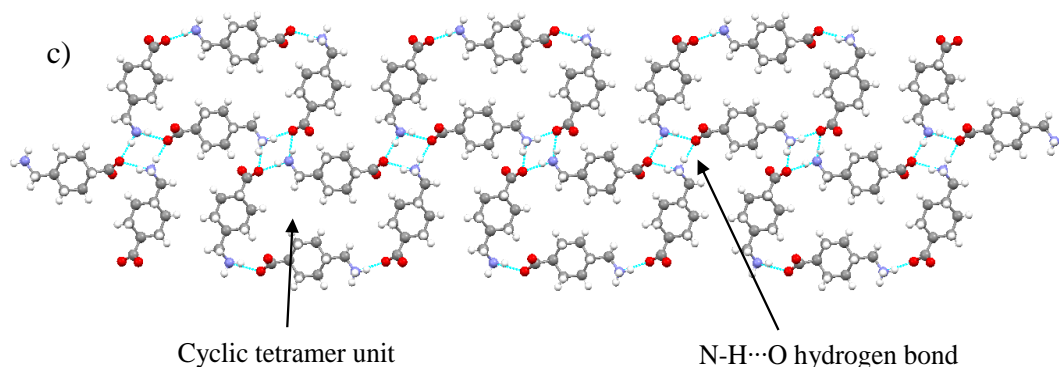
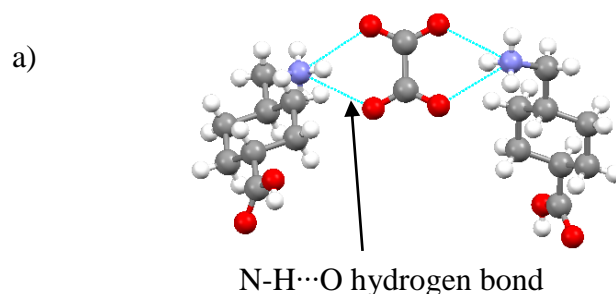


Figure 5.6: (a) Asymmetric unit (b) 2D sheet-like structure of GAA (c) 2D structure of TXA in TXA-GAA cocrystal.

TXA-OXA

It was crystallized in monoclinic crystal system with C_2/c space group. The asymmetric unit consists one molecule of TXA and half molecule of OXA and the molecules were interacted through charge assisted acid...amine heterosynthon (bifurcated) with N-H...O bond distances 2.846 Å and 2.922 Å (**Figure 5.7a**). The TXA molecule in the crystalline material forms a dimer with another TXA molecule with complimentary O-H...O hydrogen bond (2.646 Å). The neighboring supramolecular adducts were interconnected through complementary N-H...O hydrogen bond (2.749 Å) between N-H of TXA and oxygen of OXA resulting in a cyclic six component supramolecular unit (**Figure 5.7b**). This further continues to give a linear 1D tape-like structure of TXA-OXA salt (**Figure 5.7c**). The 1D tape further converts to the 2D and 3D structure by utilizing strong N-H...O hydrogen bond (2.818 Å & 2.749 Å) between TXA and OXA molecules (**Figure 5.7d**). The overall crystal structure features weak C-H...O hydrogen bond between TXA and OXA molecules.



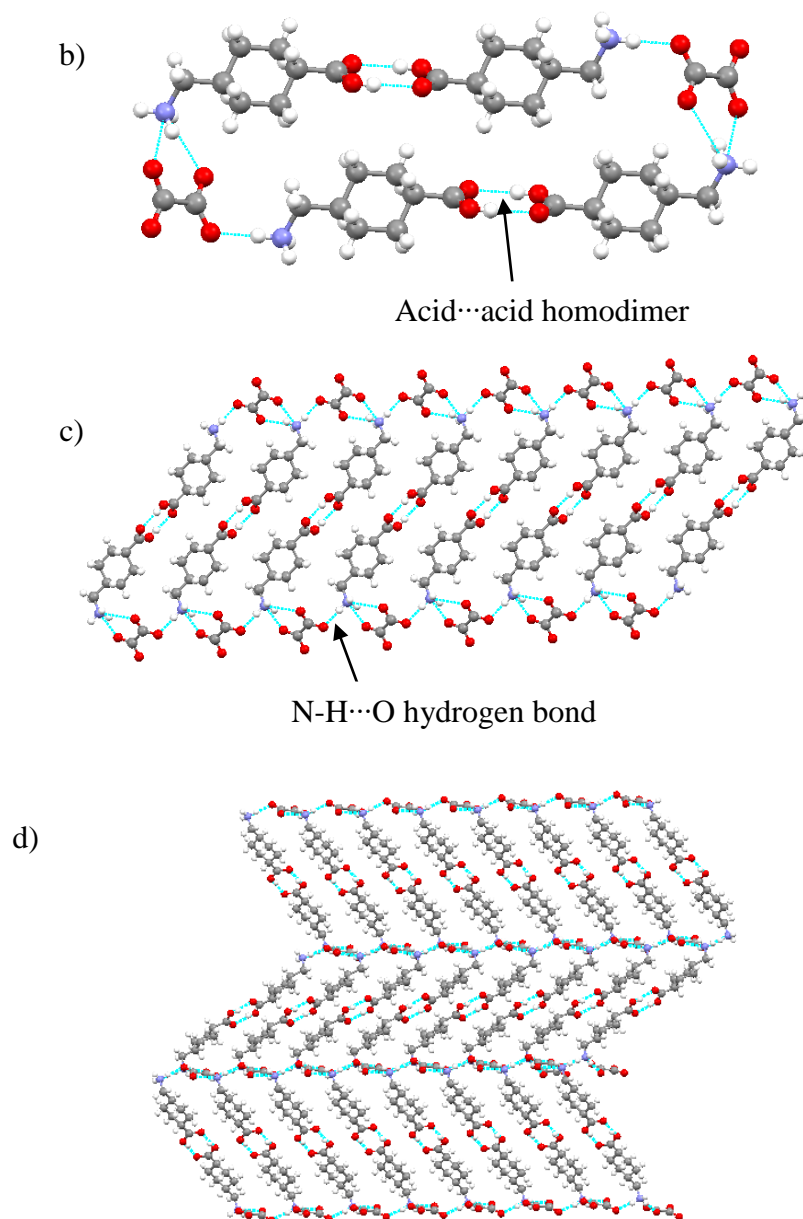
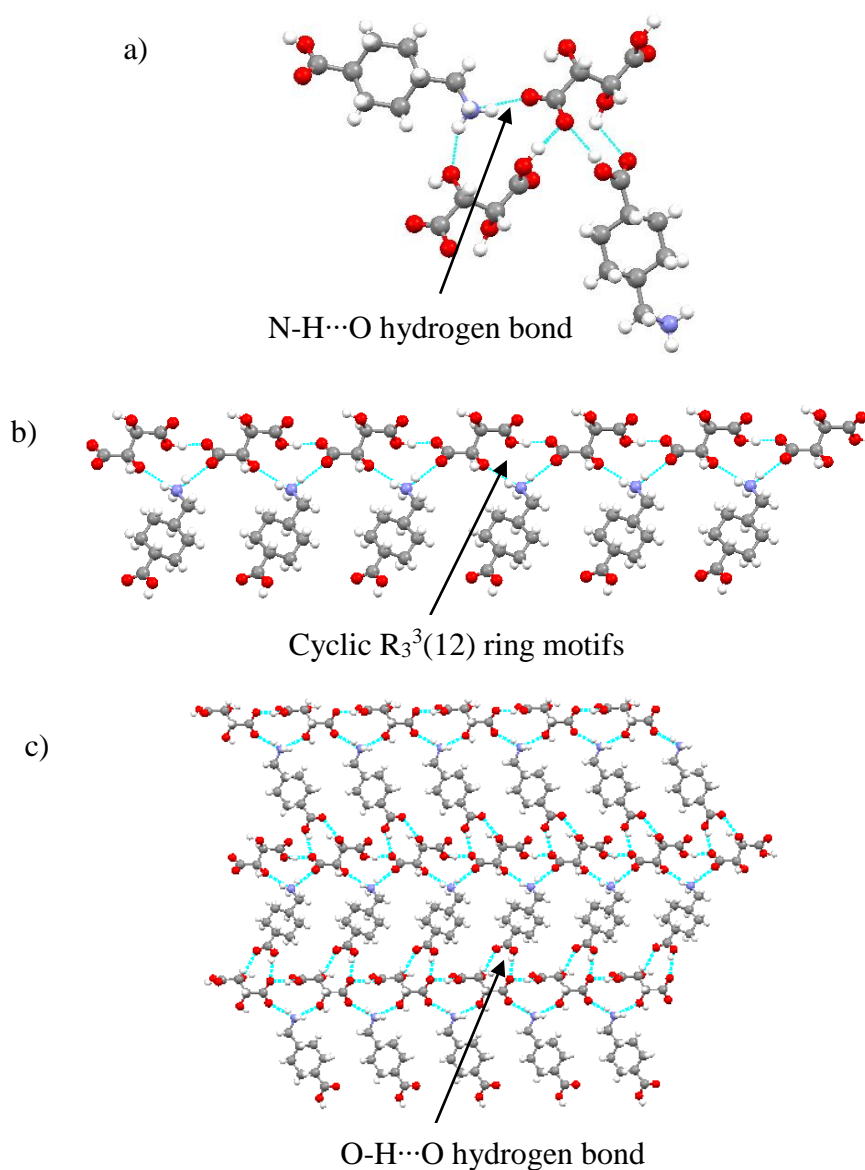


Figure 5.7: (a) Asymmetric unit (b) Cyclic six component supramolecular unit (c) 1D tape-like structure (d) 3D structure of TXA-OXA salt.

TXA-TTA

It was crystallized in monoclinic crystal system with space group $P 2_1$. The asymmetric unit consists of two molecules each of TXA and TTA (**Figure 5.8a**). The molecules in the asymmetric unit were interconnected through N-H...O (2.780 Å & 2.857 Å) and O-H...O hydrogen bond (2.789 Å & 2.626 Å). One carboxylate group of TTA forms a hydrogen bond with an acid group of neighboring TTA (2.565 Å) and the amine group of TXA (2.780 Å), the TXA molecule in turn connected to TTA forming a cyclic

$R_3^3(12)$ ring motifs. This further continues to give the 1D structure of TXA-TTA salt (**Figure 5.8b**). The 1D structure converts to the 2D structure by utilizing O-H \cdots O hydrogen bond involving acid group of TXA and carboxylate group of TTA (2.626 Å) and hydroxy group of TTA with the acid group of TXA (2.789 Å) (**Figure 5.8c**). The 2D structure converts to the 3D structure using N-H \cdots O (2.938 Å & 2.894 Å) hydrogen bond between TXA and TTA, O-H \cdots O hydrogen bond (2.841 Å) between two TTA molecules (**Figure 5.8d**). The overall crystal structure features weak C-H \cdots O hydrogen bond associated with TXA and TTA molecules.



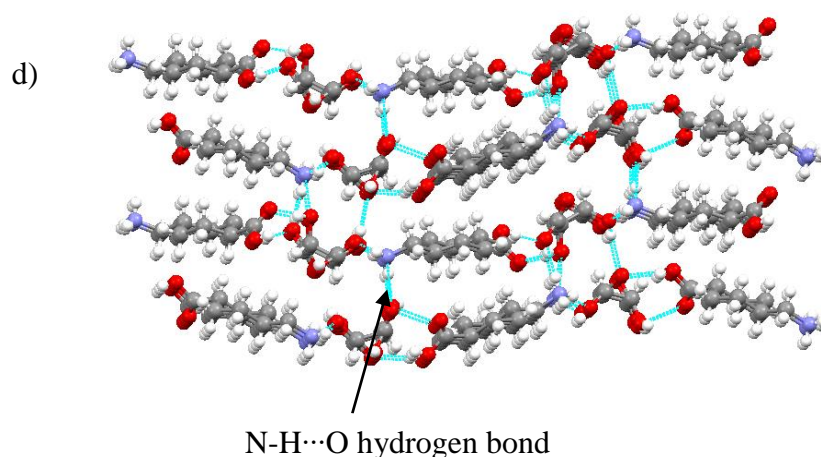
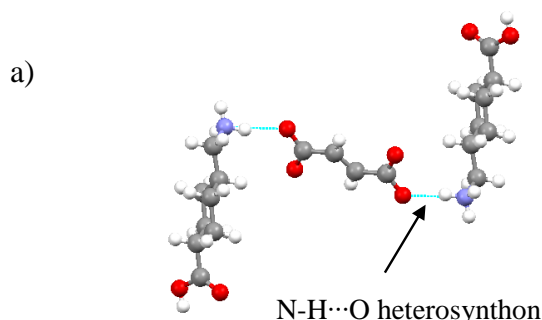


Figure 5.8: (a) Asymmetric unit (b) 1D structure (c) 2D structure (d) 3D structure of TXA-TTA salt.

TXA-FUM

It was crystallized in monoclinic crystal system with $P 2_1/n$ space group. The asymmetric unit consists of 1:0.5 molar ratio of TXA and FUM, which was interconnected through complementary N-H...O hydrogen bond (2.754 Å) (**Figure 5.9a**). The neighboring supramolecular units interacted through N-H...O hydrogen bond (2.865 Å & 2.832 Å) between TXA and FUM resulting in a cyclic tetrameric unit of TXA-FUM salt, which further self-assemble each other resulting in a 1D structure of TXA-FUM salt (**Figure 5.9b**). The 1D structure converts to the 2D and 3D structure by utilizing N-H...O hydrogen bond associated with TXA and FUM (**Figure 5.9c** & **Figure 5.9d**). The overall crystal structure features C-H...O hydrogen bond associated with TXA and FUM molecules).



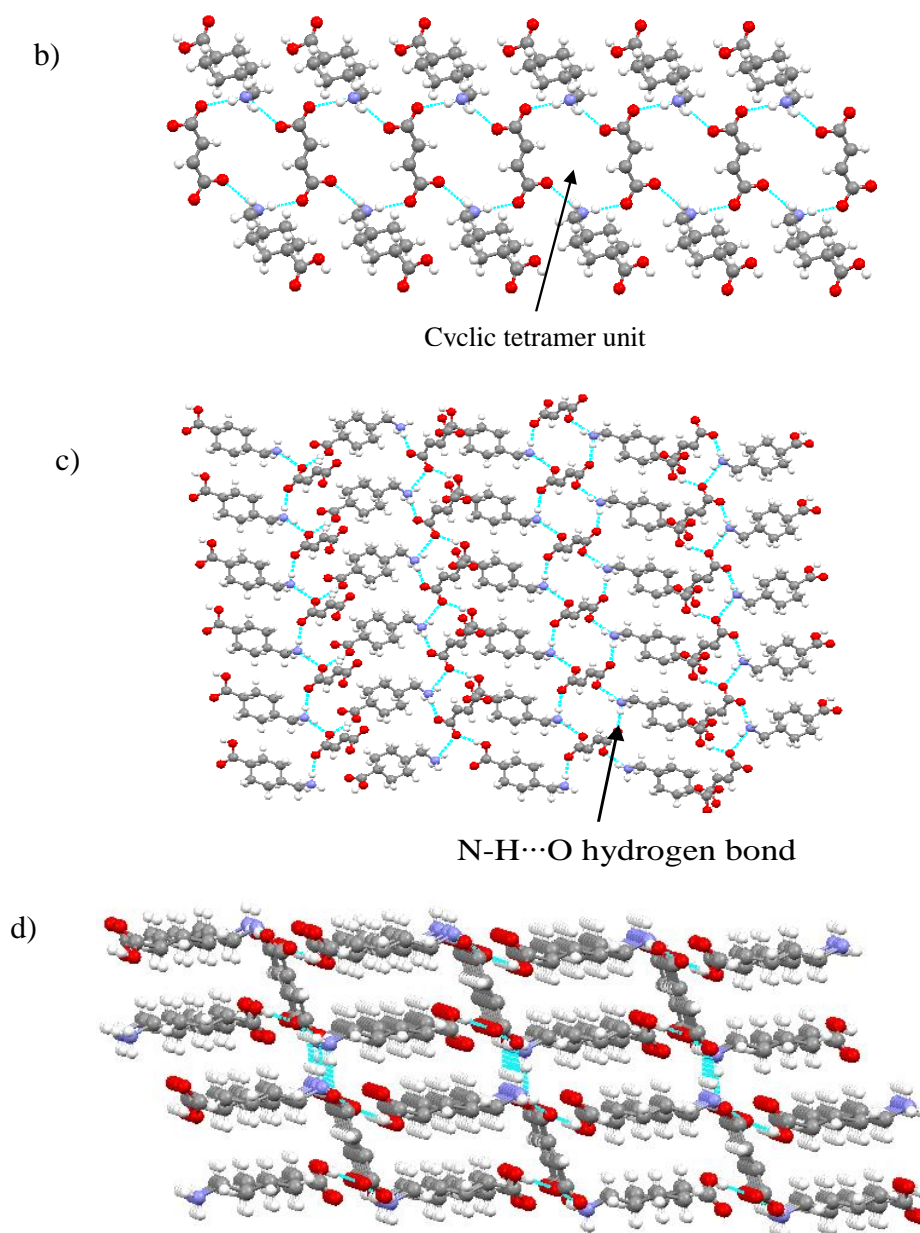


Figure 5.9: (a) Asymmetric unit (b) cyclic 1D structure (c) 2D structure (d) 3D structure of TXA-FUM salt stabilized via N-H...O hydrogen bond.

TXA-SUA

This salt was crystallized in monoclinic crystal system with $P 2_1/n$ space group. The asymmetric unit contains one molecule of TXA and half molecule of SUA which was interconnected through N-H...O hydrogen bond (2.919 Å) (**Figure 5.10a**). The adjacent supramolecular units in the crystalline material were interconnected through complementary N-H...O hydrogen bond (2.842 Å) between TXA and SUA resulting in a cyclic tetrameric unit, which further continues resulting in a 1D structure of TXA-

SUA salt (**Figure 5.10b**). The 1D structure converts to 2D and then 3D structure using N-H \cdots O associated with TXA and SUA molecules (**Figure 5.10c**). The crystal structure also features weak C-H \cdots O hydrogen bond associated with TXA and SUA molecules.

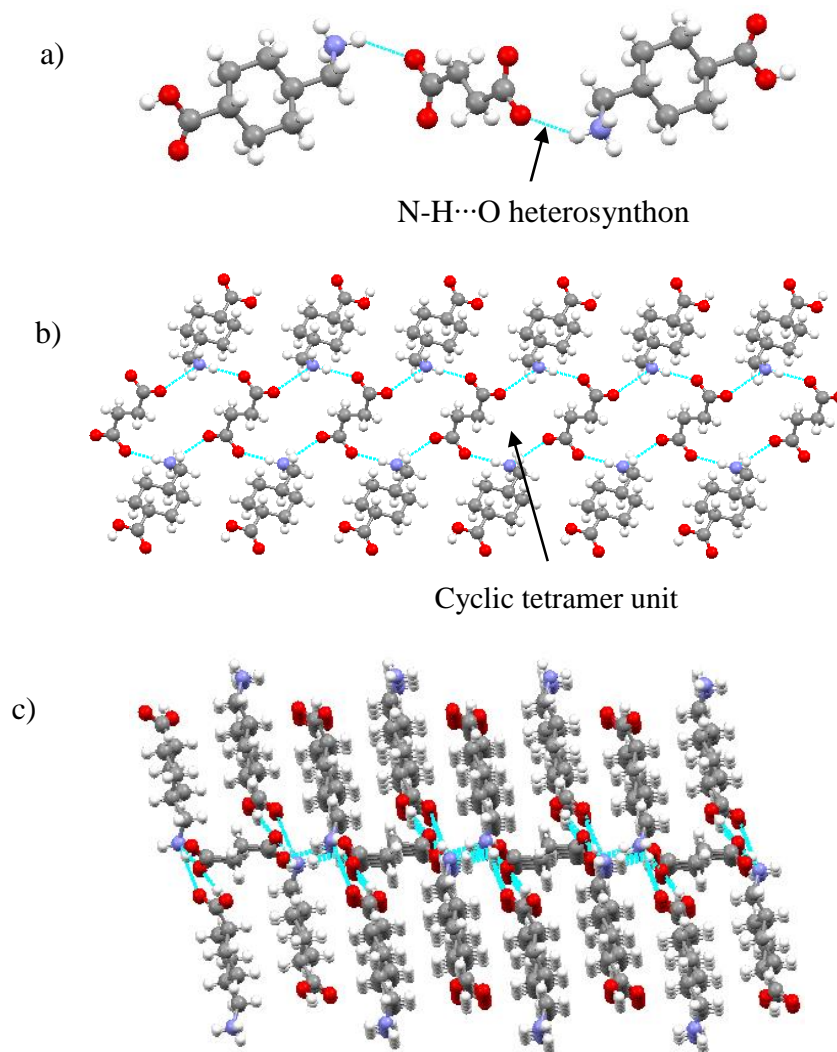


Figure 5.10: (a) Asymmetric unit (b) cyclic 1D structure (c) 3D structure of TXA-SUA salt stabilized via N-H \cdots O hydrogen bond.

TXA-CRA

A 1:1 cocrystal of TXA with CRA was obtained, it was crystallized in monoclinic crystal system with P 2₁/n space group. TXA molecule exists as zwitter ion in the crystalline material. The molecules were interconnected through O-H \cdots O hydrogen bond between CRA and TXA with a bond distance of 2.524 Å (**Figure 5.11a**). TXA molecule in the crystalline material forms a cyclic tetramer unit in the crystal structure with R₄⁴(12) graph sets via N-H \cdots O hydrogen bond (2.748 Å & 2.865 Å). This

tetrameric unit further interconnected through N-H \cdots O hydrogen bond (2.865 Å) resulting in a cyclic 1D chain like structure of TXA molecule in TXA-CRA cocrystal (**Figure 5.11b**). These interactions further repeat in the crystalline material resulting 2D structure of TXA molecule in TXA-CRA cocrystal (**Figure 5.11c**). This 2D structure converts to the 3D structure by interacting with CRA molecule via N-H \cdots O hydrogen bond (2.957 Å) and O-H \cdots O hydrogen bond (2.524 Å) between TXA and CRA molecules. The crystal structure features weak C-H \cdots O hydrogen bond between TXA and CRA molecules.

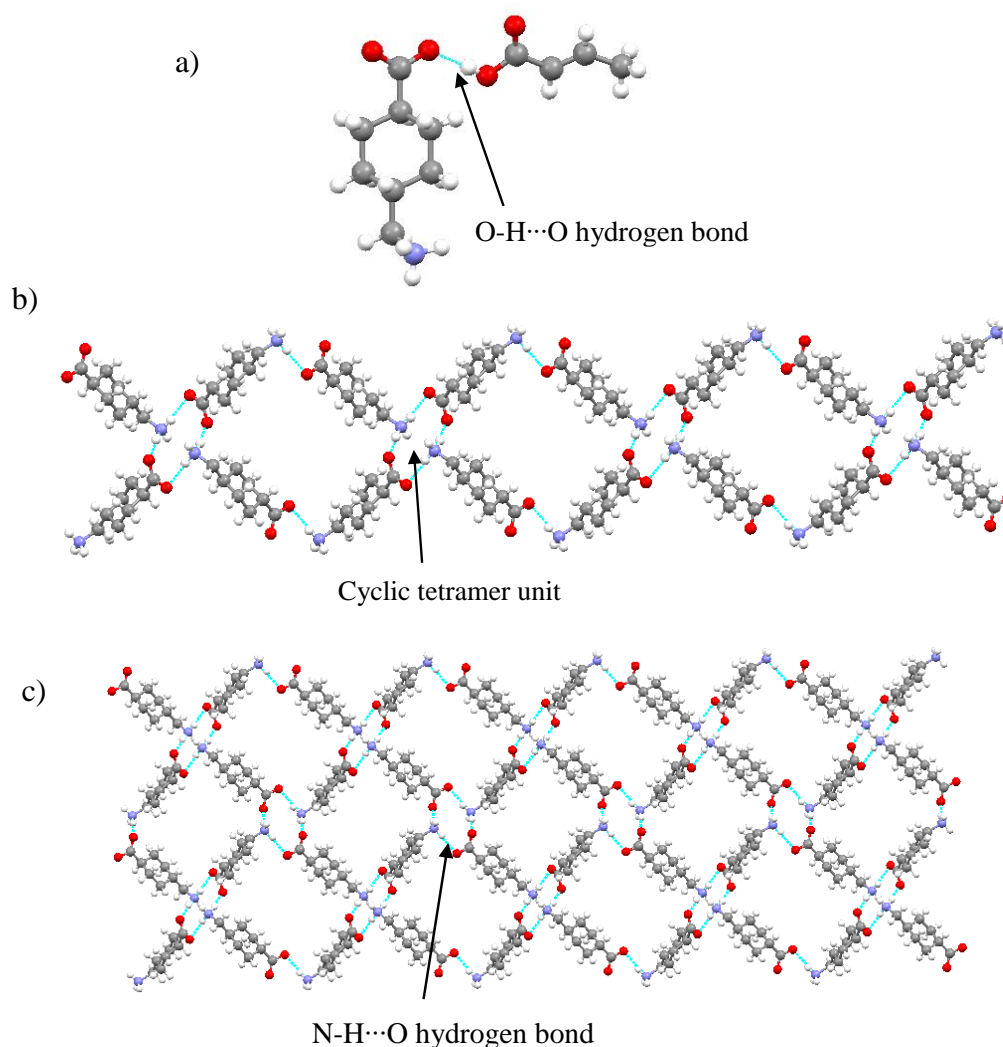


Figure 5.11: (a) Asymmetric unit (b) 1D chain-like structure of TXA (c) 2D chain-like structure of TXA in TXA-CRA cocrystal.

Table 5.2a: The crystal structure details and the crystallographic parameters of TXA salt/cocrystal.

Crystal structure details	TXA-SAL	TXA-3HBA	TXA-2,4HBA	TXA-2,5HBA	TXA-2,6HBA	TXA-GAA
CCDC number	1554428	1554429	1554430	1554432	1554436	1554437
Mol. formula	C ₁₅ H ₂₁ NO ₅	C ₁₅ H ₂₃ NO ₆	C ₁₅ H ₂₁ NO ₆	C ₁₅ H ₂₁ NO ₆	C ₁₅ H ₂₁ NO ₆	C ₁₅ H ₂₁ NO ₇
Molar mass	295.33	313.34	311.33	311.33	311.33	327.33
crystal system	monoclinic	triclinic	monoclinic	monoclinic	triclinic	monoclinic
Space group	P 2 ₁ /n	P -1	P 2 ₁ /n	P 2 ₁ /n	P -1	P 2 ₁ /n
a / Å	9.161(2)	8.076(6)	9.1202(3)	9.4748(3)	7.8714(2)	7.9528(2)
b / Å	14.045(3)	8.744(6)	14.2078(4)	7.7754(3)	8.6385(2)	12.3445(3)
c / Å	12.051(3)	24.464(18)	11.8890(3)	19.9385(7)	12.7164(3)	16.4631(4)
α / °	90	82.808(10)	90	90	82.6030(10)	90
β / °	104.987(3)	86.708(9)	104.5420(10)	101.035(2)	77.0710(10)	102.6550(10)
γ / °	90	64.525(8)	90	90	63.9810(10)	90
Volume/ Å ³	1497.8(6)	1547.4(19)	1491.20(8)	1441.72(9)	756.88(3)	1576.97(7)
Z	4	4	4	4	2	4
Density [g/cm ³]	1.310	1.345	1.387	1.434	1.366	1.379
μ (Mo Kα) [mm ⁻¹]	0.098	0.104	0.107	0.111	0.106	0.109
T/K	296(2)	296(2)	296(2)	296(2)	296(2)	296(2)
Reflns collected	3447	6974	2935	2828	2664	3101
Unique rflns	2483	5089	2654	2633	2353	2793
Parameter refined	274	420	283	283	281	289
R ₁ (I > 2σ)	0.0427	0.0474	0.0365	0.0393	0.0430	0.0350
wR ₂ (I > 2σ)	0.1274	0.1412	0.1196	0.0996	0.1331	0.0867
GOF	0.975	1.048	0.933	1.038	0.978	0.956

Table 5.2b: The crystal structure details and the crystallographic parameters of TXA salt/cocrystal.

Crystal structure details	TXA-OXA	TXA-TTA	TXA-FUM	TXA-SUA	TXA-CRA
CCDC number	1554438	1554439	1554440	1554441	1554442
Mol. formula	C ₉ H ₁₆ N O ₄	C ₁₂ H ₂₁ N O ₈	C ₁₀ H ₁₇ N O ₄	C ₁₀ H ₁₈ N O ₄	C ₁₂ H ₂₁ N O ₄
Molar mass	202.23	307.30	215.25	216.25	243.30
crystal system	monoclinic	monoclinic	Monoclinic	monoclinic	monoclinic
Space group	C 2/c	P 2 ₁	P 2 ₁ /n	P 2 ₁ /n	P 2 ₁ /n
a /Å	10.647(7)	7.2398(9)	10.4554(7)	11.0902(12)	6.560(3)
b /Å	7.419(5)	24.813(3)	6.6648(4)	6.9234(7)	14.988(6)
c /Å	27.585(19)	8.2219(10)	16.0018(9)	15.0839(16)	13.295(5)
α / °	90	90	90	90	90
β / °	97.182(16)	93.440(6)	98.030(4)	102.7980(10)	97.233(5)
γ / °	90	90	90	90	90
Volume/ Å ³	2162(3)	1474.4(3)	1104.12(12)	1129.4(2)	1296.7(8)
Z	8	4	4	4	4
Density [g/cm ³]	1.243	1.385	1.295	1.272	1.246
μ (MoKα) [mm ⁻¹]	0.097	0.117	0.100	0.098	0.093
T/K	296(2)	296(2)	296(2)	296(2)	296(2)
Reflns collected	2110	5770	2537	2613	3025
Unique rflns	1442	5532	1994	1900	1890
Parameter refined	142	548	139	138	236
R ₁ (I > 2σ)	0.0586	0.0383	0.0803	0.0543	0.0519
wR ₂ (I > 2σ)	0.1436	0.1098	0.2278	0.1422	0.1547
GOF	1.054	1.017	1.051	1.057	0.899

Table 5.3: The geometrical parameters hydrogen bond interactions in the molecular salt/cocrystal of TXA.

Cocrystal	D-H...A ^a	H...A / Å	D...A / Å	<D-H...A / °	Symmetry code
TXA-SAL	O3-H1...O2	1.619	2.537	152.49	x, y, z
	N1-H19...O2	1.828	2.777	173.58	x+1/2, -y+3/2, z-1/2
	N1-H18...O4	2.568	3.053	111.93	x+1/2, -y+3/2, z-1/2
	N1-H18...O3	2.295	3.200	159.04	-x+1, -y+1, -z+1
	N1-H20...O1	2.073	2.913	153.36	-x+1/2, y+1/2, -z+1/2
	N1-H20...O5	2.503	3.001	114.92	-x+1/2, y+1/2, -z+1/2
	O4-H21...O1	1.789	2.647	177.37	x, y, z
TXA-3HBA	O9-H24...O8	1.820	2.639	176.31	x-1, y, z
	O1-H3...O3	1.799	2.614	172.56	x-1, y, z
	O11-H30...O10	1.823	2.630	167.85	x, y, z
	N00B-H17...O6	1.945	2.823	168.52	x-1, y, z
	N00B-H18...O7	2.004	2.859	160.54	x-1, y, z
	N00B-H19...O7	2.068	2.953	172.76	-x+2, -y+1, -z+1
	O5-H8...O4	1.884	2.692	168.06	x+1, y, z
	N00D-H38...O2	2.068	2.953	173.13	-x, -y+2, -z+1
	N00D-H37...O2	2.010	2.862	159.87	x-1, y, z+1
	N00D-H36...O12	2.034	2.918	171.96	x-1, y, z
	C5-H25...O11	2.639	3.261	124.86	x, y, z
	C15-H22...O9	2.551	3.163	121.07	x, y, z
	C28-H39...O1	2.548	3.198	124.41	x, y, z+1
	O10-H29...O8	1.809	2.750	172.45	x-1, y, z
	O10-H28...O4	2.251	3.037	158.44	-x+1, -y+1, -z+1
O4-H49...O3	1.775	2.716	172.76	x, y, z	
O4-H48...O12	2.404	3.053	146.54	-x+1, -y+2, -z+1	
TXA-2,4HBA	N1-H7...O3	1.837	2.762	174.69	x-1/2, -y+3/2, z+1/2
	O1-H13...O4	1.723	2.627	173.62	x, y, z
	N1-H6...O4	1.972	2.873	164.64	-x+1/2, y+1/2, -z+3/2
	N1-H8...O5	2.325	3.233	159.54	-x, -y+1, -z+1
	O6-H16...O2	1.906	2.840	169.82	x+1/2, -y+1/2, z-1/2
	O5-H18...O3	1.644	2.542	153.86	x, y, z
TXA-2,5HBA	C10-H4...O4	2.604	3.202	120.03	-x, -y, -z+1
	N1-H17...O5	1.923	2.854	165.33	x, y-1, z
	N1-H18...O4	1.988	2.871	160.69	-x+1, -y, -z+1
	N1-H19...O3	1.783	2.783	174.23	x+1, y-1, z
	O1-H5...O4	1.869	2.716	163.84	-x, -y, -z+1
	O2-H3...O3	1.690	2.558	153.48	x, y, z
	O6-H21...O1	1.977	2.756	160.89	x, y+1, z
TXA-2,6HBA	O5-H2...O6	1.851	2.652	165.23	-x+2, -y+2, -z
	C12-H8...O6	2.588	3.540	169.74	-x+2, -y+1, -z
	C6-H21...O1	2.594	3.407	146.65	x-1, y, z

	O3-H18...O1	1.575	2.502	159.80	x, y, z
	N1-H11...O3	2.005	2.895	160.60	-x+1, -y+1, -z+1
	N1-H10...O5	2.477	3.162	129.40	x, y-1, z
	N1-H10...O4	2.163	2.974	143.26	x+1, y-1, z
	N1-H12...O1	2.041	2.854	143.99	x, y-1, z
	N1-H12...O2	2.149	3.013	152.39	x, y-1, z
	O4-H17...O2	1.535	2.509	153.89	x, y, z
TXA-GAA	O4-H23...O7	2.617	3.100	119.05	x, y, z
	O4-H23...O6	1.693	2.511	174.86	x, y, z
	O2-H22...O6	1.829	2.690	167.80	x-1/2, -y+3/2, z-1/2
	O3-H3...O5	1.921	2.746	155.17	x-1/2, -y+3/2, z-1/2
	O1-H5...O2	2.309	2.758	114.39	x, y, z
	O1-H5...O3	2.302	2.907	129.94	-x+1/2, y+1/2, -z+1/2
	N1-H15...O7	1.886	2.765	161.12	x+1/2, -y+1/2, z+1/2
	N1-H15...O4	2.630	3.096	112.50	x+1/2, -y+1/2, z+1/2
	N1-H13...O7	1.934	2.814	157.58	-x+1/2, y-1/2, -z+3/2
	N1-H14...O2	2.620	3.260	127.73	-x+1, -y+1, -z+1
N1-H14...O5	2.150	2.930	142.78	-x+3/2, y-1/2, -z+3/2	
TXA-OXA	O004-H004...O1	1.839	2.647	167.98	-x+3/2, -y+5/2, -z+1
	N1-H3...O002	1.832	2.749	176.12	x, y-1, z
	N1-H1...O001	1.855	2.818	174.36	x, y, z
	N1-H2...O001	2.140	2.922	142.16	-x+3/2, y-1/2, -z+3/2
	N1-H2...O002	2.139	2.846	132.76	-x+3/2, y-1/2, -z+3/2
TXA-TTA	C18-H2...O14	2.528	3.356	148.78	x+1, y, z
	C22-H12...O7	2.532	3.398	157.69	x-1, y, z+1
	N2-H17...O11	2.537	2.953	110.62	-x+1, y+1/2, -z
	N2-H17...O9	1.985	2.846	177.65	-x+1, y+1/2, -z
	N2-H18...O6	2.001	2.857	150.25	-x+1, y+1/2, -z
	N2-H19...O7	1.917	2.780	158.35	-x+2, y+1/2, -z
	O3-H24...O8	1.575	2.565	173.76	x-1, y, z
	O3-H24...O7	2.654	3.363	128.47	x-1, y, z
	O6-H25...O7	2.088	2.611	122.35	x, y, z
	O6-H25...O13	2.412	3.047	136.14	x+1, y, z-1
	O11-H29...O15	1.795	2.740	165.02	x, y, z
	O13-H28...O10	1.730	2.548	168.20	x-1, y, z
	O12-H27...O8	2.103	2.841	156.04	x-1, y, z
	C16-H36...O3	2.646	3.551	142.47	-x+1, y-1/2, -z+1
	N1-H33...O5	2.147	2.938	149.90	-x+1, y-1/2, -z
	N1-H33...O4	2.207	2.893	134.96	-x+1, y-1/2, -z
	N1-H34...O14	1.851	2.806	166.34	-x, y-1/2, -z+1
	N1-H35...O12	1.912	2.796	166.17	-x+1, y-1/2, -z+1
	O16-H40...O9	1.853	2.647	174.30	x-1, y, z
	O2-H41...O8	1.906	2.626	161.44	x-1, y, z
O5-H26...O1	2.245	2.789	113.55	x+1, y, z	

TXA-FUM	N1-H1A...O1	1.957	2.832	167.34	$x-1/2, -y+3/2, z+1/2$
	N1-H1B...O2	2.046	2.865	152.55	$x-1/2, -y+1/2, z+1/2$
	N1-H1B...O3	2.537	3.089	120.86	$x-1/2, -y+1/2, z+1/2$
	N1-H1C...O1	1.881	2.754	166.14	$-x+1, -y+1, -z+1$
	O4-H4...O2	1.776	2.595	178.24	x, y, z
TXA-SUA	N1-H1A...O4	1.967	2.842	167.45	$x+1/2, -y+3/2, z-1/2$
	N1-H1B...O3	2.155	2.920	143.66	$x+1/2, -y+1/2, z-1/2$
	N1-H1B...O2	2.407	3.053	129.69	$x+1/2, -y+1/2, z-1/2$
	N1-H1C...O4	1.988	2.832	157.77	$-x+1, -y+1, -z+1$
	N1-H1C...O3	2.535	3.304	145.05	$-x+1, -y+1, -z+1$
	O1-H1...O3	1.709	2.529	178.41	x, y, z
	C10-H10B...O1	2.619	3.585	174.37	$-x+1/2, y-1/2, -z+1/2$
TXA-CRA	O2-H2...O3	1.704	2.524	178.60	$x-1, y, z$
	C1-H11...O4	2.603	3.437	141.31	$x-1/2, -y+3/2, z+1/2$
	N1-H14...O3	1.981	2.865	166.75	$-x+1/2, y+1/2, -z+1/2$
	N1-H14...O4	2.586	3.294	136.02	$-x+1/2, y+1/2, -z+1/2$
	N1-H15...O3	2.504	3.188	137.62	$x-1/2, -y+3/2, z+1/2$
	N1-H15...O1	2.253	2.957	139.58	$x+1/2, -y+3/2, z+1/2$
	N1-H16...O4	1.753	2.748	172.30	$x+1/2, -y+3/2, z+1/2$

^a D=donor, A=acceptor

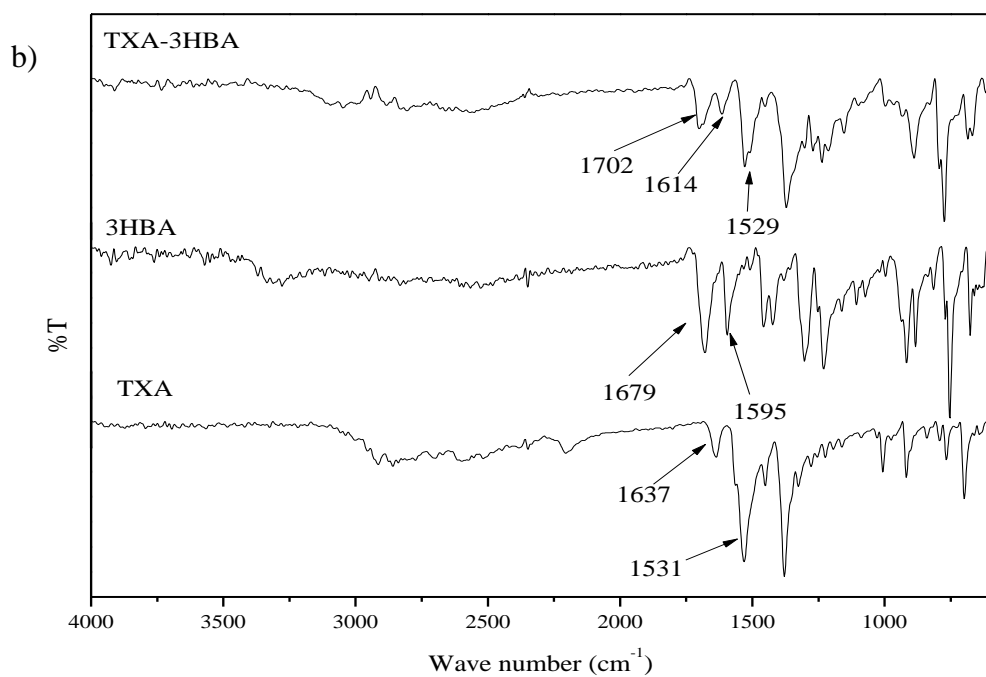
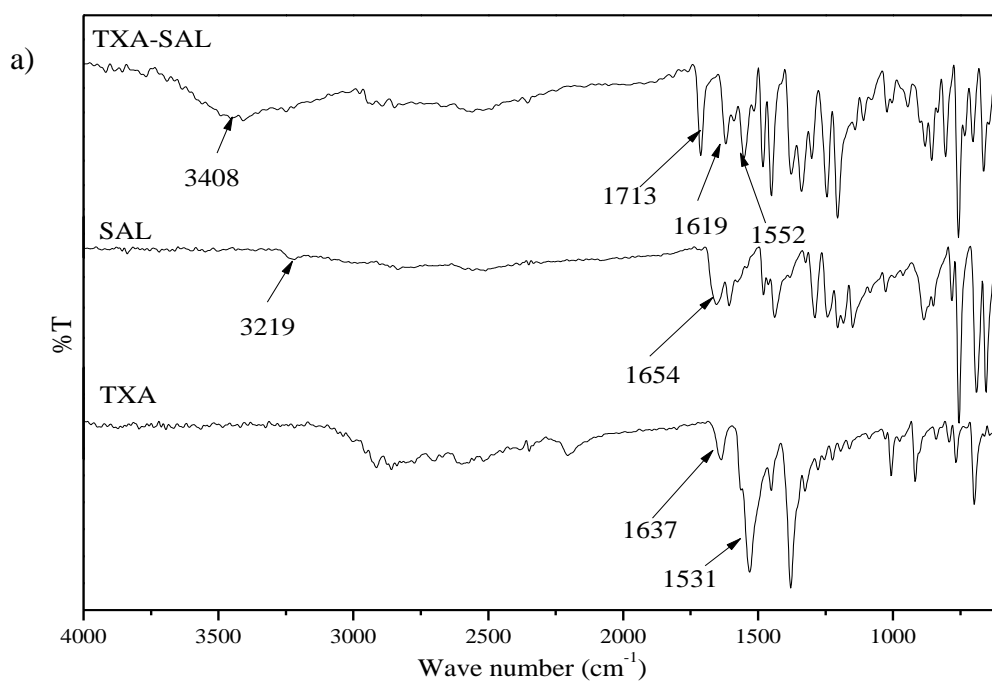
5.3.2 FT-IR spectroscopy

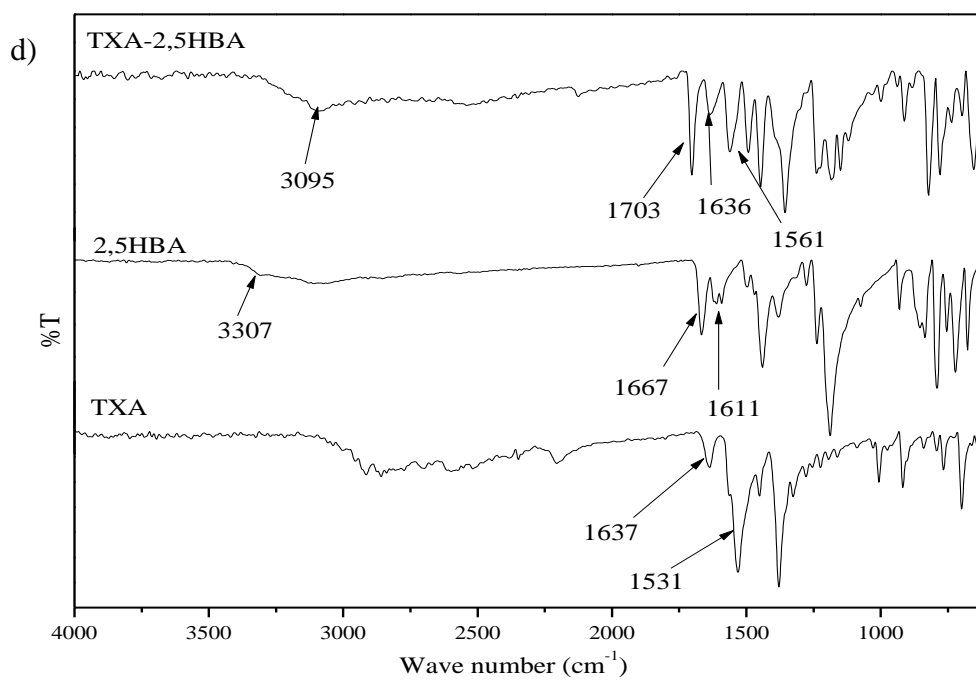
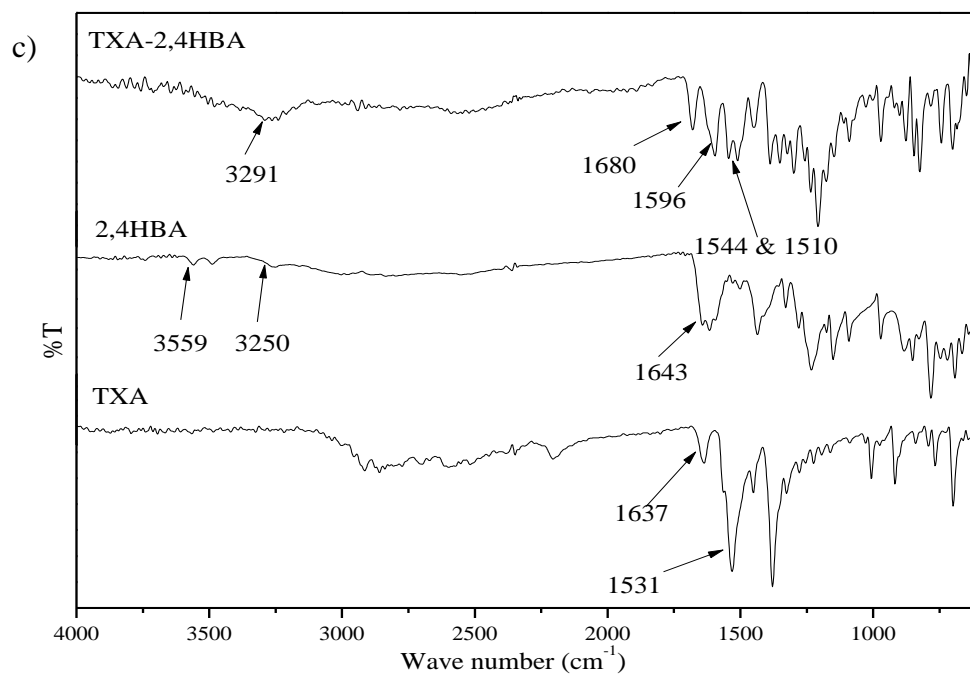
FT-IR spectroscopy was performed for all the synthesized salt/cocrystal and compared the spectrum with their individual starting materials spectra in order to construe the salt/cocrystal formation. The shift in carbonyl group of acid or amide derivatives is common when the group is involved in intermolecular interactions. In the present study, acid derivatives have been used for salt/cocrystal synthesis, and the TXA molecule exists as zwitter ion in the solid state. The carbonyl group of TXA was observed at 1531 cm^{-1} and $-\text{NH}_3^+$ bending frequency was observed at 1637 cm^{-1} . Since the salt formation was observed in most of the cases except TXA-GAA and TXA-CRA, the TXA molecule in these salts exists as acid rather than carboxylate due to the proton transfer from cofomer to an amino group. Therefore, the new carbonyl stretching frequency of TXA appeared around 1700 cm^{-1} in all the salts, which indicates the formation of new crystalline material. In TXA-GAA and TXA-CRA slight shift in the carbonyl stretching frequency of cofomers observed in the cocrystal. In these cocrystals, the carboxylate stretching and $-\text{NH}_3^+$ bending frequency were observed similar to that TXA as such. In TXA-TTA salt, two carbonyl stretching frequency

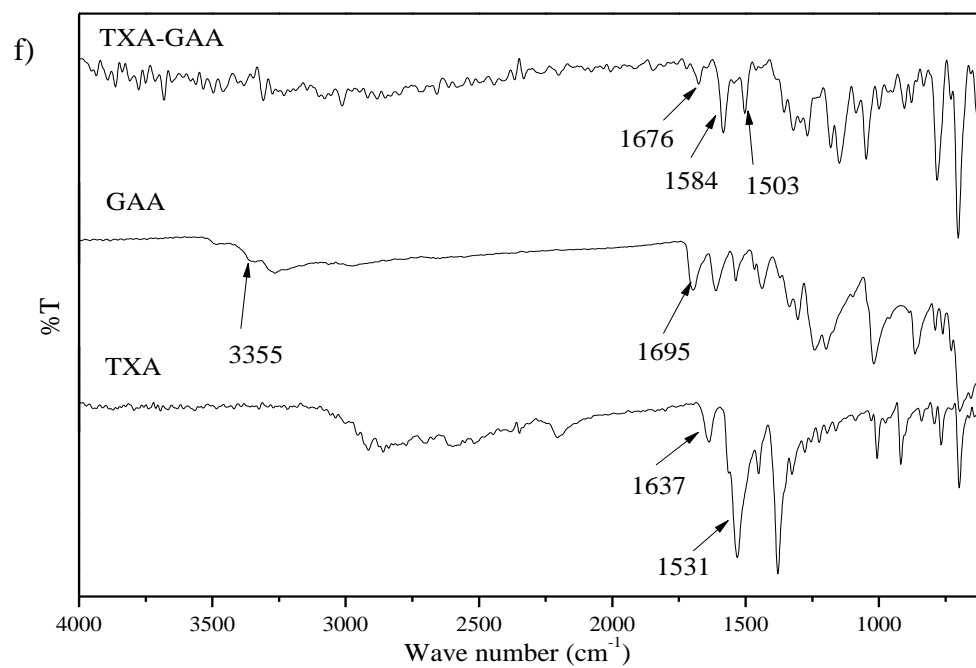
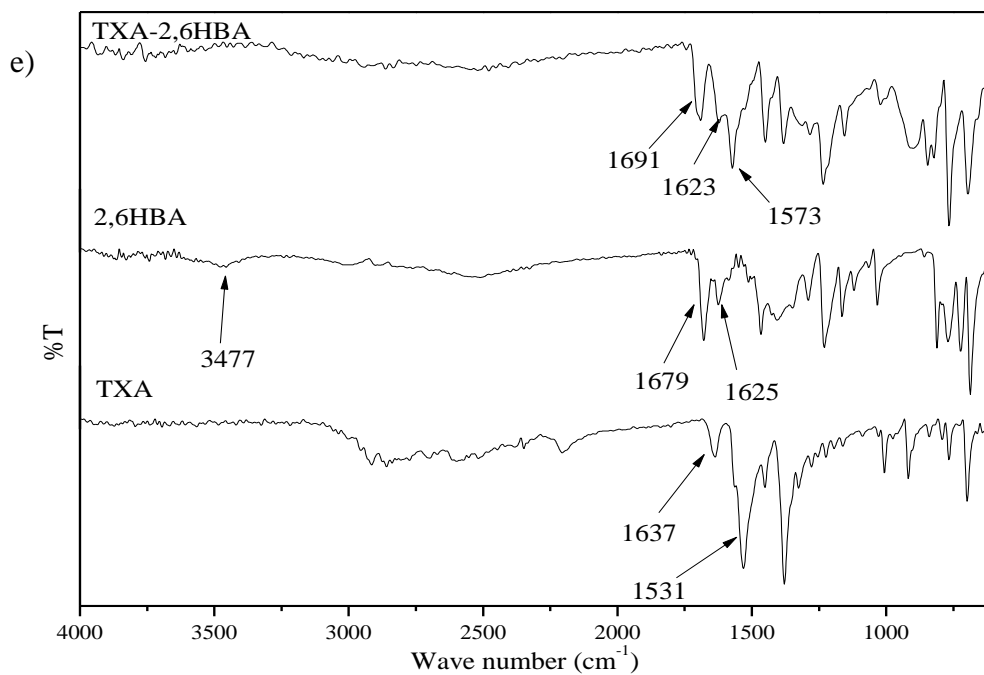
observed at 1724 cm^{-1} and 1692 cm^{-1} which correspond to the acid group of TXA and TTA respectively. The detailed list of stretching and bending frequencies are shown in **Table 5.4**. The comparison spectra of TXA salt/cocrystal with their starting material are shown in **Figure 5.12**.

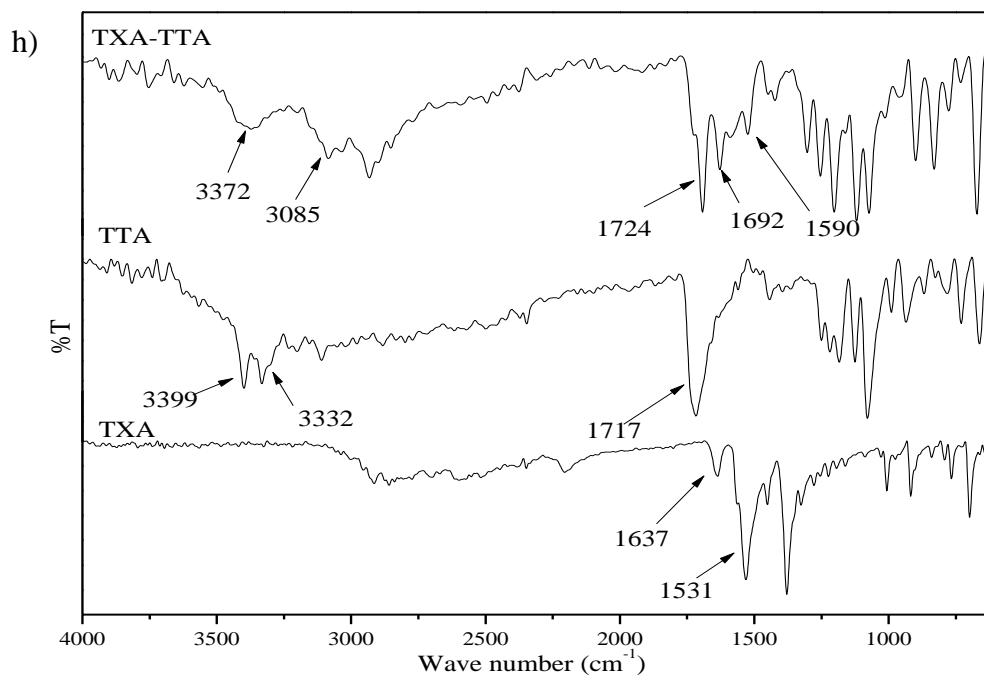
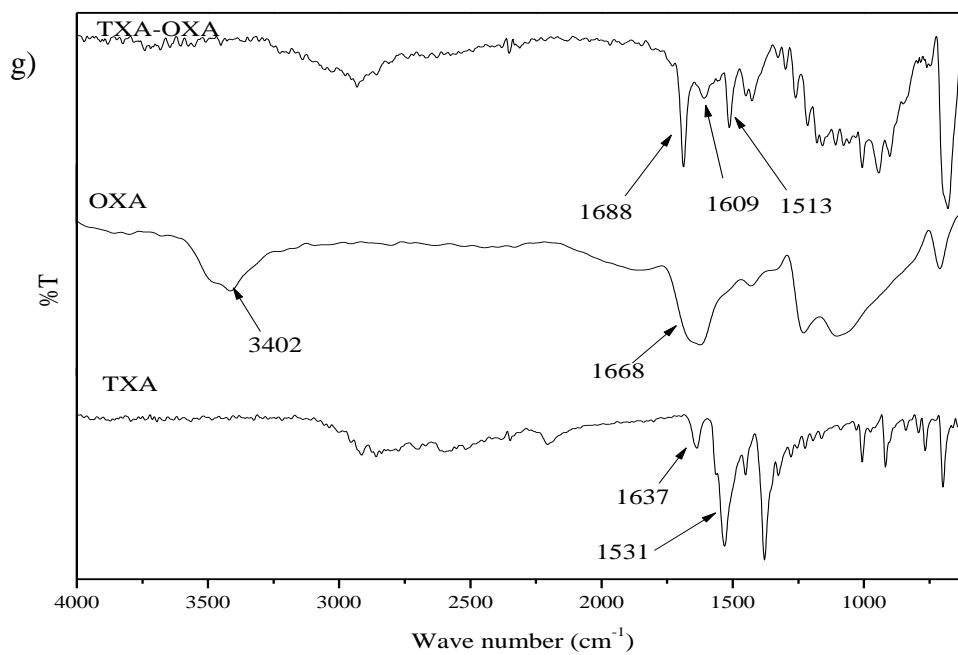
Table 5.4: FT-IR stretching frequencies of TXA, cofomers and the salt/cocrystals of TXA.

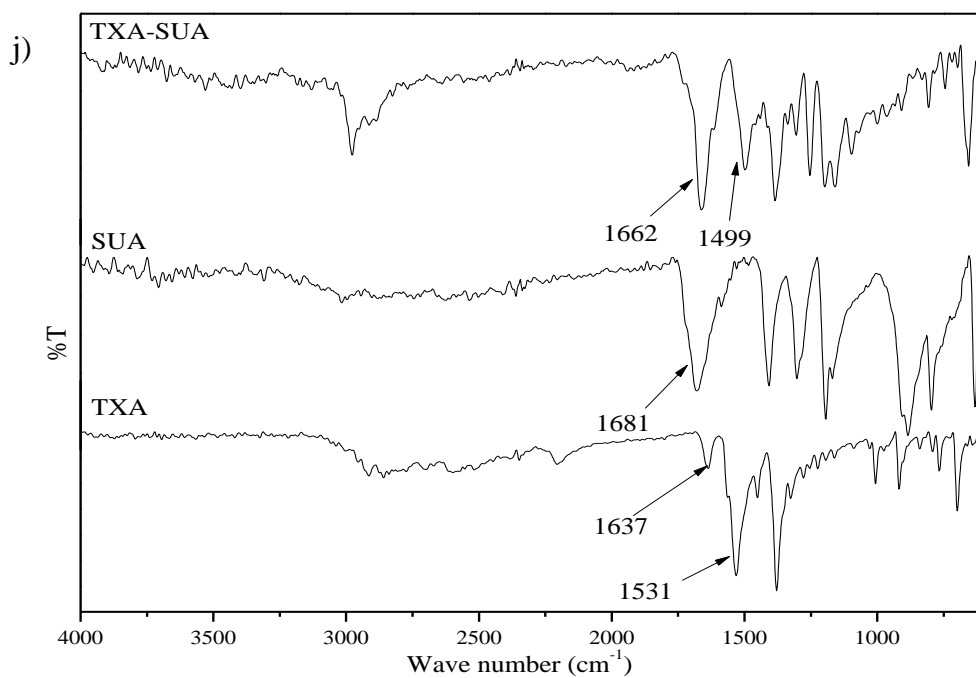
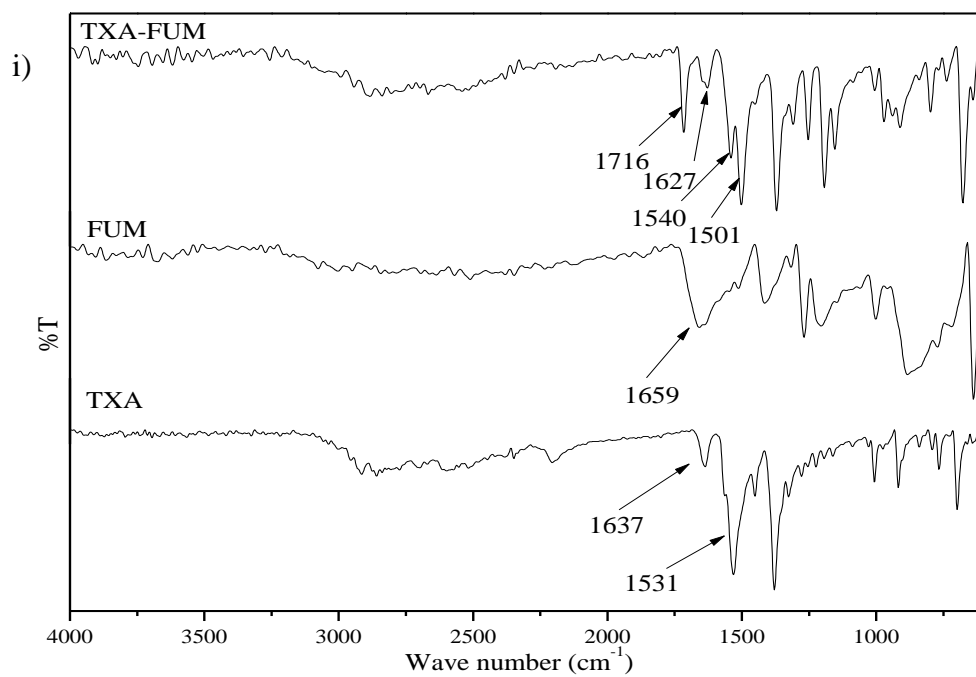
API/Cofomer/Salt/ Cocrystal	-C=O stretching frequency (cm^{-1})	-NH ₃ ⁺ bending frequency (cm^{-1})	-OH/-NH stretching frequency (cm^{-1})
TXA	1531	1637	-
SAL	1654	-	3219
3HBA	1679	-	-
2,4HBA	1643	-	3559
2,5HBA	1667	-	3307
2,6HBA	1679	-	3477
GAA	1695	-	3355
OXA	1668	-	3402
TTA	1717	-	3399, 3332
FUM	1659	-	-
SUA	1681	-	-
CRA	1697	-	-
TXA-SAL	1713	1619	3408
TXA-3HBA	1702	1614	-
TXA-2,4HBA	1680	1596	3291
TXA-2,5HBA	1703	1636	3095
TXA-2,6HBA	1691	1623	-
TXA-GAA	1676, 1584	1503	-
TXA-OXA	1688	1609	-
TXA-TTA	1724, 1692	1590	3372, 3085
TXA-FUM	1716	1627	-
TXA-SUA	1662	-	-
TXA-CRA	1686, 1528	1634	-











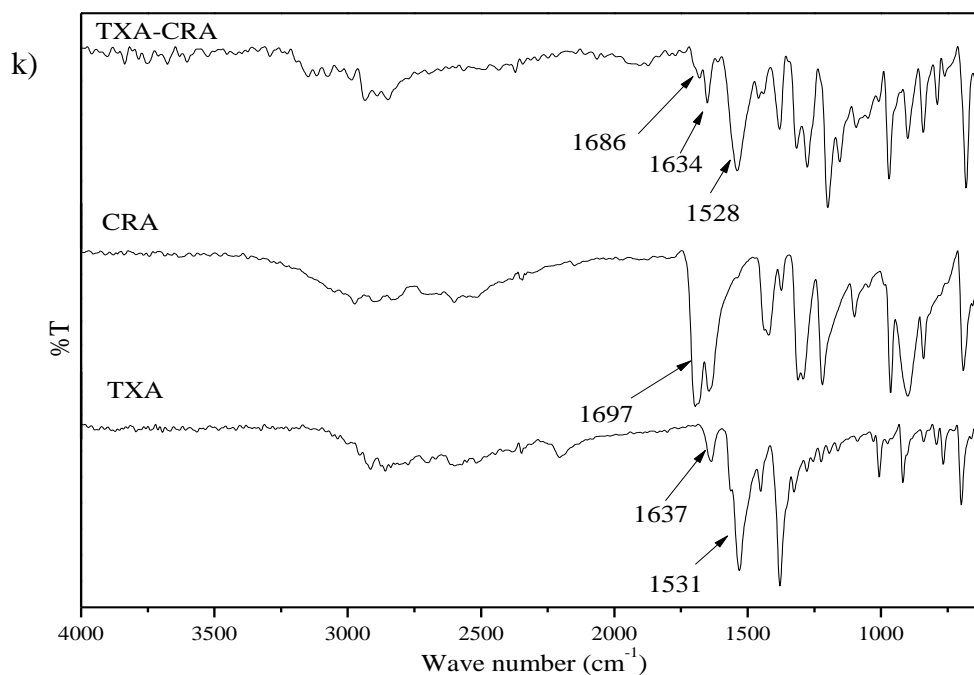


Figure 5.12: Comparison of FT-IR spectra of TXA salt/cocrystal with starting materials (a) TXA-SAL, (b) TXA-3HBA, (c) TXA-2,4HBA, (d) TXA-2,5HBA, (e) TXA-2,6HBA, (f) TXA-GAA, (g) TXA-OXA, (h) TXA-TTA, (i) TXA-FUM, (j) TXA-SUA, and (k) TXA-CRA.

5.3.3 DSC and POM analysis

The DSC analysis of all the synthesized salt/cocrystal in the present study were performed in order to determine the accurate melting point and to determine the phase purity of the bulk samples. The melting point of TXA, coformer, and the salt/cocrystal is displayed in **Table 5.5**. Except for TXA-3HBA and TXA-2,4HBA, all the other synthesized salts and the cocrystals exhibited single endotherm in the thermogram substantiated the phase purity of the synthesized molecular adducts. In TXA-3HBA salt, due to the presence of water molecule in the crystalline material, an endothermic peak is observed around 100 °C for the release of water from the material, and the peak at 201 °C corresponds to the melting of the salt. In TXA-2,4HBA salt, two endothermic peaks are observed probably due to the phase transformation in the crystalline material. In the carboxylic acid derivatives, all the salts exhibited a melting point in between that of the melting point of starting materials except TXA-FUM salt, where it melts at below the melting temperature of starting materials. The melting point of TXA-GAA cocrystal is found to be less than the melting of the corresponding starting materials, whereas,

TXA-CRA cocrystal melts at higher temperature (268.79 °C), though the melting temperature of CRA is around 70-73 °C. The higher melting temperature of this cocrystal may be due to the stronger primary interactions in the crystalline material. The DSC thermogram of the synthesized salt/cocrystal is shown in **Figure 5.13**.

POM analysis of the synthesized salt/cocrystal further supports the DSC analysis for the chemical stability of the salt/cocrystal. The POM images of the crystals were taken at different temperature in order see the changes in surface morphology. The clear morphological changes were observed for TXA-3HBA and TXA-2,4HBA salts as these exhibited two melting temperatures. TXA-2,4HBA salt found to decompose after 230 °C. The POM images of the synthesized salt/cocrystal is shown in **Figure 5.14**.

Table 5.5: Melting points of TXA, cofomers and the salt/cocrystals of TXA.

API melting temperature (°C)	Cofomer melting temperature (°C)	Salt/cocrystal melting temperature (°C)
TXA (274.31)	SAL (158)	200.45
	3HBA (202)	201.04
	2,4HBA (223.06)	190.02 & 231.51
	2,5HBA (214.54)	211.6
	2,6HBA (169.28)	214.16
	GAA hydrate (78.6 & 256.5)	218.66
	OXA (101.5)	224.89
	TTA (171-174)	195.63
	FUM (287)	265.47
	SUA (184)	239.12
	CRA (70-73)	268.79

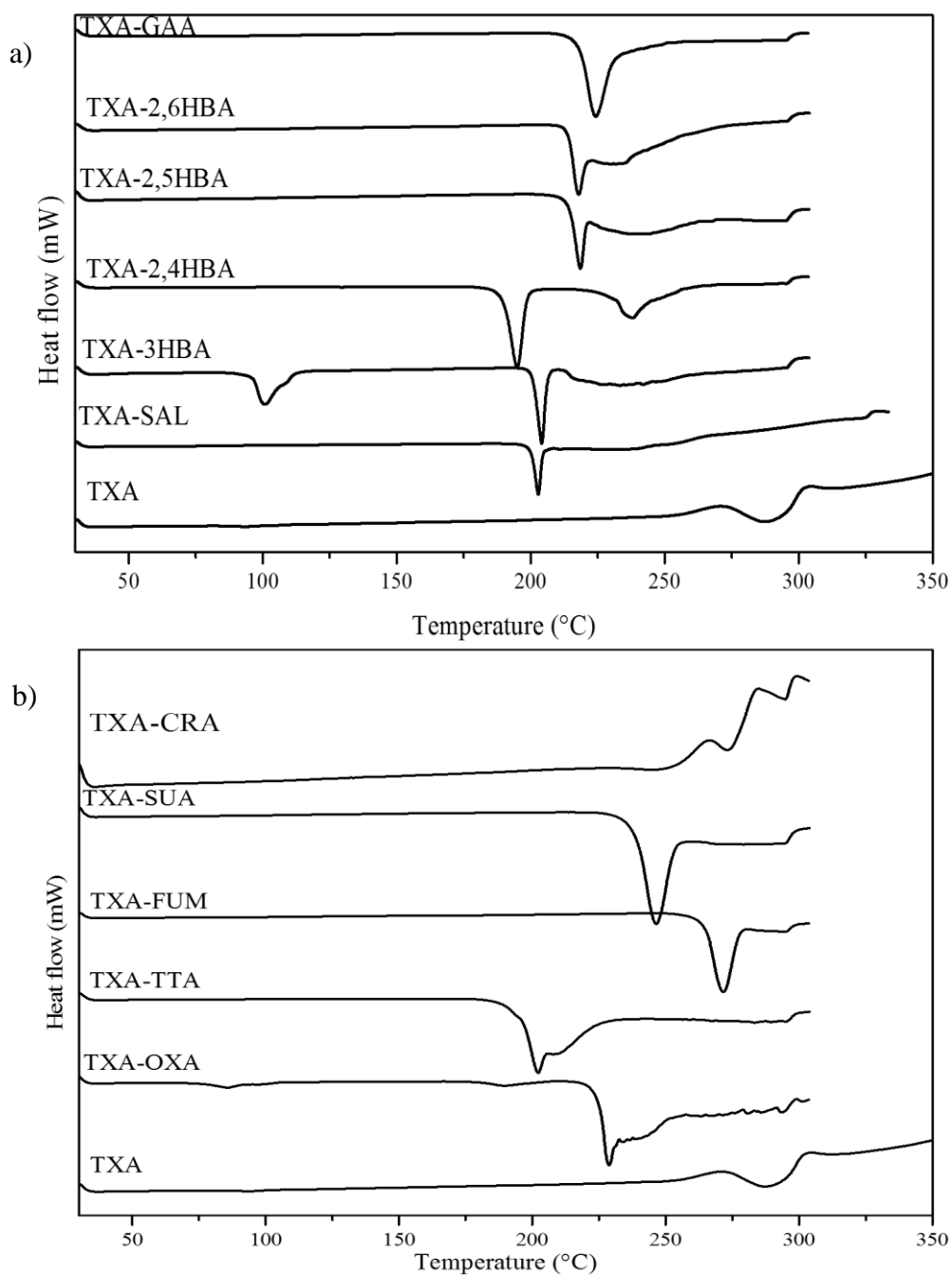


Figure 5.13: DSC thermograms of TXA salt/cocrystal (a) TXA-Sal, TXA-3HBA, TXA-2,4HBA, TXA-2,5HBA, TXA-2,6HBA, and TXA-GAA (b) TXA-OXA, TXA-TTA, TXA-FUM, TXA-SUA, and TXA-CRA.

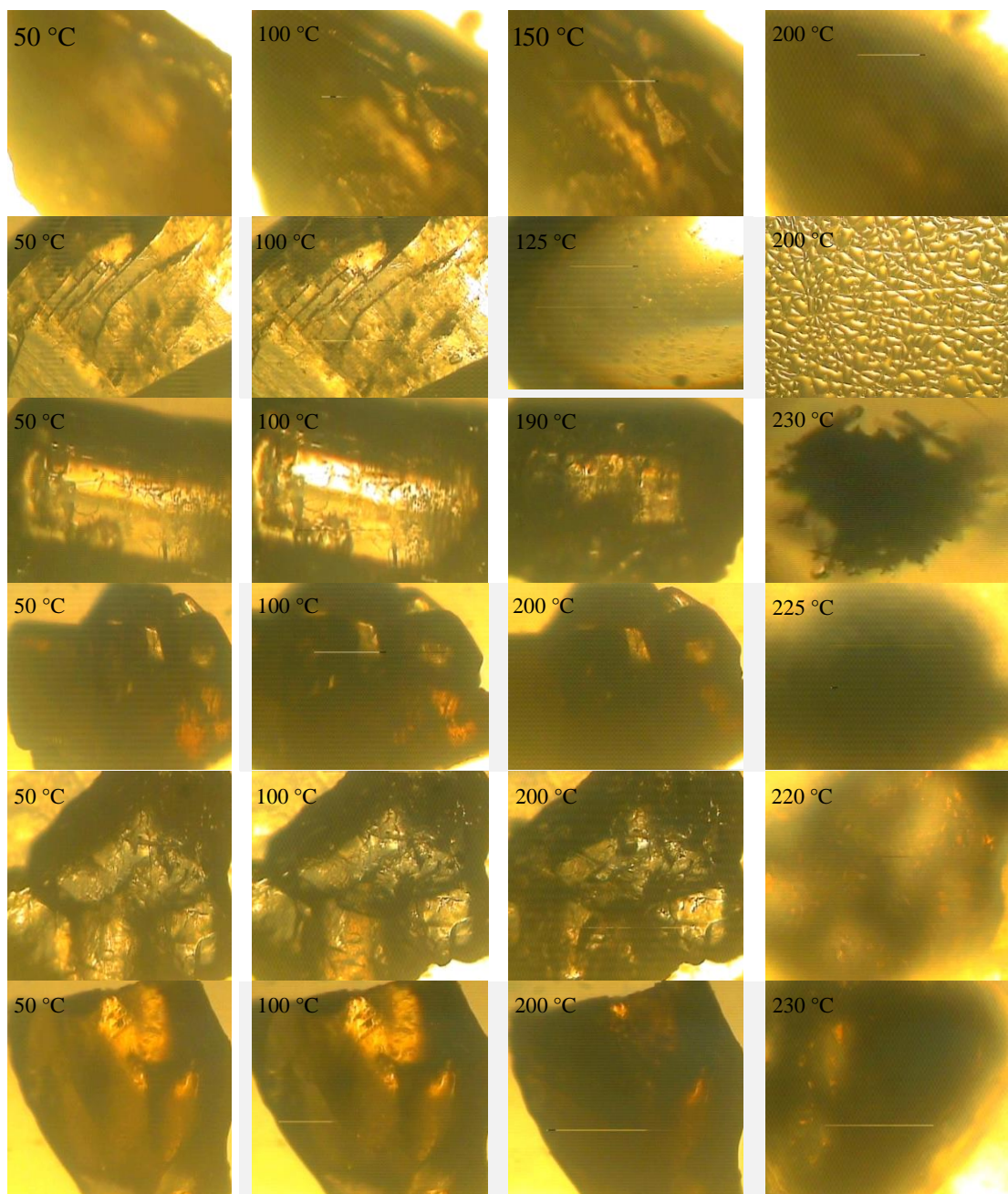


Figure 5.14 (a): POM images of salt/cocrystal of TXA with benzoic acid derivatives at various temperature. 1st row (from top): TXA-SAL, 2nd row: TXA-3HBA, 3rd row: TXA-2,4HBA, 4th row: TXA-2,5HBA, 5th row: TXA-2,6HBA, 6th row: TXA-GAA.

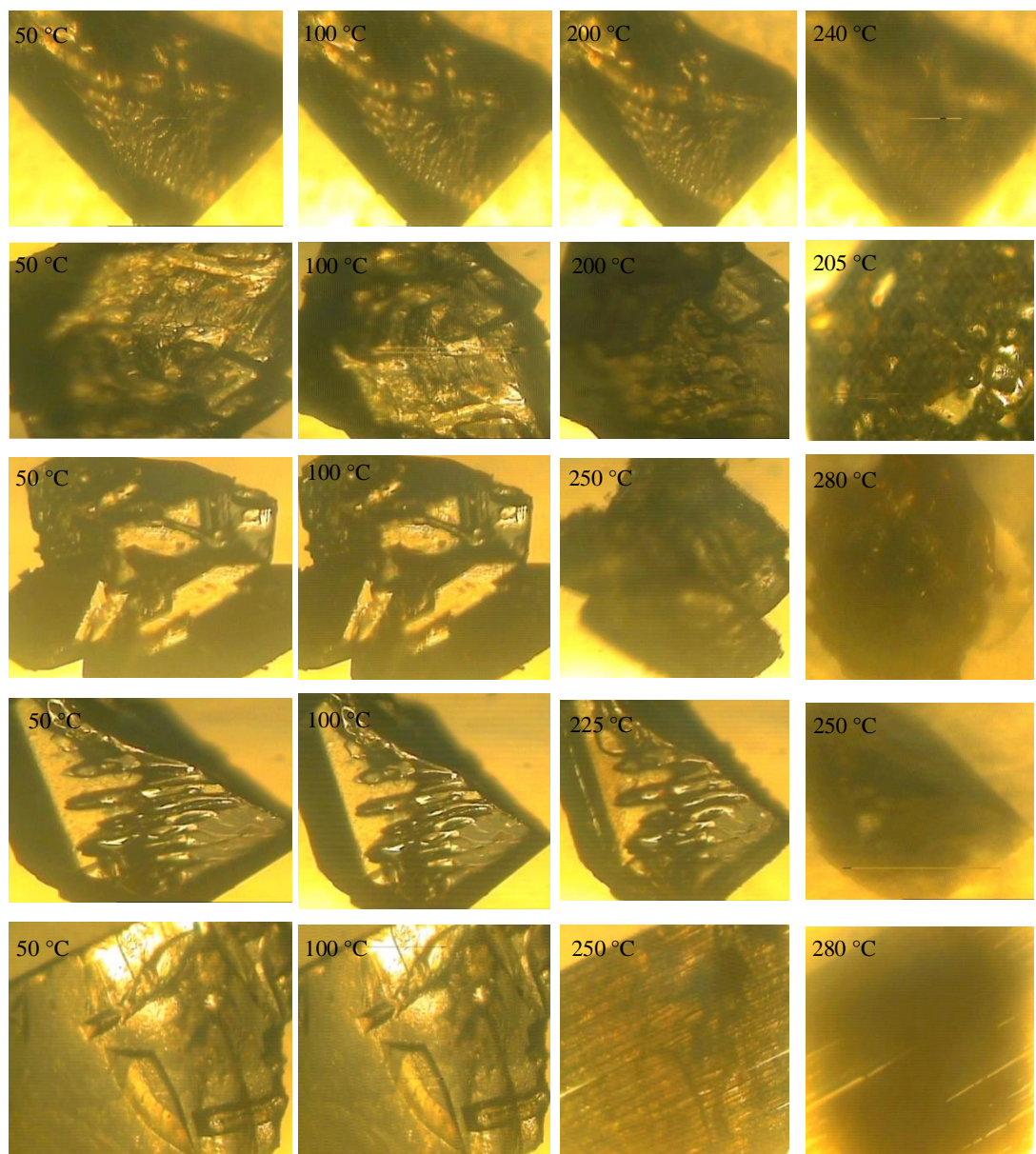


Figure 5.14 (b): POM images of salt/cocrystal of TXA with carboxylic acid derivatives at various temperature. 1st row (from top): TXA-OXA, 2nd row: TXA-TTA, 3rd row: TXA-FUM, 4th row: TXA-SUA, 5th row: TXA-CRA.

5.3.4 Structural comparison of salt/cocrystal

In all the synthesized salt/cocrystal, the robust primary supramolecular synthon involved was $-O-H\cdots O=C$, $-N-H\cdots O$, $-O-H\cdots O-H$ hydrogen bonds. The TXA molecule in the synthesized salts were found to exist as $HOOC-R-CH_2-NH_3^+$, where R is cyclohexyl group. However, in cocrystal, TXA molecule exists as zwitter ion. In the

crystal structure of TXA-SAL, molecules interacted through O-H...O hydrogen bond between TXA and SAL. The carbonyl group of both TXA and SAL were involved in a hydrogen bond with $-\text{NH}_3^+$ group of TXA molecule. However, in TXA-3HBA, it was crystallized as monohydrate and the carboxylic acid group of TXA is involved in a hydrogen bond with a water molecule. Further, the carboxyl group of 3HBA forms a hydrogen bond with hydroxy group of 3HBA, the amino group of TXA molecule and with a water molecule. Due to the presence of water molecule and the involvement of 3-hydroxy group in hydrogen bond the crystal density for TXA-3HBA were found to be higher when compared to TXA-SAL salt.

When compared to the structural property of dihydroxybenzoic acid salt/cocrystal of TXA, all the salts/cocrystal except TXA-2,6HBA were crystallized in monoclinic crystal system with $P 2_1/n$ space group. Whereas TXA-2,6HBA was crystallized in triclinic crystal system. Though these salts/cocrystals were crystallized in same space group, the interactions involved and the crystal packing were found to be entirely different. In TXA-2,4HBA salt, the molecules interacted through O-H...O hydrogen bond between an acid group of TXA and the carboxyl group of 2,4HBA and the 4-hydroxy group of 2,4HBA forms hydrogen bond with carbonyl group of TXA molecule. However, in TXA-2,5HBA salt, the molecules interacted through N-H...O hydrogen bond between TXA and 2,5HBA and the acid group of TXA forms a hydrogen bond with a 5-hydroxy group of 2,5HBA molecule. In TXA-2,6HBA salt, strong two point heterosynthon between the amino group of TXA and the carboxyl group of 2,6HBA were observed. Here, the acid group of TXA forms dimer with another TXA molecule and the hydroxy group of TXA-2,6HBA were involved in weak N-H...O hydrogen bond with TXA molecule. When compared to the crystal density of these three molecular salts, TXA-2,5HBA exhibited highest crystal density of 1.434 g/cm^3 , and this may be attributed to the involvement of a hydroxy group of 2,5HBA in intermolecular hydrogen bonding. In TXA-2,5HBA salt, the 5-hydroxy group forms strong O-H...O hydrogen bond with the carboxyl group of TXA and 2,5HBA molecules. However, in TXA-2,4HBA salt, the 4-hydroxy group forms a hydrogen bond with the only carbonyl group of TXA molecule. Therefore, the crystal density was found to be lower than TXA-2,5HBA salt. TXA-2,6HBA exhibited lowest crystal density as the

hydroxy group was involved in an only weak hydrogen bond with $-\text{NH}_3^+$ group of TXA molecule.

When related with secondary interaction (i.e. $\text{C-H}\cdots\pi$) with respect to benzoic acid derivatives of TXA salt/cocrystal, all salt/cocrystal except TXA-2,5HBA and TXA-2,6HBA exhibited $\text{C-H}\cdots\pi$ interaction in the crystal structure. In TXA-2,5HBA and TXA-2,6HBA salts, the arrangement of molecules in the crystal structure was found to be different and the molecules were involved in $\text{C-H}\cdots\text{O}$ hydrogen bond rather than $\text{C-H}\cdots\pi$ interaction. In TXA-2,5HBA, the acid group of TXA formed a hydrogen bond with 5th $-\text{OH}$ group of 2,5HBA, whereas in TXA-2,6HBA salt, acid group of TXA formed a dimer with another TXA molecule, thereby $\text{C-H}\cdots\text{O}$ hydrogen bond between TXA molecules is favored over $\text{C-H}\cdots\pi$ interaction. The weak $\text{C-H}\cdots\text{O}$ hydrogen bond was found to be common for all the salt/cocrystal of TXA.

In the molecular salts of TXA with dicarboxylic acid derivatives, all the salts except TXA-TTA displayed 1:0.5 molecular stoichiometry in the asymmetric unit and in all these salts charge assisted acid \cdots amine heterosynthon was observed. In TXA-TTA salt, apart from acid \cdots amine heterosynthon, carboxylate group of TTA is involved in a hydrogen bond with an acid group of another TTA molecule. Off all these salts, the density was found to be higher for TXA-TTA salts, due to the larger number of interactions involved with TTA molecule. In the cocrystals of TXA-GAA and TXA-CRA, the robust $\text{O-H}\cdots\text{O}$ heterosynthon between the acid group of coformer and carboxylate group of TXA molecule was observed. TXA-FUM and TXA-SUA salts were found to be isostructural with similar bond lengths and bond angles. Further, the cell volume of these salts was found to be similar. The isostructurality is determined based on the isostructural parameters π and \mathcal{E} .

$$\pi = ((a + b + c) / (a' + b' + c')) - 1, \text{ for } a + b + c > a' + b' + c'$$

Where, a , b , c and a' , b' , c' are the orthogonal lattices parameters of TXA-FUM and TXA-SUA salts respectively.

$$\begin{aligned} \pi &= (33.122 / 33.0975) - 1 \\ &= 0.000740 \end{aligned}$$

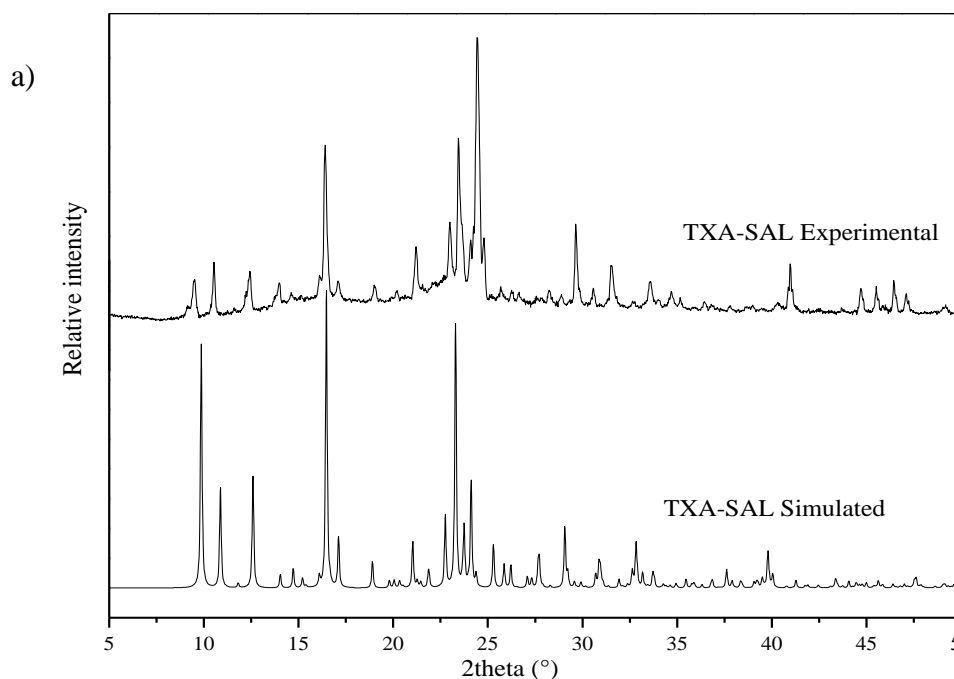
$$\mathcal{E} = (v' / v)^{1/3} - 1, \text{ where } v \text{ and } v' \text{ are the cell volume such that } v' > v$$

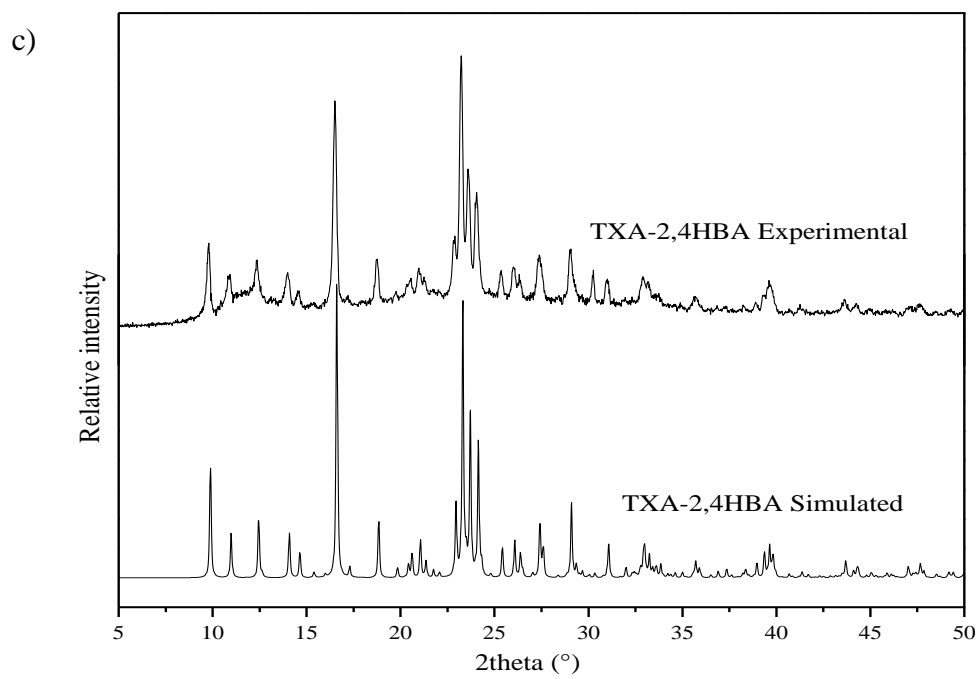
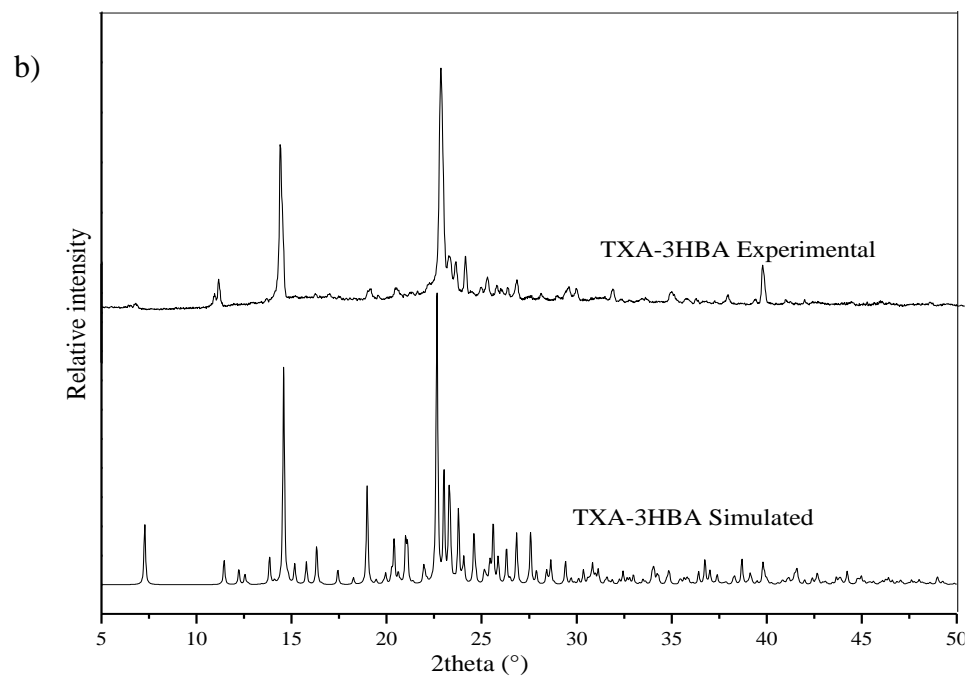
$$\begin{aligned} \mathcal{E} &= (1129.4 / 1104.12)^{1/3} - 1 \\ \mathcal{E} &= 0.00757 \end{aligned}$$

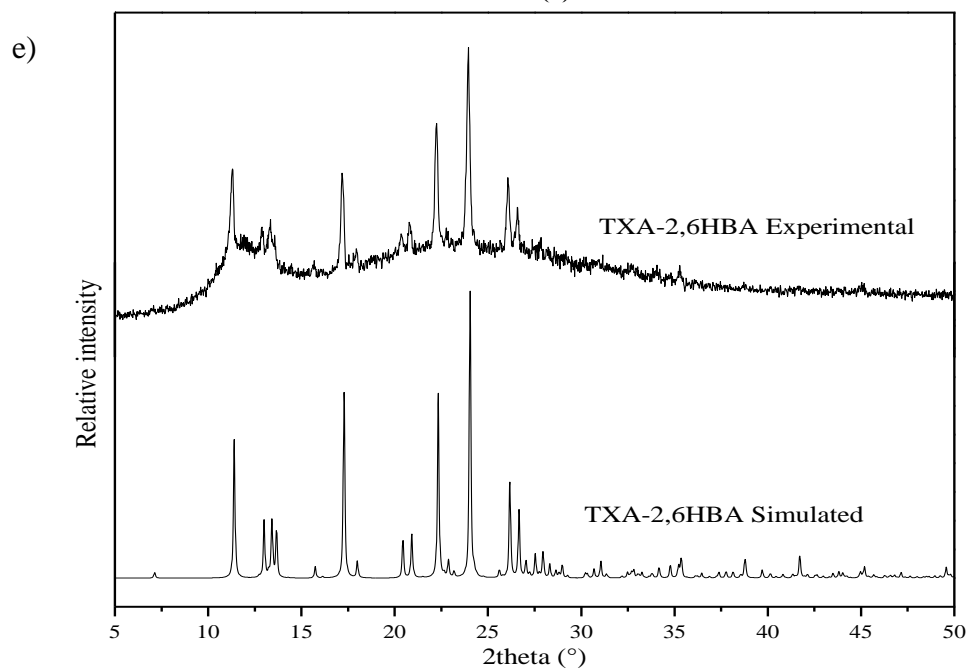
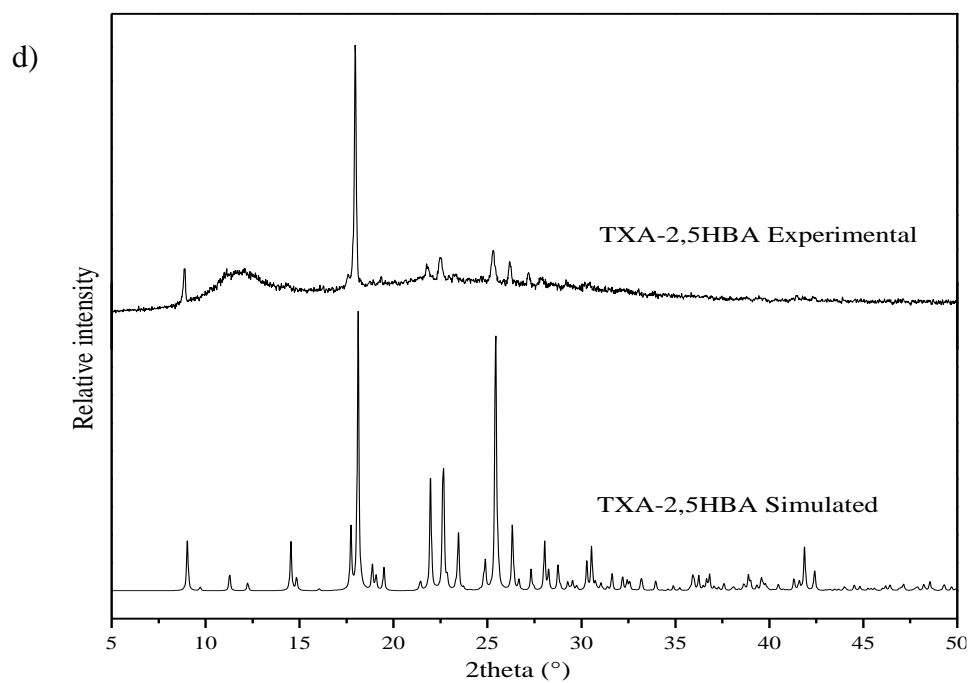
The isostructural parameters were found to be close to zero for TXA-FUM and TXA-SUA salts indicating the similarity in these crystal structures. The only difference observed was the involvement of $-\text{CH}_2$ group of TXA molecule ($-\text{CH}_2\text{-NH}_3^+$) in hydrogen bonding with the carboxyl group of another TXA molecule in TXA-SUA salt.

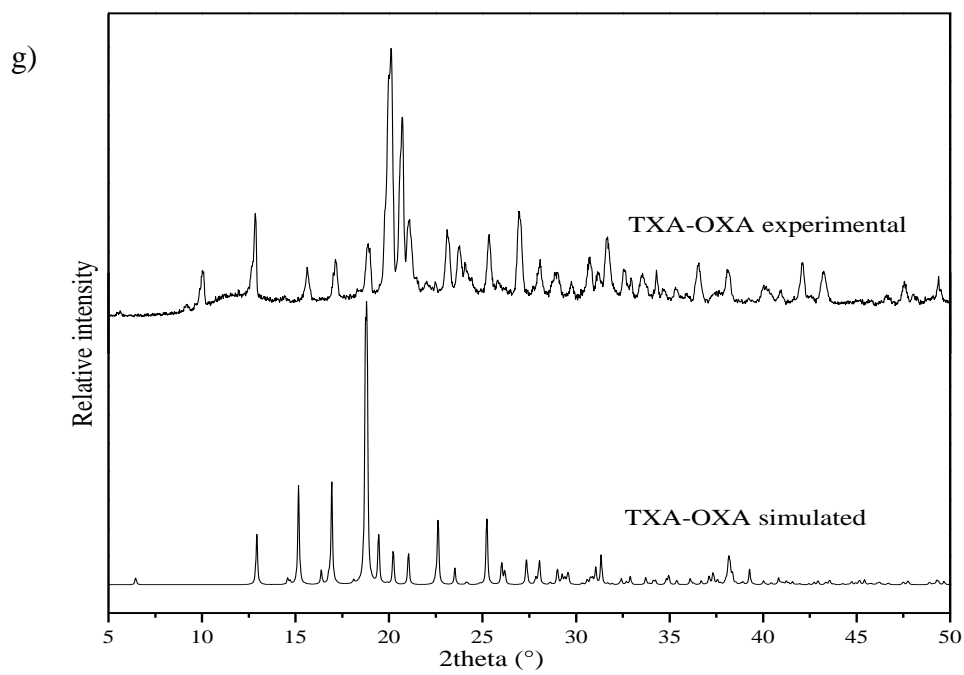
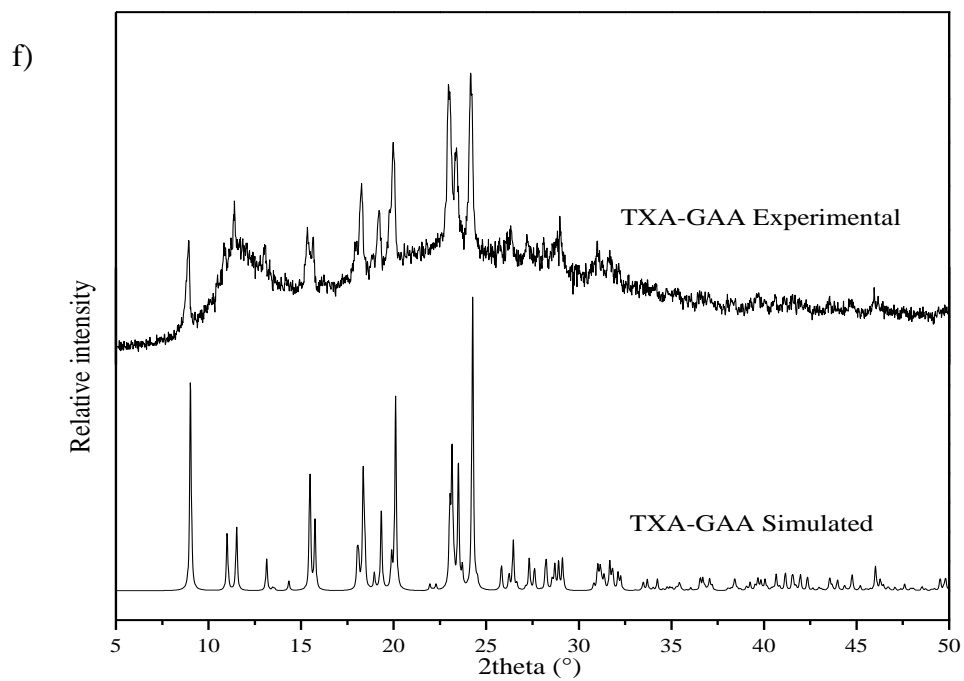
5.3.5 PXRD analysis

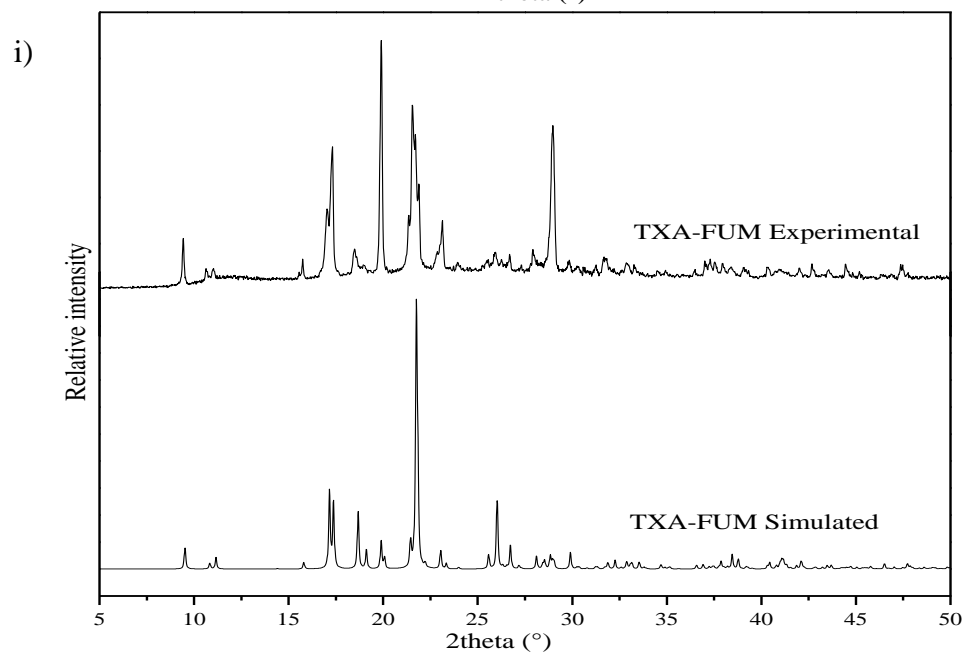
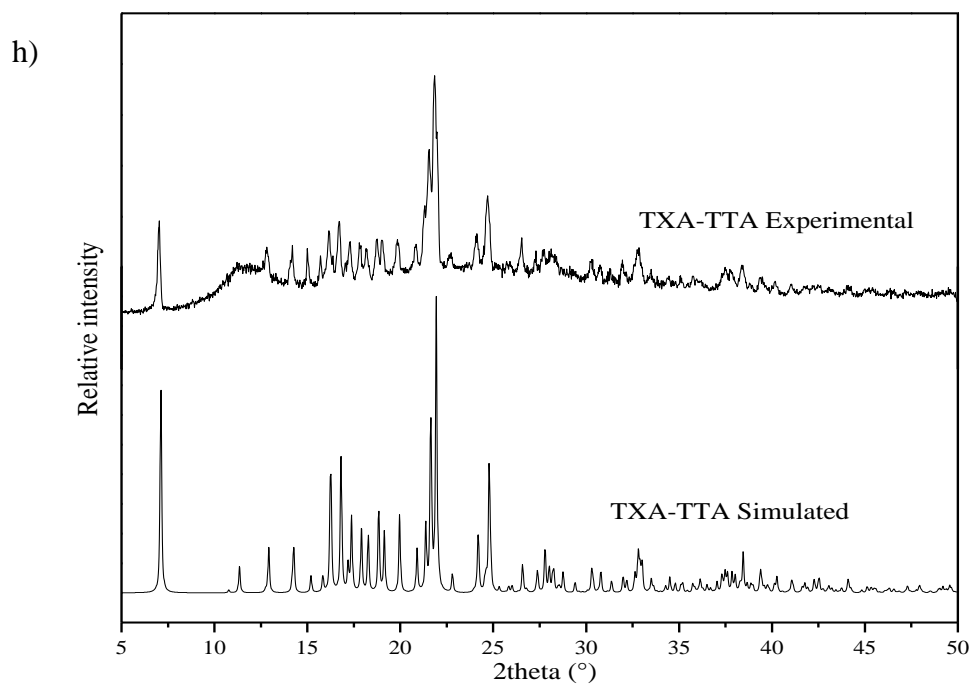
PXRD technique is a reliable characterization tool to ascertain the formation of new crystalline phases. The product formation in the salt/cocrystal screening experiment can be distinguished by comparing the diffraction patterns of starting materials. The presence or absence of diffraction peak in the newly formed crystalline material confirms the formation of new crystalline phases. In the present study, PXRD of the synthesized salt/cocrystal was performed and compared the diffraction patterns with the simulated patterns obtained from SC-XRD analysis. The overlay of the two PXRD patterns confirms the homogeneity of crystalline material in the bulk composition of all the synthesized salt/cocrystal (**Figure 5.15**). The broad peak around $2\theta=12^\circ$ is due to the instrumental error.











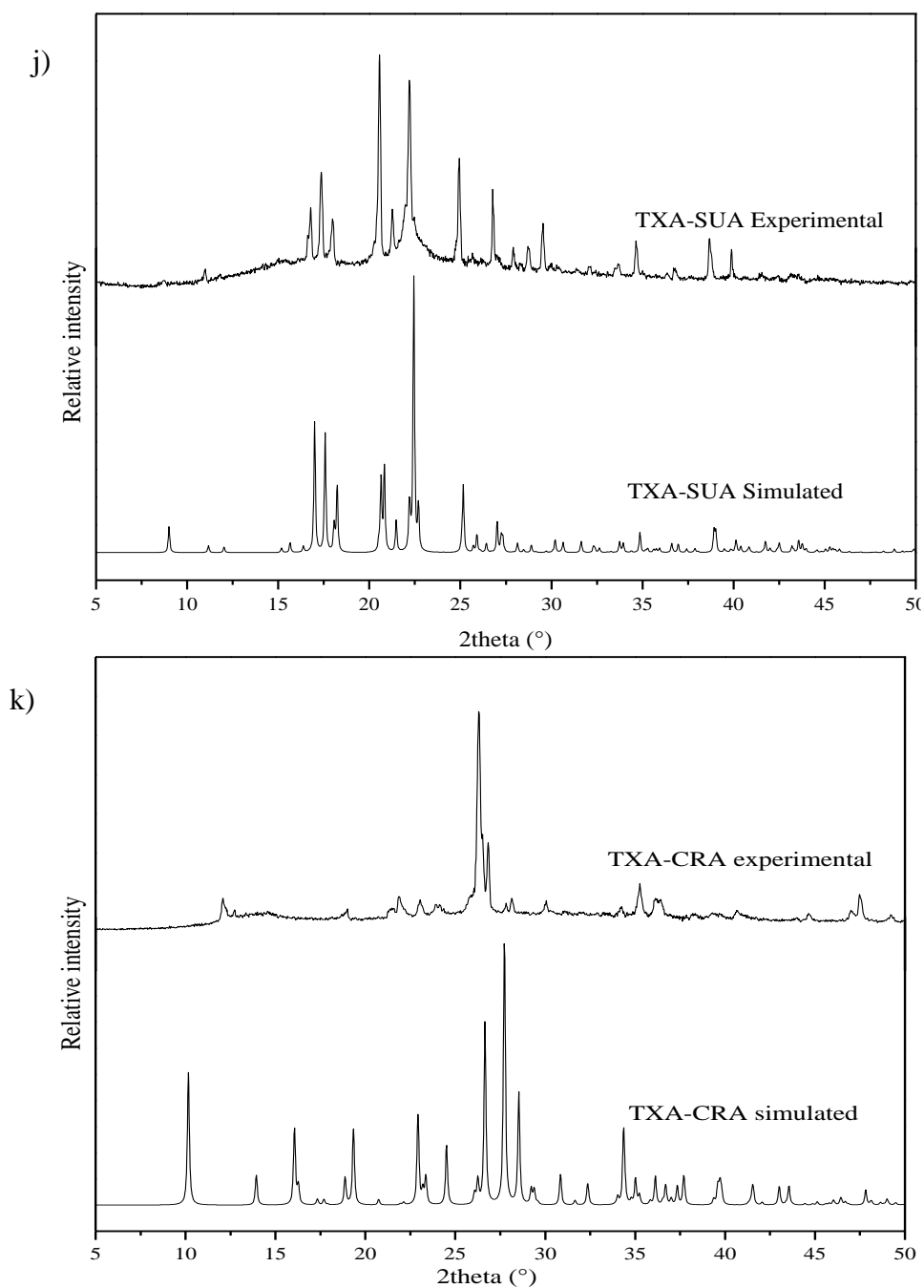


Figure 5.15: PXRD comparison plots of simulated and experimental patterns of TXA salt/cocrystal (a) TXA-SAL, (b) TXA-3HBA, (c) TXA-2,4HBA, (d) TXA-2,5HBA, (e) TXA-2,6HBA, (f) TXA-GAA, (g) TXA-OXA, (h) TXA-TTA, (i) TXA-FUM, (j) TXA-SUA, and (k) TXA-CRA.

5.3.6 DFT calculations

DFT calculations were performed for all the synthesized salt and cocrystals of TXA using Gaussian 09 Becke's three-parameter set with Lee-Yang-Parr modification

(B3LYP) with the 6-31G(d,p) basis set. The calculations were performed to better understand the geometry of the molecular structure present in the crystalline adducts in aqueous medium. The IE values of the molecular adducts were calculated in all the cases and it support the obtained crystal structure from SC-XRD analysis. Three Different hypothetical structures were constructed by changing the carboxylic acid and amine functionalities of TXA molecule in the case of TXA-GAA and TXA-CRA molecule to better demonstrate the stability of the molecular adducts (**Figure 5.16**). From the interaction energy it was found that the cocrystal structure (structure 3) is more stable compared to salt in both TXA-GAA and TXA-CRA adducts. The salt/cocrystal energy, TXA energy, coformer energy, and the IE values are given in the **Table 5.6**. The optimized structures obtained from DFT study is shown in **Figure 5.17**. **Table 5.6:** The total energy, coformer energy, and the IE value of the salt/cocrystals of TXA.

System	E _T (kJ/mol)	E _A (kJ/mol)	E _c (kJ/mol)	IE (kJ/mol)
TXA-SAL	-2665508.023	-1363001.79	-1302444.955	-61.27768134
TXA-3HBA	-5732416.563	-2726020.201	-3006195.211	-201.1511833
TXA-2,4HBA	-2863013.505	-1363001.79	-1499953.841	-57.87441897
TXA-2,5HBA	-2862999.632	-1363001.79	-1499923.33	-74.5121941
TXA-2,6HBA	-2863040.318	-1363001.79	-1499951.711	-86.8168624
TXA-GAA structure 1	-3060362.522	-1362934.617	-1697410.9	-17.00583084
TXA-GAA structure 2	-3060469.311	-1363001.79	-1697410.9	-56.62182181
TXA-GAA structure 3	-3060431.333	-1362934.617	-1697410.9	-85.8168252
TXA-OXA	-3719456.784	-2726005.144	-993322.6781	-128.9619161
TXA-TART	-2957819.381	-1363001.79	-1594771.55	-46.04119333
TXA-FUMA	-3922694.202	-2726006.273	-1196569.61	-118.3198116
TXA-SUA	-3925912.209	-2726018.76	-1199795.284	-98.1640266
TXA-CRA structure 1	-2167732.369	-1362934.617	-804720.567	-23.5948224
TXA-CRA structure 2	-2167777.074	-1363001.79	-804720.567	-54.71659097
TXA-CRA structure 3	-2167678.779	-1362934.617	-804720.567	-77.18503186

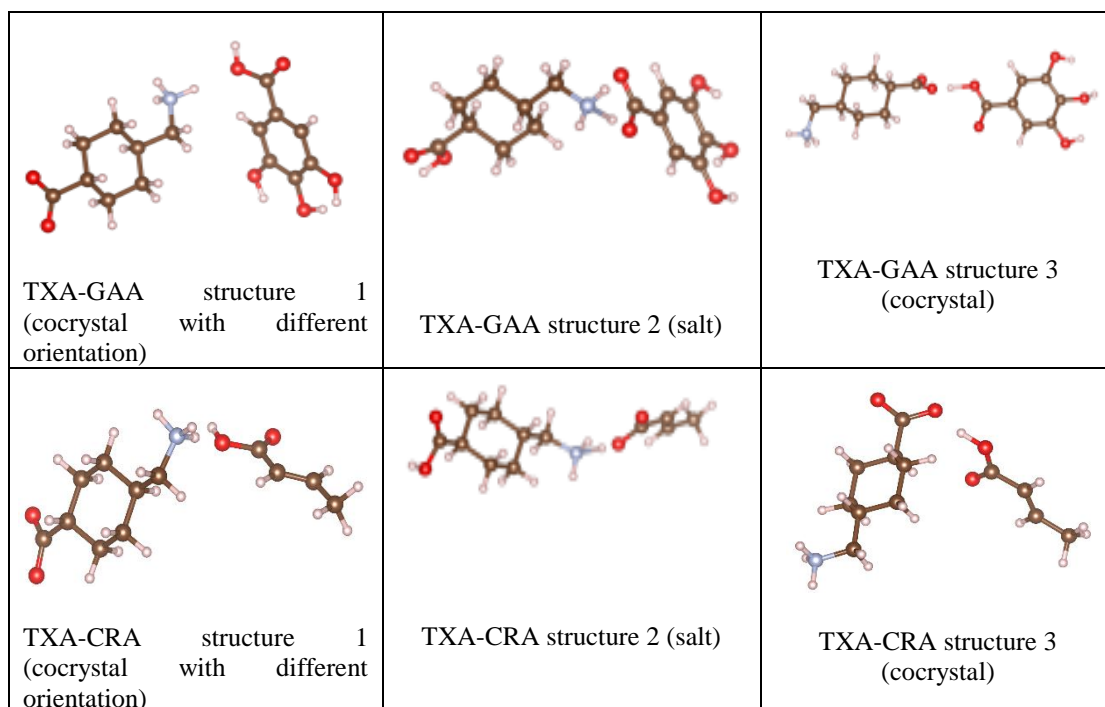


Figure 5.16: The optimized hypothetical structures drawn for TXA-GAA and TXA-CRA cocrystal.

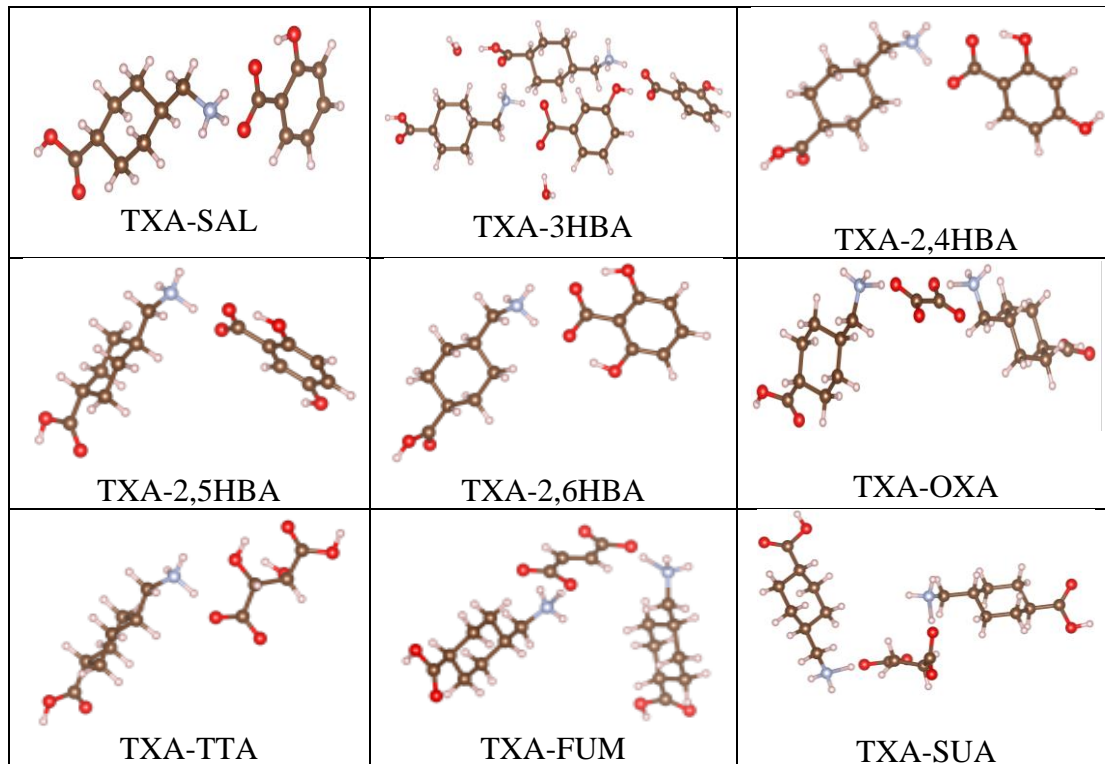


Figure 5.17: The optimized structures of molecular salts of TXA.

5.3.7 Stability study

The chemical stability of pharmaceutical products has greater importance due to its intrinsic effects safety and efficacy of drug molecules. The FDA and ICH guidelines clearly state the requirement of stability testing data to understand the quality of the drug substance changes with time under the influence of various environmental factors. In the present work, long-term stability study at ambient condition is performed (25-30 °C & 60-65% RH) for a period of six months and the phase purity of the material is determined by PXRD techniques by comparing the diffraction patterns of initial and final samples. Since all the salt/cocrystals were synthesized in aqueous media, the stability study at accelerated humidity condition is not performed. From the long term stability study, it was found that all the salt/cocrystals of TXA are stable for a period of six months at ambient conditions (**Figure 5.18-5.21**).

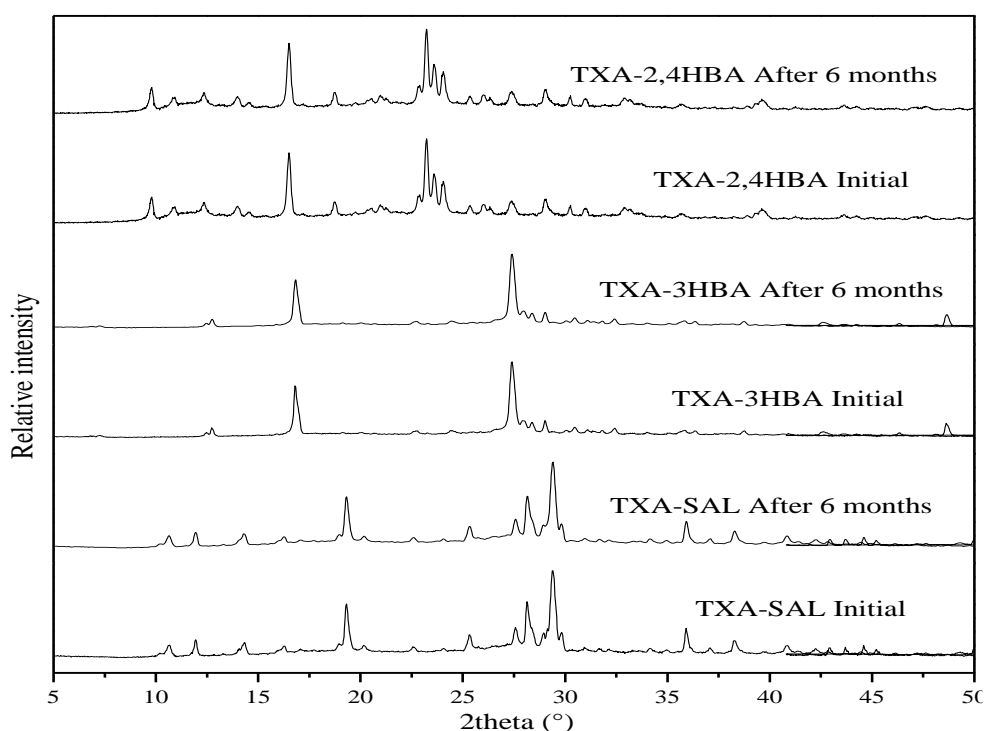


Figure 5.18: The PXRD comparison plots of (initial and after six months) TXA-SAL, TXA-3HBA, and TXA-2,4HBA salts.

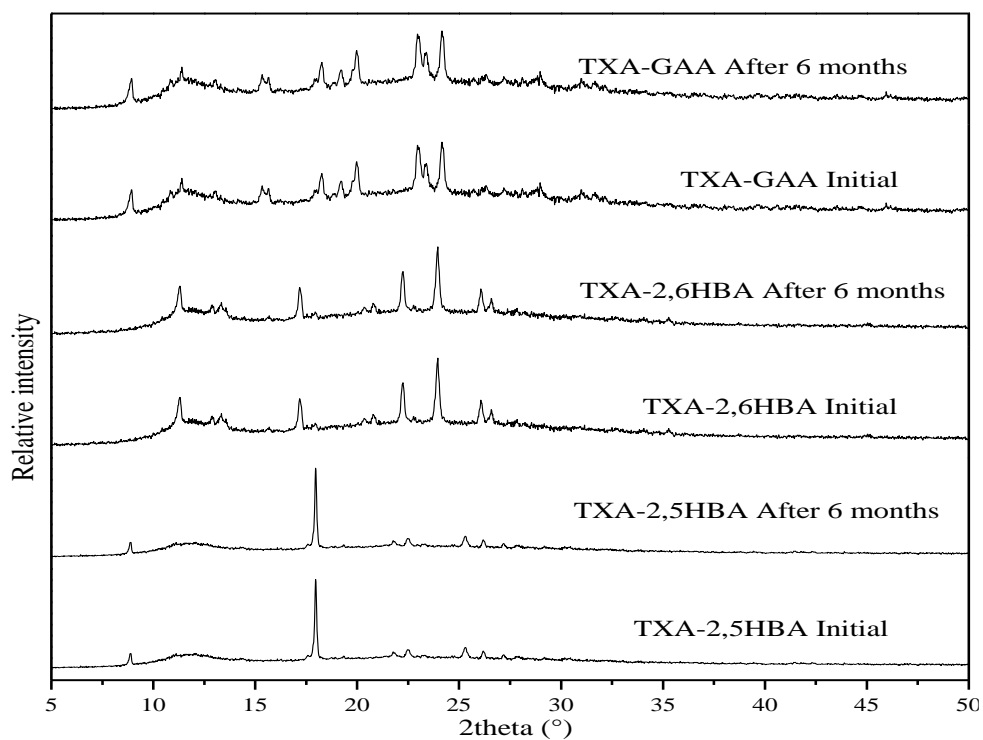


Figure 5.19: The PXR D comparison plots of (initial and after six months) TXA-2,5HBA and TXA-2,6HBA salts, and TXA-GAA cocrystal.

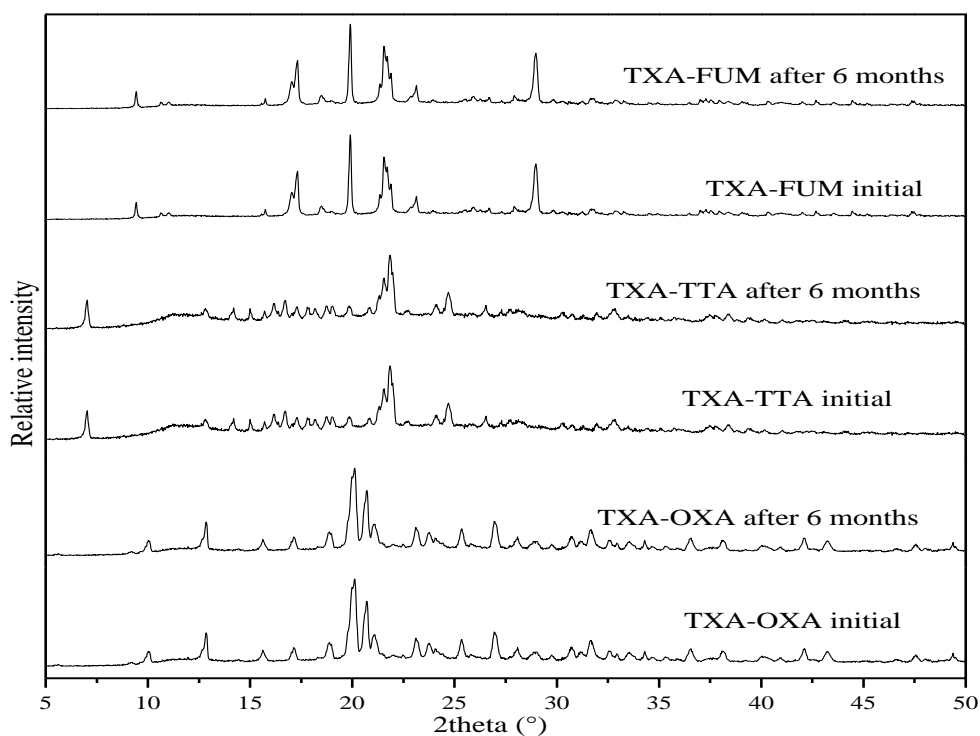


Figure 5.20: The PXR D comparison plots of (initial and after six months) TXA-OXA and TXA-TTA, and TXA-FUM salts.

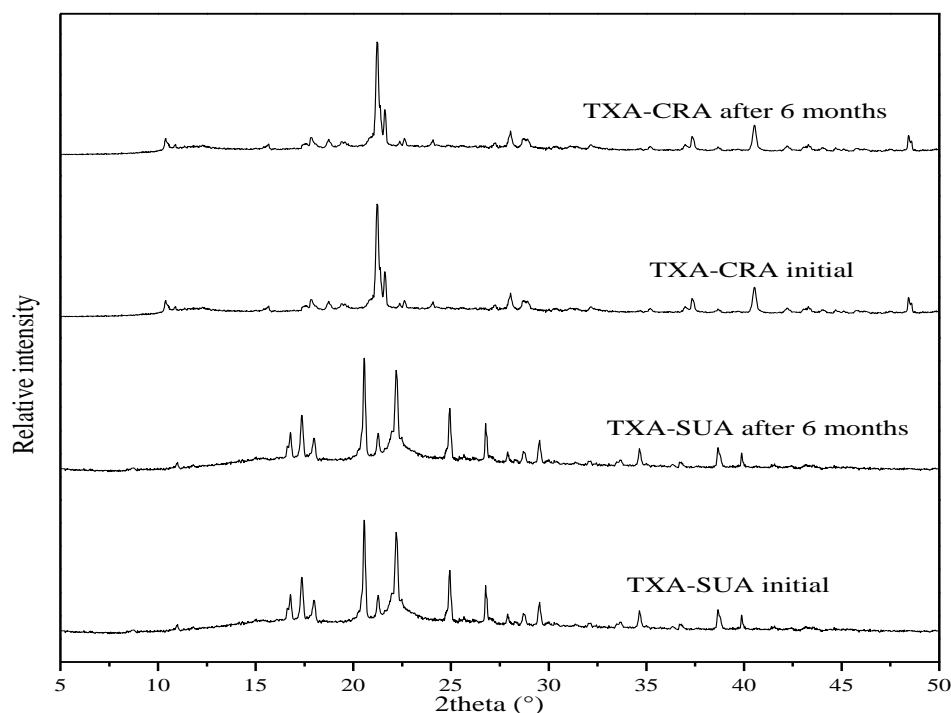


Figure 5.21: The PXRD comparison plots of (initial and after six months) TXA-SUA salt and TXA-CRA cocrystal.

5.4 CONCLUSIONS

In summary, nine molecular salts and two cocrystals of an antifibrinolytic hemostatic drug tranexamic acid were synthesized by solvent evaporation method. The detailed structural characterization study was done using various spectral, thermal and XRD techniques. Crystal structure analysis by SC-XRD techniques revealed that in all the synthesized salt/cocrystal, the robust primary supramolecular synthon involved was $-O-H\cdots O=C$, $-N-H\cdots O$, $-O-H\cdots O-H$ hydrogen bonds. All the cofomers/counter ions were of GRAS molecule and therefore these molecular adducts may be useful for the development of new drug products of TXA molecule which may have enhanced absorption in the gastrointestinal tract. The molecular salts namely, TXA-FUM and TXA-SUA were found to be isostructural based on the isostructural parameters π and ϵ . From the DFT calculation study, it was found that the cocrystal structure is more favored over salt in the case of TXA-GAA and TXA-CRA. The long-term stability study of these salt/cocrystal revealed that these salt/cocrystal are stable for about six months at ambient conditions and subsequently the salts TXA-SAL and TXA-2,5HBA offers for the synthesis of combination drug of TXA API.

CHAPTER 6

***DESIGN, SYNTHESIS, CHARACTERIZATION, AND
EVALUATION OF PHYSICOCHEMICAL
PROPERTIES OF COCRYSTAL/SALT OF ANTI-
FUNGAL DRUG FLUCYTOSINE***

This chapter describes the design and synthesis of pharmaceutical salt/cocrystal of anti-fungal drug flucytosine. The detailed structural study based on SC-XRD analysis is explained, and the hygroscopicity of the synthesized cocrystal/salt at accelerated humidity condition is evaluated and compared the hygroscopicity with parent flucytosine drug molecule.

6.1 INTRODUCTION

5-Fluorocytosine (4-amino-5-fluoro-1,2-dihydropyrimidine-2-one) (FLC) is a fluorinated analogue of nucleobase cytosine (**Figure 6.1**). It is an anti-metabolite which acts as an antifungal agent. Its pharmaceutical action involves the conversion of fluorocytosine into fluorouracil by deamination by the enzyme cytosine deaminase (CD) present in the fungal cell. It is also introduced as a potential drug for cancer treatment in combination with CD. According to BCS classification, the FLC is BCS class III drug due to high solubility and low permeability in water medium. The main drawback of this API is that it is highly hygroscopic in nature. This poor solid state stability cause challenges during the manufacture and storage of FLC drug.

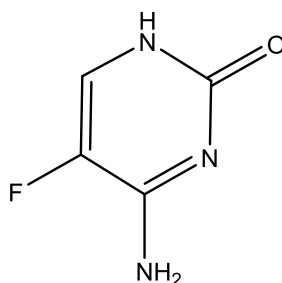
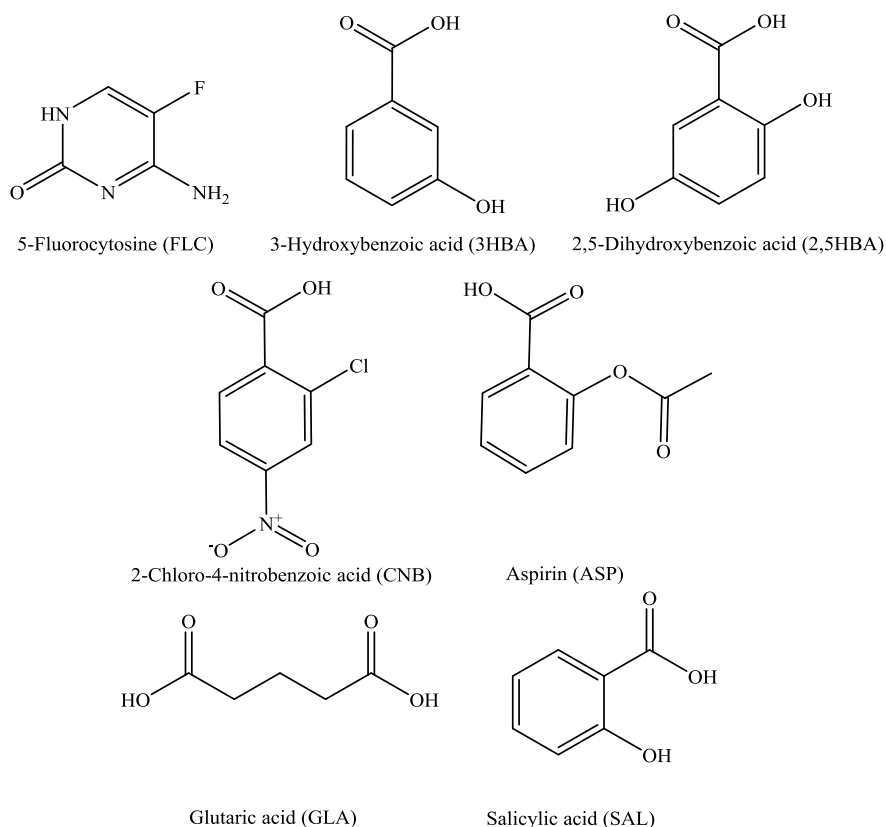


Figure 6.1: Molecular structure of 5-fluorocytosine.

Numerous reports on cocrystal/salt of FLC drug molecule was found in the literature. Various salts of FLC were reported in the literature with maleic acid, oxalic acid, fumaric acid (2013), salicylic acid (SA), sulfosalicylic acid (SSA) (2012) and HCl (2006). Perumalla et al. (2013) successfully synthesized eight new salts, both cytosinium and hemicytosinium, with strong acids like hydrobromic acid, hydroiodic acid, nitric acid and saccharine. It is found that among these new FLC salts, the anhydrous FLC/saccharine salt holds the potential for pharmaceutical application due to its superior solid-state stability and accepted safety profile in humans.

Cecilia et al. (2014) have been synthesized 1:1 cocrystals of FLC with adipic acid, succinic acid, benzoic acid, terephthalic acid, and malic acid based on the ΔpK_a values. The crystal structure data showed that in the first four cocrystals instead of heterodimer two different homodimer were observed by the interaction of two adjacent FLC molecules through N-H \cdots O and N-H \cdots N hydrogen bonds respectively. In contrast to other crystal structures, the cocrystal with malic acid exhibits an intermediate supramolecular synthon between salt and cocrystal. Other reported cocrystals include nitrouracil, 2-amino pyrimidine, N-acetyl creatinine, 6-aminouracil, 6-aminoisocytosine, acyclovir, biuret, 6-acetamidouracil, and 6-methylisocytosine. The conformational analysis of these cocrystals showed that the cocrystal with biuret exhibit energetically stable trans form and 6-acetamidouracil exhibit less stable cis form. The cocrystallization with 5-nitrouracil resulted in a crystal structure which contains two neutral FLC molecule hydrogen bonded to a pair and the crystal structure contains conventional N-H \cdots O, O-H \cdots O, N-H \cdots N, N-H \cdots N hydrogen bonds. Lin et al. (2014) synthesized 2:1 conjugate acid-base cocrystal and 1:1 salt hydrate of FLC with acesulfame, a sweetening agent both exhibit enhanced phase stability against hydration. It was observed that FLC content is higher in 2:1 acid base cocrystal and it exhibit comparatively high thermal stability than the 1:1 salt hydrate. Perumalla et al. (2016) developed pharmaceutically acceptable conjugate acid base cocrystals of FLC with HCl and acesulfame with excellent physical stability, tabletability and good flowability.

In the present study, we report five molecular salt/cocrystal of FLC with various GRAS molecules such as 3-hydroxybenzoic acid (3HBA), 2,5-dihydroxybenzoic acid (2,5HBA), 2-chloro-4-nitrobenzoic acid (CNB), aspirin (ASP), and glutaric acid (GLA). The cocrystal synthesis in the present work with ASP in aqueous medium resulted in hydrolysis of ASP and a salt of FLC with salicylic acid (SAL) is obtained in the crystallization process. The molecular diagrams of FLC and the cofomer molecules are shown in **Scheme 6.1**. Since the major drawback of FLC drug is that it experiences hydration when exposed to the atmosphere and this causes a major challenge in formulation and storage of this drug molecule. Therefore, in the present work, we have studied the effect of humidity (accelerated humidity conditions) on the storage of the newly synthesized salt/cocrystals of FLC drug. Further, the present work describes the detailed structural study and structural comparison of the synthesized salt/cocrystals.



Scheme 6.1: Molecular structures of FLC and the coformer chosen in the study.

6.2 EXPERIMENTAL SECTION

FLC was purchased from TCI Chemicals and used as such. 3-hydroxybenzoic acid, 2,5-dihydroxybenzoic acid, 2-chloro-4-nitrobenzoic acid, aspirin, and glutaric acid were purchased from sigma Aldrich. These chemicals were used as such without further purification. Purified distilled water is used for all the cocrystal/salt synthesis.

6.2.1 Synthesis salts/cocrystals

Salts/cocrystals of FLC were synthesized by solvent evaporation method.

FLC-3HBA: The equimolar ratio of FLC (50 mg, 0.3873 mmol) and 3HBA (53.49 mg, 0.3873 mmol) were taken in a 25 mL beaker and dissolved the material in 10 mL of water at 80 °C. This clear solution is allowed for slow evaporation at room temperature. Colorless needle-shaped crystals were obtained after 7 days.

FLC-2,5HBA: The equimolar amount of FLC (50mg, 0.3873mmol) and 2,5HBA (59.69 mg, 0.3873 mmol) were dissolved individually in 10 mL of water at 80 °C, this clear solution is then mixed together and again heated to 80 °C to ensure the complete

dissolution followed by slow evaporation at room temperature yielded pale yellow colored block-shaped crystals of FLC-2,5HBA cocrystal after 5 days.

FLC-CNB: The equimolar ratio of FLC (50 mg, 0.3873 mmol) and CNB (78.06 mg, 0.3873 mmol) were dissolved in 15 mL of water at 60 °C. The clear solution is then allowed to room temperature and then kept for slow evaporation. Pale yellow colored block-shaped crystals were collected after 7 days.

FLC-ASP: FLC (50 mg, 0.3873 mmol) and ASP (69.77 mg, 0.3873 mmol) were taken in the equimolar ratio in a 25 mL beaker and dissolved individually in 10 mL of water at 80 °C. This clear solution is then mixed together, again heated to 80 °C and then allowed to cool to room temperature and kept for slow evaporation. Colorless block-shaped crystals were obtained after 7 days. The crystal confirmed to be FLC-SAL salt rather than FLC-ASP cocrystal. Multiple crystallization trials with non-aqueous solvent did not yield cocrystal of FLC with ASP.

FLC-GLA: The equimolar ratio of FLC (50 mg, 0.3873 mmol) and GLA (51.17 mg, 0.3873 mmol) were taken in a small beaker and dissolved it in 15 mL of water. Heated this mixture to 60 °C to ensure the complete dissolution followed by slow evaporation at room temperature. Colorless block-shaped crystals were obtained after 7 days by filtration.

6.2.2 Single crystal X-ray diffraction analysis (SC-XRD)

Data collections were done on Rigaku XtaLAB Mini diffractometer with X-ray generator operating at 50 kV and 12 mA, using MoK α radiation of wavelength 0.71073 Å at 293 K. Data were collected with χ fixed at 54° and for different settings of ϕ (0° and 360°), keeping the scan width of 0.5°, exposure time of 3 s, the sample to detector distance of 50 mm. The complete intensity data sets were processed using CRYSTAL CLEAR. The crystal structure was solved by a direct method and refined by full-matrix least squares method of F^2 using SHELXS and SHELXL programs. All the SC-XRD figures corresponds to the crystal structures were drawn using Mercury 3.8 software.

6.3 RESULTS AND DISCUSSION

FLC is a weak base having pKa value 3.26 for pyrimidine N. The ΔpK_a comparison with the selected coformer molecule is tabulated in **Table 6.1** for the salt/cocrystal prediction. It is observed that the ΔpK_a values for 3HBA, ASP, and GLA were found to be below 0 demonstrating the possibility of cocrystal formation. Since the hydrolysis of ASP is observed in an aqueous medium, the resulted crystal was found to be a salt with SAL. The ΔpK_a for CNB and 2,5HBA falls under salt-cocrystal continuum. All the newly formed crystalline adducts were subjected to melting point and FT-IR analysis in order to confirm the salt/cocrystal formation. After the confirmation of new crystalline adducts formation, the materials were characterized further by SC-XRD, PXRD, DSC, and ^1H NMR analysis.

Table 6.1: The pKa and ΔpK_a values of FLC and the coformers.

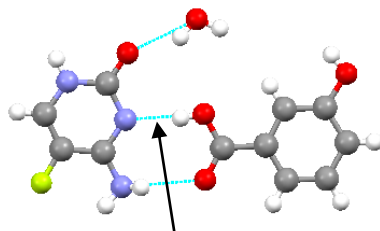
API	pKa1	Coformer	pKa2	ΔpK_a (pKa1-pKa2)	Molecular adducts formed
FLC	3.26	3HBA	3.8	-0.54	Cocrystal
		2,5HBA	2.5	0.76	Cocrystal
		CNB	1.96	1.3	Salt
		ASP	3.4	-0.14	-
		GLA	4.34	-1.08	Cocrystal
		SAL	2.97	0.29	Salt

6.3.1 SC-XRD analysis of FLC salt/cocrystal

FLC-3HBA

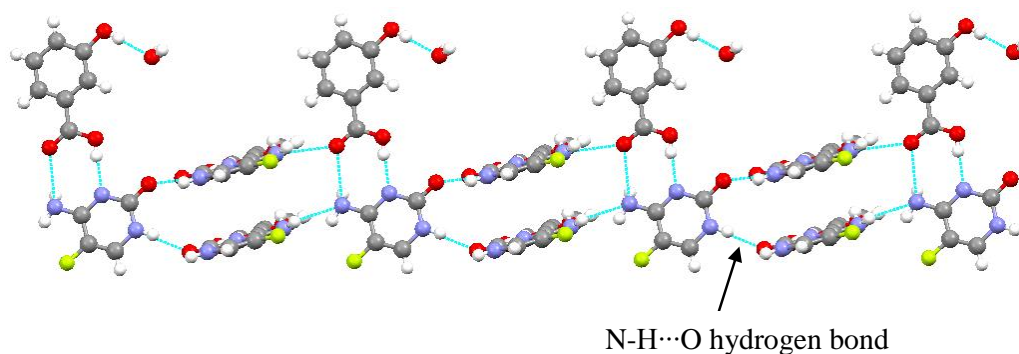
It was crystallized in monoclinic crystal system with $P 2_1$ space group. It was crystallized as monohydrate, the asymmetric unit includes one molecule each of FLC, 3HBA, and a water molecule (**Figure 6.2**). Primary interactions comprised of O-H \cdots N and N-H \cdots O hydrogen bond (2.684 Å & 2.848 Å) between 3HBA and FLC molecule. The water molecule forms a hydrogen bond with a 3-hydroxy group of 3HBA with O-H \cdots O bond distance of 2.747 Å. Neighboring supramolecular adducts in the crystal structure interconnected through N-H \cdots O hydrogen bond (2.949 Å) resulting in a 2D structure of FLC-3HBA cocrystal (**Figure 6.3**). The overall crystal structure here features O-H \cdots O hydrogen bond between a water molecule and FLC, O-H \cdots O between two water molecules, weak C-H \cdots O, C-H \cdots F, & N-H \cdots O hydrogen bond between FLC

and 3HBA molecules (**Figure 6.4**). Crystallographic parameters, refinement details and geometry of intermolecular interaction in FLC salt/cocrystal are shown in **Table 6.2** and **Table 6.3**. Color code for the atoms are gray: carbon, off-white: hydrogen, red: oxygen, blue: nitrogen, light green: fluorine, green: chlorine.



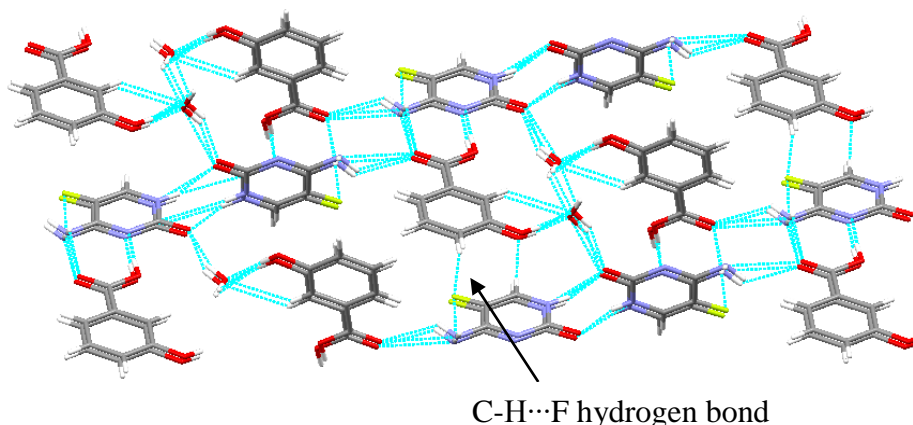
O-H...N heterosynthon

Figure 6.2: Asymmetric unit of FLC-3HBA cocrystal.



N-H...O hydrogen bond

Figure 6.3: 2D structure of FLC-3HBA cocrystal.



C-H...F hydrogen bond

Figure 6.4: 3D structure of FLC-3HBA cocrystal stabilized via C-H...O and C-H...F hydrogen bond.

FLC-2,5HBA

It was crystallized in monoclinic crystal system with $P 2_1/c$ space group, the asymmetric unit in the crystal structure constitutes one molecule each of FLC and 2,5HBA. The

molecules interacted through two point heterosynthons between acid and amide group of 2,5HBA and FLC respectively with O-H \cdots O and N-H \cdots O bond distance of 2.481 Å and 2.805 Å (**Figure 6.5a**). Two neighboring supramolecular adducts interconnected through N-H \cdots O hydrogen bond (3.00 Å) and O-H \cdots O hydrogen bond (2.724 Å) between FLC and 2,5HBA resulting in a cyclic tetrameric unit of FLC-2,5HBA cocrystal (**Figure 6.5b**). This tetrameric unit further interconnected via N-H \cdots O hydrogen bond involving -NH of the amino group of FLC and O of the hydroxyl group of GEA (2.834 Å) resulting in 1D chain-like structure of FLC-2,5HBA cocrystal (**Figure 6.6**). 1D chain further converts to the 2D structure by utilizing C-H \cdots O hydrogen bond (3.173 Å) between aromatic C-H of FLC and O-H of 2,5HBA resulting in two-dimensional sheet-like structure of FLC-2,5HBA cocrystal (**Figure 6.7**). This 2D structure converts to the 3D structure using the π - π interaction between FLC and 2,5HBA with centroid to centroid bond distance of 3.352 Å.

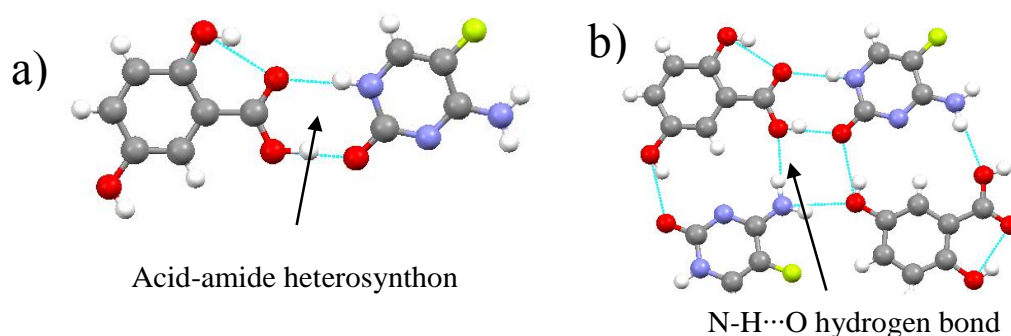


Figure 6.5: Asymmetric unit (a) and tetrameric unit (b) of FLC-2,5HBA cocrystal.

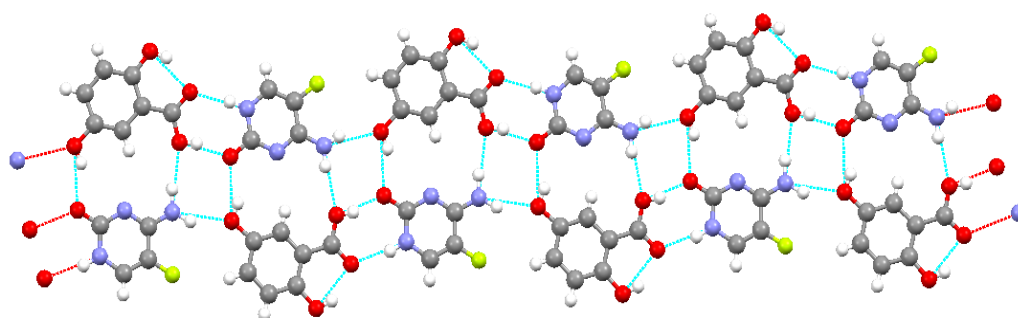


Figure 6.6: 1D chain-like structure of FLC-2,5HBA cocrystal.

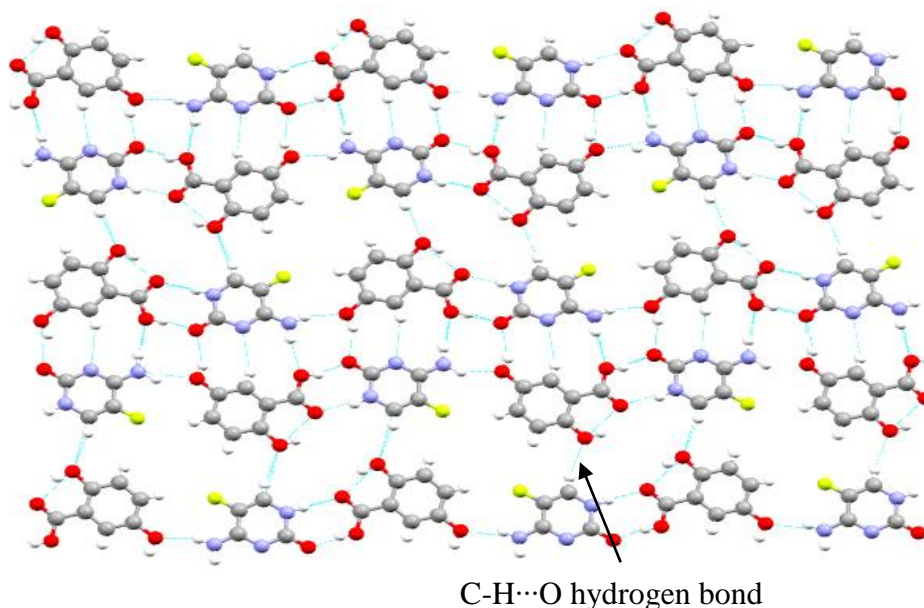


Figure 6.7: 2D sheet-like structure of FLC-2,5HBA cocrystal.

FLC-CNB

Good quality crystals were not obtained in this case and therefore the crystal structures could not solve with good R factor. The asymmetric unit in the crystal structure consists of one molecule each of FLC and CNB which was crystallized in monoclinic crystal system with $P 2/n$ space group. Proton transfer from acid group of CNB to pyramidal nitrogen is observed. The molecules interacted through N-H...O hydrogen bond (2.772 Å) between FLC and CNB (**Figure 6.8**). The amide group of FLC in the crystal structure forms an amide-amide homodimer (2.850 Å), and this dimer connected to the neighboring dimer via N-H...O hydrogen bond (2.866 Å) between FLC molecules, which further continues resulting in the 2D structure of FLC-CNB cocrystal (**Figure 6.9**). This further convert to the 3D structure using O...O chalcogen bond between two CNB molecules. The overall crystal structure features weak secondary C-H...O hydrogen bond between C-H of FLC and O of nitro group of CNB molecules.

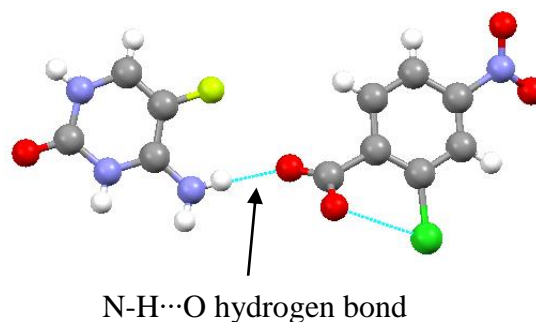


Figure 6.8: Asymmetric unit of FLC-CNB salt.

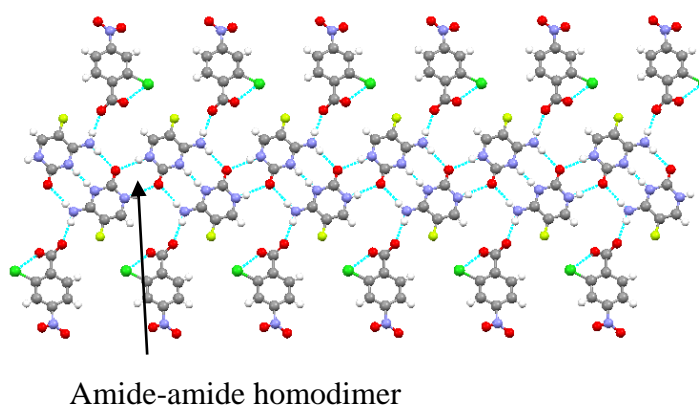


Figure 6.9: 2D sheet-like structure of FLC-CNB salt.

FLC-SAL

Cocrystallization of FLC with ASP unexpectedly yielded FLC-SAL salt due to the hydrolysis of ASP molecule in water media which was already reported by Prabhakaran et al. in the year 2001. Since, the stability study of this salt is not carried out previously, we have included the crystal structure in the present study in order to show the stability of this salt towards hydration. It was crystallized in monoclinic crystal system with $P 2_1/n$ space group. Here the charge assisted acid-pyrimidine heterosynthon was observed between the molecules with N-H...O bond distance of 2.785 Å & 2.762 Å (**Figure 6.10**). Neighboring molecular units were interconnected through strong N-H...O hydrogen bond (2.721 Å) between FLC and SAL molecule resulting in a 2D structure of FLC-SAL salt (**Figure 6.11**). The overall crystal structure of this salt features weak C-H...O, C-H...F and π - π interaction between FLC and SAL molecules.

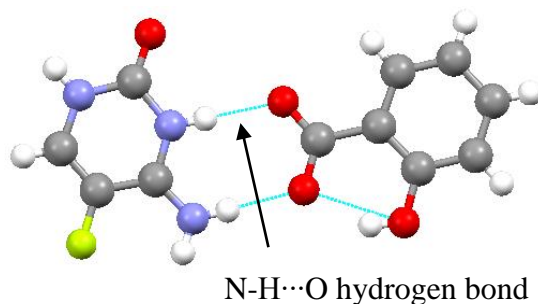


Figure 6.10: Asymmetric unit of FLC-SAL salt.

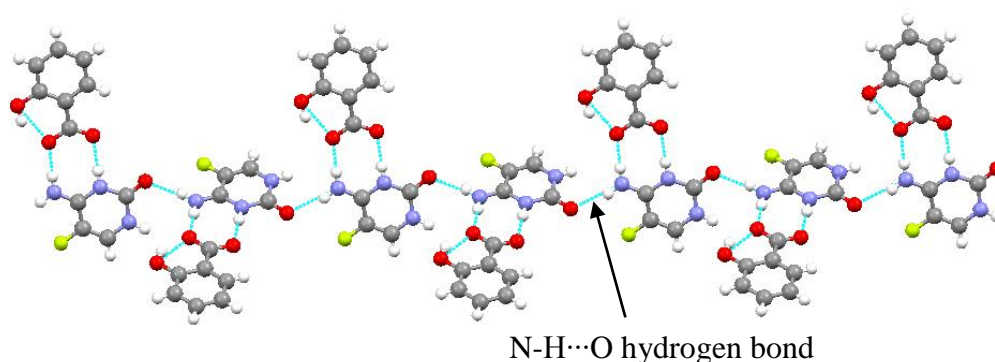


Figure 6.11: 2D structure of FLC-CNB stabilized by N-H...O hydrogen bond.

FLC-GLA

It was crystallized in monoclinic crystal system in the $P 2_1/c$ space group. Cocrystal is formed in 2:1 ratio of FLC and GLA even though 1:1 ratio of FLC and GLA is used for cocrystallization. Cocrystal is formed through acid-carbonyl heterosynthon between GLA and FLC with O-H...O bond distances 2.599 Å and 2.624 Å (bond angle 171.23° and 163.63°) respectively (**Figure 6.12**). This molecular adduct further interconnected to the neighboring adducts through N-H...O homosynthon between FLC molecule with bond distances 2.872 Å, 2.820 Å, N-H...O hydrogen bond between FLC and GLA (bond distances 2.855 Å, 2.892 Å) and N-H...N homosynthon between FLC molecule (bond distances 2.924 Å, 2.916 Å) resulting in a cyclic six component supramolecular unit. This further continues to give a cyclic one-dimensional and two-dimensional structure of FLC-GLA cocrystal (**Figure 6.13**). Two-dimensional structure converts to the 3D structure by utilizing the C-H...F hydrogen bond between C-H of GLA and F of FLC (3.371 Å) (**Figure 6.14**). The overall crystal structure features the C-H...O hydrogen bond between FLC and carboxylic group of GLA.

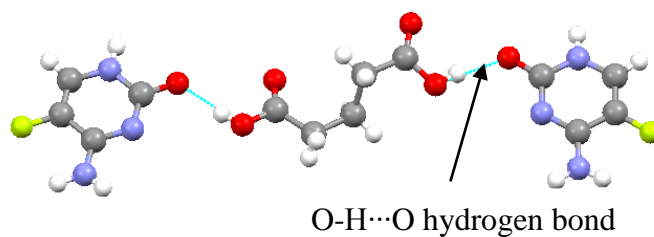


Figure 6.12: Asymmetric unit of FLC-GLA cocrystal.

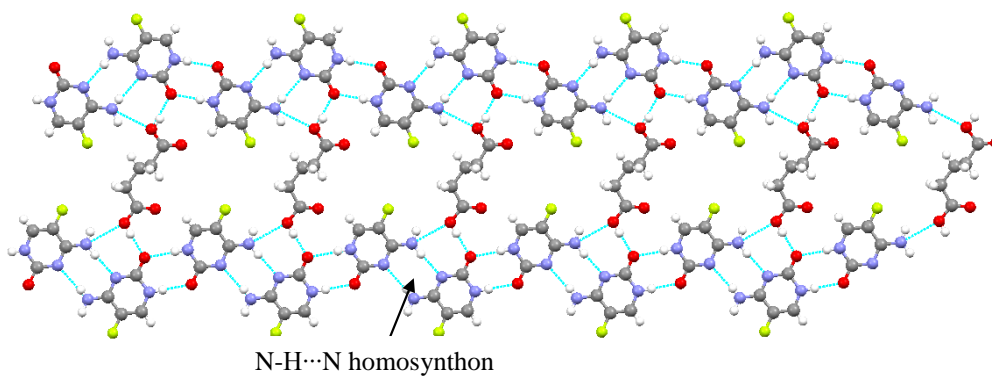


Figure 6.13: Cyclic 1D chain-like structure of FLC-GLA cocrystal.

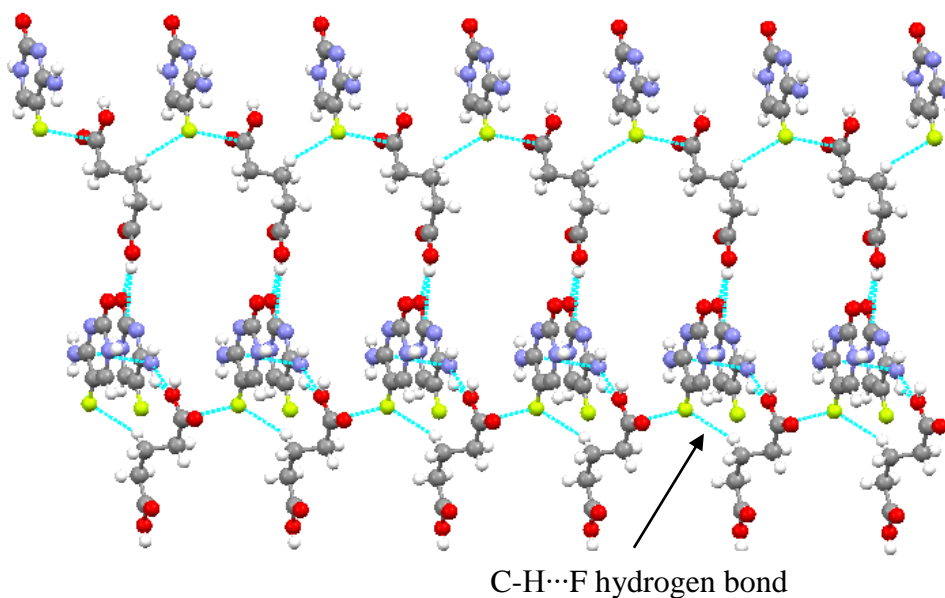


Figure 6.14: 3D structure of FLC-GLA cocrystal stabilized by C-H...F hydrogen bond.

Table 6.2: Crystallographic parameters and refinement details of FLC salt/cocrystal.

Crystal structure details	FLC-3HBA	FLC-2,5HBA	FLC-CNB	FLC-SAL	FLC-GLA
CCDC number	1578369	1578356	-	1578366	1543795
Mol. formula	C ₁₁ H ₁₂ FN ₃ O ₅	C ₁₁ H ₁₀ FN ₃ O ₅	C ₁₁ H ₈ FCIN ₄ O ₅	C ₁₁ H ₁₀ FN ₃ O ₄	C ₁₃ H ₁₆ F ₂ N ₆ O ₆
Molar mass	285.24	283.22	330.66	267.22	390.32
crystal system	Monoclinic	monoclinic	Monoclinic	Monoclinic	monoclinic
Space group	P 2 ₁	P 2 ₁ /c	P 2/n	P 2 ₁ /n	P 2 ₁ /c
a / Å	8.903(3)	5.455(15)	9.731(5)	8.178(3)	10.0742(8)
b / Å	5.2836(15)	14.57(4)	8.497(4)	10.516(3)	24.810(2)
c / Å	13.527(4)	14.53(4)	17.101(9)	13.540(4)	6.8938(6)
α / °	90.000(4)	90	90.00	90	90
β / °	97.941(7)	96.13(4)	97.039(9)	101.774(16)	105.058(6)
γ / °	90.000(7)	90	90.00	90	90
Volume/ Å ³	630.2(3)	1148(5)	1403.3(12)	1139.9(6)	1663.9(2)
Z	2	4	4	4	4
Density [g/cm ³]	1.503	1.639	1.565	1.557	1.558
μ (MoKα) [mm ⁻¹]	0.129	0.141	0.314	0.131	1.211
T/K	296	293(2)	293(2)	293(2)	296(2)
Reflns collected	2249	2700	3153	2564	2722
Unique rflns	1859	1661	1783	1864	1936
Parameter refined	188	187	200	173	308
R ₁ (I > 2σ)	0.0554	0.0738	0.2020	0.0507	0.0632
wR ₂ (I > 2σ)	0.1438	0.1886	0.5096	0.1359	0.1795
GOF	0.997	0.945	1.393	1.248	1.024

Table 6.3: Geometrical parameters of hydrogen bond interactions in FLC salt/cocrystal.

Cocrystal/ Salt	D-H...A ^a	D-H...A/ Å	D...A/ Å	∠D-H...A/ °	Symmetry Code
FLC- 3HBA	N3-H7...O4	1.911	2.749	164.18	-x+2, y+1/2, -z+2
	O1-H2...N2	1.875	2.684	168.71	x-1, y+1, z
	N1-H9...O2	2.296	2.848	122.01	x+1, y-1, z
	N1-H8...O2	2.344	2.949	127.58	-x+1, y-1/2, -z+1
	C10-H5...O3	2.569	3.496	175.31	x, y+1, z
	C14-H11...F1	2.474	3.389	168.06	x, y-1, z
	O3-H6...O5	1.929	2.747	175.70	-x+1, y-1/2, -z+2
	O5-H1...O4	2.009	2.777	149.78	x-1, y+1, z
O5-H3...O5	2.611	3.347	145.51	-x+1, y-1/2, -z+2	
FLC- 2,5HBA	O3-H8...O4	1.843	2.558	144.97	x, y, z
	O2-H5...O1	1.990	2.724	148.58	x+1, y, z
	N1-H4...O4	1.955	2.805	169.29	-x+2, y-1/2, -z+1/2
	N3-H2...O5	2.169	3.000	162.32	x-1, y, z
	N3-H1...O2	2.070	2.834	147.50	-x+2, y+1/2, -z+1/2
	C7-H6...N2	2.559	3.424	154.86	x+1, y, z
	C8-H3...O3	2.291	3.173	158.18	x+1, -y+1/2, z+1/2
	O5-H7...O1	1.432	2.481	168.39	-x+2, y+1/2, -z+1/2
	O5-H7...N1	2.681	3.508	134.53	-x+2, y+1/2, -z+1/2
FLC-CNB	O7-H2...C11	2.636	3.068	114.43	x, y, z
	O7-H2...N2	2.450	3.190	150.58	x+1, y, z
	N2-H5...O2	1.968	2.819	170.18	-x, -y+1, -z
	N3-H8...O2	1.996	2.855	176.51	-x, -y, -z
	N3-H7...O6	1.903	2.758	171.89	-x+3/2, y-1, -z+1/2
	C10-H6...O5	2.553	3.046	113.52	x, y, z
FLC-SAL	O2-H1...O3	1.828	2.549	145.94	x, y, z
	N2-H8...O4	1.926	2.785	175.86	-x+1, -y, -z
	N1-H7...O3	1.904	2.762	175.00	-x+1, -y, -z
	N1-H6...O1	2.040	2.885	167.33	x-1/2, -y+1/2, z-1/2
	N3-H9...O4	1.881	2.721	164.99	x+1/2, -y+1/2, z+1/2
	C6-H2...O3	2.652	3.541	160.16	-x+1/2, y+1/2, -z+1/2
FLC-GLA	C7-H9...O1	2.188	3.035	150.10	-x, y+1/2, -z+1/2
	O2-H4...O3	1.790	2.624	163.91	x, y, z
	N6-H6...O3	1.925	2.820	178.80	-x, y+1/2, -z+1/2
	N4-H7...N1	2.184	2.961	171.04	-x+1, y+1/2, -z+3/2
	O5-H5...O6	1.789	2.599	171.52	x, y, z
	C2-H13...O4	2.621	3.170	118.57	x, y, z
	N2-H3...O6	2.024	2.872	174.04	-x, y-1/2, -z+1/2
	N3-H1...O5	2.290	2.855	123.66	-x+1, y-1/2, -z+3/2
	N4-H8...O2	2.239	2.893	126.69	-x+1, y+1/2, -z+3/2

	C11-H2...O4	2.177	3.016	146.68	-x, y-1/2, -z+1/2
	N3-H16...N5	2.019	2.924	172.62	-x+1, y-1/2, -z+3/2

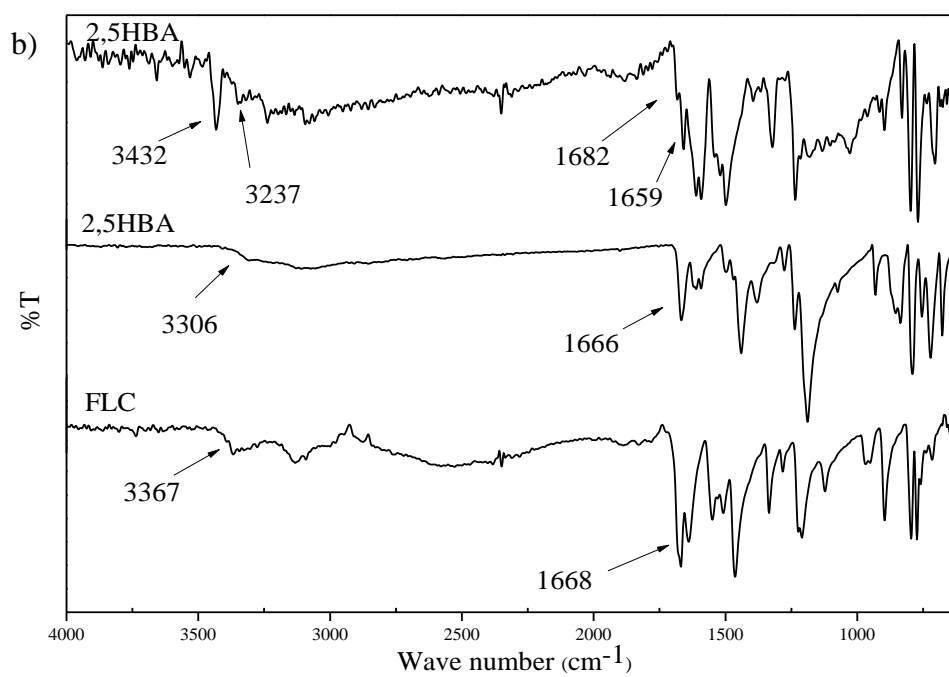
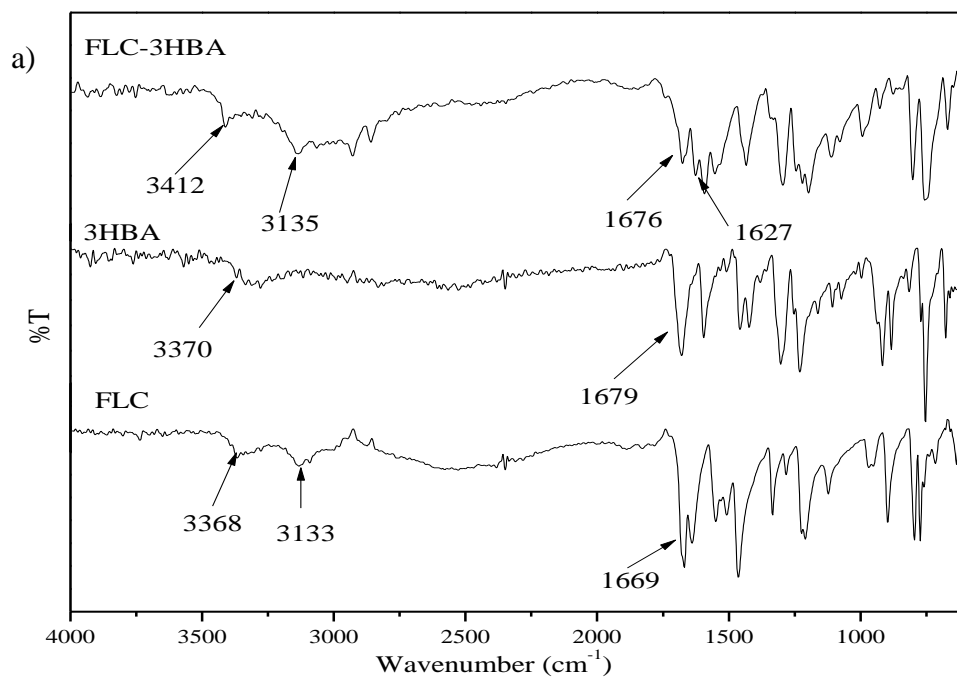
^a D=donor, A=acceptor

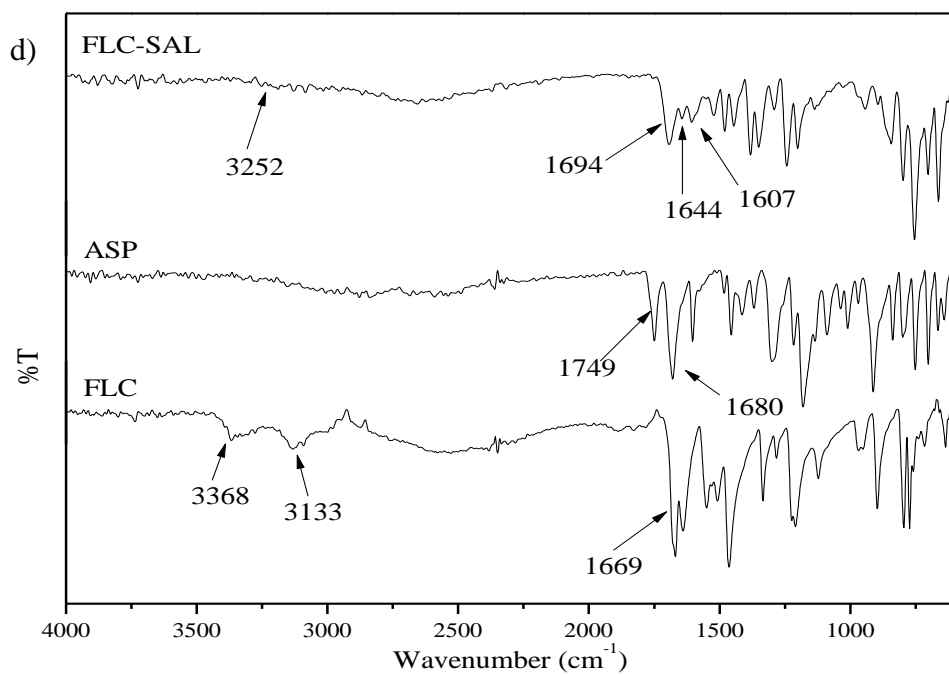
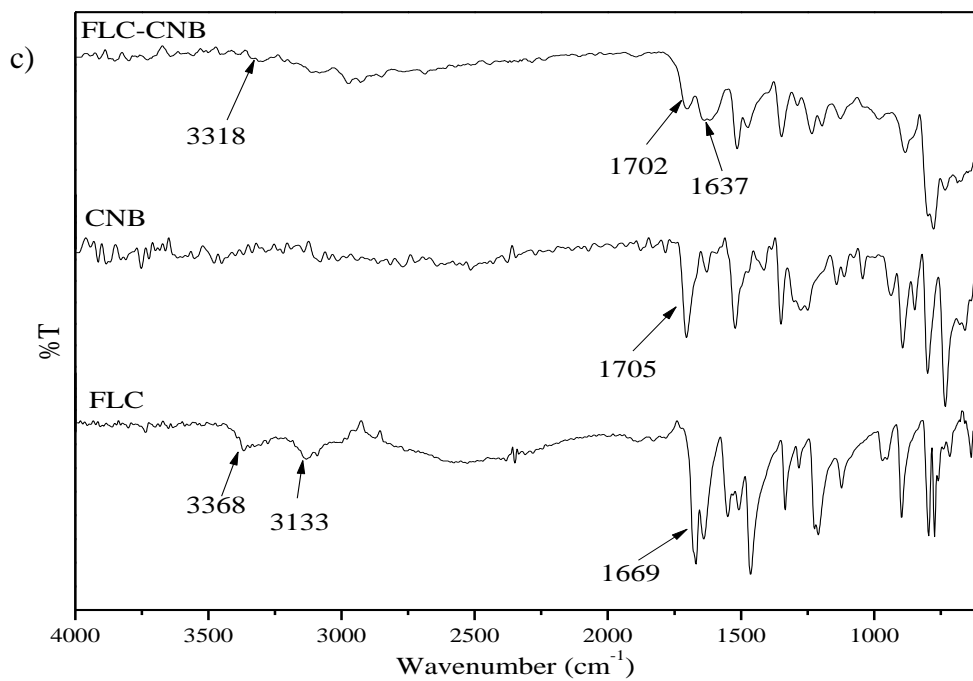
6.3.2 FT-IR spectroscopy

A clear-cut evidence for the formation of new crystalline material was observed at the initial stages of the experimentation by FT-IR spectroscopy. The changes in the stretching frequencies of the functional groups present in the FLC molecule and in the coformer molecule were observed in all the newly formed crystalline materials. The detailed comparison of stretching frequencies of various functional groups in the crystalline material are displayed in **Table 6.4**. The hydrolysis of ASP molecule in an aqueous medium during cocrystallization is clearly distinguishable in the IR spectrum, where the disappearance of the carbonyl stretching frequency corresponds to ester group of ASP was observed in the newly formed crystalline material. The FT-IR comparison spectra with respect to starting materials are shown in **Figure 6.15**.

Table 6.4: FT-IR Stretching frequencies of cocrystal/salt and starting materials.

API, coformer and cocrystal	-C=O stretch (amide) (cm ⁻¹)	-C=O stretch (acid) (cm ⁻¹)	-NH ₂ /-OH stretch (cm ⁻¹)
FLC	1669	-	3368, 3133
CNB	-	1705	-
2,5HBA	-	1667	3307
ASP	-	1749, 1679	-
3HBA	-	1679	3370
GLA	-	1684	-
FLC-3HBA	1627	1676	3412, 3135
FLC-2,5HBA	1659	1682	3432, 3237
FLC-CNB	1637	1702	3318
FLC-SAL	1694	1607	3251
FLC-GLA	1647	1684	3461,3079





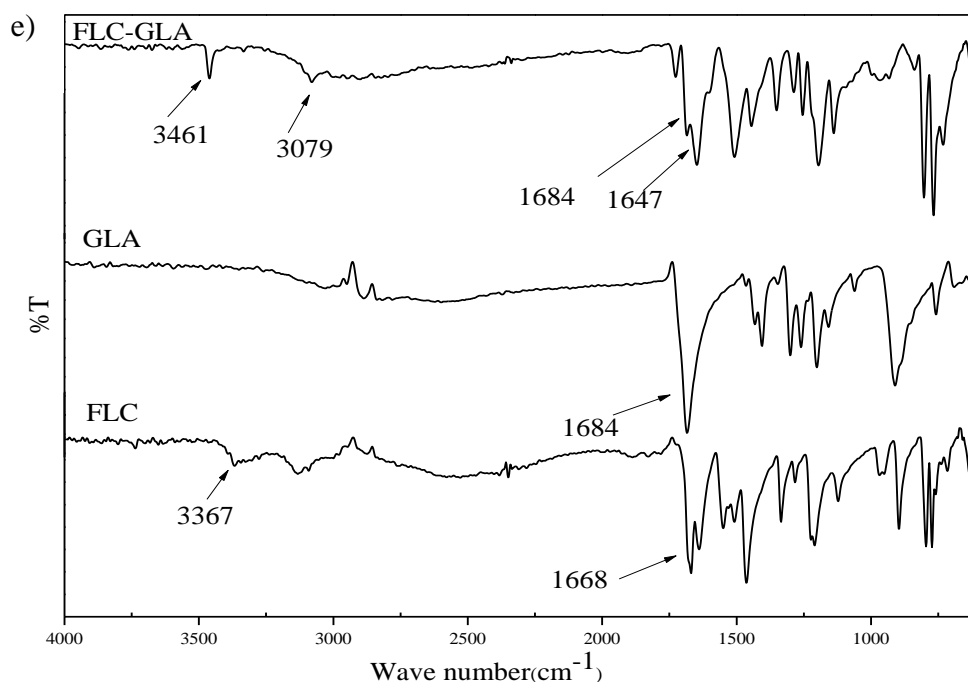


Figure 6.15: FT-IR spectra of FLC cocrystal/salt with starting materials: a) FLC-3HBA, b) FLC-2,5HBA, c) FLC-CNB, d) FLC-SAL, e) FLC-GLA.

6.3.3 DSC & POM analysis

DSC analysis was performed to determine the exact melting temperature of salt/cocrystals. Three of the synthesized cocrystals/salts melts exactly in between the melting temperature of FLC and cofomers. The cocrystal FLC-3HBA melts at a lower temperature when compared with FLC and 3HBA. The lower melting of FLC-3HBA is attributed to the presence of water molecule in the crystalline structure. A broad melting temperature was observed for this cocrystal hydrate. The broad melting temperature is probably due to the release of water molecule followed by the melting of the cocrystal. Off all these crystal structures, FLC-2,5HBA possess highest crystal density and therefore, the melting temperature found to be higher for this cocrystal. FLC-3HBA exhibits lowest crystal density and hence lower melting temperature. The melting temperature of FLC, cofomers, and the synthesized cocrystal/salt are shown in **Table 6.5**. The DSC thermogram is shown in **Figure 6.16**.

The images of the cocrystal/salt structure at different temperatures were captured using POM instrument to demonstrate the cocrystal stability. There was no

obvious phase change was observed for the cocrystal/salt during heating till the melting temperature. However, for FLC-3HBA cocrystal, phase change was observed at around 115 °C due to the removal of a water molecule from the crystal structure. The images of the synthesized cocrystal/salt are shown in **Figure 6.17**.

Table 6.5: Melting points of FLC, coformer, and the synthesized salt/cocrystal.

API Onset temperature (°C)	Coformer melting point (°C)	Cocrystal /salt	Onset temperature (°C)	Crystal density (g/cm ³)
FLC (302.85)	3HBA (196.40)	FLC-3HBA	116.69	1.503
	2,5HBA (204.5)	FLC-2,5HBA	243.69	1.639
	CNB (140.20)	FLC-CNB	204.81	1.565
	SAL (158.60)	FLC-SAL	226.16	1.557
	GLA (95.00)	FLC-GLA	198.75	1.558

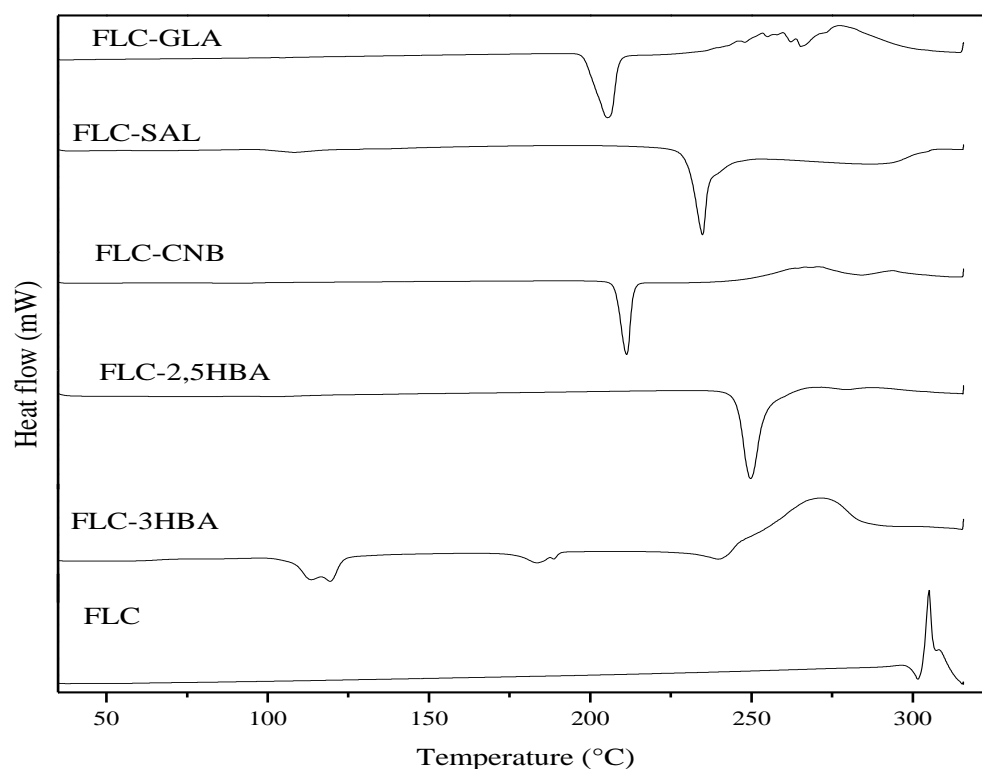


Figure 6.16: DSC thermograms of FLC and FLC salt/cocrystal.

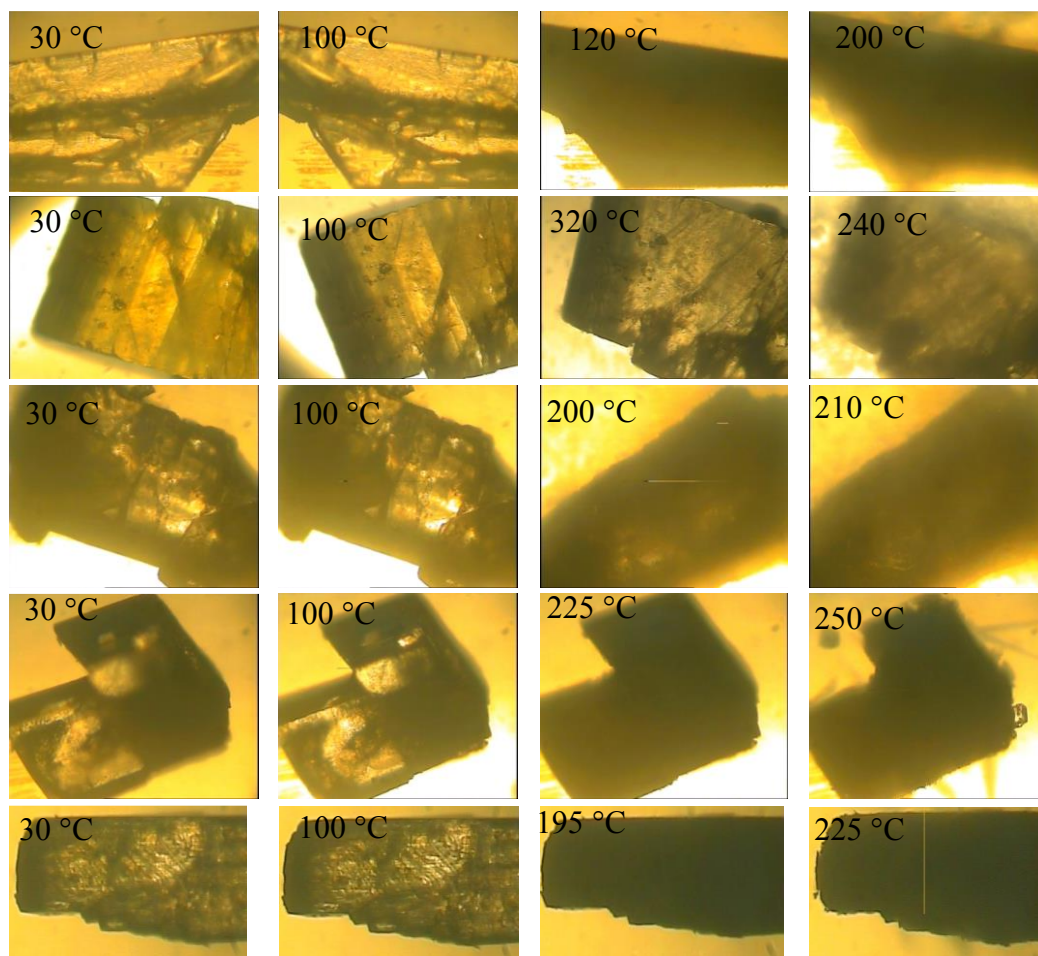


Figure 6.17: POM images of (1st row from top) FLC-3HBA, (2nd row) FLC-2,5HBA, (3rd row) FLC-CNB, (4th row) FLC-SAL, and (5th row) FLC-GLA at various temperature.

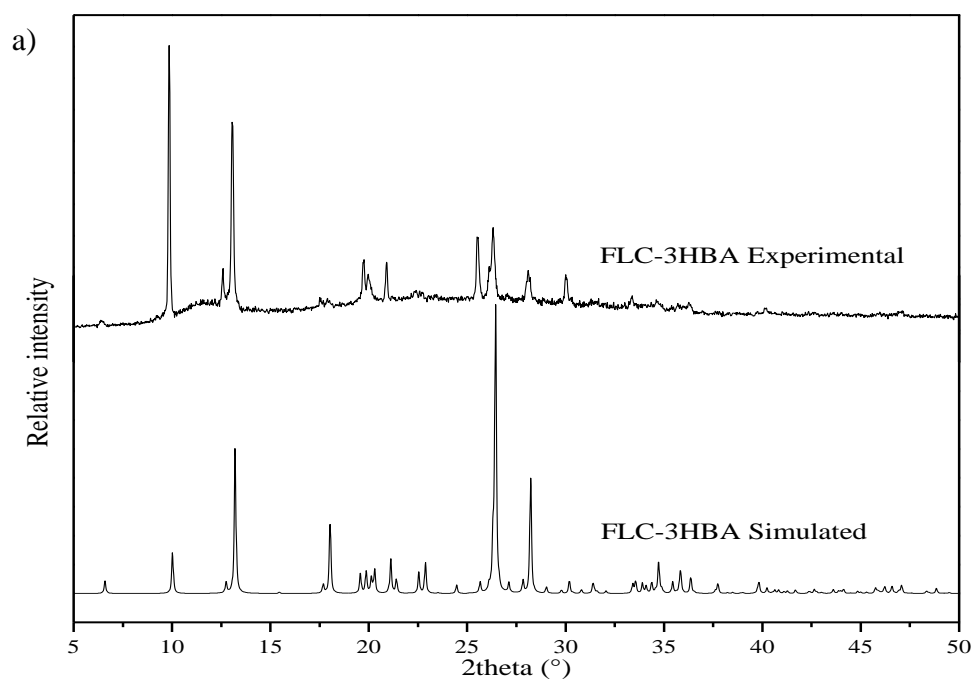
6.3.4 Structural comparison of synthesized salt/cocrystal

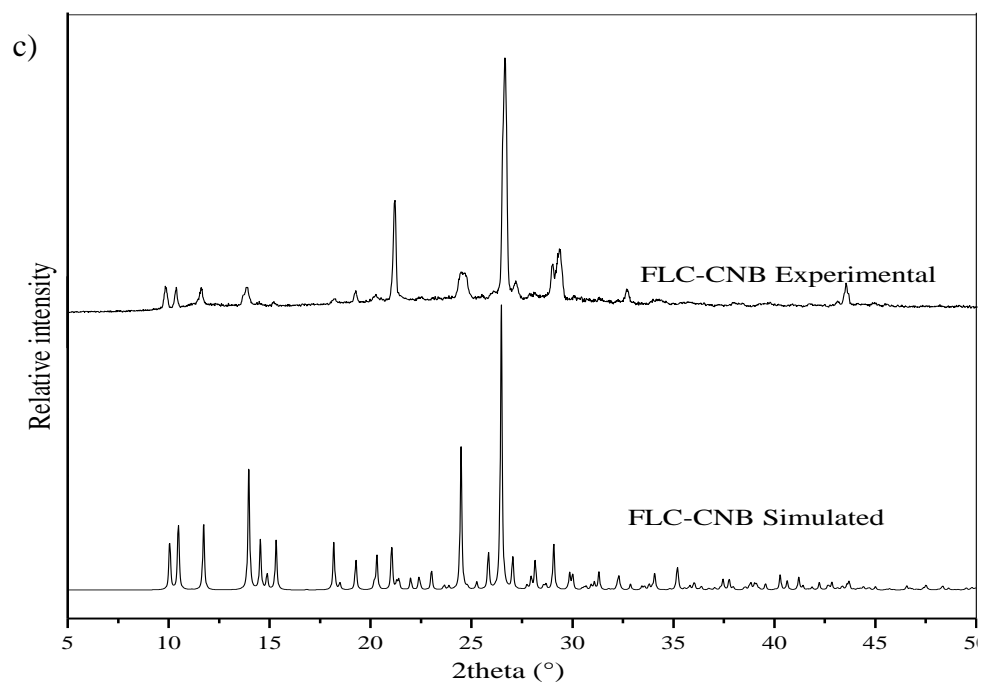
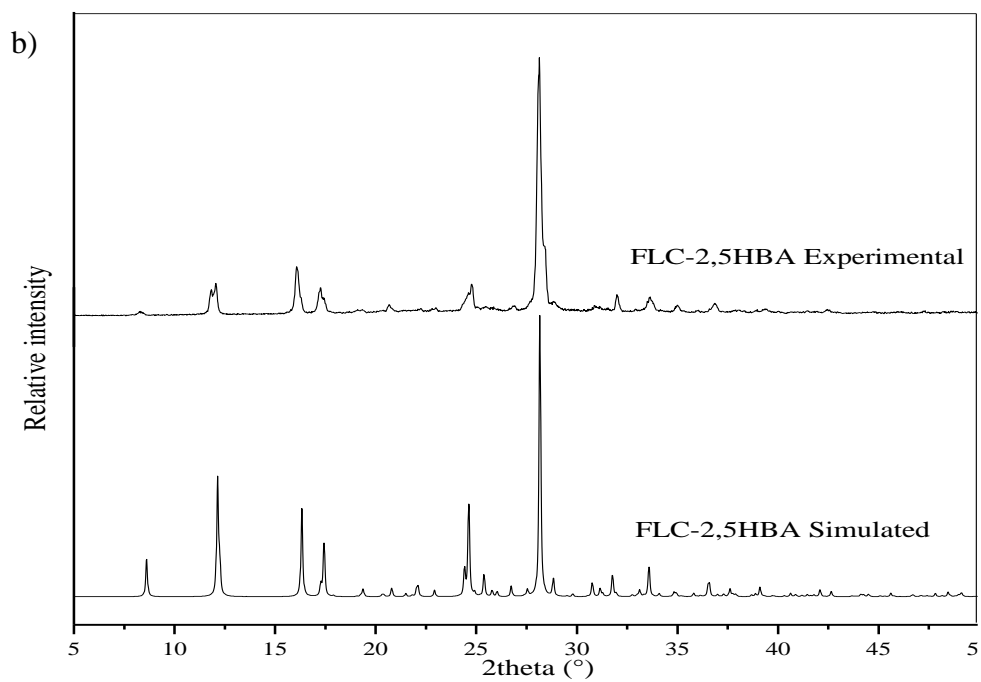
In all the crystal structures, except FLC-CNB, the primary supramolecular interactions involved acid-amide, acid-pyrimidine and acid-carbonyl heterosynthon between FLC and the coformer molecules. FLC-3HBA was crystallized as the monohydrate, due to this, two endothermic peaks observed for this cocrystal where initial endothermic peak corresponding to the release of a water molecule from the crystal lattice. Off all these crystal structures, crystal density was found to be higher for FLC-2,5HBA. This is probably due to the involvement of hydroxy group in intermolecular interactions with FLC molecule. When compared with the secondary interactions, except FLC-2,5HBA cocrystal, all the other crystal structures, utilized

weak C-H \cdots F hydrogen bond, whereas, FLC-2,5HBA stabilized via π - π interaction between FLC and 2,5HBA. FLC-CN \cdots B salt stabilized via O \cdots O chalcogen bond.

6.3.5 PXRD analysis

The PXRD analysis was performed in order to demonstrate the homogeneity of the synthesized salt/cocrystals. All the synthesized salt/cocrystals in the present work were found to be homogeneous by comparing the PXRD patterns of simulated and the experimentally determined PXRD patterns. The overlay of the experimental and simulated PXRD patterns of the synthesized salt/cocrystals are shown in **Figure 6.18**.





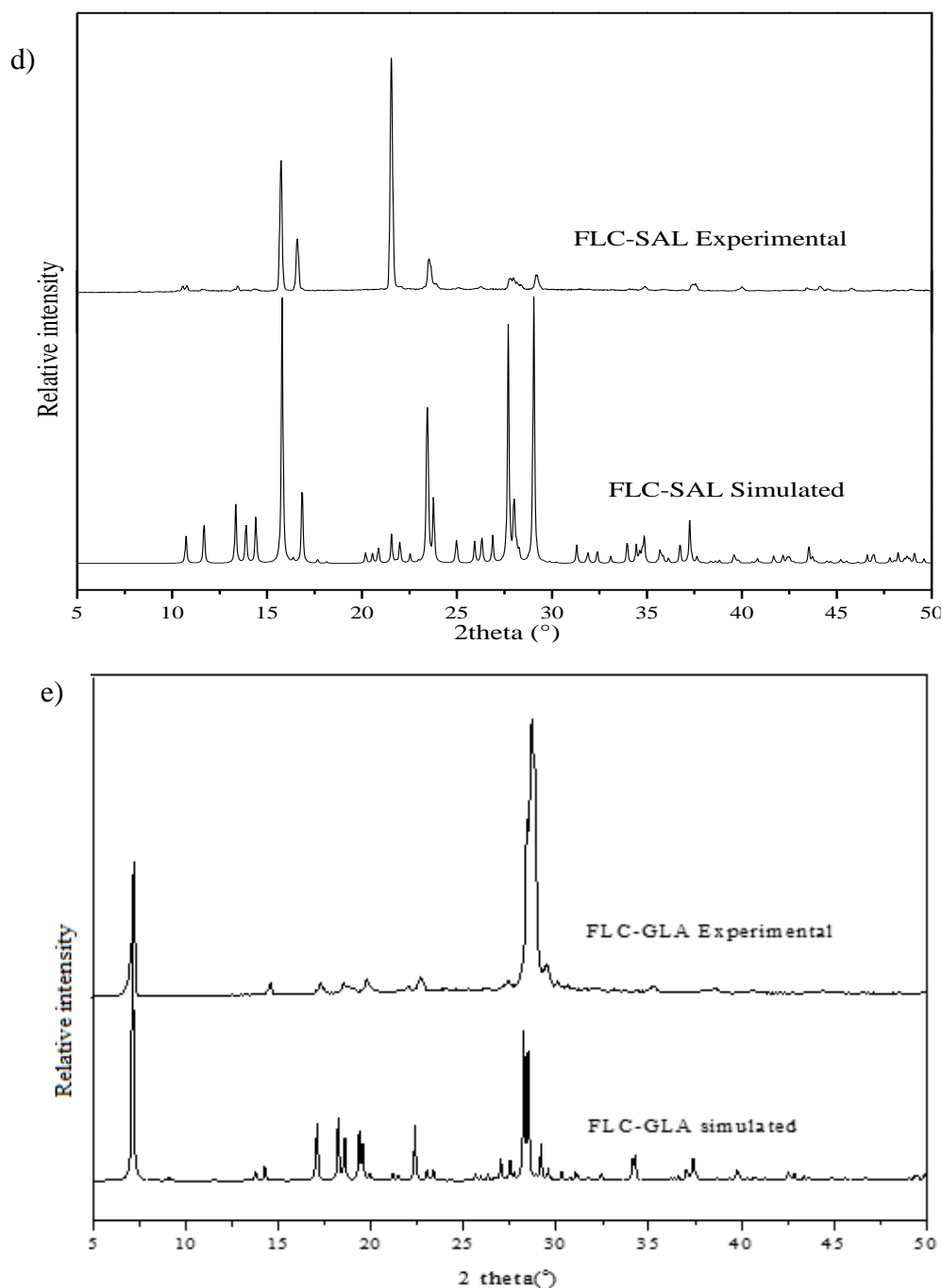


Figure 6.18: PXRD overlapping plots of simulated and experimental patterns: a) FLC-3HBA, b) FLC-2,5HBA, c) FLC-CNB, d) FLC-SAL, and e) FLC-GLA.

6.3.6 ^1H NMR spectroscopy

^1H NMR analysis confirmed molecular stoichiometry of the synthesized salt/cocrystals and it further substantiated the results obtained from the SC-XRD

analysis. The spectral details of the cocrystals are depicted below. The ^1H NMR spectrum of salt/cocrystals is shown in **Figure 6.19**.

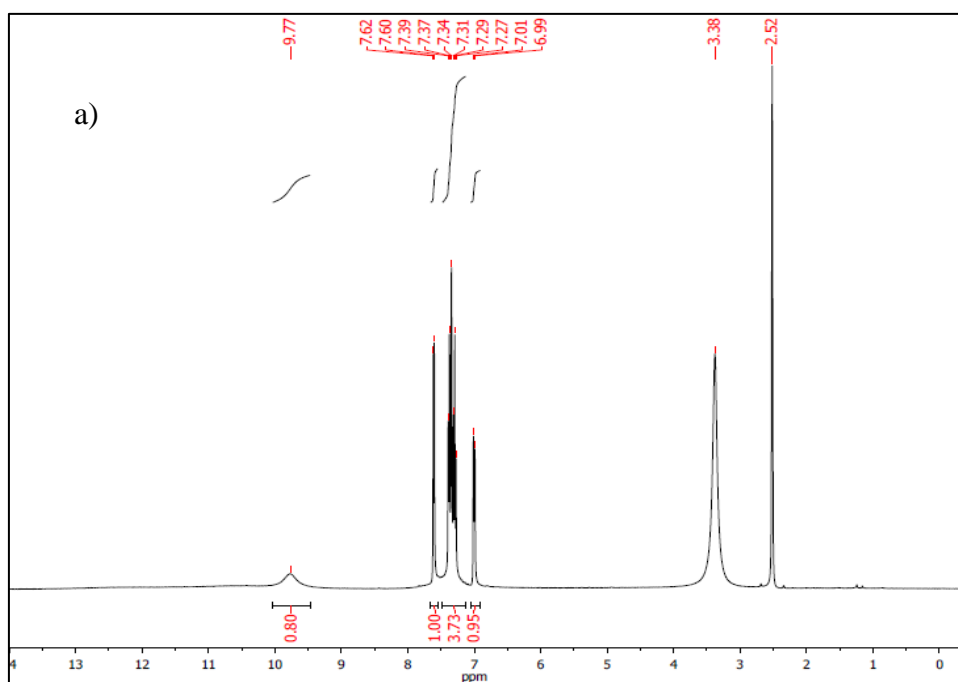
FLC-3HBA (400 MHz, DMO-d_6): δ ppm- 9.77 (1H, s), 7.62-7.60 (1H, d ($J=8$ Hz)), 7.39-7.27 (4H, m), 7.01-6.99 (1H, d ($J=8$ Hz)).

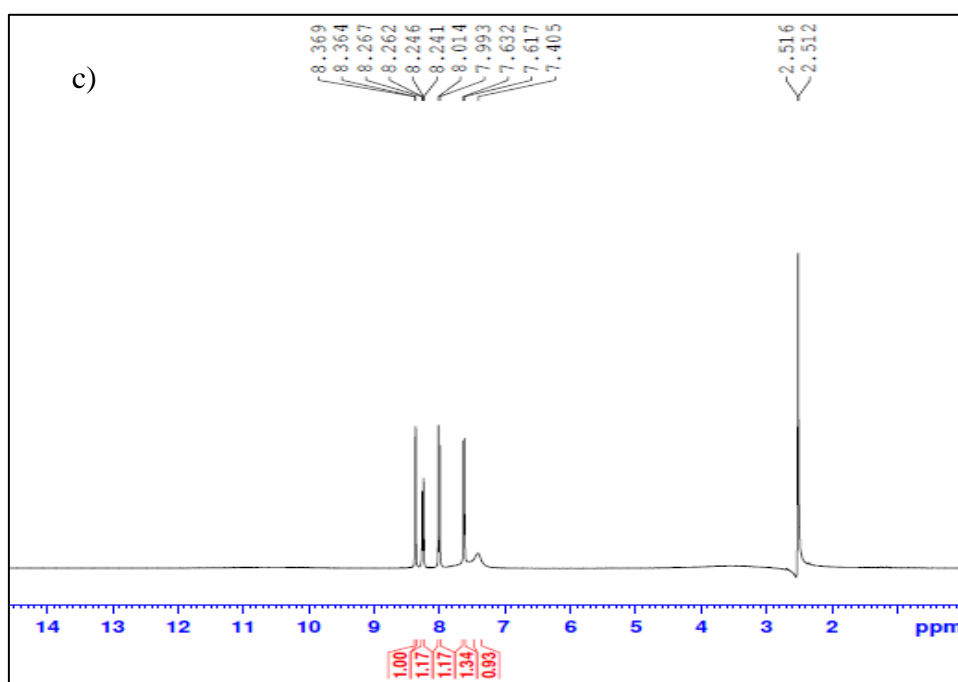
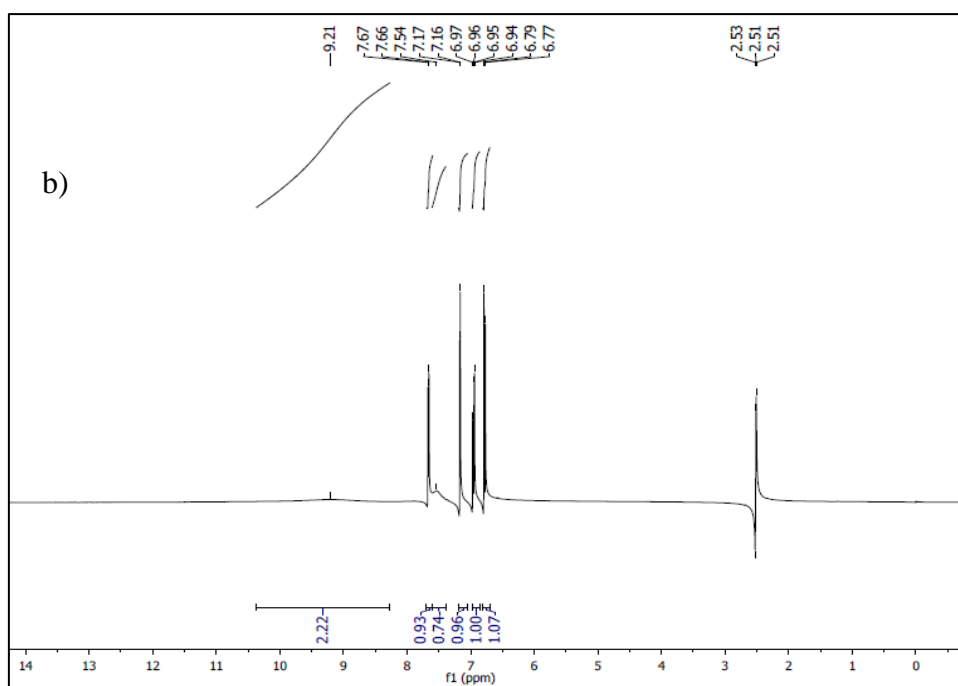
FLC-2,5HBA (400 MHz, DMSO-d_6): δ ppm-9.212 (2H, s), 7.672-7.656 (1H, d ($J=6.4$ Hz)), 7.54 (1H, s), 7.164-7.171 (1H, d ($J=2.8$ Hz)), 6.969-6.939 (1H, dd ($J=3.2$ Hz)), 6.7916.769 (1H, d ($J=8.8$ Hz)).

FLC-CNB (400 MHz, DMO-d_6) δ ppm- 8.37-8.36 (1H, d ($J=4$ Hz)), 8.27-8.24 (1H, dd ($J=4$ Hz)), 8.01-7.99 (1H, d ($J=8$ Hz)), 7.63-72 (1H, d ($J=4$ Hz)), 7.41 (1H, s).

FLC-SAL (400 MHz, DMO-d_6) δ ppm- 7.81-7.79 (1H, d ($J=8$ Hz)), 7.67-7.65 (1H, d ($J=8$ Hz)), 7.52-7.48 (1H, t ($J=8$ Hz)), 6.95-6.90 (2H, m).

FLC-GLA (400 MHz, DMSO-d_6): δ ppm-12.02 (1H, s), 10.36 (1H, m), 7.597-7.582 (2H, d ($J=6$ Hz)), 7.325 (2H, s), 2.257-2.221 (4H, t ($J=7.2$ Hz)), 1.733-1.659 (2H, q ($J=7.2$ Hz)).





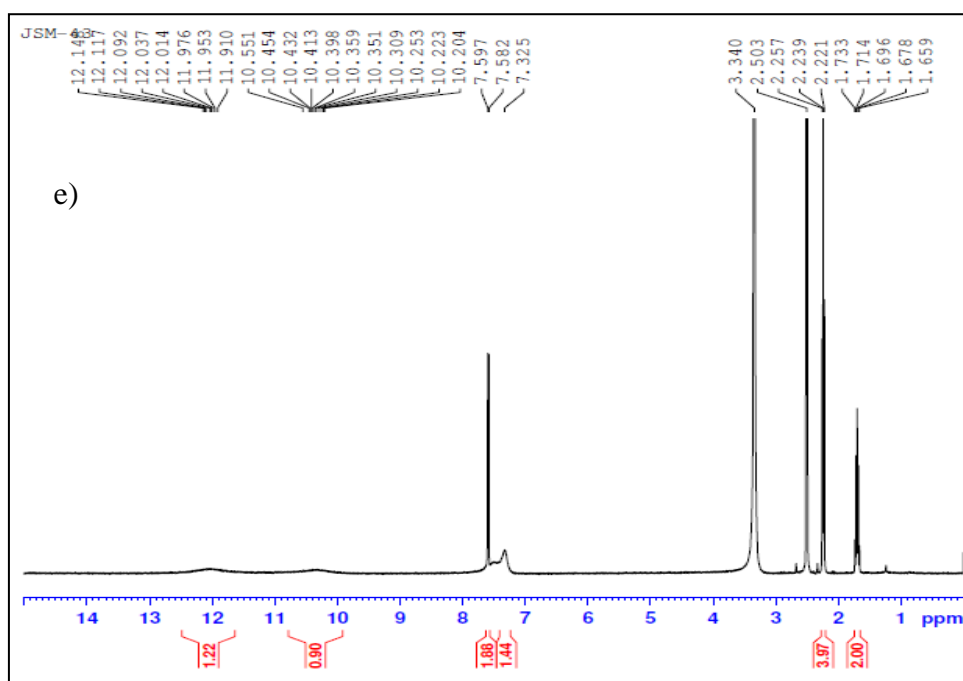
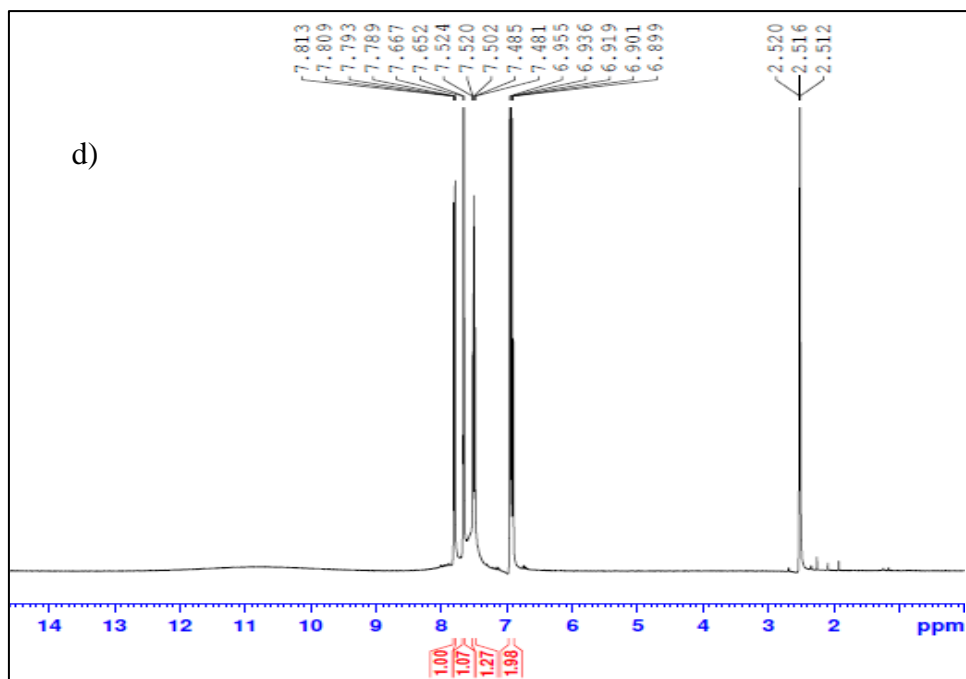


Figure 6.19: ^1H NMR spectra of FLC salt/cocrystals: s) FLC-3HBA, b) FLC-2,5HBA, c) FLC-CNB, d) FLC-SAL, and e) FLC-GLA.

6.3.7 Stability study

Since, the FLC molecule is found to be highly hygroscopic in nature, our present work focused on the stability of synthesized salt/cocrystal at accelerated conditions. Stability study of all the salt/cocrystals were performed in accelerated humid condition (90-95% Relative Humidity (RH)) at room temperature by conventional weight loss method. All the cocrystals/salt were kept in a desiccator which was filled with a saturated solution of potassium nitrate in order to maintain the humidity of 90-95% RH for a period of seven days. The weight of the samples under study was monitored regularly (every 12 hours), and at the end of the experiment, hygroscopicity is measured by TGA analysis. It was observed that FLC-2,5HBA and FLC-GLA cocrystal were found to be non-hygroscopic at ~90-95% RH conditions, and FLC-CNB & FLC-SAL were found to be moderately hygroscopic where the weight loss was found to be about ~-0.35% between 40-120 °C. FLC-3HBA was found to be hygroscopic with about 6% weight loss between 40-120 °C (**Table 6.6**). However, when compared with FLC alone, these cocrystal/salt exhibits superior solid state stability at accelerated humidity conditions. TGA plots are shown in **Figure 6.20**. In the literature report, only three salts of FLC were found which exhibited superior solid state stability. Salts such as HCl, saccharine, and acesulfame were found to be non-hygroscopic at accelerated conditions (0-90% RH), which boosts the possibility of preparing new solid forms of FLC API with improved stability. Similarly, the hygroscopicity study in the present work exhibited superior solid state stability at accelerated conditions. The salt/cocrystal namely FLC-2,5HBA, FLC-CNB, FLC-SAL, and FLC-GLA offers not only for the development for the new drug product but also for the development of a new drug-drug product with better stability which may overcome the disadvantage of FLC drug due to hydration.

Table 6.6: Percentage weight loss between 40 to 120 °C in the salt/cocrystal of FLC at 70-75% RH and at 90-95% RH.

Crystal forms	% wt. loss (between 40-120 °C) at 90-95% RH
FLC	-14.98
FLC-3HBA	-6.46
FLC-2,5HBA	0
FLC-CNB	-0.347
FLC- SAL	-0.380
FLC-GLA	-0.0351

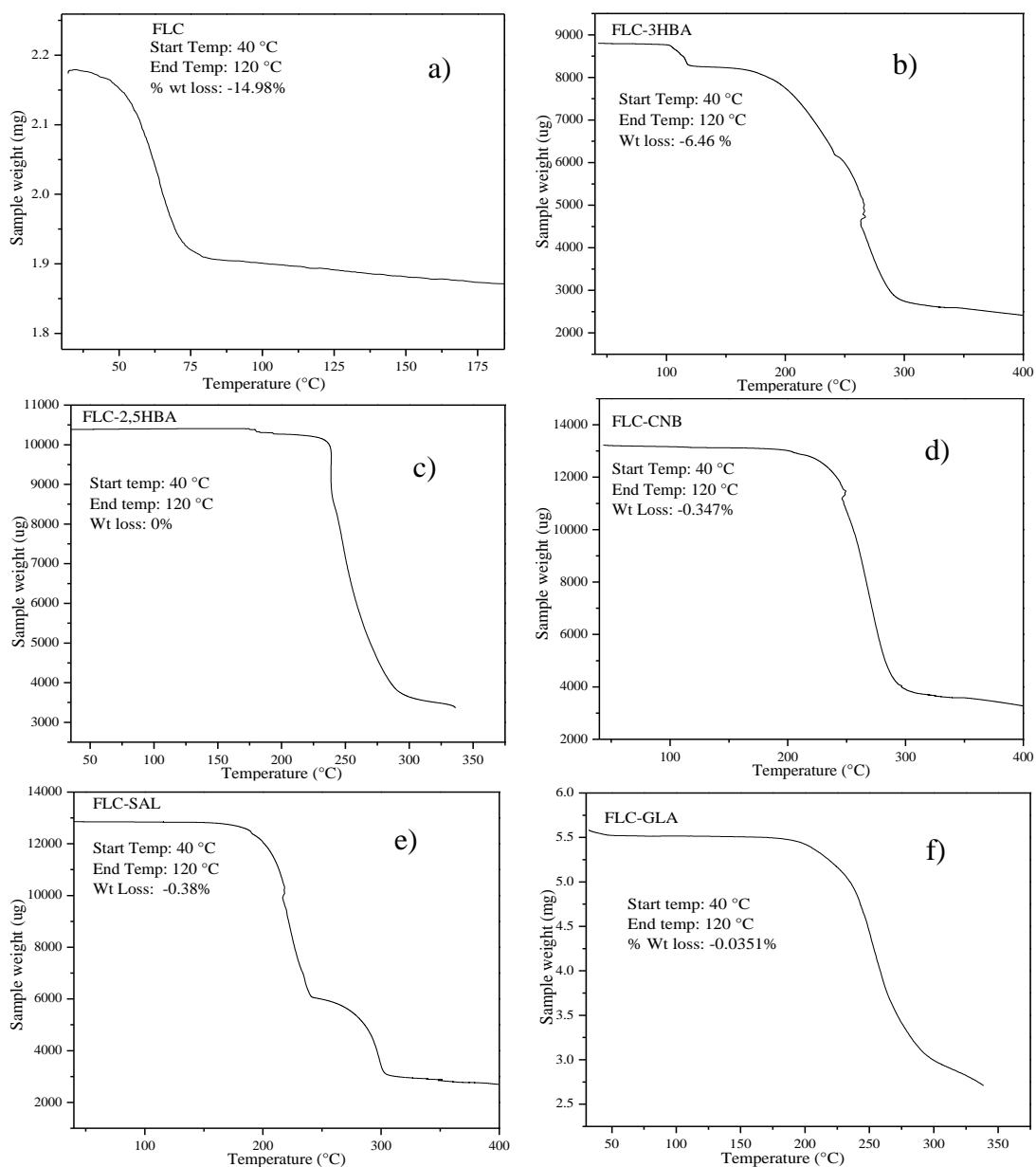


Figure 6.20: TGA plots of FLC and the FLC cocystal/salt: a) FLC, b) FLC-3HBA, c) FLC-2,5HBA, d) FLC-CNB, and e) FLC-SAL, and f) FLC-GLA.

6.4 CONCLUSIONS

In conclusion, five molecular salt/cocystals of anti-fungal drug flucytosine were synthesized by a solvent evaporation method, and the crystal structures were determined by SC-XRD analysis. FLC-3HBA was crystallized as a monohydrate. CocrySTALLIZATION with ASP in aqueous medium resulted in the hydrolysis of ester group of ASP, and a new salt of FLC-SAL obtained in the crystallization experiment.

Hygroscopicity study at accelerated humidity condition showed that the synthesized cocrystal/salt are stable towards hydration even at ~90-95% RH condition at room temperature, except FLC-3HBA cocrystal. Therefore, the salt/cocrystal namely, FLC-2,5HBA, FLC-CNB, and FLC-SAL are a better candidate for the development of new drug-drug products, and the cocrystal namely FLC-GLA is an alternate option for the development of new drug product of FLC with improved stability.

CHAPTER 7

SUMMARY AND CONCLUSIONS

This Chapter briefly explains the summary and conclusions drawn from the present research work.

7.1 SUMMARY OF PRESENT WORK

Owing to the poor aqueous solubility of some of the commercial drug products, the usage of the drug products in the market are limited. In this context, “Pharmaceutical cocrystal” finds its application. Pharmaceutical cocrystal is an alternate pathway for the modification of physicochemical properties of the drug ingredients without affecting its biological activity. Traditionally, the salt formation was the only known method to modify the physicochemical properties of the active drug ingredients, later, the method of Cocrystallization was introduced. Cocrystallization techniques can be employed for the drug molecule which does not possess any ionization site. The formation of salt or cocrystal can be predicted based on the pKa thumb rule. i.e., if the difference in the pKa value (pKa base-pKa acid), (ΔpK_a) < -1 , then there will not be any proton transfer, the resultant component will be a cocrystal. If the $\Delta pK_a > 4$, there will be a complete proton transfer results in the formation of molecular salts. The region in between -1 to 4 is the salt/cocrystal continuum.

The field of crystal engineering in last two decades has gained a lot of attention from pharmaceutical scientists due to its application in pharmaceutical cocrystal. The cocrystallization experiments of BCS Class II or Class IV drugs with water-soluble GRAS cofomers have shown a tremendous increment in water solubility of poorly soluble drug molecules. In order to improve the solubility and dissolution profile of a poorly water-soluble drug molecule, highly water-soluble cofomer have to be chosen for the cocrystallization technique. Further, literature reports show that pharmaceutical cocrystallization can result in the increase of the stability of drug molecule. Furthermore, multidrug cocrystal preparation is an added advantage, where, two drug molecules can be administrated in a single dosage form.

Owing to the above merits of pharmaceutical cocrystals, a series of few active drug ingredients have been chosen with poor or high aqueous solubility and screened for salt/cocrystallization with GRAS and non-GRAS substances. The physicochemical

properties such as solubility and stability are evaluated and compared the results with parent APIs. The overall research work can be summarized as,

- ❖ A series of active pharmaceutical ingredients was chosen, which was having low and high aqueous solubility. The active ingredients chosen were anti-inflammatory drug (flufenamic acid, mefenamic acid, tolfenamic acid, naproxen, and ethenzamide), anti-viral drug (2-chloro-4-nitrobenzoic acid), anti-tuberculosis drug (ethionamide), anti-fibrinolytic hemostatic drug (tranexamic acid), and anti-fungal drug (flucytosine). All the synthesized salt/cocrystal structures were determined by SC-XRD techniques and were further characterized by spectroscopic (^1H NMR, UV-Vis, and FT-IR), Thermal (DSC, POM, and TGA), and PXRD techniques.
- ❖ The solubility study was performed for the cocrystal/salt of flufenamic acid, ethenzamide, 2-chloro-4-nitrobenzoic acid, and ethionamide in both aqueous and 0.1 N HCl medium. The results were compared with parent APIs.
- ❖ Stability study (long-term stability and hygroscopicity) was carried out for most of the synthesized cocrystal/salt. Due to the instability of flucytosine drug ingredients towards hydration, hygroscopicity study was performed for the synthesized salt/cocrystal at accelerated humidity condition (~90-95% RH, 25 °C). All the obtained results were compared with parent API.
- ❖ Isostructurality of the molecular salt was deduced in the case of salts of tranexamic acid, mefenamic acid, and tolfenamic acid based on the isostructurality parameters π and ε .
- ❖ Conformational analysis of the synthesized molecular salts was carried out in the case of ethionamide, mefenamic acid, tolfenamic acid, and naproxen.
- ❖ DFT calculations were performed for molecular salt/cocrystal of tranexamic acid to better demonstrate the molecular structure and to support crystal structures determined from the SC-XRD analysis.

7.2 CONCLUSIONS

The following conclusion has been deduced from each working chapter based on the experimental results.

- ❖ Four novel pharmaceutical cocrystals, namely FFA-CNB, FFA-ETZ, ETZ-SNP, and CNB-SNP were reported. The solubility and stability associated with the cocrystals were studied. The increment in the solubility of FFA was observed in the cocrystals in both purified water and 0.1 N HCl solution. No improvement in the solubility was observed for ETZ and CNB in the cocrystal with SNP.
- ❖ Four molecular salts of anti-tuberculosis drug ETH, namely ETH-CNB, ETH-2,3HBA, ETH-2,6HBA, and ETH-DNB were reported. It was observed that the solubility of ETH in these salts follow the order of ETH-CNB>ETH-2,6HBA>ETH-2,3HBA>ETH in purified water. However, no increment in the solubility of these salts in 0.1N HCl solution was observed.
- ❖ A series of six molecular salts of three different APIs were reported with different pyridyl derivatives namely, MFA-4AP, MFA-DMAP, TFA-4AP, TFA-DMAP, NPX-4AP, and NPX-2AP. In the crystal structure, 4AP salts of MFA and TFA, DMAP salts of MFA and TFA were found to be isostructural based on the isostructural parameters π and ϵ . The 4AP salts of all the three APIs were found to be stable for a time period of six months at ambient temperature.
- ❖ Nine molecular salts and two cocrystals of an antifibrinolytic hemostatic drug TXA were synthesized and their crystal structures were studied using SC-XRD technique. DFT calculation study supported the newly formed crystalline adducts based on interaction energy. All the synthesized salt/cocrystals were found to be stable for about six months at ambient conditions.
- ❖ Five molecular salt/cocrystal of anti-fungal drug FLC with GRAS cofomers such as FLC-3HBA, FLC-2,5HBA, FLC-CNB, FLC-SAL, and FLC-GLA were reported. The hygroscopicity study of the molecules was done at accelerated conditions. All the synthesized salt/cocrystal exhibited superior solid-state stability at accelerated conditions when compared with FLC alone.

7.3 SCOPE FOR FUTURE WORK

Pharmaceutical cocrystallization is an alternate pathway for the improvement of physicochemical properties of APIs. The synthesized salt/cocrystal in the present work can be of greater benefits in the future for the development of new drug products including drug-drug products. Further, the dissolution study in both water and 0.1 N

HCl solution, in-vitro, and in-vivo study of the synthesized cocrystals can give a clear idea about the possibility of development of new drug products with improved physicochemical properties. Furthermore, these APIs can be used for salt/cocrystallization experiments with water-soluble cofomers including amino acids and also with other drug ingredients to explore the possibility of new drug products with enhanced properties.

CHAPTER 8

REFERENCES

- Aakeroy, C. B. and Seddon, K.R. (1993). "The hydrogen bond and Crystal engineering." *Chem. Soc. Rev.*, 22, 397-407.
- Aakeroy, C.B. (1997). "Crystal engineering: strategies and architectures." *Acta Cryst.*, B53, 569-586.
- Abourahma, H., Cocuzza, D. S., Melendez, J. and Urban, J. M. (2011). Pyrazinamide cocrystals and the search for polymorphs. *CrystEngComm*, 13 (21), 6442-6450.
- Adalder, T. K., Sankolli, R. and Dastidar, P. (2012). "Homo-or heterosynthon? A crystallographic study on a series of new cocrystals derived from pyrazinecarboxamide and various carboxylic acids equipped with additional hydrogen bonding sites." *Cryst. Growth Des.*, 12 (5), 2533-2542.
- Ahmed, H., Shimpi, M. R. and Velaga, S. P. (2017). "Relationship between mechanical properties and crystal structure in cocrystals and salt of paracetamol." *Drug Dev. Ind. Pharm.*, 43 (1), 89-97.
- Aitipamula, S. and Vangala, V. R. (2017). "X-Ray Crystallography and its Role in Understanding the Physicochemical Properties of Pharmaceutical Cocrystals." *J. Indian Inst. Sci.*, 1-17.
- Aitipamula, S., Banerjee, R., Bansal, A. K., Biradha, K., Cheney, M. L., Choudhury, A. R., ... and Ghogale, P. P. (2012). "Polymorphs, salts, and cocrystals: What's in a name?." *Cryst. Growth Des.*, 12 (5), 2147-2152.
- Aitipamula, S., Chow, P. S. and Tan, R. B. (2009). "Trimorphs of a pharmaceutical cocrystal involving two active pharmaceutical ingredients: potential relevance to combination drugs." *CrystEngComm*, 11, 1823-1827.
- Aitipamula, S., Chow, P. S. and Tan, R. B. (2009). "Dimorphs of a 1: 1 cocrystal of ethenzamide and saccharin: solid-state grinding methods result in metastable polymorph." *CrystEngComm*, 11 (5), 889-895.

Aitipamula, S., Chow, P. S. and Tan, R. B. (2010). “Conformational and enantiotropic polymorphism of a 1: 1 cocrystal involving ethenzamide and ethylmalonic acid.” *CrystEngComm*, 12 (11), 3691-3697.

Aitipamula, S., Chow, P. S. and Tan, R. B. (2010). “Polymorphs and solvates of a cocrystal involving an analgesic drug, ethenzamide, and 3, 5-dinitrobenzoic acid.” *Cryst. Growth Des.*, 10 (5), 2229-2238.

Aitipamula, S., Wong, A. B., Chow, P. S. and Tan, R. B. (2014). “Cocrystallization with flufenamic acid: comparison of physicochemical properties of two pharmaceutical cocrystals.” *CrystEngComm*, 16, 5793-5801.

Aitipamula, S., Wong, A. B., Chow, P. S. and Tan, R. B. (2012). “Pharmaceutical cocrystals of ethenzamide: structural, solubility and dissolution studies.” *CrystEngComm*, 14 (24), 8515-8524.

Almansa, C., Mercè, R., Tesson, N., Farran, J., Tomàs, J. and Plata-Salamán, C. R. (2017). “Co-crystal of Tramadol Hydrochloride–Celecoxib (ctc): A Novel API-API Co-crystal for the Treatment of Pain.” *Cryst. Growth Des.*, 17 (4), 1884-1892.

Alshryda, S., Sarda, P., Sukeik, M., Nargol, A., Blenkinsopp, J. and Mason, J.M. (2011). “Tranexamic acid in total knee replacement.” *J. Bone Jt. Surg., Br.*, 93, 1577-1585.

Ando, S., Kikuchi, J., Fujimura, Y., Ida, Y., Higashi, K., Moribe, K. and Yamamoto, K. (2012). “Physicochemical characterization and structural evaluation of a specific 2: 1 cocrystal of naproxen–nicotinamide.” *J. Pharm. Sci.*, 101, 3214-3221.

André, V., Fernandes, A., Santos, P. P. and Duarte, M. T. (2011). “On the track of new multicomponent gabapentin crystal forms: synthon competition and pH stability.” *Cryst. Growth Des.*, 11, 2325-2334.

Aoki, S., Mizutani, T. and Danjo, K. (2000). “Studies on the number of contacts between ibuprofen and Ethenzamide using thermal analysis.” *Chem. Pharm. Bull.*, 48, 140-141.

- Ayuko, W. O., Kinchington, D. and Ng, T. (1997). "Agonists in the costimulation of tcr/cd3-induced t-lymphocytes." 81 PIXXD2 WO 9734593 A1.
- Badhani, B., Sharma, N. and Kakkar, R. (2015). "Gallic acid: a versatile antioxidant with promising therapeutic and industrial applications." *RSC Advances*, 5, 27540-27557.
- Bag, P. P., Ghosh, S., Khan, H., Devarapalli, R. and Reddy, C. M. (2014). "Drug–drug salt forms of ciprofloxacin with diflunisal and indoprofen." *CrystEngComm*, 16, 7393-7396.
- Barsky, I., Bernstein, J., Stephens, P. W. and Stone, K. H. (2008). "The study of the polymorphic system of 2-chloro-4-nitrobenzoic acid." *New J. Chem.*, 32, 1747-1753.
- Beatty, A.M. (2003). "Open-framework coordination complexes from hydrogen-bonded networks: toward host/guest complexes." *Coord. Chem. Rev.*, 246, 131-143.
- Benny, P. J., Shibumon, G., Sunny, K. and Cincy, G. (2010). "2, 3-dihydroxybenzoic acid: an effective antifungal agent isolated from Flacourtia inermis fruit." *Int. J. Chem. Pharm. Res.*, 2, 101-105.
- Bernhardson, D., Brandt, T. A., Hulford, C. A., Lehner, R. S., Preston, B. R., Price, K., ... and Thuma, B. (2014). "Development of an early-phase bulk enabling route to sodium-dependent glucose cotransporter 2 inhibitor ertugliflozin." *Org. Process Res. Dev.*, 18 (1), 57-65.
- Bhatt, P. M., Azim, Y., Thakur, T. S. and Desiraju, G. R. (2008). "Cocrystals of the anti-HIV drugs lamivudine and zidovudine." *Cryst. Growth Des.*, 9, 951-957.
- Bhosale, S., Sisson, A.L., Talukdar, P., Fürstenberg, A., Banerji, N., Vauthey, E., Bollot, G., Mareda, J., Röger, C., Würthner, F. and Sakai, N. (2006). "Photoproduction of proton gradients with π -stacked fluorophore scaffolds in lipid bilayers." *Science*, 313, 84-86.

- Bi, W., Louvain, N., Mercier, N., Luc, J. and Sahraoui, B. (2007). "Type structure, which is composed of organic diammonium, triiodide and hexaiodobismuthate, varies according to different structures of incorporated cations." *CrystEngComm*, 9, 298-303.
- Bian, S., Doh, H. J., Zheng, J., Kim, J. S., Lee, C. H. and Kim, D. D. (2003). "In vitro evaluation of patch formulations for topical delivery of gentisic acid in rats." *Eur. J. Pharm. Sci.*, 18 (2), 141-147.
- Biradha, K., Su, C. Y. and Vittal, J. J. (2011). "Recent developments in crystal engineering." *Cryst. Growth Des.*, 11 (4), 875-886.
- Bis, J. A., Vishweshwar, P., Weyna, D. and Zaworotko, M. J. (2007). "Hierarchy of supramolecular synthons: Persistent hydroxy pyridine hydrogen bonds in cocrystals that contain a cyano acceptor." *Mol. Pharm.*, 4, 401-416.
- Callahan, J. C., Cleary, G. W., Elefant, M., Kaplan, G., Kensler, T. and Nash, R. A. (1982). "Equilibrium moisture content of pharmaceutical excipients." *Drug Dev. Ind. Pharm.*, 8, 355-369.
- Chadha, K., Karan, M., Chadha, R., Bhalla, Y. and Vasisht, K. (2017). "Is failure of cocrystallization actually a failure? Eutectic formation in cocrystal screening of hesperetin." *J. Pharm. Sci.* 106, 2026–2036.
- Chadha, R., Rani, D. and Goyal, P. (2017). "Supramolecular Cocrystals of Gliclazide: Synthesis, Characterization and Evaluation." *Pharm. Res.*, 34 (3), 552-563.
- Cheney, M. L., McManus, G. J., Perman, J. A., Wang, Z. and Zaworotko, M. J. (2007). "The role of cocrystals in solid-state synthesis: cocrystal-controlled solid-state synthesis of imides." *Cryst. Growth Des.*, 7 (4), 616-617.
- Cheney, M. L., Weyna, D. R., Shan, N., Hanna, M., Wojtas, L. and Zaworotko, M. J. (2011). "Cofomer selection in pharmaceutical cocrystal development: a case study of a meloxicam aspirin cocrystal that exhibits enhanced solubility and pharmacokinetics." *J. Pharm. Sci.*, 100, 2172-2181.

- Cherukuvada, S., Bolla, G., Sikligar, K. and Nangia, A. (2013). "4-Aminosalicylic acid adducts." *Cryst. Growth Des.*, 13, 1551-1557.
- Cherukuvada, S., Kaur, R. and Row, T. N. G. (2016). "Co-crystallization and small molecule crystal form diversity: from pharmaceutical to materials applications." *CrystEngComm*, 18 (44), 8528-8555.
- Childs, S. L., Stahly, G. P. and Park, A. (2007). "The salt-cocystal continuum: the influence of crystal structure on ionization state." *Mol. Pharm.*, 4, 323-338.
- Choudhary, M. I., Naheed, N., Abbaskhan, A., Musharraf, S. G. and Siddiqui, H. (2008). "Phenolic and other constituents of fresh water fern *Salvinia molesta*." *Phytochemistry*, 69, 1018-1023.
- Colleter, J. C. and Gadret, M. (1968). "Crystalline structure of antitubercular compounds. I. Crystalline structure of the hydrochloride of ethionamide." *Acta Crystallogr., Sect. B: Struct. Crystallogr. Cryst. Chem.*, 24, 513-519.
- Colleter, J. C. and Gadret, M. (1968). "Structure cristalline de composés antituberculeux. II. Structure cristalline du bromhydrate d'éthionamide. Comparaison avec celle du chlorhydrate d'éthionamide." *Acta Crystallogr., Sect. B: Struct. Crystallogr. Cryst. Chem.*, 24, 519-525.
- Cruz-Cabeza, A. J. (2012). "Acid–base crystalline complexes and the p K a rule." *CrystEngComm*, 14, 6362-6365.
- Cynamon, M. H. and Sklaney, M. (2003). "Gatifloxacin and ethionamide as the foundation for therapy of tuberculosis." *Antimicrob. Agents Chemother.*, 47, 2442-2444.
- da Silva, C. C., de Oliveira, R., Tenorio, J. C., Honorato, S. B., Ayala, A. P. and Ellena, J. (2013). "The continuum in 5-fluorocytosine. Toward salt formation." *Cryst. Growth Des.*, 13 (10), 4315-4322.

- da Silva, C. C., Pepino, R. D. O., de Melo, C. C., Tenorio, J. C. and Ellena, J. (2014). "Controlled Synthesis of New 5-Fluorocytosine Cocrystals Based on the p K a Rule." *Cryst. Growth Des.*, 14 (9), 4383-4393.
- Dai, X. L., Li, S., Chen, J. M. and Lu, T. B. (2016). "Improving the membrane permeability of 5-fluorouracil via cocrystallization." *Cryst. Growth Des.*, 16 (8), 4430-4438.
- Das, B. and Srivastava, H. K. (2017). "Influence of Local Chemical Environment in Formation of Multicomponent Crystals of L-Tryptophan with N-Heterocyclic Carboxylic Acids: Unusual Formation of Double Zwitterions." *Cryst. Growth Des.*, 17, 3796–3805.
- de Melo, C. C., da Silva, C. C., Pereira, C. C., Rosa, P. C. and Ellena, J. (2016). "Mechanochemistry applied to reformulation and scale-up production of Ethionamide: salt selection and solubility enhancement." *Eur. J. Pharm. Sci.*, 81, 149-156.
- de Melo, C. C., de Sousa Carvalho, P., Diniz, L. F., D'Vries, R. F., Ayala, A. P. and Ellena, J. (2016). "Supramolecular synthesis and thermochemical investigations of pharmaceutical inorganic isoniazid salts." *CrystEngComm*, 18 (34), 6378-6388.
- de Vries, E. J., Kantengwa, S., Ayamine, A. and Báthori, N. B. (2016). "Testing the limits of synthon engineering: salts of salicylic and sulfosalicylic acid with nucleobases and derivatives." *CrystEngComm*, 18 (39), 7573-7579.
- Delaney, S. P., Smith, T. M. and Korter, T. M. (2014). "Conformational origins of polymorphism in two forms of flufenamic acid." *J. Mol. Struct.*, 1078, 83-89.
- Delori, A., Eddleston, M. D. and Jones, W. (2013). "Cocrystals of 5-fluorouracil." *CrystEngComm*, 15 (1), 73-77.
- Deng, J. H., Lu, T. B., Sun, C. C. and Chen, J. M. (2017). "Dapagliflozin-citric acid cocrystal showing better solid state properties than dapagliflozin." *Eur. J. Pharm. Sci.*, 104, 255-261.

- Desiraju, G. R. (2007). "Crystal engineering: A holistic view." *Angew. Chem. Int. Ed.*, 46, 8342 – 8356.
- Desiraju, G. R. (2010). "Crystal engineering: A brief overview." *Chem. Sci.*, 122, 667–675.
- Desiraju, G. R. (2013). "Crystal engineering: from molecule to crystal." *J. Am. Chem. Soc.*, 135, 9952-9967.
- Desiraju, G. R. and Parshall, G. W. (1989). "Crystal engineering: the design of organic solids." *Mater. Sci. Monogr.*, 54.
- Desiraju, G.R. (1995). "Supramolecular Synthons in Crystal Engineering-A new organic synthesis." *Angew Chem., Int. Ed. Engl.*, 34, 2311-2327.
- Desiraju, J. R., Vittal, J. J. and Ramanan A. (2011). "Crystal engineering A Text Book." World Scientific, Singapore.
- Diniz, L. F., Carvalho, P. S., de Melo, C. C. and Ellena, J. (2017). "Development of a salt drug with improved solubility: Ethionamide nitrate." *J. Mol. Struct.*, 1137, 119-125.
- Diniz, L. F., Souza, M. S., Carvalho, P. S., da Silva, C. C., D'Vries, R. F. and Ellena, J. (2017). "Novel Isoniazid cocrystals with aromatic carboxylic acids: Crystal engineering, spectroscopy and thermochemical investigations." *J. Mol. Struct.*, 1153, 58-68
- Drozd, K. V., Manin, A. N., Churakov, A. V. and Perlovich, G. L. (2017). "Drug-drug cocrystals of antituberculous 4-aminosalicylic acid: Screening, crystal structures, thermochemical and solubility studies." *Eur. J. Pharm. Sci.*, 99, 228-239.
- Du, Y., Cai, Q., Xue, J., Zhang, Q. and Qin, D. (2017). "Structural investigation of the cocrystal formed between 5-fluorocytosine and fumaric acid based on vibrational spectroscopic technique." *Spectrochim. Acta, Part A*, 178, 251-257.
- Duan, X., Huang, Y., Agarwal, R. and Lieber, C. M. (2003). "Single-nanowire electrically driven lasers." *Nature*, 421, 241-245.

- Duarte, Í., Andrade, R., Pinto, J. F. and Temtem, M. (2016). “Green production of cocrystals using a new solvent-free approach by spray congealing.” *Int. j. pharm.*, 506 (1), 68-78.
- Dunn, C. J. and Goa, K. L. (1999). “Tranexamic acid: a review of its use in surgery and other indications.” *Drugs*, 57, 1005-1032.
- E. Castro, R. A., Ribeiro, J. D., Maria, T. M., Ramos Silva, M., Yuste-Vivas, C., Canotilho, J. and Eusébio, M. E. S. (2011). “Naproxen cocrystals with pyridinecarboxamide isomers.” *Cryst. Growth Des.*, 11, 5396-5404.
- Eriksson, O., Kjellman, H., Pilbrant, Å. and Schannong, M. (1974). “Pharmacokinetics of tranexamic acid after intravenous administration to normal volunteers.” *Eur. J. Clin. Pharmacol.*, 7, 375-380.
- Evans, O. R. and Lin, W. (2002). “Crystal engineering of NLO materials based on metal-organic coordination networks.” *Acc. Chem. Res.*, 35, 511-522.
- Évora, A. O., Castro, R. A., Maria, T. M., Rosado, M. T., Ramos Silva, M., Matos Beja, A., ... and Eusébio, M. E. S. (2011). “Pyrazinamide-diflunisal: A new dual-drug co-crystal.” *Cryst. Growth Des.*, 11 (11), 4780-4788.
- Fabian, L. and Kalman, A. (1999). “Volumetric measure of isostructurality.” *Acta Crystallogr., Sect. B: Struct. Sci.*, 55, 1099-1108.
- Fábián, L., Hamill, N., Eccles, K. S., Moynihan, H. A., Maguire, A. R., McCausland, L. and Lawrence, S. E. (2011). “Cocrystals of fenamic acids with nicotinamide.” *Cryst. Growth Des.*, 11, 3522-3528.
- Fiuza, S. M., Gomes, C., Teixeira, L. J., Da Cruz, M. G., Cordeiro, M. N. D. S., Milhazes, N. and Marques, M. P. M. (2004). “Phenolic acid derivatives with potential anticancer properties—a structure–activity relationship study. Part 1: Methyl, propyl and octyl esters of caffeic and gallic acids.” *Bioorg. Med. Chem.*, 12, 3581-3589.
- Fukte, S. R., Wagh, M. P. and Rawat, S. (2014). “Coformer selection: An important tool in cocrystal formation.” *Int. J. Pharmaceutics*, 6, 7, 9-14.

- Gadade, D. D., Kulkarni, D. A., Rathi, P. B., Pekamwar, S. S. and Joshi, S. S. (2017). "Solubility Enhancement of Lornoxicam by Crystal Engineering." *Indian J. Pharm. Sci.*, 79 (2), 277-286.
- Ganin, E. V., Minacheva, L. K., Koroeva, L. V. and Sergienko, V. S. (2010). "Bis (2-alkyl-4-thiocarbamoyl-4-pyridinium) hexafluorosilicates." *Russ. J. Inorg. Chem.*, 55, 1209-1215.
- George, S., Benny, P. J., Kuriakose, S., George, C. and Gopalakrishnan, S. (2011). "Antiprotozoal activity of 2, 3-dihydroxybenzoic acid isolated from the fruit extracts of *Flacourtia inermis* Roxb." *Medicinal Plants-Int. J. Phytomed. Rel. Ind.*, 3, 237-241.
- George, S., Benny, P. J., Sunny, K. and Cincy, G. (2011). "Antibiotic activity of 2, 3-dihydroxybenzoic acid isolated from *Flacourtia inermis* fruit against multi drug resistant bacteria." *Asian J. Pharm. Clin. Res.*, 4, 126-130.
- Ghosh, R., Chakraborty, A., Maiti, D. K. and Puranik, V. G. (2006). "Crystal or low molecular mass organogel based on sugar-derived chiral pyrano [2, 3-b] naphtho [1, 2-e] pyrans." *Org. Lett.*, 8 (6), 1061-1064.
- Ghosh, S. and Reddy, C. M. (2012). Elastic and bendable caffeine cocrystals: Implications for the design of flexible organic materials. *Angew. Chem., Int. Ed.*, 51 (41), 10319-10323.
- Giron, D. (2001). "Investigation of polymorphism and pseudo polymorphism in pharmaceuticals by combined thermo analytical techniques." *J. Therm. Anal. Calorim.*, 64, 37-60.
- Gonnade, R. G. and Sangtani, E. (2017). "Polymorphs and Cocrystals: A Comparative Analysis." *J. Indian Inst. Sci.*, 1-34.
- Gopi, S. P., Banik, M. and Desiraju, G. R. (2016). "New Cocrystals of Hydrochlorothiazide: Optimizing Solubility and Membrane Diffusivity." *Cryst. Growth Des.*, 17 (1), 308-316.

- Goud, N. R., Khan, R. A. and Nangia, A. (2014). "Modulating the solubility of sulfacetamide by means of cocrystals." *CrystEngComm*, 16 (26), 5859-5869.
- Graziano, J. H., Grady, R. W. and Cerami, A. (1974). "The identification of 2, 3-dihydroxybenzoic acid as a potentially useful iron-chelating drug." *J. Pharmacol. Exp. Ther.*, 190, 570-575.
- Gobelny, P., Mukherjee, A. and Desiraju, G. R. (2011). "Drug-drug cocrystals: Temperature-dependent proton mobility in the molecular complex of isoniazid with 4-aminosalicylic acid." *CrystEngComm*, 13, 4358-4364.
- Gobelny, P., Mukherjee, A. and Desiraju, G. R. (2011). "Drug-drug co-crystals: Temperature-dependent proton mobility in the molecular complex of isoniazid with 4-aminosalicylic acid." *CrystEngComm*, 13 (13), 4358-4364.
- Grootveld, M. and Halliwell, B. (1988). "2, 3-Dihydroxybenzoic acid is a product of human aspirin metabolism." *Biochem. Pharmacol.*, 37, 271-280.
- Gunnam, A., Suresh, K., Ganduri, R. and Nangia, A. (2016). "Crystal engineering of a zwitterionic drug to neutral cocrystals: a general solution for floxacins." *Chem. Commun.*, 52, 12610-12613.
- Haneef, J. and Chadha, R. (2017). "Drug-Drug Multicomponent Solid Forms: Cocrystal, Coamorphous and Eutectic of Three Poorly Soluble Antihypertensive Drugs Using Mechanochemical Approach." *AAPS PharmSciTech*, 1-12.
- He, H., Jiang, L., Zhang, Q., Huang, Y., Wang, J. R. and Mei, X. (2015). "Polymorphism observed in dapsone-flavone cocrystals that present pronounced differences in solubility and stability." *CrystEngComm*, 17 (34), 6566-6574.
- Heifets, L. B. (1982). "Synergistic Effect of Rifampin, Streptomycin, Ethionamide, and Ethambutol on Mycobacterium intracellulare 1, 2." *Am. Rev. Respir. Dis.*, 125, 43-48.
- Hiendrawan, S. T. E. V. A. N. U. S., Veriansyah, B. A. M. B. A. N. G., Widjojokusumo, E. D. W. A. R. D., Soewandhi, S. N., Wikarsa, S. and Tjandrawinata, R. R. (2016).

Simultaneous cocrystallization and micronization of paracetamol-dipicolinic acid cocrystal by supercritical antisolvent (SAS). *Int. J. Pharm. Pharm. Sci.*, 8, 89-98.

Hiippala, S., Strid, L., Wennerstrand, M., Arvela, V., Mäntylä, S., Ylinen, J. and Niemelä, H. (1995). "Tranexamic acid (Cyklokapron) reduces perioperative blood loss associated with total knee arthroplasty." *Br. J. Anaesth.*, 74, 534-537.

Hirasawa, N., Okamoto, H. and Danjo, K. (1999). "Lactose as a low molecular weight carrier of solid dispersions for carbamazepine and ethenzamide." *Chem. Pharm. Bull.*, 47, 417-420.

<http://www.drugbank.ca/drugs/DB06637>

Huang, F., Zhang, H. and Banfield, J. F. (2003). "Two-stage crystal-growth kinetics observed during hydrothermal coarsening of nanocrystalline ZnS." *Nano Lett.*, 3 (3), 373-378.

Hulme, A. T. and Tocher, D. A. (2005). "4-Amino-5-fluoropyrimidin-2 (1H)-one-2-amino-5-fluoropyrimidin-4 (3H)-one-water (1/1/1)." *Acta Crystallogr., Sect. E: Struct. Rep. Online*, 61 (7), o2112-o2113.

Hulme, A. T. and Tocher, D. A. (2006). "The discovery of new crystal forms of 5-fluorocytosine consistent with the results of computational crystal structure prediction." *Cryst. Growth Des.*, 6 (2), 481-487.

Itai S., Nemoto M., Kouchiwa S., Murayama H. and Nagai T. (1985). "Influence of wetting factors on the dissolution behavior of flufenamic acid." *Chem. Pharm. Bull.*, 33, 5464-5473.

Jarzemska, K. N., Hoser, A. A., Kamiński, R., Madsen, A. Ø., Durka, K. and Woźniak, K. (2014). Combined experimental and computational studies of pyrazinamide and nicotinamide in the context of crystal engineering and thermodynamics. *Cryst. Growth Des.*, 14 (7), 3453-3465.

- Jiang, L., Huang, Y., Zhang, Q., He, H., Xu, Y. and Mei, X. (2014). "Preparation and solid-state characterization of dapsone drug–drug cocrystals." *Cryst. Growth Des.*, 14, 4562-4573.
- Kadoya, S. H. I. Z. U. O., Hanazaki, F. U. M. I. E. and Iitaka, Y. O. I. C. H. I. (1966). "The crystal structures of trans and cis-4-aminomethylcyclohexane-1-carboxylic acid hydrohalides." *Acta Crystallogr.*, 21, 38-49.
- Kale, D. P., Zode, S. S. and Bansal, A. K. (2017). "Challenges in Translational Development of Pharmaceutical Cocrystals." *J. Pharm. Sci.*, 106 (2), 457-470.
- Kalman, A. P. L. A. G., Párkányi, L. and Argay, G. (1993). "Classification of the isostructurality of organic molecules in the crystalline state." *Acta Crystallogr., Sect. B: Struct. Sci.*, 49, 1039-1049.
- Kang, Y., Gu, J. and Hu, X. (2017). Syntheses, structure characterization and dissolution of two novel cocrystals of febuxostat. *J. Mol. Struct.*, 1130, 480-486.
- Kaur, R. and Guru Row, T. N. (2012). Polymorphic Anhydrous Cocrystals of Gallic Acid and Acetamide from Methanol: Pointers toward a Stable Cocrystal Form. *Cryst. Growth Des.*, 12 (6), 2744-2747.
- Kawano, O., Sawabe, T., Misaki, N. and Fukawa, K. (1978). "Studies on combination dosing. III. Aspirin and ethenzamide." *The Japanese Journal of Pharmacology*, 28, 829-835.
- Kerr, H. E., Softley, L. K., Suresh, K., Hodgkinson, P. and Evans, I. R. (2017). "Structure and physicochemical characterization of a naproxen–picolinamide cocrystal." *Acta Crystallogr., Sect. C: Struct. Chem.*, 73 (3), 168-175.
- Khare, S. G., Jena, S. K., Sangamwar, A. T., Khullar, S. and Mandal, S. K. (2017). "Multicomponent Pharmaceutical Adducts of α -Eprosartan: Physicochemical Properties and Pharmacokinetic Study." *Cryst. Growth Des.*, 17 (4), 1589-1599.

- Kinchington, D., Ng, T., Mathews, N., Tisdale, M., Devine, D. and Ayuko, W. O. (1997). "T cell costimulation by derivatives of benzoic acid." *Antiviral Chem. Chemother.*, 8 (2), 121-130.
- Konno T. (1990). "Physical and chemical changes of medicinals in mixtures with adsorbents in the solid state. IV. Study on reduced-pressure mixing for practical use of amorphous mixtures of flufenamic acid." *Chem. Pharm. Bull.*, 38, 2003-2007.
- Korth-Bradley, J. M., Mayer, P., Mansfield, D., Tucker, H. and Wu, D. (2014). "Comparative Bioavailability Study of Single-Dose Film-Coated and Sugar-Coated Ethionamide Tablets in Healthy Volunteers." *Clin. Ther.*, 36, 982-987.
- Krc, J. (1977). "Crystallographic properties of flufenamic acid." *Microscope*, 25, 31-45.
- Krishna, G. R., Shi, L., Bag, P. P., Sun, C. C. and Reddy, C. M. (2015). "Correlation among crystal structure, mechanical behavior, and tabletability in the co-crystals of vanillin isomers." *Cryst. Growth Des.*, 15 (4), 1827-1832.
- Kumari, H., Zhang, J., Erra, L., Barbour, L. J., Deakyne, C. A. and Atwood, J. L. (2013). "Cocrystals of gabapentin with C-alkylresorcin [4] arenes." *CrystEngComm*, 15, 4045-4048.
- Kurozumi, K., Tamiya, T., Ono, Y., Otsuka, S., Kambara, H., Adachi, Y., ... and Ohmoto, T. (2004). "Apoptosis induction with 5-fluorocytosine/cytosine deaminase gene therapy for human malignant glioma cells mediated by adenovirus." *J. Neuro-Oncol.*, 66 (1), 117-127.
- Lee, D. I., Yoon, M. J. and Lee, P. S. (2014). U.S. Patent Application No. 14/779,927.
- Lemmer, H. (2012). "Thermal kinetics and crystal structure of dapsone polymorphs and solvates (Doctoral dissertation, North-West University)."
- Lemmerer, A. (2012). "Covalent assistance to supramolecular synthesis: modifying the drug functionality of the antituberculosis API isoniazid in situ during co-crystallization with GRAS and API compounds." *CrystEngComm*, 14 (7), 2465-2478.

- Li, H., Wen, H., Stowell, J. G., Morris, K. R. and Byrn, S. R. (2010). "Crystal quality and physical reactivity in the case of flufenamic acid (FFA)." *J. Pharm. Sci.*, 99, 3839-3848.
- Li, S., Chen, J. M. and Lu, T. B. (2014). "Synthon polymorphs of 1: 1 co-crystal of 5-fluorouracil and 4-hydroxybenzoic acid: their relative stability and solvent polarity dependence of grinding outcomes." *CrystEngComm*, 16 (28), 6450-6458.
- Liu, Y., Pukala, T. L., Musgrave, I. F., Williams, D. M., Dehle, F. C. and Carver, J. A. (2013). "Gallic acid is the major component of grape seed extract that inhibits amyloid fibril formation." *Bioorg. Med. Chem. Lett.*, 23, 6336-6340.
- López-Mejías, V., Kampf, J. W. and Matzger, A. J. (2012). "Nonamorphism in flufenamic acid and a new record for a polymorphic compound with solved structures." *J. Am. Chem. Soc.*, 134, 9872-9875.
- Lorico, A., Masturzo, P., Villa, S., Salmona, M., Semeraro, N. and De Gaetano, G. (1986). "Gentisic acid: an aspirin metabolite with multiple effects on human blood polymorphonuclear leukocytes." *Biochem. Pharmacol.*, 35, 2443-2445.
- Lou, M., Mao, S. H., Luo, Y. H., Zhao, P. and Sun, B. W. (2015). "Synthesis, co-crystal structure and characterization of pyrazinamide with m-hydroxybenzoic acid, p-hydroxybenzoic acid and 3, 4-dihydroxy benzoic acid." *Resea Res. Chem. Intermed.*, 41 (5), 2939-2951.
- Louis, T., Low, J. N. and Tollin, P. (1982). "5-Fluoro-Cytosine, C₄H₄FN₃O. H₂O." *Cryst. Struct. Commun.*, 11 (3), 1059-1064.
- Louvain, N.; Mercier, N. and Boucher, F. (2009). "r- to -(dmes)BiI₅ (dmes) Dimethyl(2-ethylammonium)sulfonium Dication): Umbrella Reversal of Sulfonium in the Solid State and Short I · · · I Interchain ContactssCrystal Structures, Optical Properties, andTheoretical Investigations of 1D Iodobismuthates." *Inorg. Chem.*, 48, 879-888.

- Majumder, J., Yedoti, P. and Dastidar, P. (2015). A supramolecular topical gel derived from a non-steroidal anti-inflammatory drug, fenoprofen, is capable of treating skin inflammation in mice. *Org. Biomol. Chem.*, 13 (8), 2300-2309.
- Manin, A. N., Voronin, A. P., Manin, N. G., Vener, M. V., Shishkina, A. V., Lermontov, A. S. and Perlovich, G. L. (2014). "Salicylamide cocrystals: screening, crystal structure, sublimation thermodynamics, dissolution, and solid-state DFT calculations." *J. Phys. Chem. B*, 118 (24), 6803-6814.
- Mannava, M. C., Suresh, K. and Nangia, A. (2016). "Enhanced Bioavailability in the Oxalate Salt of the Anti-Tuberculosis Drug Ethionamide." *Cryst. Growth Des.*, 16, 1591-1598.
- Mannava, M. C., Suresh, K. and Nangia, A. (2016). "Enhanced bioavailability in the oxalate salt of the anti-tuberculosis drug ethionamide." *Cryst. Growth Des.*, 16 (3), 1591-1598.
- Mannava, M. C., Suresh, K. and Nangia, A. (2016). "Enhanced bioavailability in the oxalate salt of the anti-tuberculosis drug ethionamide." *Cryst. Growth Des.*, 16 (3), 1591-1598.
- Manoj, K., Tamura, R., Takahashi, H. and Tsue, H. (2014). "Crystal engineering of homochiral molecular organization of naproxen in cocrystals and their thermal phase transformation studies." *CrystEngComm*, 16, 5811-5819.
- Mashhadi, S. M. A., Yunus, U., Bhatti, M. H. and Tahir, M. N. (2014). Isoniazid cocrystals with anti-oxidant hydroxy benzoic acids. *J. Mol. Struct.*, 1076, 446-452.
- Mashhadi, S. M. A., Yunus, U., Bhatti, M. H., Ahmed, I. and Tahir, M. N. (2016). "Synthesis, characterization, solubility and stability studies of hydrate cocrystal of antitubercular Isoniazid with antioxidant and anti-bacterial Protocatechuic acid." *J. Mol. Struct.*, 1117, 17-21.
- McCormack, P. L. (2012). "Tranexamic acid: a review of its use in the treatment of hyper fibrinolysis." *Drugs*, 72, 585-617.

- Mekala, R., Jagdish, P., Mathammal, R. and Sangeetha, K. (2017). "Screening and Structural Elucidation of the Zwitterionic Cocrystal o-Picolinic acid with p-Nitro aniline." *J. Mol. Struct.*
- Min, W. U., Xingang, L., Yu, X., Qi, C., Xiurong, H. U., Jun, Z., and Guping, T. (2017). "Synthesis, characterization and antitumor activity of 5-fluorouracil-nicotinamide cocrystal." *J. Zhejiang Univ., Sci. Med. Sci.*, 46 (2), 127.
- Mohamed, A. A. and Matijević, E. (2012). "Preparation and characterization of uniform particles of flufenamic acid and its calcium and barium salts." *J. Colloid Interface Sci.*, 381, 198-201.
- Mohamed, S., Tocher, D. A., Vickers, M., Karamertzanis, P. G. and Price, S. L. (2009). "Salt or cocrystal? A new series of crystal structures formed from simple pyridines and carboxylic acids." *Cryst. Growth Des.*, 9, 2881-2889.
- Mohana, M., Muthiah, P. T. and McMillen, C. D. (2017). "Supramolecular hydrogen-bonding patterns in 1: 1 cocrystals of 5-fluorouracil with 4-methylbenzoic acid and 3-nitrobenzoic acid." *Acta Crystallogr., Sect. C: Struct. Chem.*, 73 (3), 259-263.
- Mohana, M., Thomas Muthiah, P. and McMillen, C. D. (2017). "Supramolecular architectures in two 1: 1 cocrystals of 5-fluorouracil with 5-bromothiophene-2-carboxylic acid and thiophene-2-carboxylic acid." *Acta Crystallogr., Sect. C: Struct. Chem.*, 73 (6).
- Moiescu-Goia, C., Muresan-Pop, M. and Simon, V. (2017). "New solid state forms of antineoplastic -fluorouracil with anthelmintic piperazine." *J. Mol. Struct.*, 1150, 37-43.
- Mondal, P. K., Rao, V., Mittapalli, S. and Chopra, D. (2017). Exploring Solid State Diversity and Solution Characteristics in a Fluorine-Containing Drug Riluzole. *Cryst. Growth Des.*, 17 (4), 1938-1946.
- Mudit, D., Bhardwaj, Y., Keshavarao, P. K. and Selvam, P. (2011). "Enhancing solubility and dissolution of mefenamic acid by freeze drying using β -cyclodextrin." *Int. Res. J. Pharm*, 2, 146-150.

- Murikipudi, V., Gupta, P. and Sihorkar, V. (2013). "Efficient throughput method for hygroscopicity classification of active and inactive pharmaceutical ingredients by water vapor sorption analysis." *Pharm. Dev. Technol.*, 18, 348-358.
- Nangia, A. (2008). "Conformational polymorphism in organic crystals." *Acc. Chem. Res.*, 41, 595-604.
- Nanubolu, J. B. and Ravikumar, K. (2017). "Designing a new cocrystal of olanzapine drug and observation of concomitant polymorphism in a ternary cocrystal system." *CrystEngComm*, 19 (2), 355-366.
- Nanubolu, J. B. and Ravikumar, K. (2017). "Designing a new cocrystal of olanzapine drug and observation of concomitant polymorphism in a ternary cocrystal system." *CrystEngComm*, 19 (2), 355-366.
- Neurohr, C., Erriguible, A., Laugier, S. and Subra-Paternault, P. (2016). "Challenge of the supercritical antisolvent technique SAS to prepare cocrystal-pure powders of naproxen-nicotinamide." *Chem. Eng. J.*, 303, 238-251.
- Neurohr, C., Erriguible, A., Laugier, S. and Subra-Paternault, P. (2016). "Challenge of the supercritical antisolvent technique SAS to prepare cocrystal-pure powders of naproxen-nicotinamide." *Chem. Eng. J.*, 303, 238-251.
- Neurohr, C., Marchivie, M., Lecomte, S., Cartigny, Y., Couvrat, N., Sanselme, M. and Subra-Paternault, P. (2015). "Naproxen–Nicotinamide Cocrystals: Racemic and Conglomerate Structures Generated by CO₂ Antisolvent Crystallization." *Cryst. Growth Des.*, 15, 4616-4626.
- Nilsson, I. M. (1980). "Clinical pharmacology of aminocaproic and tranexamic acids." *J. Clin. Pathol.*, 33(Suppl. 14), 41-47.
- Nishiyama, T., Kawamura, Y., Kawamoto, K., Matsumura, H., Yamamoto, N., Ito, T., ... and Sakai, T. (1985). "Antineoplastic effects in rats of 5-fluorocytosine in combination with cytosine deaminase capsules." *Cancer res.*, 45 (4), 1753-1761.

- Oruganti, M., Khade, P., Das, U. K. and Trivedi, D. R. (2016). “The hierarchies of hydrogen bonds in salts/cocrystals of isoniazid and its Schiff base—a case study.” *RSC Advances*, 6 (19), 15868-15876.
- Oruganti, M., Khade, P., Das, U. K. and Trivedi, D. R. (2016). The hierarchies of hydrogen bonds in salts/cocrystals of isoniazid and its Schiff base—a case study. *RSC Advances*, 6 (19), 15868-15876.
- Pandey, N. K., Sehal, H. R., Garg, V., Gaur, T., Kumar, B., Singh, S. K., ... and Sharma, P. (2017). Stable Co-crystals of Glipizide with Enhanced Dissolution Profiles: Preparation and Characterization. *AAPS PharmSciTech*, 1-12.
- Pathak, C. D., Savjani, K. T., Gajjar, A. K. and Savjani, J. K. (2013). “Cocrystal formation of paracetamol with indomethacin and mefenamic acid: An efficient approach to enhance solubility.” *Int. J. Pharm. Pharm. Sci.*, 5, 414-419.
- Patil, S., Ujalambkar, V. and Mahadik, A. (2017). “Electrospray technology as a probe for cocrystal synthesis: Influence of solvent and cofomer structure.” *J. Drug Delivery Sci. Technol.*, 39, 217-222.
- Paulekuhn, S., Dressmann, J. and Saal, C. (2007). “Trends in Active Pharmaceutical Ingredient Salt Selection based on Analysis of the Orange Book Database.” *J. Med. Chem.*, 50, 6665-6672.
- Pentikäinen, P. J., Neuvonen, P. J. and Backman, C. (1981). “Human pharmacokinetics of tolfenamic acid, a new anti-inflammatory agent.” *Eur. J. Clin. Pharmacol.*, 19, 359-365.
- Perumalla, S. R., Pedireddi, V. R. and Sun, C. C. (2013). “Design, synthesis, and characterization of new 5-fluorocytosine salts.” *Mol. Pharmaceutics*, 10 (6), 2462-2466.
- Perumalla, S. R., Pedireddi, V. R. and Sun, C. C. (2013). “Protonation of cytosine: cytosinium vs hemicytosinium duplexes.” *Cryst. Growth Des.*, 13 (2), 429-432.

- Petty, T. L. and Mitchell, R. S. (1962). "Successful Treatment of Advanced Isoniazid- and Streptomycin-Resistant Pulmonary Tuberculosis with Ethionamide, Pyrazinamide, and Isoniazid 1." *Am. Rev. Respir. Dis.*, 86, 503-512.
- Portalone, G. (2011). "Solid-phase molecular recognition of cytosine based on proton-transfer reaction. Part II. Supramolecular architecture in the cocrystals of cytosine and its 5-Fluoroderivative with 5-Nitrouracil." *Chem. Cent. J.*, 5 (1), 51.
- Portalone, G. and Colapietro, M. (2006). "Redetermination of 5-Fluorocytosine monohydrate." *Acta Crystallogr., Sect. E: Struct. Rep. Online*, 62 (3), o1049-o1051.
- Portalone, G. and Colapietro, M. (2007). "Asymmetric base pairing in the complex 5-fluorocytosinium chloride/5-fluorocytosine monohydrate." *J. Chem. Crystallogr.*, 37 (2), 141-145.
- Prasad, K. D., Cherukuvada, S., Ganduri, R., Stephen, L. D., Perumalla, S. and Guru Row, T. N. (2015). "Differential Cocrystallization Behavior of Isomeric Pyridine Carboxamides toward Antitubercular Drug Pyrazinoic Acid." *Cryst. Growth Des.*, 15 (2), 858-866.
- Pringsheim, T., Davenport, W. J. and Dodick, D. (2008). "Acute treatment and prevention of a menstrually related migraine headache Evidence-based review." *Neurol.*, 70, 1555-1563.
- Przybyłek, M., Ziółkowska, D., Mroczyńska, K. and Cysewski, P. (2016). "Propensity of salicylamide and ethenzamide cocrystallization with aromatic carboxylic acids." *Eur. J. Pharm. Sci.*, 85, 132-140.
- Qiao, N., Li, M., Schlindwein, W., Malek, N., Davies, A. and Trappitt, G. (2011). "Pharmaceutical cocrystals: an overview." *Int. J. Pharm.*, 419, 1-11.
- Ranjan, S., Devarapalli, R., Kundu, S., Vangala, V. R., Ghosh, A. and Reddy, C. M. (2017). "Three new hydrochlorothiazide cocrystals: Structural analyses and solubility studies." *J. Mol. Struct.*, 1133, 405-410.

- Ranjan, S., Devarapalli, R., Kundu, S., Vangala, V. R., Ghosh, A. and Reddy, C. M. (2017). "Three new hydrochlorothiazide cocrystals: Structural analyses and solubility studies." *J. Mol. Struct.*, 1133, 405-410.
- Ranzani, L. S. and Aldea, A. F. (2014). *U.S. Patent No. 8,846,744*. Washington, DC: U.S. Patent and Trademark Office.
- Ravikumar, N., Gaddamanugu, G. and Solomon, K. A. (2013). "Structural, spectroscopic (FT-IR, FT-Raman) and theoretical studies of the 1: 1 cocrystal of isoniazid with p-coumaric acid." *J. Mol. Struct.*, 1033, 272-279.
- Reddy, L. S., Bethune, S. J., Kampf, J. W. and Rodriguez-Hornedo, N. (2008). "Cocrystals and salts of gabapentin: pH dependent cocrystal stability and solubility." *Cryst. Growth Des.*, 9 (1), 378-385.
- Rossi, S. (2013). "Australian Medicines Handbook." Adelaide: The Australian Medicines Handbook Unit Trust. ISBN 978-0-9805790-9-3.
- Rutherford, J. S. (1997). "On comparing lattice parameters among isostructural molecular crystals." *Acta Chim. Hun.*, 134, 395-405.
- Saha, B. K., Saha, A. and Rather, S. A. (2017). Shape and Geometry Corrected Statistical Analysis on Halogen··· Halogen Interactions. *Crystal Growth & Design*, 17(5), 2314-2318.
- Sangeetha, N. M. and Maitra, U. (2005). "Supramolecular gels: Functions and uses." *Chem. Soc. Rev.*, 34, 821-836.
- Sangtani, E., Mandal, S. K., Sreelakshmi, A. S., Munshi, P. and Gonnade, R. G. (2017). "Salts and Cocrystals of Furosemide with Pyridines: Differences in π -Stacking and Color Polymorphism." *Cryst. Growth Des.*, 17 (6), 3071-3087.
- Santra, R., Ghosh, N. and Biradha, K. (2008). "Crystal engineering with acid and pyridine heteromeric synthon: neutral and ionic co-crystals." *New J. Chem.*, 32 (10), 1673-1676.

- Sarceviča, I., Kons, A. and Orola, L. (2016). "Isoniazid cocrystallisation with dicarboxylic acids: vapochemical, mechanochemical and thermal methods." *CrystEngComm*, 18 (9), 1625-1635.
- Sarmah, K. K., Boro, K., Arhangeliskis, M. and Thakuria, R. (2017). "Crystal structure landscape of ethenzamide: a physicochemical property study." *CrystEngComm*, 19 (5), 826-833.
- Sarmah, K. K., Rajbongshi, T., Bhowmick, S. and Thakuria, R. (2017). "First-line antituberculosis drug, pyrazinamide, its pharmaceutically relevant cocrystals and a salt." *Acta Crystallogr., Sect. B: Struct. Sci., Cryst. Eng. Mater.*, 73 (5), 1007-1016.
- Schultheiss, N. and Newman, A. (2009). "Pharmaceutical Cocrystal and Their Physicochemical Properties." *Cryst. Growth Des.*, 9, 2950-2967.
- Sekhon, B. S. (2005). "Pharmaceutical Cocrystals-An Update." *Int. Bull. Drug Res.*, 1, 24-39.
- Sekhon, B. S. (2009). "Pharmaceutical cocrystals-a review."
- Sekhon, B. S. (2012). "Drug-drug cocrystals." *Daru, J. Pharm. Sci.*, 20, 1.
- Sekhon, B., 2009. "Pharmaceutical co-crystals—a review." *Ars Pharmaceutica*, 50, 99–117.
- Sheldrick, G. M. (2014). "SHELXL-2014, Program for structure refinement." Universität of Göttingen, Göttingen.
- Shepard, C. C. (1976). "Combinations involving dapsone, rifampin, clofazimine, and ethionamide in the treatment of *M. leprae* infections in mice." *Int. J. Lepr*, 44, 135-139.
- Skorupska, E., Jeziorna, A. and Potrzebowski, M. J. (2016). "Thermal Solvent-Free Method of Loading of Pharmaceutical Cocrystals into the Pores of Silica Particles: A Case of Naproxen/Picolinamide Cocrystal." *J. Phys. Chem. C*, 120 (24), 13169-13180.
- Sokal, A., Pindelska, E., Szeleszczuk, L. and Kolodziejcki, W. (2017). "Pharmaceutical properties of two ethenzamide-gentisic acid cocrystal polymorphs: Drug release

profiles, spectroscopic studies and theoretical calculations.” *Int. J. Pharm.*, 522 (1), 80-89.

Solomon, K. A., Blacque, O. and Venkatnarayan, R. (2017). “Molecular salts of 2, 6-dihydroxybenzoic acid (2, 6-DHB) with N-heterocycles: Crystal structures, spectral properties and Hirshfeld surface analysis.” *J. Mol. Struct.*, 1134, 190-198.

Sousa, M., Ousingawatt, J., Seitz, R., Puntheeranurak, S., Regalado, A., Schmidt, A. and Kunzelmann, K. (2007). “An extract from the medicinal plant *Phyllanthus acidus* and its isolated compounds induce airway chloride secretion: a potential treatment for cystic fibrosis.” *Mol. pharmacol.*, 71, 366-376.

Srivastava, K., Shimpi, M. R., Srivastava, A., Tandon, P., Sinha, K. and Velaga, S. P. (2016). “Vibrational analysis and chemical activity of paracetamol–oxalic acid cocrystal based on monomer and dimer calculations: DFT and AIM approach.” *RSC Advances*, 6 (12), 10024-10037.

Sugandha, K., Kaity, S., Mukherjee, S., Isaac, J., & Ghosh, A. (2014). “Solubility enhancement of ezetimibe by a cocrystal engineering technique.” *Cryst. Growth Des.*, 14 (9), 4475-4486.

Sultan, S. M., Alzamil, I. Z., Alrahman, A. M. A., Altamrah, S. A. AND Asha, Y. (1986). “Use of cerium (IV) sulphate in the spectrophotometric determination of paracetamol in pharmaceutical preparations.” *Analyst*, 111, 919-921.

Suresh, K. and Nangia, A. (2014). “Lornoxicam salts: crystal structures, conformations, and solubility.” *Cryst. Growth Des.*, 14, 2945-2953.

Svahn, C. M., Merenyi, F., and Karlsson, L. (1986). “Tranexamic acid derivatives with enhanced absorption.” *J. Med. Chem.*, 29, 448-453.

Svahn, C. M., Merenyi, F., Karlsson, L. E. and Hanshoff, G. (1984). U.S. Patent No. 4,483,867. Washington, DC: U.S. Patent and Trademark Office.

- Swapna, B., Maddileti, D. and Nangia, A. (2014). "Cocrystals of the tuberculosis drug isoniazid: polymorphism, isostructurality, and stability." *Cryst. Growth Des.*, 14 (11), 5991-6005.
- Thipparaboina, R., Thumuri, D., Chavan, R., Naidu, V. G. M. and Shastri, N. R. (2017). Fast dissolving drug-drug eutectics with improved compressibility and synergistic effects. *Eur J. Pharm. Sci.*, 104, 82-89.
- Tilborg, A., Leyssens, T., Norberg, B. and Wouters, J. (2013). "Structural study of prolinium/fumaric acid zwitterionic cocrystals: focus on hydrogen-bonding pattern involving zwitterionic (ionic) heterosynthons." *Cryst. Growth Des.*, 13, 2373-2389.
- Tilborg, A., Norberg, B. and Wouters, J. (2014). "Pharmaceutical salts and cocrystals involving amino acids: A brief structural overview of the state-of-art." *Eur. J. Pharm. Sci.*, 74, 411-426.
- Tilborg, A., Springuel, G., Norberg, B., Wouters, J. and Leyssens, T. (2013). "On the influence of using a zwitterionic coformer for cocrystallization: structural focus on naproxen–proline cocrystals." *CrystEngComm*, 15 (17), 3341-3350.
- Titapiwatanakun, V., Basit, A. W. and Gaisford, S. (2016). "A New Method for Producing Pharmaceutical Co-crystals: Laser Irradiation of Powder Blends." *Cryst. Growth Des.*, 16 (6), 3307-3312.
- Tomita, K. and Takano, T. (1992). "Interaction of flufenamic acid on ethanol metabolism in rat." *Ind. health*, 30, 85-95.
- Trask, A. V. (2007). "An overview of pharmaceutical cocrystals as intellectual property." *Mol. pharmaceutics*, 4, 301-309.
- Tumanova, N., Tumanov, N., Robeyns, K., Filinchuk, Y., Wouters, J. and Leyssens, T. (2014). "Structural insight into cocrystallization with zwitterionic co-formers: cocrystals of S-naproxen." *CrystEngComm*, 16, 8185-8196.

- Tumanova, N., Tumanov, N., Robeyns, K., Filinchuk, Y., Wouters, J. and Leyssens, T. (2014). "Structural insight into cocrystallization with zwitterionic co-formers: cocrystals of S-naproxen." *CrystEngComm*, 16 (35), 8185-8196.
- Tutughamiarso, M. and Egert, E. (2012). "Cocrystals of 5-fluorocytosine. II. Cofomers with variable hydrogen-bonding sites." *Acta Crystallogr., Sect. B: Struct. Sci.*, 68 (4), 444-452.
- Tutughamiarso, M., Bolte, M. and Egert, E. (2009). "New pseudopolymorphs of 5-fluorocytosine." *Acta Crystallogr., Sect. C: Cryst. Struct. Commun.*, 65 (11), o574-o578.
- Tutughamiarso, M., Wagner, G. and Egert, E. (2012). "Cocrystals of 5-fluorocytosine. I. Cofomers with fixed hydrogen-bonding sites." *Acta Crystallogr., Sect. B: Struct. Sci.*, 68 (4), 431-443.
- Uehara, H., Otsuka, H. and Izumi, K. (1998). "Modifying effects of a mixture of acetaminophen, aspirin, dipyron and ethenzamide on a multiorgan initiation model and its carcinogenicity in male F344 rats." *Cancer lett.*, 135, 83-90.
- Vangala, V. R., Chow, P. S. and Tan, R. B. (2011). "Characterization, physicochemical and photo-stability of a co-crystal involving an antibiotic drug, nitrofurantoin, and 4-hydroxybenzoic acid." *CrystEngComm*, 13 (3), 759-762.
- Vangala, V. R., Chow, P. S. and Tan, R. B. (2012). "Co-crystals and co-crystal hydrates of the antibiotic nitrofurantoin: structural studies and physicochemical properties." *Cryst. Growth Des.*, 12 (12), 5925-5938.
- Vayá, I., Jiménez, M. C. and Miranda, M. A. (2005). "Stereo differentiation in the fluorescence of naproxen-arginine salts in the solid state." *Tetrahedron: Asymmetry*, 16, 2167-2171.
- Vermes, A., Guchelaar, H. J. and Dankert, J. (2000). "Flucytosine: a review of its pharmacology, clinical indications, pharmacokinetics, toxicity and drug interactions." *J. Antimicrob. Chemother.*, 46 (2), 171-179.

- Wang, J. R., Ye, C., Zhu, B., Zhou, C. and Mei, X. (2015). "Pharmaceutical cocrystals of the anti-tuberculosis drug pyrazinamide with dicarboxylic and tricarboxylic acids." *CrystEngComm*, 17 (4), 747-752.
- Wang, L., Wen, X., Li, P., Wang, J., Yang, P., Zhang, H. and Deng, Z. (2014). "2:1 5-Fluorocytosine–acesulfame CAB cocrystal and 1:1 5-fluorocytosine–acesulfame salt hydrate with enhanced stability against hydration." *CrystEngComm*, 16 (36), 8537-8545.
- Wellington, K. and Wagstaff A. J. (2003). "Tranexamic acid: a review of its use in the management of menorrhagia." *Drugs*, 63, 1417-1433.
- Wenger, M. and Bernstein, J. (2008). "An alternate crystal form of gabapentin: a cocrystal with oxalic acid." *Cryst. Growth Des.*, 8, 1595-1598.
- Winder, C. V., Wax, J., Serrano, B., Jones, E. M. and McPhee, M. L. (1963). "Anti-inflammatory and antipyretic properties of N-(α , α , α -Trifluoro-m-tolyl) anthranilic acid (CI-440; flufenamic acid)." *Arthritis & Rheum.*, 6, 36-47.
- Wittering, K. E., Agnew, L. R., Klapwijk, A. R., Robertson, K., Cousen, A. J. P., Cruickshank, D. L. and Wilson, C. C. (2015). "Crystallisation and physicochemical property characterisation of conformationally-locked cocrystals of fenamic acid derivatives." *CrystEngComm*, 17, 3610-3618.
- World Health Organization (WHO), 19th WHO Model List of Essential Medicines (April 2015).
- Würthner, F., & Schmidt, R. (2006). "Electronic and Crystal Engineering of Acenes for Solution-Processible Self-Assembling Organic Semiconductors." *ChemPhysChem*, 7 (4), 793-797.
- Xu, G., & McLeod, H. L. (2001). "Strategies for enzyme/prodrug cancer therapy." *Clin. Cancer Res.*, 7 (11), 3314-3324.
- Zaworotko, M. J. (2007). "Molecules to crystals, crystals to molecules... and back again?." *Cryst. Growth Des.*, 7, 4-9.

LIST OF PUBLICATIONS

Papers Published/Communicated in International Journals

- i. **Nechipadappu, S. K.** and Trivedi, D. R. (2017). "Structural and physicochemical characterization of pyridine derivative salts of anti-inflammatory drugs." *J. Mol. Struct.*, 1141, 64-74.
- ii. **Nechipadappu, S. K.**, Tekuri, V. and Trivedi, D. R. (2017). "Pharmaceutical Co-Crystal of Flufenamic Acid: Synthesis and Characterization of Two Novel Drug-Drug Co-Crystal." *J. Pharm. Sci.*, 106(5), 1384-1390.
- iii. **Nechipadappu, S. K.** and Trivedi, D. R. (2017). "Pharmaceutical salts of ethionamide with GRAS counter ion donors to enhance the solubility." *Eur. J. Pharm. Sci.*, 96, 578-589.
- iv. **Nechipadappu, S. K.**, Ramachandran, J., Shivalingegowda, N., Lokanath, N. K., & Trivedi, D. R. (2018). Synthesis of cocrystals/salts of flucytosine: Structure and stability. *New J. Chem.*, 42, 5433-5446.
- v. **Nechipadappu, S. K.**, Reddy, I. R., Tarafder, K., & Trivedi, D. R. "Crystal Engineering of Anti-Fibrinolytic Hemostatic drug Tranexamic acid: Structural, DFT, and Stability Study of Salt/Cocrystal with GRAS Molecules." *Cryst. Growth & Des.* (Manuscript is under revision).
- vi. **Nechipadappu, S. K.**, & Trivedi, D. R. (2018). "Cocrystal of Nutraceutical Sinapic Acid with Active Pharmaceutical Ingredients Ethenzamide and 2-Chloro-4-Nitrobenzoic Acid: Equilibrium Solubility and Stability Study." *J. Mol. Struct.* 1171, 898-905.
- vii. **Nechipadappu, S. K.**, Lokanath, N. K., Kumara, K. and Trivedi, D. R. (2017). "Drug-Drug Cocrystal of Anti-Fungal Drug 5-Fluorocytosine with improved stability." (Manuscript is to be communicated).

Papers presented in national/international conferences

- i. **Nechipadappu, S. K.** and Trivedi, D. R. (2015). "A novel pharmaceutical cocrystal of flufenamic acid with 2-chloro-4-nitro benzoic acid to improve the physicochemical properties of flufenamic acid." Paper presented at "International conference on Contemporary Advances in Science and Technology (IC-CAST 2015)." August 7-8, 2015 at Banaras Hindu University, Varanasi.

-
- ii. Nechipadappu, S. K. and Trivedi, D. R. (2016). “Pharmaceutical cocrystal of flufenamic acid with ethenzamide: structural, solubility and stability study.” Paper presented at “International conference on science and technology: Future challenges and solutions (STFCS - 2016).” August 8-9, 2016 at University of Mysore, Mysore.
- iii. Nechipadappu, S. K. and Trivedi, D. R. (2016). “Structural and stability study of pyridine derivative salts of anti-inflammatory drug naproxen.” Paper presented at “International conference on science and technology: Future challenges and solutions (STFCS - 2016).” August 8-9, 2016 at University of Mysore, Mysore.
- iv. Nechipadappu, S. K. Shivalingegowda, N., Kumar, V., and Trivedi, D. R. (2017). “A Drug-drug Cocrystal of Isoniazid with Anti-Oxidant Syringic acid: Study of Structural and Stability Aspects.” Paper presented at “International conference on Crystal Ball Vision on Science & Engineering for Societal Upliftment.” August 7-8, 2017 at CSIR-National Institute of Oceanography (CSIR-NIO), Goa.

CURRICULUM VITAE

Sunil Kumar N

Nechipadappu House, Mulleria Post

Kasaragod, Kerala, India-671543

E-mail ID: nsunilkumar123@gmail.com

Mobile: +91-8050184189

EDUCATION

2014-2018 Ph. D (Crystal Engineering)

Department of Chemistry, NITK Surathkal

Thesis Title: "Design & Synthesis of A Few Pharmaceutical Cocrystals/Salts by Crystal Engineering Approach and Study of Their Physicochemical Properties."

Supervisor: Dr. Darshak R. Trivedi

2008-2010 M. Sc (Chemistry)

Department of Chemistry, NITK Surathkal

2005-2008 B. Sc (Physics, Chemistry, Maths)

Canara College, Mangalore (Affiliated to Mangalore University)

RESEARCH EXPERIENCE

12/2014 to Present as Research Scholar

Department of Chemistry,

National Institute of Technology Karnataka, India

06/2010 to 12/2014 as ASSOCIATE-II

Apotex Pharmachem India Pvt Ltd

Research area: Research and Development of Active Pharmaceutical Ingredients.

SKILLS/EXPERTISE

- ❖ Working experience on literature survey and patent evaluation.
- ❖ Process development of Active Pharmaceutical Ingredients (API).
- ❖ Expertise in handling both small (milligrams) and scale up batches (kilograms) of various active pharmaceutical ingredients (API's) and their intermediates and implementation of process at plant level.

-
- ❖ Reference standards-Identification, synthesis and characterization of impurities, intermediates/related compounds and drug substance.
 - ❖ Proficient in multi-step synthesis and reaction monitoring by TLC, NMR, HPLC, UPLC, and LCMS.
 - ❖ Safe handling of pyrophoric (air sensitive) reagents like Pd/C, Pt/C, Rh/Al₂O₃, NaH, LiAlH₄ etc.
 - ❖ Safe handling of water-reactive reagents like n-BuLi, n-hexyl lithium, NaBH₄.
 - ❖ Purification techniques like crystallization, re-precipitation, column chromatography etc.
 - ❖ Documentations related to reference standard reports, process development reports etc.
 - ❖ Handling of NMR instrument, spray drier, lyophilizer, autoclave and pH meter.
 - ❖ Expert in handling analytical instruments like FT-IR, UV-Vis, TGA, POM, and DSC.
 - ❖ Expert in handling Bruker Apex-II Single Crystal X-ray Diffractometer and proficient in solving structures using SHELXL software.
 - ❖ Interpretation of analytical results- NMR, LCMS, HPLC, IR, UV, CHNS, HRMS, etc.
 - ❖ Working knowledge of Microsoft office, Chem Draw, MestReNova, Origin Pro, Mercury, and Platon etc.

RESEARCH PUBLICATIONS

Papers published/communicated in international journals

1. **Nechipadappu, S. K.**, and Trivedi, D. R. (2017). "Pharmaceutical salts of ethionamide with GRAS counter ion donors to enhance the solubility." *Eur. J. Pharm. Sci.*, 96, 578-589.
2. **Nechipadappu, S. K.**, Tekuri, V., and Trivedi, D. R. (2017). "Pharmaceutical Co-Crystal of Flufenamic Acid: Synthesis and Characterization of Two Novel Drug-Drug Co-Crystal." *J. Pharm. Sci.*, 106, 1384-1390.
3. **Nechipadappu, S. K.**, and Trivedi, D. R. (2017). "Structural and physicochemical characterization of pyridine derivative salts of anti-inflammatory drugs." *J. Mol. Struct.*, 1141, 64-74.

-
4. Hariprasad, V. M., **Nechipadappu, S. K.** and Trivedi, D. R. (2016). "Cocrystals of Ethenzamide: Study of Structural and Physicochemical Properties." *Cryst. Growth Des.*, 16, 4473-4481.
 5. Madhavi Oruganti, M., **Nechipadappu, S. K.**, Khade, P. A., & Trivedi, D. R. (2017). "Solid State Versatility of the Molecular Salt/Cocrystal of 2-Chloro-4-Nitrobenzoic Acid: A Case Study on Halogen Bond." *ACS Omega*, 2017, 2(10), 7146–7162.
 6. **Nechipadappu, S. K.**, Ramachandran, J., Shivalingegowda, N., Lokanath, N. K., & Trivedi, D. R. (2018). Synthesis of cocrystals/salts of flucytosine: Structure and stability. *New J. Chem.*, 42, 5433-5446.
 7. **Nechipadappu, S. K.**, Reddy, I. R., Tarafder, K., & Trivedi, D. R. "Crystal Engineering of Anti-Fibrinolytic Hemostatic drug Tranexamic acid: Structural, DFT, and Stability Study of Salt/Cocrystal with GRAS Molecules." *Cryst. Growth & Des.* (Manuscript is under revision).
 8. **Nechipadappu, S. K.**, & Trivedi, D. R. (2018). "Cocrystal of Nutraceutical Sinapic Acid with Active Pharmaceutical Ingredients Ethenzamide and 2-Chloro-4-Nitrobenzoic Acid: Equilibrium Solubility and Stability Study." *J. Mol. Struct.* 1171, 898-905.
 9. **Nechipadappu, S. K.**, Lokanath, N. K., Kumara, K. & Trivedi, D. R. (2017). "Drug-Drug Cocrystal of Anti-Fungal Drug 5-Fluorocytosine with improved stability." (Manuscript is to be communicated).
 10. Javoor, M. J., **Nechipadappu, S. K.**, Lokanath, N. K., Kumara, K. & Trivedi, D. R. (2018). "Cocrystals of Anti-Tuberculosis Drug Pyrazinamide with Hydroxybenzoic Acids: Solubility and Stability Study." (Manuscript is to be communicated).

Papers presented in national/international conferences

1. Kumar, N. S., and Trivedi, D. R. (2015). "A novel pharmaceutical cocrystal of flufenamic acid with 2-chloro-4-nitro benzoic acid to improve the physicochemical properties of flufenamic acid." Paper presented in "International conference on

Contemporary Advances in Science and Technology (IC-CAST 2015).” August 7-8, 2015 at Banaras Hindu University, Varanasi.

2. Kumar, N. S., and Trivedi, D. R. (2016). “Pharmaceutical cocrystal of flufenamic acid with ethenzamide: structural, solubility and stability study.” Paper presented at “International conference on science and technology: Future challenges and solutions (STFCS - 2016).” August 8-9, 2016 at University of Mysore, Mysore.

REFERENCE

1. Dr. Darshak R. Trivedi

Assistant Professor, Department of Chemistry
National Institute of Technology Karnataka, Surathkal
Mangalore, Karnataka-575 025, INDIA
Email: darshak_rtrivedi@yahoo.co.in

2. Dr. Samimul Islam

Group Leader, Apotex Pharmachem India Pvt. Ltd
Bommasandra, Jigani Link Road, Bangalore, INDIA
Email: sislam4@gmail.com